THE STOCHASTIC DYNAMICS OF SYSTEMS IN SWITCHING ENVIRONMENTS

A thesis submitted to the University of Manchester
for the degree of Doctor of Philosophy
in the Faculty of Science and Engineering

2018

Peter G. Hufton
School of Physics and Astronomy

Contents

Word count 59,689

List of Tables

List of Figures

The University of Manchester

Peter G. Hufton
Doctor of Philosophy
The stochastic dynamics of systems in switching environments
July 20, 2018

No physical or biological system can fully be decoupled from its surroundings; the effect of the environment on such a system therefore needs to be understood. In this thesis, we present a number of methods to understand the dynamics of stochastic systems coupled to a time-varying environment. We focus primarily on the case of an environment which randomly switches between conditions, however deterministic environments are also considered. For all our methods and applications, the starting point is an individual-based model: a microscopic description of the system.

The first model-reduction method we develop considers an approximation to the dynamics in the limit of a large system. As the system's size approaches infinity, its dynamics can be approximated by a piecewise-deterministic Markov process (PDMP), where the dynamics are characterised by deterministic motion in between random switches of the environment; this approximation neglects the effects of demographic noise. We go beyond this approximation and explicitly include the effects of demographic stochasticity, resulting in a description of the system as a stochastic differential equation with switching. We derive an expression for the stationary distribution for certain cases, and show how this method leads to strong agreement with simulations.

The second method considers the dynamics of a system in an environment when there is a large separation between systemic and environmental time scales. In the limit in which environment's time scale is infinitely faster than the system's—the adiabatic limit—the environmental dynamics can be eliminated. For fast, but finite, environments we show how reduced master equations can be derived beyond this adiabatic limit. These are characterised by bursting events not found in the original master equation. The above two methods can be combined to consider scenarios with both a large system and fast environmental switching. This results in a range of different approximation schemes valid in different situations. New methods are also developed for the approximation of first-passage times, subject to a deterministic environment.

Applications of these methods to models in biology, medicine, and otherwise, are explored. One focus is on bet-hedging strategies in populations of cells: in the face of uncertain environmental conditions, cells are understood to switch between phenotypes with different growth properties. We present a microscopic model of such a system, and use the PDMP to derive analytical expressions for the mean instantaneous growth rates and thereby study bet-hedging. Another study considers a large genetic network, representing an embryonic stem cell. We derive a simplified model, where the system is a high-dimensional population of gene-products, and we show how the PDMP can be used as an efficient method of simulation. We also consider applications to normal tissue complications, which are caused by damage to normal cells in the radiotherapy of neighbouring cancer cells. Our approaches provide an approximation to the first and second moments of normal tissue complication probabilities in the limit of a large, but finite, population of cells. Other applications considered include a bi-stable genetic circuit and crack propagation.

Declaration

No portion of the work referred to in the thesis has been submitted in support of an application for another degree or qualification of this or any other university or other institute of learning.

Copyright Statement

i. The author of this thesis (including any appendices and/or schedules to this thesis) owns certain copyright or related rights in it (the "Copyright") and s/he has given The University of Manchester certain rights to use such Copyright, including for administrative purposes.

ii. Copies of this thesis, either in full or in extracts and whether in hard or electronic copy, may be made **only** in accordance with the Copyright, Designs and Patents Act 1988 (as amended) and regulations issued under it or, where appropriate, in accordance with licensing agreements which the University has from time to time. This page must form part of any such copies made.

iii. The ownership of certain Copyright, patents, designs, trade marks and other intellectual property (the "Intellectual Property") and any reproductions of copyright works in the thesis, for example graphs and tables ("Reproductions"), which may be described in this thesis, may not be owned by the author and may be owned by third parties. Such Intellectual Property and Reproductions cannot and must not be made available for use without the prior written permission of the owner(s) of the relevant Intellectual Property and/or Reproductions.

iv. Further information on the conditions under which disclosure, publication and commercialisation of this thesis, the Copyright and any Intellectual Property and/or Reproductions described in it may take place is available in the University IP Policy (see http://documents.manchester.ac.uk/DocuInfo.aspx?DocID=487), in any relevant Thesis restriction declarations deposited in the University Library, The University Library's regulations (see http://www.manchester.ac.uk/library/aboutus/regulations) and in The University's Policy on Presentation of Theses.

Acknowledgements

I would like to thank the Engineering and Physical Sciences Research Council (EPSRC) and the University of Manchester for funding my research. I would like to thank Tobias Galla and Alan McKane for their supervision over the course of my PhD, and also my collaborators Yen Ting Lin, Davit Potoyan, Esther Lee, and Elizabeth Buckingham-Jeffery. Thanks also to my colleagues in the Complex Systems and Statistical Physics Group for their brilliant minds and support: Toby, Pete, César, Luis, Louise, Mike, Francisco, Joe, Laura, and Ernseto; and similarly to my office mates: Pierre, Wissam, Rory, and Henry. Thanks also to the biological physics department: B.B., Gareth, Dave, Craig, Haibo, Erick, Charlie, Daniela, Henry, Vinay, Jess, Johanna, Sean, Jack and Hannah; and likewise my close friends: Tom, Jake, Aileen, Elliot, Noel, and especially Rebeca. Thanks go out to my housemates (I couldn't have afforded the rent without you). And, of course, my family: ma, pa, Lizz, Mitch, the girls, Phil, and Abigail.

Chapter 1

Introduction

> It is not because things are difficult that we do not dare; it is because we do not dare that they are difficult.
>
> *Seneca* (5 BC – 65 AD)

1.1 Systems in switching environments

An introduction to statistical physics. Statistical physics arises from the need to understand a world which is simply too complex. Consider a balloon with 10^{23} individual interacting gas particles, each with a certain momentum and position: the system's microscopic properties. Using a computer to simulate the precise dynamics of each of these quantities is well beyond our current capabilities. Still, theoretically, if one knew the initial conditions of the system and the precise nature of the physical interactions between the particles, could one not model the system's dynamics and calculate a later state of the system with certainty? Such a question was considered in 1814, and has come to be referred to as Laplace's demon [1]. The answer, it seems, is no. Firstly, one would have to know all initial conditions with infinite precision: our recent understanding of chaos [2] shows that any deviation in the initial conditions, however small, grows exponentially with passing time. As a result any error in a model quickly prevents us from describing the microscopic properties of the system. Secondly, the success of quantum mechanics presses us to make another conclusion: all evidence suggests the universe is intrinsically probabilistic. We are forced to conclude

that we cannot predict the future with certainty. But most importantly, what use would knowing all this information be? In practise a few macroscopic variables, such as pressure, volume, and temperature, are sufficient to describe the system's behaviour. Statistical physics, then, arises from a need to understand the emergent phenomena of an impossibly complicated microscopic system and its unpredictable environment. Thus at the core of statistical physics is the study of which elements are essential in the description of a complex system. Such elements become the necessary ingredients of an effective model.

The successes of this approach can be seen by the achievements of non-equilibrium statistical physics. These achievements are not isolated to any one area; rather they are spread throughout innumerable scientific disciplines and impossible to list comprehensively. For example, economical applications have allowed physicists to understand the nature of financial processes [3], while sociological applications have allowed us to understand behaviours ranging from the flow of traffic and stampedes [4, 5] to explaining the racial segregation of neighbourhoods using a model initially proposed to describe atomic spins [6]. The analysis of models of infectious diseases have shaped medical policy [7–9]. Through research of statistical physics, we even shed light on the assembly and evolution of life itself [10, 11].

In this thesis we identify one inalienable constituent of many complex systems to be its dynamical environment. All processes in nature are to some extent dependent on an environment. Physical and biological systems can exchange energy, information, or particles with their surroundings. The need to understand a general class of problem necessitates a careful analysis of the effects of environmental noise, and for us to identify the reduced variables and dynamics which allow us to conceptualise environmental effects.

Deterministic environmental dynamics. In many cases environments are best characterised as deterministic. In studies of the dynamics of disease, seasonal variations in temperature, behaviour, and resource availability are known to exert strong pressures on populations [12]; extensions to the susceptible-infectious-recovered (SIR) model have incorporated time-dependent rates [13, 14]. The effects of periodic variations have also been considered in ecological models of extinction [15]. Even in controlled medical applications one can identify such an environment: Brachytherapy,

the treatment of cancer using a sealed radiation source, irradiates cancer cells and nearby normal cells with a rate which varies in time as the source decays.

Bacterial persistence presents another important example of such behaviour. Microbial cells have been shown to switch between phenotypes as a survival strategy to react to changing environments, including variations in temperature and concentrations of nutrients and toxins. In certain settings, this environment can be deterministic: in laboratory experiments, the dynamics of phenotypic switching as a survival strategy are often studied using periodic application of antibiotics [16–18]. Such dynamics are understandably important due to our continued interest in antibiotic resistance.

Continuous stochastic environmental dynamics. In general, however, the dynamical environment is itself unpredictable. For example, in real bacterial populations outside of a laboratory setting, we expect environmental changes to occur outside of any strictly regimented regime. In ecological models, environmental fluctuations may arise from changes in the availability of food, pressure from predation, and weather; stochastic environments have therefore been considered in studies of extinction, fixation, and competition [19–25]. Similarly, the role of continuous stochastic environmental noise on evolutionary processes has been a subject of study [26, 27].

The dividing line between system and environment is not always clear, and in some sense arbitrary. In theory, one could incorporate elements of the environment into the system, resulting in a ever-increasingly complicated joint system. The system, then, is perhaps best described as the populations in which we are strictly interested.

Noise is understood to play a crucial role within the dynamics of gene expression, including being an indispensable part of the cellular decision making process, enabling cell specialization and bet-hedging strategies [28, 29]. Many authors identify a source of environmental noise which arises from variations in the copy numbers of molecules underlying the machinery of gene expression [30,31], affecting the rates on transcription and translation. The effects of such environmental sources of noise on biochemical networks has been an important area of theoretical research, where it has been shown to induce bistability [32, 33] and modify switching rates [34–36]. Recent studies have incorporated the effects of this environmental noise into simple kinetic models through production and degradation rates which vary stochastically in time [37,38]. This source of environmental noise is distinct from the kind considered in this thesis:

Switching environments. For many applications it is more realistic to assume an environment consists of discrete states; the environment switches between these states stochastically, having a pronounced effect on the model parameters of the system to which it is coupled. For example, in the context of genetic networks, noise arises from temporal variations in the binding configurations of genes: each potential configuration of a gene's promoter site corresponds to a discrete state. A change to this configuration may activate or repress the gene, vastly changing the rate of transcription of mRNA [39]. In models of bacterial persistence, the environment may represent the presence of antibiotics or a host immune response, each of which can be modelled as a random environment with discrete states [40, 41]. In certain ecological models an environment may occasionally switch to describe a short-lived catastrophe, causing a major change to the population [20, 42]. Predator-prey models and other ecological models have been considered in switching environments in order to account for abrupt changes in growth rates and carrying capacities arising from weather variations and the availability of nutrients [43–47]. A recent game theoretical study of fixation in switching environments shows that switching environments can work in a mutant's favour to increase the probability of fixation [48]. Further examples can be found in models of voter behaviour [49], and the failure of mechanical components due to different modes of operation [50–55].

Systems coupled to switching environments are subject to two sources of noise: environmental noise, arising from stochasticity in environmental switches, and demographic (or intrinsic) noise, arising from unpredictability of the system itself. This latter source is caused by random births and deaths of individuals. Intrinsic noise is understood play an important role in many models. For example, it has shown to cause macroscopic changes of behaviour in populations by sustaining oscillations [56–58]. Our goal is to better understand the dynamics of systems under the influence of both these sources of noise. This involves the development, understanding, and application of model-reduction schemes to reduce complex problems to their necessary elements.

In the aforementioned examples and the majority of this thesis, the processes describing the system and the environment are Markov jump processes: the system and the environment each hop stochastically between discrete states in continuous time.

Such processes will be referred to as individual-based models, since each possible state refers to a certain number of individuals in the population of the system. The time-evolution of the joint probability of processes occupying a specific state is described exactly by a master equation.

Although both system and environment are formally described by the master equation, an environment as discussed here differs from a system in a number of crucial ways. Firstly, environmental states are typically few in number, while a system may have many possible states. Binary environments, in particular, are used extensively in the aforementioned models; in such cases, the variation in the environment is sometimes referred to as dichotomous noise [59]. Secondly, a change in environmental state often causes an abrupt change in dynamics. This can be seen in the context of genetic models, where the binding or unbinding of a particular molecule to a promoter site can have a drastic effect on the production of mRNA molecules [39]. Similarly in models of antibiotic resistance, the introduction of antibiotics to a population of bacteria can serve to favour one phenotype over another and thereby reverse the direction of flow [40,41]. As a result of these differences the environmental states cannot be treated as a continuum. Thus many simplifying approximations which work for large systems—the Kramers–Moyal expansion or the system-size expansion [60,61]—are not valid for the environment. In order to approximate the dynamics of systems in switching environmental conditions different techniques are needed.

We proceed by discussing existing methods which are used to understand the dynamics of systems in switching environments.

1.2 Existing methods

1.2.1 Exact approaches for analysing systems in switching environments

The chemical master equation is a set of first-order ordinary differential equations (ODEs) describing the time-evolution of the probability of a system (and an environment) occupying each state as a function of time [60,61]. In the simplest case where the system consists of a single species, this probability can be written $P_{n,\sigma}(t)$, where

σ is the state of the environment and n is the number of individuals in the system[1]. The master equation then takes the general form

$$\frac{\mathrm{d}}{\mathrm{d}t}P_{n,\sigma}(t) = \sum_{n',\sigma'} A_{n'\to n,\sigma'\to\sigma} P_{n',\sigma'}(t), \tag{1.1}$$

where **A** describes the rate of transition from one state to another. The master equation is an exact description of the dynamics of the underlying individual-based model. However, only for the simplest models can the master equation be solved analytically [60–62]. For other cases, analytical results are only available by performing an approximation.

Integration of the master equation. The master equation, however, may be integrated numerically using a Runge–Kutta method or similar [63]. In this way, one can obtain numerical results describing, for example, the time-course of the probability distribution, the stationary probability distribution, and the first-passage time through a boundary. This brute-force approach, however, has a number of disadvantages. One such shortfall is the scaling of computational difficulty with the size and complexity of the system. When the populations in the model are large, a large number of ODEs must be forward-integrated. This can have a large effect on simulation times: each additional (chemical) species in the model increases the dimensionality of the system, thereby exponentially increasing the number of ODEs and thus the computation time. For large systems, then, it can quickly become infeasible to directly integrate the chemical master equation. Another disadvantage is that integration of the master equation provides only numerical results, and so gives little insight into the underlying physics of a model. Lastly, numerical integration of the master equation itself involves a number of approximations: (1) for many models the state-space is infinite. Thus, to proceed with this method one needs to truncate an infinite series of ODEs at some finite cut-off [64]; (2) it involves selecting a finite time-step dt thereby introducing error depending on the method of integration [e.g., the fourth order Runge–Kutta introduces an error of order $(\mathrm{d}t)^4$].

Generating functions. One technique for obtaining analytical results from the master equation without approximation involves moment generating functions. This

[1]Since the space of states is discrete, the set of probabilities is strictly (up to a labelling) a vector. However, in practise the probabilities are often written as a function, e.g., $P(n, \sigma, t)$.

entails introducing the generating function $G_\sigma(z,t) = \sum_{n=0}^{\infty} z^n P_{n,\sigma}(t)$, and substituting into the master equation. Using such a method, one is able obtain exact solutions to the transient and asymptotic probability distributions for simple models [35,65–68]. Critically, however, the moment generating function method works only for the simplest cases. Specifically, this method is limited to cases where the dynamics of the underlying model are linear. Furthermore, success in using the moment-generating function to exactly solve problems for systems in switching environments has only been achieved for one dimensional systems, that is, systems containing a single species; for more complex models, approximations (such as a separation in timescales [69]) have been required. While for the simplest cases such methods provide a solution to the generating function, transforming this solution back to the space of probabilities [i.e., $P_{n,\sigma}(t)$] is difficult. Lastly, if such a solution is obtainable, the functional form is often too complicated to glean the underlying physics. Thus, to study a more general class of problem, the method of moment-generation functions is inadequate.

Monte Carlo methods. The statistics of systems in switching environments can be obtained from the master equation using kinetic Monte Carlo methods. The Gillespie algorithm, otherwise called the Stochastic Simulation Algorithm (SSA), was proposed by Gillespie in 1976 [70,71] and has seen widespread use in simulating Markov jump processes. The SSA produces a single sample path of a stochastic process without approximation; at each time this sample path has a single given state. Owing to the stochastic nature of the process, each sample path will be different. To determine the statistics of the model using this method, a large ensemble of trajectories must be simulated. The Gillespie algorithm has also been generalised to consider time-dependent transition rates and non-Markovian processes [72, 73], while an improvement to the Gillespie algorithm has been suggested which requires only a single random variable to be generated per time step [74]. Still, using this method involves the generation of a large number of random numbers, which comes at a significant computational cost. As a result, the Gillespie algorithm often does not constitute an efficient approach to obtaining the statistical properties of a model. This is especially the case when either (i) the rate at which events occur is very high, meaning a large number of events need to be simulated over a small time, as is the case when the system contains a very large population; or (ii) when the state space is very large, meaning a very large ensemble

of Gillespie simulations must be considered before the statistics are adequately representative. Similarly to the other approaches discussed so far, the Gillespie algorithm provides only numerical results, while analytical results can sometimes be more useful.

1.2.2 Approximations to systems in switching environments

The need for the approximation of the master equation derives from two main reasons. Firstly, they allow one to obtain otherwise impossible (or impractical) mathematical results. By making certain well-justified assumptions, we are often able to make simplifications which lead to new analytical results, giving real, physical insight into the properties of the model itself. Secondly, approximating the master equation can facilitate more efficient means of simulation. An example of this, as is discussed in more detail below, is the Kramers–Moyal expansion which allows for stochastic time-courses to be generated more efficiently at larger system sizes. In this way, the approximation of the master equation precipitates progress even when it does not provide a final, analytical result. One aim of this thesis is therefore to expand our understanding of approximations to systems in switching (and in Chap. 6 continuously time-varying) environments. Secondly, we use these methods in a number of applications to further our understanding of various biological processes. Below, we give an overview of existing approaches for approximating the master equation and their relevance to systems in switching environments.

The large-system limit. For systems without the complication of environmental switching, a well-developed toolset for approximating the master equation has emerged. The most prominent of these approximations rely on the following assumption: the populations of interest are large. For systems with larger sizes, the dynamics become more predictable.

The Kramers–Moyal expansion [60–62, 75, 76] is the Taylor expansion of the master equation in inverse powers of the system size; The system size is characterised by the system-size parameter Ω. Truncating this series after a finite number of terms constitutes an approximation; this is almost always done after either one or two terms. The reason for this is Pawula's theorem [60, 62] which states that the inclusion of higher-order terms contradicts the positivity of the probability density distribution, unless infinitely many terms are collected.

The truncation of the Kramers–Moyal expansion after the lowest-order terms leads to the rate equation. One introduces a rescaling of the population $x_t = n_t/\Omega$, referred to as the population density. For a one-dimensional population the rate equation has the form

$$\frac{\mathrm{d}x}{\mathrm{d}t} = v[x(t)], \tag{1.2}$$

where $v(x)$ describes the deterministic drift of the population. For the multidimensional case, this is a set of ordinary differential equations (ODEs) which again describe the deterministic drift of the system only. While useful in certain cases, this description neglects the effects of demographic noise which arises as a product of having a finite system. Even with this caveat, such rate equations have seen use in many applications, including models of infectious disease [7] and pioneering studies of predator-prey dynamics [77].

The sub-leading-order truncation of the Kramers–Moyal expansion leads to a Fokker–Planck equation (FPE), a second order partial differential equation (PDE). The finite truncation of the expansion removes the discreteness of the state space, so that that state-space becomes continuous, and rather than a probability we have a probability density. The Fokker–Planck equation in one dimension has the form

$$\frac{\partial}{\partial t}\Pi(x,t) = -\frac{\partial}{\partial x}v(x)\Pi(x,t) + \frac{1}{2\Omega}\frac{\partial^2}{\partial x^2}w^2(x)\Pi(x,t), \tag{1.3}$$

where $\Pi(x,t)$ is the probability density as a function of time. The right hand side of the FPE consists of two terms; the first, characterised by the function $v(x)$, describes the drift of the population, and the second, characterised by the function $w(x)$, describes the diffusion. This latter term accounts for the demographic noise. In general the Kramers–Moyal expansion results in process with multiplicative noise; a process where the diffusion term is a function of the random process.

Similarly, a related expansion—van Kampen's system-size expansion—also considers an expansion in powers of the inverse system size. This approach utilises an ansatz to further simplify the dynamics; we assume the random process describing the population density can be decomposed

$$x_t = \phi(t) + \Omega^{-1/2}\xi_t, \tag{1.4}$$

where $\phi(t)$ is a deterministic path which describes the drift only, and random process

ξ_t describes deviations from this path. This is referred to as the linear noise approximation (LNA), and it leads to a description of the system as an FPE with *additive* noise:

$$\frac{\mathrm{d}\phi}{\mathrm{d}t} = v[\phi(t)], \tag{1.5a}$$

$$\frac{\partial}{\partial t}\tilde{\Pi}(\xi,t) = -v'(\phi)\frac{\partial}{\partial \xi}\xi\tilde{\Pi}(\xi,t) + \frac{w^2(\phi)}{2}\frac{\partial^2}{\partial \xi^2}\tilde{\Pi}(\xi,t), \tag{1.5b}$$

where $v'(\phi)$ is the derivative of $v(\phi)$, and $\tilde{\Pi}(\xi,t)$ is the probability density of the random process ξ_t. It has been shown that this approximation is valid over limited times for any population which is sufficiently large [78]. The linear form of the noise, the independence of the noise strength from variable ξ, can be considered simpler than the multiplicative noise in the Kramers–Moyal expansion. In this way, the system-size expansion lends itself more readily to analytical solutions, however, in some circumstances where the system size is not sufficiently large, it fails to capture dynamical effects otherwise captured by multiplicative noise [79].

Monte Carlo methods can also be used in the large-system limit. Dynamics in the form of a Fokker–Planck equation can equivalently be written as a system of Itō stochastic differential equations (SDEs). For example FPE (1.3) may be rendered

$$\mathrm{d}x_t = v(x_t)\,\mathrm{d}t + \Omega^{1/2}\,w(x_t)\,\mathrm{d}W_t, \tag{1.6}$$

where W_t is the Wiener process, also referred to as Brownian motion. The Euler–Maruyama method provides a method for the integration of these SDEs, providing an approximation to a sample path of the process [80]. For large systems, this approximate approach can be much more efficient than performing the SSA with the full model.

While these large-system-size approaches are useful when all species are present in large numbers, they are not directly applicable to cases where they are coupled to environmental states which are few in number. The failure of such an approach is documented in Ref. [81], wherein the authors perform the traditional Kramers–Moyal expansion to a model where a large population of proteins (a system) coupled to the state of a small number of genes (an environment). The authors find a marked disagreement between the stationary statistics of the approximation and the full model. This motivates a more careful approach to the dynamics of systems in switching environments, where we adapt the approach of the Kramers–Moyal expansion to consider

a system which is large but an environment which is not. Before starting my PhD, such a technique was developed only for the cases of an infinitely-large system:

The piecewise-deterministic Markov process. The piecewise-deterministic Markov process (PDMP) was first introduced in a 1984 paper by Davis [82]. Such a process is characterised by continuous deterministic motion between discrete stochastic jumps. Since its inception, the PDMP has been used in applications as varied as financial risk [83] and the growth of cracks in mechanical components subject to time varying loads [52].

The PDMP can be seen as an approximation to large systems coupled to switching environments. More specifically, it is the result of approximating the system as infinitely large (and therefore deterministic), while maintaining the discreteness and randomness of the environment. For this reason, the PDMP has seen increasing use in modelling genetic regulatory networks [84–87]. In these cases a large population of proteins is coupled to an 'environment' which is typically the state of a single gene, or else a small population of mRNA molecules [88]. For the case of a one-dimensional population, the PDMP has the form

$$\frac{\mathrm{d}x_t}{\mathrm{d}t} = v_{\sigma_t}(x_t), \tag{1.7}$$

where the function $v_\sigma(x)$ describes the drift of the population when it is in environmental state σ; the state of the environment σ_t is itself described by a master equation.

Approximating the system in this way has allowed for analytical results to be produced in some cases, for example the stationary distributions for certain models were calculated in Refs. [84, 89]. A major part of the work of this thesis is using the PDMP to achieve new, analytical results. Furthermore, the deterministic treatment of the large system vastly increases the efficiency with which a process can be simulated [85]. This allows progress to be made where analytical solutions are not feasible. As such, another major component of this thesis involves utilising the PDMP to efficiently simulate large and high-dimensional models.

While the PDMP accounts for discrete switching between environmental states, it does not account for demographic noise arising from finite system sizes. This noise cannot always be ignored. For example, in Chapter 2, we show that this noise can lead to marked difference in the statistics of the stationary state. This motivates a

more accurate approximation of the full model which retains, to some approximation, the effects of this demographic noise.

Fast environmental switching. A separate approach for approximating systems in switching environments has been used when the time-scale separation between the evolution of the environment and the system is large. When the environment switches very quickly, it can be that assumed the environment is always equilibrated to its stationary state. This assumption is closely related to the quasi-steady-state assumption (QSSA), which allows fast-reacting species to be eliminated from the dynamics of chemical reactions [90–97]. For the case of a one-dimensional population, the dynamics are then described by a master equation

$$\frac{\mathrm{d}}{\mathrm{d}t}P_n(t) = \sum_n A^{\mathrm{avg}}_{n'\to n} P_{n'}(t), \tag{1.8}$$

where $\mathbf{A}^{\mathrm{avg}}$ is an effective transition rate matrix, found by averaging over the environment.

This approach, however, relies on the assumption that there is an *infinite* separation between the time scales of the system and the environment. This results in a deterministic environment, where the noise from environmental switches is entirely neglected. Even in the fast switching case, the noise from environmental switches can be important. For example, in Ref. [98] it was shown that even when fluctuations in a genetic environment occur on fast time scales, they still impart a non-negligible modification to the lifetime of an epigenetic state. Thus, it is necessary to more accurately consider the dynamics of systems in fast-switching environments, in order to re-account for this environmental noise.

1.3 New approaches to systems in switching environments and applications

The aforementioned existing approaches to systems in switching environments (the PDMP and the QSSA) ignore sources of noise which can have a significant effect on the resulting statistics. In order to effectively approximate systems in switching environments, one must introduce new methods. In the chapters which follow, we develop new methods for treating such systems, and we apply our insight to certain

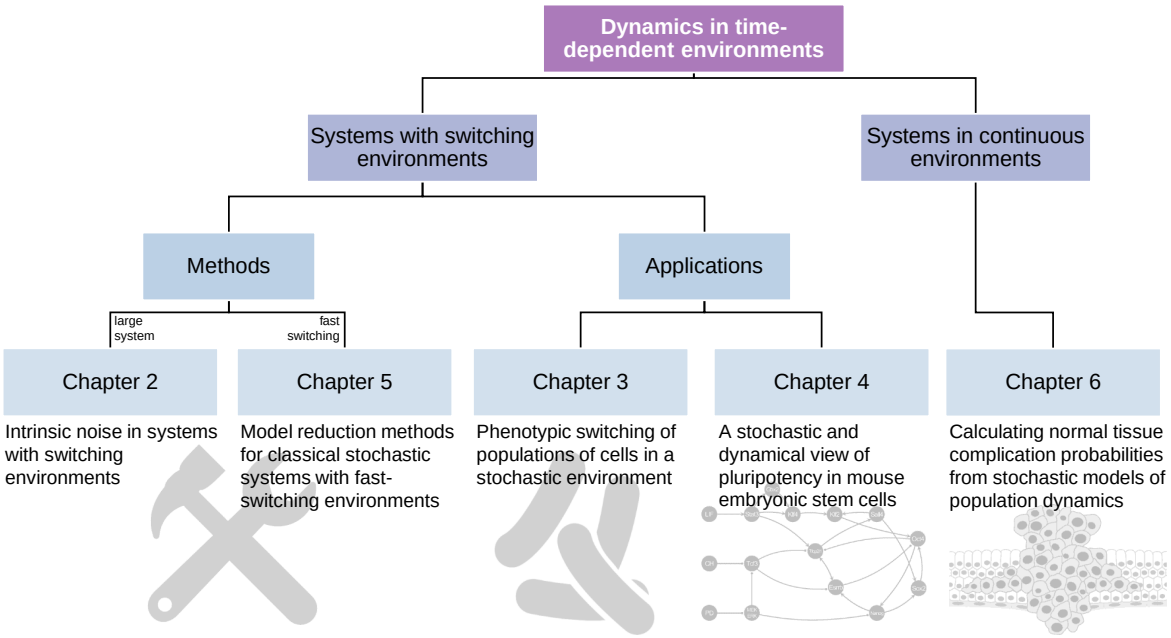

Figure 1.1: A schematic view of this thesis (Pictures reproduced from Freepik from www.flaticon.com, and Cancer Research UK / Wikimedia Commons).

important biological applications. An overview of the structure of these chapters is shown in Fig. 1.1.

Throughout this body of work, we develop a range of approximations to the master equation, allowing one to approximate the dynamics of a model suit each individual purpose. This involves putting existing approximations into context, as well as developing new approximations. A schematic of approximation schemes is presented in Fig. 1.2, in which we consider approximations in the size of the system (horizontal axis), and approximations in the time scale of environmental switching (vertical axis). Approximation schemes with a red border were developed during the course of this body of work.

Chapter 2: Intrinsic noise in systems with switching environments. In Chapter 2 we consider approximations of systems in switching environments in the large-system limit, i.e., we move horizontally along the top column of Fig. 1.2. This involves considering a Kramers–Moyal-type expansion of the system only, while maintaining the discrete, random environment. Collecting only lowest-order terms leads to a PDMP. Focusing on the case of a two-state environment and a single systemic species, we derive a general expression for the stationary state of this PDMP. However, we show that there are major qualitative and quantitative differences between

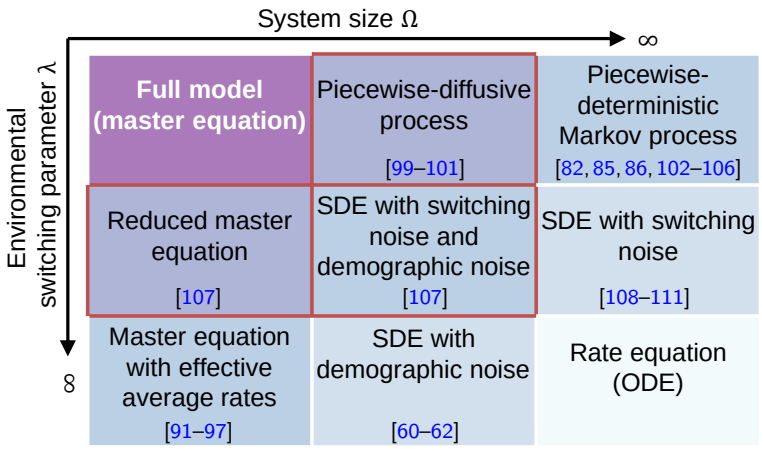

Figure 1.2: A schematic of the different schemes for approximating the individual-based model of a system in a switching environment as we increase the system size and the environmental switching rates; each column and row corresponds to a successive layer of approximation. Approximation schemes with a red border are original to this body of work.

the true stationary distribution and this lowest-order approximation. This motivates us to consider the next-order term in the Taylor expansion of the system.

The result of our higher-order expansion is a hybrid Fokker–Planck equation; an equation where the time-evolution of the system evolves according to drift and diffusion terms (i.e., Fokker–Planck-like), but where the environment is described by master-equation-like switching. This is related to a contemporary study considering dichotomous noise [100]. Such dynamics can be described by an SDE where the drift and diffusion coefficients change instantaneously between discrete environmental switches, i.e.,

$$\mathrm{d}x_t = v_{\sigma_t}(x_t)\,\mathrm{d}t + \Omega^{1/2}\, w_{\sigma_t}(x_t)\,\mathrm{d}W_t. \tag{1.9}$$

We refer to such a process as a piecewise-diffusive process. In this chapter, we focus on the statistics of the stationary state of systems in switching environments. Using an additional approximation, we are able to produce a result describing the stationary state in a closed form as an integral. We show how this has marked improved accuracy over the PDMP, and show a number of illuminating examples. Chapters 3 and 4 each contain biological applications of the techniques developed in this chapter.

Chapter 3: Phenotypic switching of populations of cells in a stochastic environment. Chapter 3 contains an application of the techniques developed in

the preceding chapter to a model rooted in biology. Thereby, we obtain original insight into a biological problem. We consider the phenomenon of bacterial phenotypic switching as a bet-hedging strategy to endure unfavourable environmental conditions. Microbial cells are understood to switch between faster-growing and more-resilient phenotypes in order to react to changes in the environment, including the presence of antibiotics, differences in temperature, and the state of a host immune response [16, 112–117]. While much previous analysis has been carried out when the environmental changes happen periodically [16, 17, 118–125] , less attention has been paid to stochastic environmental switching [40,41,126–130]. In this chapter we focus primarily on the case of a Markovian environment. Starting from an individual-based model, we derive the piecewise-diffusive process and piecewise-deterministic Markov process. Applying these technologies, we derive a closed expression for the average growth rate of bacterial populations in our model, and use this to analyse how phenotypic switching constitutes a survival strategy in a stochastically switching environment. We show that optimal phenotypic responses are non-trivial for slow and intermediate environmental processes, and we compare our results to the case of periodic environments. We also find that stochastic environmental switching produces population growth rates which are always higher than their periodic counterparts. The model can also be looked at as a host-pathogen interaction, where a host switches environments to minimise the growth rate while the pathogen attempts to maximise it. In doing so, we find a Nash-like best-response scenario for the pathogen and host environment.

Chapter 4: A stochastic and dynamical view of pluripotency in mouse embryonic stem cells. The research paper reproduced in Chapter 4 arose as a collaborative effort between the Theoretical Physics division at the University of Manchester and the Center for Theoretical Biological Physics at Rice University, Houston TX. We consider a large genetic network which describes mouse embryonic stem cells (mESCs). In this case, the instantaneous configuration of a number of genes constitutes an environmental state. Under certain chemical conditions such mESCs are pluripotent: they maintain the capacity to differentiate into every type of cell in the adult organism [131–133]. The network and underlying signalling layers are thought to describe the cell-fate decision-making process [133]. Descriptions of genetic networks have been inferred from experiments, however, these often only encode the lowest-level Boolean

information of *whether* the expression of a particular gene causes the expression of another further downstream. In this respect, they remain silent about exactly *how* one gene causes the activation of another. The underlying molecular dynamics and logic are ignored, and thereby also the role of stochasticity in gene expression.

The primary aim of Chapter 4 is to expound the benefits of using the PDMP to simulate large genetic networks. We develop an extension to the Boolean-level information to give a higher-resolution picture which explicitly accounts for molecular logic and switching between genetic states. We start from the genetic network recently inferred by Dunn *et al.* [134] describing 12 genes and three external inputs, and we introduce molecule logic describing the production, degradation, binding, and unbinding of molecules of transcription factors (TFs). This results in an individual-based model describing populations of TFs and the states of genes. In order to proceed with the smallest number of free parameters, a large number of simplifying assumptions are made, such TFs sharing the same rates, and similarly for genes. While these assumptions are chosen to be consistent with experiments as best possible, they still (in all likelihood) constitute very large approximations to the real microscopic system. In this chapter, then, we do not focus on the quantitative specifics of embryonic stem cells, but rather on: (i) the methods for the efficient simulation of large individual-based models; and (ii) qualitative results which appear to be features of the network, rather than the specific molecular dynamics. We present a mathematical framework for the efficient simulation of a high-dimensional population of TFs in a genetic environment; in this case we consider a PDMP description of the system since the populations are very large. We validate this against Monte Carlo simulation of the full chemical master equation, and report an increase in simulation efficiency of order 10^3.

Chapter 5: Model reduction methods for classical stochastic systems with fast-switching environments: reduced master equations, stochastic differential equations, and applications. In Chapter 5 we consider the dynamics of systems in switching environments in the limit that this switching is fast. We perform an expansion in this limit which is independent of the large-system approximations considered in Chapter 2. When the environmental switching is infinitely fast compared to the system—the adiabatic limit—the aforementioned QSSA applies and there is in effect no environmental noise. However, when there is a finite time-scale separation

we show that there are corrections; the dynamics can be approximated by a *reduced* master equation which contains bursting events. Bursting events are characterised by instances where two of the original system's reactions occur simultaneously (e.g., the reduced dynamics may allow two proteins to be synthesised simultaneously, even when the original dynamics did not). These approximations are shown schematically by descending the left-hand column of Fig. 1.2.

Combining the different levels of approximations in (i) the system size, and (ii) the environmental switching time scale leads to the full series of approximations shown in Fig. 1.2. In this way, we put the existing levels of approximation [81, 82, 85, 86, 91–97, 99–106, 108–111, 135] and our approximations (those shown with a red border) into a wider context. In this chapter we apply these methods to a number of different examples, biological and otherwise, and suggest how they may be useful for efficient simulation and for obtaining analytical results in the future.

Another focus of this chapter relates to negative 'rates'. In some cases, the expansion of the master equation in the fast-switching limit leads to a reduced master equation containing negative 'rates'. This is similar, at least superficially, to negative rates which appear in open quantum systems when integrating out an environment [136–138]. We consider existing approaches for the treatment of master equations with negative rates [137, 138]. We also devise a stochastic simulation algorithm in discrete time to procure sample paths in such a scenario, and provide an interpretation of bursting events in the reduced master equation.

Chapter 6: Calculating normal tissue complication probabilities and probabilities of complication-free tumour control from stochastic models of population dynamics. Chapter 6 marks a slight departure from the preceding chapters since here we consider the dynamics of a system with an environment which varies continuously and deterministically in time. We define an individual-based model of normal tissue cells subject to radiation from the radiotherapeutic treatment of neighbouring cancer cells. During the radiotherapy of cancerous cells, nearby healthy cells are also damaged, which can lead to normal tissue complications ranging from acute complications such as increased urinary frequency in the treatment of prostate cancers [139, 140], to severe neurological complications such as myelitis in neck cancers [141]. In the model we consider, the radiation protocol constitutes an environment. The

calculation of normal tissue complication probabilities (NTCP) forms an active area of research [142–145]. In our work, the mathematics of NTCP are equivalent to a first-passage time problem [146]. In this chapter, we use large-system expansion methods to approximate the distributions of first-passage times for general models in this limit. In this way, our results have implications beyond modelling cancer therapies. In the latter parts of this chapter we consider the probability of normal tissue complications for a more complicated model of cancer treatment. Using earlier research into the probability of fully eliminating all cancerous cells [147], we also consider a combined model of tumour control probabilities (TCP) and NTCP, which aims to forms a balance between the maximisation of tumour control and the minimisation of normal tissue complications.

Chapter 7: Conclusions. Finally, Chapter 7 is the conclusions chapter. In this chapter, I consider the body of work produced during my doctoral studies as a whole, including its successes, shortcomings, and areas for future research.

It is my hope that the reader of this thesis will experience even a fraction of the enjoyment that I have had in writing it over the past three and a half years.

Comments on thesis format. This thesis follows The University of Manchester's journal format: the middle chapters consist of five journal papers. The first three chapters are reproduced from three published research papers [101,148,149], while the latter two relate to submitted papers currently under review [107,150]. The papers are presented here in order of submission/publication; fortunately, this also proves optimal in terms of storytelling. To varying extents, each of these papers relates to work which was completed as part of a collaboration: I preface each chapter with details of my personal contribution to each paper. The motivation behind my decision to use the journal format is that it allowed me to focus on developing skills in writing research papers, as well as enhancing my research profile. Secondly, it is my opinion that the material contained in these five papers tells a logical and consistent story.

The papers presented herein are not without changes from their published forms. Most notably, rather than using pre-prints relating to each publication, the papers have been adapted into the appropriate thesis template. This allows for consistent pagination and sequential numbering throughout the thesis. Other minor changes have been made to improve the consistency of notation throughout the papers, with

the aim of increasing the ease of reading when considering the body of work as a whole.

1.4 Bibliography

[1] M. d. Laplace. *A Philosophical Essay on Probabilities.* Dover, Mineola NY (1814).

[2] S. H. Strogatz. Nonlinear dynamics and chaos: with applications to physics, biology, chemistry, and engineering (2000).

[3] J.-P. Bouchaud and M. Potters. *Theory of financial risk and derivative pricing: from statistical physics to risk management.* Cambridge University Press, Cambridge (2003).

[4] D. Helbing and B. Tilch. Generalized force model of traffic dynamics. *Phys. Rev. E* **58**, 133 (1998).

[5] D. Helbing, I. Farkas, and T. Vicsek. Simulating dynamical features of escape panic. *Nature* **407**, 487 (2000).

[6] T. C. Schelling. Dynamic models of segregation. *J. Math. Sociol.* **1**, 143 (1971).

[7] M. J. Keeling and P. Rohani. *Modeling infectious diseases in humans and animals.* Princeton University Press, Princeton NJ (2011).

[8] H. Heesterbeek, R. M. Anderson, V. Andreasen, S. Bansal, D. De Angelis, C. Dye, K. T. Eames, W. J. Edmunds, S. D. Frost, S. Funk, *et al.* Modeling infectious disease dynamics in the complex landscape of global health. *Science* **347**, aaa4339 (2015).

[9] Z. Wang, C. T. Bauch, S. Bhattacharyya, A. d'Onofrio, P. Manfredi, M. Perc, N. Perra, M. Salathé, and D. Zhao. Statistical physics of vaccination. *Phys. Rep.* **664**, 1 (2016).

[10] G. M. Whitesides and B. Grzybowski. Self-assembly at all scales. *Science* **295**, 2418 (2002).

[11] M. A. Nowak. *Evolutionary dynamics*. Harvard University Press, Cambridge MA (2006).

[12] S. Altizer, A. Dobson, P. Hosseini, P. Hudson, M. Pascual, and P. Rohani. Seasonality and the dynamics of infectious diseases. *Ecol. Lett.* **9**, 467 (2006).

[13] A. J. Black and A. J. McKane. Stochastic amplification in an epidemic model with seasonal forcing. *J. Theor. Biol.* **267**, 85 (2010).

[14] N. C. Grassly and C. Fraser. Seasonal infectious disease epidemiology. *Proc. Royal Soc. A* **273**, 2541 (2006).

[15] M. Assaf, A. Kamenev, and B. Meerson. Population extinction in a time-modulated environment. *Phys. Rev. E* **78**, 041123 (2008).

[16] N. Q. Balaban, J. Merrin, R. Chait, L. Kowalik, and S. Leibler. Bacterial persistence as a phenotypic switch. *Science* **305**, 1622 (2004).

[17] E. Kussell, R. Kishony, N. Q. Balaban, and S. Leibler. Bacterial persistence a model of survival in changing environments. *Genetics* **169**, 1807 (2005).

[18] H. J. Beaumont, J. Gallie, C. Kost, G. C. Ferguson, and P. B. Rainey. Experimental evolution of bet hedging. *Nature* **462**, 90 (2009).

[19] E. G. Leigh Jr. The average lifetime of a population in a varying environment. *J. Theor. Biol.* **90**, 213 (1981).

[20] R. Lande. Risks of population extinction from demographic and environmental stochasticity and random catastrophes. *Am. Nat.* **142**, 911 (1993).

[21] K. Johst and C. Wissel. Extinction risk in a temporally correlated fluctuating environment. *Theor. Popul Biol.* **52**, 91 (1997).

[22] A. Kamenev, B. Meerson, and B. Shklovskii. How Colored Environmental Noise Affects Population Extinction. *Phys. Rev. Lett.* **101**, 268103 (2008).

[23] P. L. Chesson and R. R. Warner. Environmental variability promotes coexistence in lottery competitive systems. *Am. Nat.* **117**, 923 (1981).

[24] S. Karlin and B. Levikson. Temporal fluctuations in selection intensities: case of small population size. *Theor. Popul. Biol.* **6**, 383 (1974).

[25] M. Danino, N. M. Shnerb, S. Azaele, W. E. Kunin, and D. A. Kessler. The effect of environmental stochasticity on species richness in neutral communities. *J. Theor. Biol.* **409**, 155 (2016).

[26] M. Assaf, M. Mobilia, and E. Roberts. Cooperation Dilemma in Finite Populations under Fluctuating Environments. *Phys. Rev. Lett.* **111**, 238101 (2013).

[27] A. Melbinger and M. Vergassola. The impact of environmental fluctuations on evolutionary fitness functions. *Sci. Rep.* **5**, 15211 (2015).

[28] R. Losick and C. Desplan. Stochasticity and cell fate. *Science* **320**, 65 (2008).

[29] M. N. Artyomov, J. Das, M. Kardar, and A. K. Chakraborty. Purely stochastic binary decisions in cell signaling models without underlying deterministic bistabilities. *Proc. Natl. Acad. Sci. U.S.A.* **104**, 18958 (2007).

[30] J. Paulsson. Summing up the noise in gene networks. *Nature* **427**, 415 (2004).

[31] A. Eldar and M. B. Elowitz. Functional roles for noise in genetic circuits. *Nature* **467**, 167 (2010).

[32] M. Samoilov, S. Plyasunov, and A. P. Arkin. Stochastic amplification and signaling in enzymatic futile cycles through noise-induced bistability with oscillations. *Proc. Natl. Acad. Sci. U.S.A.* **102**, 2310 (2005).

[33] G. Caravagna, G. Mauri, and A. d'Onofrio. The interplay of intrinsic and extrinsic bounded noises in biomolecular networks. *PLoS One* **8**, e51174 (2013).

[34] V. Shahrezaei, J. F. Ollivier, and P. S. Swain. Colored extrinsic fluctuations and stochastic gene expression. *Mol. Syst. Biol.* **4**, 196 (2008).

[35] B. Hu, D. A. Kessler, W.-J. Rappel, and H. Levine. Effects of input noise on a simple biochemical switch. *Phys. Rev. Lett* **107**, 148101 (2011).

[36] M. Leisner, J.-T. Kuhr, J. O. Rädler, E. Frey, and B. Maier. Kinetics of genetic switching into the state of bacterial competence. *Biophys. J* **96**, 1178 (2009).

[37] M. Assaf, E. Roberts, Z. Luthey-Schulten, and N. Goldenfeld. Extrinsic Noise Driven Phenotype Switching in a Self-Regulating Gene. *Phys. Rev. Lett.* **111**, 058102 (2013).

[38] E. Roberts, S. Be'er, C. Bohrer, R. Sharma, and M. Assaf. Dynamics of simple gene-network motifs subject to extrinsic fluctuations. *Phys. Rev. E* **92**, 062717 (2015).

[39] T. B. Kepler and T. C. Elston. Stochasticity in transcriptional regulation: origins, consequences, and mathematical representations. *Biophys. J.* **81**, 3116 (2001).

[40] M. Thattai and A. Van Oudenaarden. Stochastic gene expression in fluctuating environments. *Genetics* **167**, 523 (2004).

[41] E. Kussell and S. Leibler. Phenotypic diversity, population growth, and information in fluctuating environments. *Science* **309**, 2075 (2005).

[42] B. Cairns, J. Ross, and T. Taimre. A comparison of models for predicting population persistence. *Ecol. Model.* **201**, 19 (2007).

[43] Q. Luo and X. Mao. Stochastic population dynamics under regime switching. *J. Math. Anal. Appl.* **334**, 69 (2007).

[44] C. Zhu and G. Yin. On competitive Lotka–Volterra model in random environments. *J. Math. Anal. Appl.* **357**, 154 (2009).

[45] R. West, M. Mobilia, and A. M. Rucklidge. Survival behavior in the cyclic Lotka-Volterra model with a randomly switching reaction rate. *Phys. Rev. E* **97**, 022406 (2018).

[46] K. Wienand, E. Frey, and M. Mobilia. Evolution of a Fluctuating Population in a Randomly Switching Environment. *Phys. Rev. Lett.* **119**, 158301 (2017).

[47] K. Wienand, E. Frey, and M. Mobilia. Eco-Evolutionary Dynamics of a Population with Randomly Switching Carrying Capacity. *arXiv preprint arXiv:1712.07939* (2017).

[48] P. Ashcroft, P. M. Altrock, and T. Galla. Fixation in finite populations evolving in fluctuating environments. *J. R. Soc. Interface* **11**, 20140663 (2014).

[49] J. Hidalgo, S. Suweis, and A. Maritan. Species coexistence in a neutral dynamics with environmental noise. *J. Theor. Biol.* **413**, 1 (2017).

[50] J. Chiquet and N. Limnios. A method to compute the transition function of a piecewise deterministic Markov process with application to reliability. *Stat. Probab. Lett.* **78**, 1397 (2008).

[51] J. Chiquet, M. Eid, and N. Limnios. Modelling and estimating the reliability of stochastic dynamical systems with Markovian switching. *Rel. Eng. & Syst. Safety* **93**, 1801 (2008).

[52] J. Chiquet, N. Limnios, and M. Eid. Piecewise deterministic Markov processes applied to fatigue crack growth modelling. *J. Stat. Plan. Inf.* **139**, 1657 (2009).

[53] A. Lorton, M. Fouladirad, and A. Grall. A methodology for probabilistic model-based prognosis. *Eur. J. Oper. Res.* **225**, 443 (2013).

[54] H. Zhang, F. Dufour, Y. Dutuit, and K. Gonzalez. Piecewise deterministic Markov processes and dynamic reliability. *Proc. Inst. Mech. Eng., Part O: J. Risk and Reliab.* **222**, 545 (2008).

[55] A. Lorton, M. Fouladirad, and A. Grall. Computation of remaining useful life on a physic-based model and impact of a prognosis on the maintenance process. *Proc. Inst. Mech. Eng., Part O: J. Risk and Reliab* **227**, 434 (2013).

[56] A. J. McKane and T. J. Newman. Predator-prey cycles from resonant amplification of demographic stochasticity. *Phys. Rev. Lett.* **94**, 218102 (2005).

[57] D. Alonso, A. J. McKane, and M. Pascual. Stochastic amplification in epidemics. *J. Royal Soc. Interface* **4**, 575 (2007).

[58] R. P. Boland, T. Galla, and A. J. McKane. Limit cycles, complex Floquet multipliers, and intrinsic noise. *Phys. Rev. E* **79**, 051131 (2009).

[59] W. Horsthemke. Noise induced transitions. In *Non-Equilibrium Dynamics in Chemical Systems*, pages 150–160. Springer, New York NY (1984).

[60] C. W. Gardiner. *Handbook of Stochastic Methods*. Springer-Verlag, Berlin (2004).

[61] N. G. van Kampen. *Stochastic Processes in Physics and Chemistry*. North-Holland, Amsterdam (2007).

[62] H. Risken. *The Fokker–Planck Equation: Methods of Solution and Applications*. Springer-Verlag, Berlin (1989).

[63] G. B. Arfken, H. J. Weber, and F. E. Harris. *Mathematical methods for physicists: a comprehensive guide*. Academic Press, Cambridge MA (2011).

[64] B. Munsky and M. Khammash. The finite state projection algorithm for the solution of the chemical master equation. *J. Chem. Phys* **124**, 044104 (2006).

[65] N. Kumar, T. Platini, and R. V. Kulkarni. Exact distributions for stochastic gene expression models with bursting and feedback. *Phys. Rev. Lett.* **113**, 268105 (2014).

[66] R. Grima, D. Schmidt, and T. Newman. Steady-state fluctuations of a genetic feedback loop: An exact solution. *J. Chem. Phys.* **137**, 035104 (2012).

[67] J. Peccoud and B. Ycart. Markovian modeling of gene-product synthesis. *Theor. Popul Biol.* **48**, 222 (1995).

[68] J. Hornos, D. Schultz, G. Innocentini, J. Wang, A. Walczak, J. Onuchic, and P. Wolynes. Self-regulating gene: an exact solution. *Phys. Rev. E* **72**, 051907 (2005).

[69] V. Shahrezaei and P. S. Swain. Analytical distributions for stochastic gene expression. *Proc. Natl. Acad. Sci. U.S.A.* **105**, 17256 (2008).

[70] D. T. Gillespie. A general method for numerically simulating the stochastic time evolution of coupled chemical reactions. *J. Comput. Phys.* **22**, 403 (1976).

[71] D. T. Gillespie. Exact stochastic simulation of coupled chemical reactions. *J. Phys. Chem.* **81**, 2340 (1977).

[72] D. F. Anderson. A modified next reaction method for simulating chemical systems with time dependent propensities and delays. *J. Chem. Phys.* **127**, 214107 (2007).

[73] M. Boguná, L. F. Lafuerza, R. Toral, and M. Á. Serrano. Simulating non-Markovian stochastic processes. *Phys. Rev. E* **90**, 042108 (2014).

[74] M. A. Gibson and J. Bruck. Efficient exact stochastic simulation of chemical systems with many species and many channels. *J. Phys. Chem. A* **104**, 1876 (2000).

[75] H. A. Kramers. Brownian motion in a field of force and the diffusion model of chemical reactions. *Physica* **7**, 284 (1940).

[76] J. Moyal. Stochastic processes and statistical physics. *J R Stat Soc Series B Stat Methodol.* **11**, 150 (1949).

[77] A. J. Lotka. Undamped oscillations derived from the law of mass action. *J. Am. Chem. Soc.* **42**, 1595 (1920).

[78] E. Wallace, D. Gillespie, K. Sanft, and L. Petzold. Linear noise approximation is valid over limited times for any chemical system that is sufficiently large. *IET Syst. Biol.* **6**, 102 (2012).

[79] T. Biancalani, L. Dyson, and A. J. McKane. Noise-induced bistable states and their mean switching time in foraging colonies. *Phys. Rev. Lett.* **112**, 038101 (2014).

[80] D. Talay. Numerical solution of stochastic differential equations (1994).

[81] A. Duncan, S. Liao, T. Vejchodskỳ, R. Erban, and R. Grima. Noise-induced multistability in chemical systems: Discrete versus continuum modeling. *Phys. Rev. E* **91**, 042111 (2015).

[82] M. H. Davis. Piecewise-deterministic Markov processes: A general class of non-diffusion stochastic models. *J. Roy. Statist. Soc. Ser. B* **46**, 353 (1984).

[83] P. Embrechts and H. Schmidli. Ruin estimation for a general insurance risk model. *Advances in applied probability* pages 404–422 (1994).

[84] S. Zeiser, U. Franz, and V. Liebscher. Autocatalytic genetic networks modeled by piecewise-deterministic Markov processes. *J. Math. Biol.* **60**, 207 (2010).

[85] S. Zeiser, U. Franz, O. Wittich, and V. Liebscher. Simulation of genetic networks modelled by piecewise deterministic Markov processes. *IET Syst. Biol.* **2**, 113 (2008).

[86] H. Ge, H. Qian, and X. S. Xie. Stochastic phenotype transition of a single cell in an intermediate region of gene state switching. *Phys. Rev. Lett.* **114**, 078101 (2015).

[87] P. C. Bressloff. Stochastic switching in biology: from genotype to phenotype. *J. Phys. A* **50**, 133001 (2017).

[88] Y. T. Lin and T. Galla. Bursting noise in gene expression dynamics: linking microscopic and mesoscopic models. *J. R. Soc. Interface* **13**, 20150772 (2016).

[89] I. Bena. Dichotomous Markov noise: exact results for out-of-equilibrium systems. *Int. J. Mod. Phys. B* **20**, 2825 (2006).

[90] J. Bowen, A. Acrivos, and A. Oppenheim. Singular perturbation refinement to quasi-steady state approximation in chemical kinetics. *Chem. Eng. Sci.* **18**, 177 (1963).

[91] L. A. Segel and M. Slemrod. The quasi-steady-state assumption: a case study in perturbation. *SIAM Rev.* **31**, 446 (1989).

[92] E. L. Haseltine and J. B. Rawlings. Approximate simulation of coupled fast and slow reactions for stochastic chemical kinetics. *J. Chem. Phys.* **117**, 6959 (2002).

[93] C. V. Rao and A. P. Arkin. Stochastic chemical kinetics and the quasi-steady-state assumption: application to the Gillespie algorithm. *J. Chem. Phys.* **118**, 4999 (2003).

[94] J. Goutsias. Quasiequilibrium approximation of fast reaction kinetics in stochastic biochemical systems. *J. Chem. Phys.* **122**, 184102 (2005).

[95] H. Qian, P.-Z. Shi, and J. Xing. Stochastic bifurcation, slow fluctuations, and bistability as an origin of biochemical complexity. *Phys. Chem. Chem. Phys.* **11**, 4861 (2009).

[96] C. D. Pahlajani, P. J. Atzberger, and M. Khammash. Stochastic reduction method for biological chemical kinetics using time-scale separation. *J. Theor. Biol.* **272**, 96 (2011).

[97] J. Kim, K. Josic, and M. R. Bennett. The Validity of Quasi-Steady-State Approximations in Discrete Stochastic Simulations. *Biophys. J.* **107**, 783 (2014).

[98] A. M. Walczak, J. N. Onuchic, and P. G. Wolynes. Absolute rate theories of epigenetic stability. *Proc. Natl. Acad. Sci. U.S.A.* **102**, 18926 (2005).

[99] X. Mao and C. Yuan. *Stochastic Differential Equations with Markovian Switching.* Imperial College Press, London (2006).

[100] D. A. Potoyan and P. G. Wolynes. Dichotomous noise models of gene switches. *J. Chem. Phys.* **143**, 195101 (2015).

[101] P. G. Hufton, Y. T. Lin, T. Galla, and A. J. McKane. Intrinsic noise in systems with switching environments. *Phys. Rev. E* **93**, 052119 (2016).

[102] C. Jia. Simplification of Markov chains with infinite state space and the mathematical theory of random gene expression bursts. *Phys. Rev. E* **96**, 032402 (2017).

[103] C. Jia, M. Q. Zhang, and H. Qian. Emergent Lévy behavior in single-cell stochastic gene expression. *Phys. Rev. E* **96**, 040402 (2017).

[104] U. Herbach, A. Bonnaffoux, T. Espinasse, and O. Gandrillon. Inferring gene regulatory networks from single-cell data: a mechanistic approach. *arXiv preprint arXiv:1705.03407* (2017).

[105] Y. T. Lin, P. G. Hufton, E. J. Lee, and D. A. Potoyan. A stochastic and dynamical view of pluripotency in mouse embryonic stem cells. *PLOS Comp. Biol.* **14**, 1 (2018).

[106] Y. T. Lin and N. E. Buchler. Efficient analysis of stochastic gene dynamics in the non-adiabatic regime using piecewise deterministic Markov processes. *J. Roy. Soc. Interface* **15** (2018).

[107] P. G. Hufton, Y. T. Lin, and T. Galla. Model reduction methods for classical stochastic systems with fast-switching environments: reduced master equations, stochastic differential equations, and applications. *arXiv preprint arXiv:1803.02941* (2018).

[108] J. M. Newby and P. C. Bressloff. Quasi-steady State Reduction of Molecular Motor-Based Models of Directed Intermittent Search. *Bull. Math. Biol.* **72**, 1840 (2010).

[109] P. C. Bressloff and J. M. Newby. Path integrals and large deviations in stochastic hybrid systems. *Phys. Rev. E* **89** (2014).

[110] P. C. Bressloff. Stochastic Liouville equation for particles driven by dichotomous environmental noise. *Phy. Rev. E* **95**, 012124 (2017).

[111] P. C. Bressloff. Feynman-Kac formula for stochastic hybrid systems. *Phys. Rev. E* **95**, 012138 (2017).

[112] C. Wiuff, R. Zappala, R. Regoes, K. Garner, F. Baquero, and B. Levin. Phenotypic tolerance: antibiotic enrichment of noninherited resistance in bacterial populations. *Antimicrob. Agents Chemother.* **49**, 1483 (2005).

[113] B. R. Levin and D. E. Rozen. Non-inherited antibiotic resistance. *Nature Rev. Microbiol.* **4**, 556 (2006).

[114] W. K. Smits, O. P. Kuipers, and J.-W. Veening. Phenotypic variation in bacteria: the role of feedback regulation. *Nature Rev. Microbiol.* **4**, 259 (2006).

[115] M. Leisner, K. Stingl, E. Frey, and B. Maier. Stochastic switching to competence. *Curr. Opin. Microbiol.* **11**, 553 (2008).

[116] P. J. Choi, L. Cai, K. Frieda, and X. S. Xie. A stochastic single-molecule event triggers phenotype switching of a bacterial cell. *Science* **322**, 442 (2008).

[117] B. Hallet. Playing Dr Jekyll and Mr Hyde: combined mechanisms of phase variation in bacteria. *Curr. Opin. Microbiol.* **4**, 570 (2001).

[118] P. Patra and S. Klumpp. Emergence of phenotype switching through continuous and discontinuous evolutionary transitions. *Phys. Biol.* **12**, 046004 (2015).

[119] M. K. Belete and G. Balázsi. Optimality and adaptation of phenotypically switching cells in fluctuating environments. *Phys. Rev. E* **92**, 062716 (2015).

[120] M. Lachmann and E. Jablonka. The inheritance of phenotypes: an adaptation to fluctuating environments. *J. Theor. Biol.* **181**, 1 (1996).

[121] M. Acar, J. T. Mettetal, and A. van Oudenaarden. Stochastic switching as a survival strategy in fluctuating environments. *Nature Genet.* **40**, 471 (2008).

[122] S. Leibler and E. Kussell. Individual histories and selection in heterogeneous populations. *Proc. Natl. Acad. Sci. U.S.A.* **107**, 13183 (2010).

[123] B. Gaál, J. W. Pitchford, and A. J. Wood. Exact results for the evolution of stochastic switching in variable asymmetric environments. *Genetics* **184**, 1113 (2010).

[124] I. Lohmar and B. Meerson. Switching between phenotypes and population extinction. *Phys. Rev. E* **84**, 051901 (2011).

[125] P. Patra and S. Klumpp. Population dynamics of bacterial persistence. *PLoS One* **8**, e62814 (2013).

[126] R. Levins. *Evolution in Changing environments: some Theoretical Explorations.* Princeton University Press, Princeton NJ (1968).

[127] P. Haccou and Y. Iwasa. Optimal mixed strategies in stochastic environments. *Theor. Popul. Biol.* **47**, 212 (1995).

[128] M. J. Gander, C. Mazza, and H. Rummler. Stochastic gene expression in switching environments. *J. Math. Biol.* **55**, 249 (2007).

[129] P. Visco, R. J. Allen, S. N. Majumdar, and M. R. Evans. Switching and growth for microbial populations in catastrophic responsive environments. *Biophys. J* **98**, 1099 (2010).

[130] D. Horvath and B. Brutovsky. Study of selected phenotype switching strategies in time varying environment. *Phys. Lett. A* **380**, 1267 (2016).

[131] M. Evans. Discovering pluripotency: 30 years of mouse embryonic stem cells. *Nat. Rev. Mol. Cell. Biol.* **12**, 680 (2011).

[132] C. E. Murry and G. Keller. Differentiation of embryonic stem cells to clinically relevant populations: lessons from embryonic development. *Cell* **132**, 661 (2008).

[133] G. Martello and A. Smith. The nature of embryonic stem cells. *Ann. Rev. Cell. Dev. Biol.* **30**, 647 (2014).

[134] S.-J. Dunn, G. Martello, B. Yordanov, S. Emmott, and A. Smith. Defining an essential transcription factor program for naive pluripotency. *Science* **344**, 1156 (2014).

[135] N. Friedman, L. Cai, and X. S. Xie. Linking Stochastic Dynamics to Population Distribution: An Analytical Framework of Gene Expression. *Phys. Rev. Lett.* **97**, 168302 (2006).

[136] H.-P. Breuer, E.-M. Laine, J. Piilo, and B. Vacchini. Colloquium: Non-Markovian dynamics in open quantum systems. *Rev. Mod. Phys.* **88**, 021002 (2016).

[137] H.-P. Breuer and J. Piilo. Stochastic jump processes for non-Markovian quantum dynamics. *EPL* **85**, 50004 (2009).

[138] J. Piilo, S. Maniscalco, K. Härkönen, and K.-A. Suominen. Non-Markovian Quantum Jumps. *Phys. Rev. Lett.* **100**, 180402 (2008).

[139] E. Martinez, A. Daidone, C. Gutierrez, J. Pera, A. Boladeras, F. Ferrer, F. Pino, J. F. Suarez, A. Polo, and F. Guedea. Permanent seed brachytherapy for clinically localized prostate cancer: Long-term outcomes in a 700 patient cohort. *Brachytherapy* **14**, 166 (2015).

[140] N. Tanaka, I. Asakawa, M. Hasegawa, and K. Fujimoto. Urethral toxicity after LDR brachytherapy: experience in Japan. *Brachytherapy* **14**, 131 (2015).

[141] J.-C. Horiot, P. Bontemps, W. Van den Bogaert, R. Le Fur, D. van den Weijngaert, M. Bolla, J. Bernier, A. Lusinchi, M. Stuschke, J. Lopez-Torrecilla, *et al.* Accelerated fractionation (AF) compared to conventional fractionation

(CF) improves loco-regional control in the radiotherapy of advanced head and neck cancers: results of the EORTC 22851 randomized trial. *Radiother. Oncol.* **44**, 111 (1997).

[142] J. T. Lyman. Complication Probability as Assessed from Dose-Volume Histograms. *Radiat. Res.* **104**, S13 (1985).

[143] A. Niemierko and M. Goitein. Modeling of normal tissue response to radiation: the critical volume model. *Int. J. Radiat. Oncol. Biol. Phys.* **25**, 135 (1993).

[144] L. Hanin and M. Zaider. A mechanistic description of radiation-induced damage to normal tissue and its healing kinetics. *Phys. Med. Biol.* **58**, 825 (2013).

[145] T. Stocks, T. Hillen, J. Gong, and M. Burger. A stochastic model for the normal tissue complication probability (NTCP) and applications. *Math. Med. Biol.* **34**, 469 (2017).

[146] S. Redner. *A guide to first-passage processes.* Cambridge University Press, Cambridge (2001).

[147] M. Zaider and G. Minerbo. Tumour control probability: a formulation applicable to any temporal protocol of dose delivery. *Phys. Med. Biol.* **45**, 279 (2000).

[148] P. G. Hufton, Y. T. Lin, and T. Galla. Phenotypic switching of populations of cells in a stochastic environment. *J. Stat. Mech. Theory Exp.* **2018**, 023501 (2018).

[149] Y. T. Lin, P. G. Hufton, E. J. Lee, and D. A. Potoyan. A stochastic and dynamical view of pluripotency in mouse embryonic stem cells. *PLoS Comput Biol.* **14**, e1006000 (2018).

[150] P. G. Hufton, E. Buckingham-Jeffery, and T. Galla. Calculating normal tissue complication probabilities and probabilities of complication-free tumour control from stochastic models of population dynamics. *arXiv preprint arXiv:1803.08595* (2018).

Chapter 2

Intrinsic noise in systems with switching environments

2.1 Preface

The contents of this chapter were previously published in a paper in Physical Review E in volume 95, page 052119 in 2016 [1], which was authored by Peter G. Hufton[1], Yen Ting Lin[1], and Tobias Galla[1].

P.G.H.'s contribution includes developing the idea for the project, performing all calculations and analysis therein, coding and executing all simulations, producing all data and all figures, writing all sections of the paper, and responding to the reports of referees.

[1]Theoretical Physics, School of Physics and Astronomy, The University of Manchester, Manchester M13 9PL, United Kingdom

Abstract

We study individual-based dynamics in finite populations, subject to randomly switching environmental conditions. These are inspired by models in which genes transition between on and off states, regulating underlying protein dynamics. Similarly switches between environmental states are relevant in bacterial populations and in models of epidemic spread. Existing piecewise-deterministic Markov process (PDMP) approaches focus on the deterministic limit of the population dynamics while retaining the randomness of the switching. Here we go beyond this approximation and explicitly include effects of intrinsic stochasticity at the level of the linear-noise approximation. Specifically we derive the stationary distributions of a number of model systems, in good agreement with simulations. This improves existing approaches which are limited to the regimes of fast and slow switching.

2.2 Introduction

There is now a broad consensus that noise plays a crucial role in most dynamical systems in biology, chemistry and in the social sciences. The theory with which to describe these stochastic processes is well established and has its roots in statistical physics. Modelling tools such as master equations, Fokker–Planck equations, and Langevin dynamics are standard and can be found in a number of textbooks [2–4]. Much of this work focuses on processes between discrete interacting individuals, which can be members of a population in epidemiology [5–7], atoms or molecules in chemical reaction systems [8, 9], or proteins in the context of gene regulatory networks [10, 11]. Many of these models are Markovian and their natural description is in terms of a master equation which describes the time evolution of the underlying probability distribution of microstates.

Solving the master equation analytically is often a difficult task: only very simple linear model dynamics allow further treatment [2–4, 12, 13]. It is therefore common to employ approximation techniques, most notably ones built around the assumption that the size of the population is large, but finite. The inverse system size (or its square

root) then serves as a small parameter in which an expansion can be performed. The lowest order in this expansion corresponds to the limit of infinite systems, and provides a deterministic description devoid of stochasticity. The second-order term in the expansion introduces some stochastic effects of noise in the population, but approximates the individual-level dynamics by a simpler Gaussian process on a continuum domain [14]. These techniques have been very successful in capturing elements of noise-induced phenomena, for example the weak selection of competing species [15–19], cyclic behaviour, patterns and waves [20–22]. The main techniques used to characterise these effects are system-size expansion methods, most notably the Kramers–Moyal and van Kampen expansions. The latter is also known as the linear-noise approximation (LNA) [2, 3].

These methods are now used routinely for the analysis of individual-based models with intrinsic noise in the weak-noise limit. Most applications so far focus on systems in which the reaction rates are set by constant model parameters, and the only time dependence is in the evolution of the population of individuals itself. Recently, exceptions have gained attention [7, 23–27]. In these models, reaction rates vary continuously and deterministically in time, for example to capture periodically varying infection rates to model seasonal variation in epidemic spreading. Crucially, no additional stochasticity is introduced in these dynamics by the environment, and the only discreteness in the dynamics is in the evolution of a finite population of individuals. Other authors have considered models with an environment which varies stochastically and continuously [28–30].

For many model systems it is more realistic to assume that model parameters switch between different discrete states. This includes phases of antibiotic treatment in the context of bacteria [31, 32], genetic switches [10, 33–39], evolutionary game theory [40] and predator-prey models in switching environmental conditions [41, 42]. Such models describe two types of discreteness: that of the state of the environment and that of the population of interacting individuals. In principle, the environmental switching can occur stochastically or follow a deterministic pattern (e.g., prescribed periods of antibiotic treatment, regularly interspersed with periods of no antibiosis).

In the present work we focus on stochastically switching environments. Assuming again a large, but finite population, the demographic noise in the population can be

approximated using the above expansion techniques. The noise relating to switches in the environmental state, however, cannot be dealt with in this way: there is no large parameter to expand in when the number of environmental states is small.

In models with switching environments the lowest-order expansion in the strength of the intrinsic noise leads to a so-called 'piecewise-deterministic Markov process' (PDMP) [43,44]. In this approximation the dynamics of the population of individuals is described by deterministic rate equations between stochastic switches of the environment. This approach neglects all intrinsic stochasticity from the reaction dynamics *within* the population—the population scale is taken to be infinite. The only type of randomness retained is that of the switching of the environmental states. The application of PDMPs has recently gained attention in the description of genetic networks [33,45,46].

The PDMP approximation has been surprisingly effective in modeling systems with very large populations [33,46,47]; however, it does not produce accurate results outside this limit. Recently, an alternative approach has incorporated some effects of demographic noise, but it is only valid if there is a very large separation between the time scales of environmental switching and that of the population dynamics [38,39]. Here, we develop the theory further and construct a systematic expansion in the noise strength about the PDMP.

The remainder of this paper is organised as follows: In Section 2.3 we give a more formal introduction to the problem using a relatively simple linear model. We show how the system-size expansion can be applied in the presence of switching environments and we analytically derive the resulting stationary distribution for the linear model. In Section 2.4 we construct a more general theory and describe how the method can be applied to a larger set of model dynamics. Section 2.5 contains applications to a number of model systems with nonlinear reaction rates and/or other additional features. In Sec. 2.6 we summarise our findings and give an outlook on future work. The Appendix contains further details of the relevant calculations.

2.3 Introductory example

2.3.1 Model definition

We first focus on a simple example with linear reaction rates. We consider a population of individuals of type $\mathcal{P}$, and we write n for the number of individuals in the population at a given time. Individuals can be created and they can decay, so that the model describes a birth-death process. The death rate per individual is assumed to be a constant d. The creation rate is taken to depend on the state of the external environment; individuals are born with rate Ωb_σ, where σ represents the state of the environment. This can be summarised as follows:

$$\begin{aligned} \varnothing &\xrightarrow{\Omega b_\sigma} \mathcal{P}, \\ \mathcal{P} &\xrightarrow{d} \varnothing, \end{aligned} \tag{2.1}$$

for times at which the environment is in state σ. The parameter Ω has been introduced as per normal convention to set a typical scale of the population size [2, 3]. If the environment were to be fixed at σ the number of individuals in the system would fluctuate around the value $\Omega b_\sigma/d$ in the long run. These fluctuations can be expected to be of order $\Omega^{1/2}$ and reflect the demographic stochasticity.

At any given time, the state of the full system is completely described by the state σ of the environment and the number of individuals in the population n. We restrict ourselves to cases in which the environment has two states, $\sigma \in \{0, 1\}$. The switching between these states is assumed to be independent of the state of the population n and it occurs with constant rates. We write λ_1 for the rate of switching from state 0 to state 1, and λ_0 for the rate of switching from state 1 to state 0.

This stylised model can be interpreted in the context of genetic networks as follows [10]. The two states of the environment, often labelled as $\mathcal{G}_0$ and $\mathcal{G}_1$, correspond to regimes in which a certain promoter—a region on DNA which initiates transcription—is either inactive ($\mathcal{G}_0$) or activated ($\mathcal{G}_1$). A protein ($\mathcal{P}$) is produced with rates b_0 and b_1 in the corresponding state. Independently of the state of the gene, proteins degrade at a constant rate d. This simple model has been studied for example in

Refs. [10, 38, 39, 46, 48], and it can be written in the form

$$\begin{aligned} \mathcal{G}_0 &\xrightarrow{\Omega b_0} \mathcal{G}_0 + \mathcal{P}, \\ \mathcal{G}_1 &\xrightarrow{\Omega b_1} \mathcal{G}_1 + \mathcal{P}, \\ \mathcal{G}_0 &\xrightarrow{\lambda_1} \mathcal{G}_1, \\ \mathcal{G}_1 &\xrightarrow{\lambda_0} \mathcal{G}_0, \\ \mathcal{P} &\xrightarrow{d} \varnothing. \end{aligned} \tag{2.2}$$

The reaction rates of this model are linear in n. It is possible to develop exact solutions to linear models of this type using a generating-function approach [12, 13, 48–51]. However, such solutions are often limited to simple model systems and frequently they only provide limited insight into the actual physical dynamics. We use this linear model to introduce our approximation method. In later sections we will then apply this approach to cases with nonlinear reaction rates, where an exact solution is no longer feasible.

2.3.2 Simulation of results and general behaviour

To illustrate the general behaviour of the model, we first show the outcome of a set of characteristic simulations in Fig. 2.1. Panels (a, c, e) depict individual simulation runs. In each of these panels a trajectory of the population density $x(t) = n(t)/\Omega$ is shown as a solid line, and the switching of the environmental states is indicated by the shading of the background. Panel (a) shows an example of relatively slow switching. In each environmental state, the population tends to a fixed point, $\phi^*_\sigma = b_\sigma/d$, specific to the environment. It then fluctuates about this fixed point. The stationary distribution (b) is bimodal. As the switching rate is increased, panels (c) and (d), the stochastic dynamics spends more time in between the two fixed points and the bimodality of the stationary distribution is lost; we observe a nearly flat distribution between the two fixed points. At very fast switching, panels (e) and (f), the stationary distribution becomes unimodal, peaked at a value between the two fixed points. The system spends most of its time fluctuating about a point in the interior of phase space, away from either of the two fixed points.

We set out to characterise this behaviour analytically, and our aim is to approximate the stationary outcome of the dynamics. We will develop a general approximation

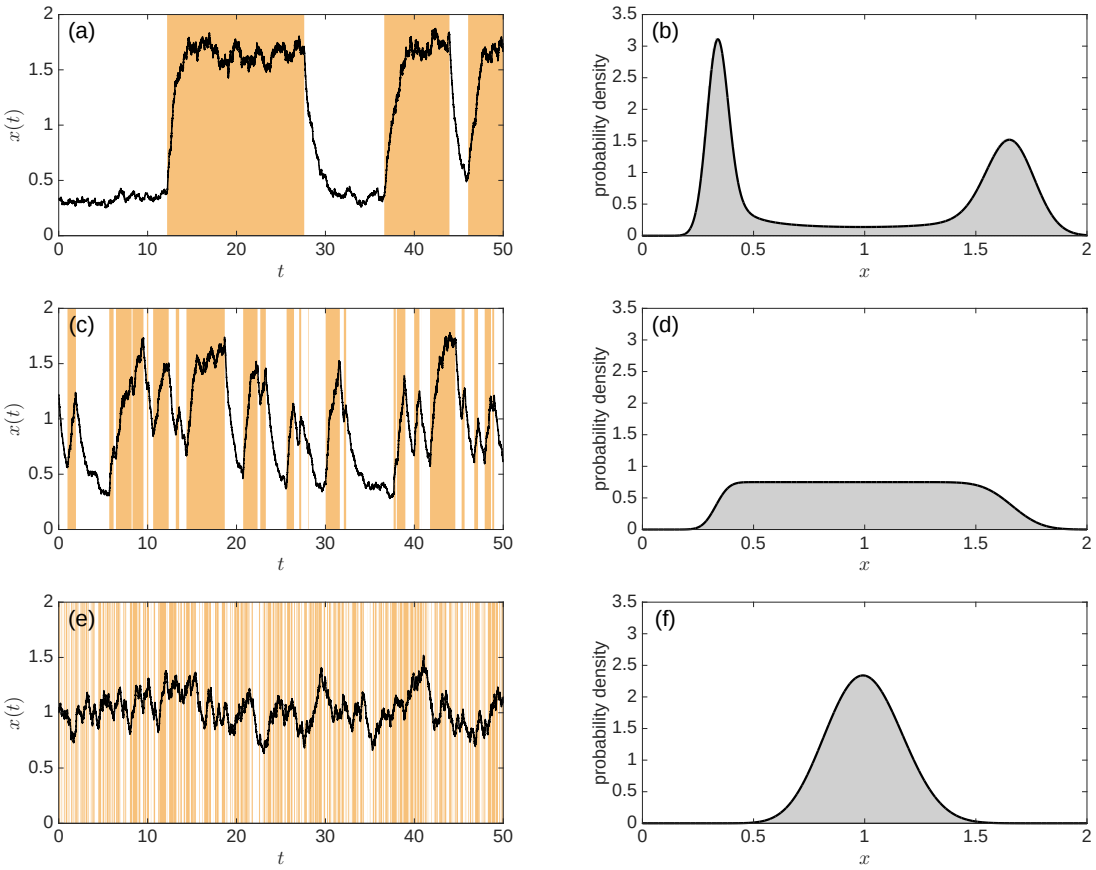

Figure 2.1: Sample paths of the dynamics and the stationary distribution of the linear birth-death process described by Eq. (2.2). Panels (a) and (b) show the regime of slow environmental switching ($\lambda_1 = \lambda_0 = 0.1$), panels (c) and (d) show intermediate environmental switching ($\lambda_1 = \lambda_0 = 1$), and (e) and (f) show fast environmental switching ($\lambda_1 = \lambda_0 = 10$). Panels (a, c, e) show individual trajectories (solid line) and the state of the environment (shaded background). Panels (b, d, f) on the right show the stationary distribution from simulations, averaged over multiple runs (histogram). We also plot the theoretical prediction for the stationary distribution $\Pi^*(x)$ obtained from Eqs. (2.16), shown as solid lines for the three scenarios. The trajectories and stationary distributions have been obtained by application of the Gillespie algorithm [52, 53]. Model parameters are $b_0 = 1/3$, $b_1 = 5/3$, $d = 1$ and $\Omega = 150$.

technique, which is applicable to a wider class of models, in the next section. Before we do this, it is useful to outline our approach and to describe the main steps of the analysis in the simple model defined in Eqs. (2.2).

2.3.3 Master equation

We write $n(t)$ for the number of individuals at time t, and $\sigma(t)$ for the state of the environment. These follow random-jump Markov processes [3]. We write $P(n, \sigma, t)$ for the probability to find the system and environment in state (n, σ) at time t. We will frequently suppress the explicit time dependence to keep the notation compact.

The master equation governing the time evolution of this distribution can then be written as

$$\begin{aligned} \frac{\mathrm{d}}{\mathrm{d}t}P(n,0) &= \mathcal{M}_0 P(n,0) - \lambda_1 P(n,0) + \lambda_0 P(n,1), \\ \frac{\mathrm{d}}{\mathrm{d}t}P(n,1) &= \mathcal{M}_1 P(n,1) + \lambda_1 P(n,0) - \lambda_0 P(n,1). \end{aligned} \tag{2.3}$$

These equations consist of two components. The operators $\mathcal{M}_0$ and $\mathcal{M}_1$ characterise the creation and removal of individuals assuming a fixed state of the environment. They are given by

$$\mathcal{M}_\sigma = \Omega b_\sigma \left(\mathcal{E}^{-1} - 1\right) + d\left(\mathcal{E} - 1\right) n, \tag{2.4}$$

where $\mathcal{E}$ is the shift operator [2]: $\mathcal{E}f(n) = f(n+1)$. It is important to note that operators, such as $\mathcal{E}$ or $\mathcal{M}_\sigma$, act on everything that follows to their right throughout our paper, e.g., $\mathcal{E}nf(n) = (n+1)f(n+1)$. The latter two terms in the master equation describe the switching between the two environmental states.

The master equation (2.3) describes the time evolution of the full process, and in our analysis, we wish to calculate the joint stationary distribution of the number of individuals n and environmental state σ, $P^*(n, \sigma)$.

2.3.4 Approximation of the master equation

We now proceed to approximate the above master equation. To this end, it is useful to define the population density $x(t) = n(t)/\Omega$. Assuming that the typical system size Ω is large but finite, the operators, $\mathcal{M}_0$ and $\mathcal{M}_1$, can be approximated by a Taylor

expansion in powers of small parameter Ω^{-1},

$$\mathcal{M}_\sigma \approx \mathcal{L}_\sigma = -\partial_x(b_\sigma - xd) + \frac{1}{2\Omega}\partial_x^2(b_\sigma + xd). \tag{2.5}$$

This is the Kramers–Moyal expansion [2, 3] in terms of the variable $x = n/\Omega$, while keeping the state of the environment, σ, discrete. We write $\mathcal{L}_\sigma$ for the operators obtained from this expansion, retaining only leading and sub-leading orders in Ω^{-1}. The state of the system is now expressed in terms of x and σ, and we will write $\Pi(x, \sigma)$ for the resulting probability density. The explicit time-dependence is again suppressed in this notation.

Substituting this into the master equation (2.3) allows us to approximate the process by

$$\begin{aligned} \partial_t\Pi(x,0) &= \mathcal{L}_0\Pi(x,0) - \lambda_1\Pi(x,0) + \lambda_0\Pi(x,1), \\ \partial_t\Pi(x,1) &= \mathcal{L}_1\Pi(x,1) + \lambda_1\Pi(x,0) - \lambda_0\Pi(x,1). \end{aligned} \tag{2.6}$$

This expansion differs from the standard Kramers–Moyal expansion in that the environmental states are not included in the expansion. Equation (2.6) accordingly is not a standard Fokker–Planck equation; it retains the discrete switching terms, akin to terms in the master equation of a conventional telegraph process. Equations (2.6) describe a diffusion process with a Markovian switching in between two sets of drift and diffusion [54, 55], which we refer to as a piecewise-diffusive process.

Since Eqs. (2.6) contain multiplicative noise, it is difficult to solve these equations directly. In the following sections, we propose an approximation method to analyse these dynamics. Our approach is similar to the conventional linear-noise approximation, and describes the effects of intrinsic noise to sub-leading order.

2.3.5 Leading-order approximation: piecewise-deterministic Markov process

In the above expansion we have retained leading and sub-leading terms in Ω^{-1}. To proceed, it is useful to first consider the leading-order terms only, i.e., to study the limit $\Omega \to \infty$. We obtain

$$\begin{aligned} \partial_t\Pi(\phi,0) &= -\partial_\phi(b_0 - d\phi)\Pi(\phi,0) - \lambda_1\Pi(\phi,0) + \lambda_0\Pi(\phi,1), \\ \partial_t\Pi(\phi,1) &= -\partial_\phi(b_1 - d\phi)\Pi(\phi,1) + \lambda_1\Pi(\phi,0) - \lambda_0\Pi(\phi,1), \end{aligned} \tag{2.7}$$

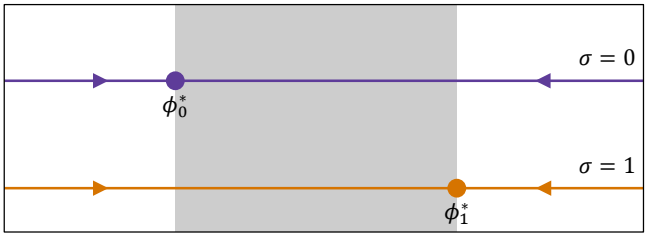

Figure 2.2: Illustration of the Liouville flow of the model described by Eq. (2.7). Arrows indicate the Liouville flow in each of the two environments, stable fixed points are shown as filled circles. The PDMP converges into the interval between the two fixed points (shaded region) at long times.

where we have written $\phi = \lim_{\Omega\to\infty} n/\Omega$ to indicate that we have taken the limit of infinite populations. In this limit operators $\mathcal{L}_\sigma$ are Liouville operators describing deterministic flow of ϕ. The functional form of this flow at any one time is entirely determined by the state of the environment, σ. The process $\phi(t)$ is a piecewise deterministic Markov process [43, 44, 54, 56], a random process composed of deterministic motion in between the discrete environmental transitions. The PDMP is a description of the system which accounts for the stochasticity of the switching only; the demographic noise on the other hand is neglected in the above truncation after the leading-order term.

The long-term behaviour of the system can be determined from inspection of the Liouville operators. In each state σ the process tends towards a stable fixed point, $\phi_\sigma^* = b_\sigma/d$. In the following, we assume that $b_0 < b_1$ so that $\phi_0^* < \phi_1^*$. The dynamics can be illustrated by the flow diagram in Fig. 2.2. When the environment is in state 0 the trajectory of the PDMP moves towards ϕ_0^*, and when the environment switches the direction is reversed towards ϕ_1^*. In the long-run, the PDMP will always take values in the interval between the fixed points ϕ_0^* and ϕ_1^*.

The stationary distribution of the PDMP, $\Pi^*(\phi,\sigma)$, can be found by setting the derivatives with respect to time in Eqs. (2.7) to zero, followed by integration and rearrangement. Further details are discussed in a more general setting in the next section. For the linear model defined in Eqs. (2.1) we find

$$\begin{aligned}\Pi^*(\phi,0) &= \mathcal{N}\frac{(\phi-\phi_0^*)^{\frac{\lambda_1}{d}}\,(\phi_1^*-\phi)^{\frac{\lambda_0}{d}}}{\phi-\phi_0^*},\\ \Pi^*(\phi,1) &= \mathcal{N}\frac{(\phi-\phi_0^*)^{\frac{\lambda_1}{d}}\,(\phi_1^*-\phi)^{\frac{\lambda_0}{d}}}{\phi_1^*-\phi},\end{aligned} \tag{2.8}$$

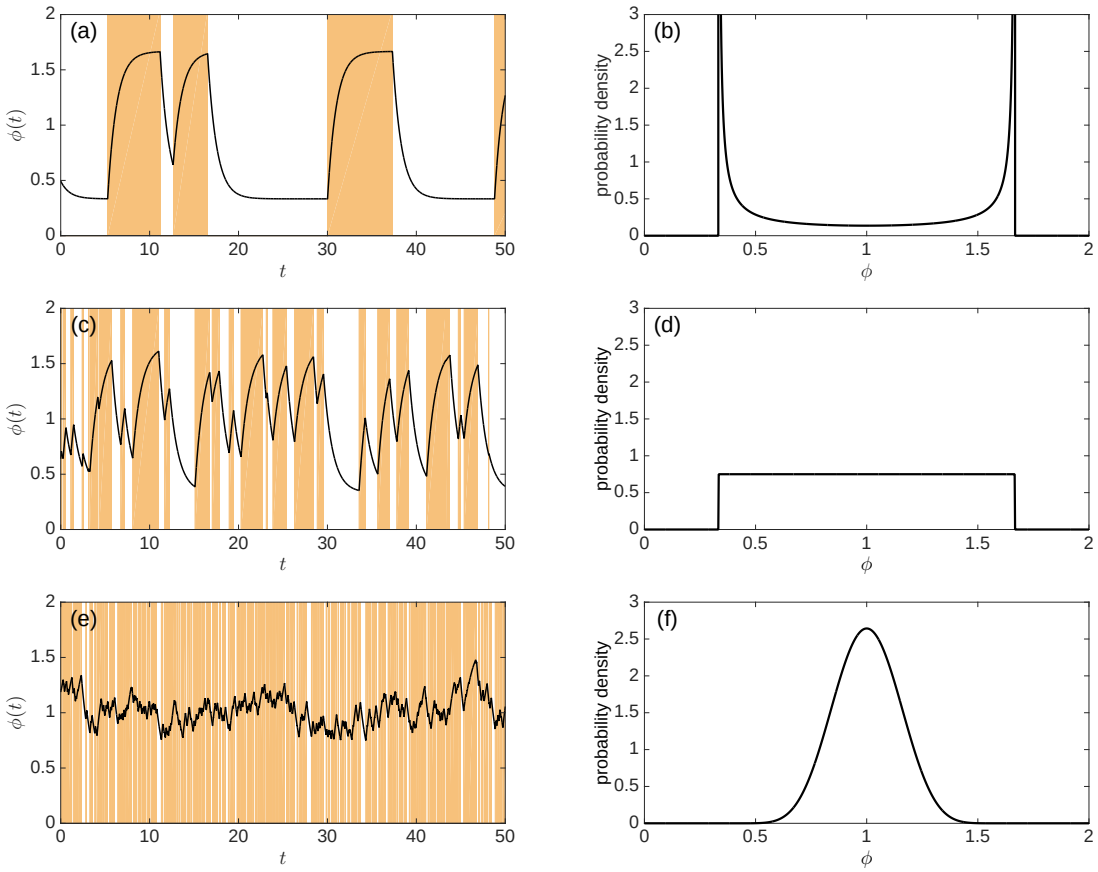

Figure 2.3: Sample paths and stationary distributions of the PDMP for the linear model in infinite populations. Panels (a) and (b) show the regime of slow environmental switching ($\lambda_1 = \lambda_0 = 0.1$), panels (c) and (d) show intermediate environmental switching ($\lambda_1 = \lambda_0 = 1$) and (e) and (f) show fast environmental switching ($\lambda_1 = \lambda_0 = 10$). Panels (a, c, e) show individual trajectories (solid line) and the state of the environment (shaded background). Panels (b, d, f) show the stationary distribution of the PDMP, as obtained from from Eq. (2.8). Comparison with Fig. 2.1 shows that this stationary distribution does not adequately reflect the stationary distribution of the full noisy process in finite populations. The sample paths have been obtained by Runge–Kutta integration of Eq. (2.11) between randomly-generated exponential switching times. Model parameters are $b_0 = 1/3$, $b_1 = 5/3$, $d = 1$ and $\Omega = 150$.

for $\phi \in (\phi_0^*, \phi_1^*)$. The pre-factor $\mathcal{N}$ is a normalisation constant, determined by the condition

$$\int_{\phi_0^*}^{\phi_1^*} [\Pi^*(\phi, 0) + \Pi^*(\phi, 1)] \, \mathrm{d}\phi = 1. \tag{2.9}$$

This result is consistent with those reported by other authors [46, 56, 57].

2.3.6 Comparison against simulations

In Fig. 2.3 we illustrate the behaviour of the PDMP. Panels (a, c, e) show individual time series for slow, medium and fast switching of the environment (parameters are as in Fig. 2.1). Panels (b, d, f) depict the corresponding stationary distributions of the PDMP, as obtained from Eqs. (2.8). For slow switching rates, the marginal stationary distribution $\Pi^*(\phi) = \Pi^*(\phi, 0) + \Pi^*(\phi, 1)$ is bimodal, with singularities at the endpoints. In this regime, the PDMP typically spends enough time in each environment between switches to come close to the corresponding fixed point. For fast switching $\Pi^*(\phi)$ is unimodal. In this situation, the system typically does not have sufficient time to reach the vicinity of the fixed points. An intermediate case is shown in panels (c) and (d). For this particular choice of parameters, the resulting stationary distribution is seen to be flat between the two fixed points, ϕ_0^* and ϕ_1^*.

Comparison of the stationary distributions of the PDMP with those of the process in finite populations (Fig. 2.1) shows that the PDMP approximation recovers some of the qualitative features of the full system, but not all. The transition from a bimodal to a unimodal shape is successfully reproduced. On the other hand, the singularities for slow switching rates seen in the stationary state of the PDMP are not observed in the full process. The PDMP is confined to the interval (ϕ_0^*, ϕ_1^*), while the intrinsic noise in finite populations allows for fluctuations on both sides of ϕ_0^* and ϕ_1^*. Thus the support of the stationary distribution of the model with intrinsic noise includes concentrations below ϕ_0^* and above ϕ_1^*.

These results stress the significance of intrinsic noise for the dynamics of the system. In order to approximate the stationary behaviour to a better accuracy, it is necessary to include higher-order terms in the above Kramers–Moyal expansion. The corresponding formalism is well established for systems without random switches of the environment, and it takes the form of an expansion about the deterministic path of the infinite system

[27]. In our case, the leading-order behaviour (the PDMP) is a stochastic process itself due to the randomness of the environmental switching. The sub-leading description we discuss below is hence an expansion about this random process.

2.3.7 Sub-leading order: linear-noise approximation

Before we present a more detailed account of the expansion to sub-leading order (Section 2.4), we briefly outline the general idea. For a fixed realisation of the environmental switching process, $\sigma(t)$, we decompose the dynamics of the population as follows:

$$x(t) = \phi(t) + \frac{1}{\sqrt{\Omega}}\xi(t). \tag{2.10}$$

This is along the lines of the system-size expansion in systems with time-dependent rates [27, 58]. For a given path of the environment, $\sigma(t)$, the trajectory $\phi(t)$ of the resulting PDMP is given by the solution of

$$\dot{\phi}(t) = b_{\sigma(t)} - d\phi(t), \tag{2.11}$$

where the birth rate $b_{\sigma(t)}$ at time t is determined by the state of the environment at that time, $\sigma(t)$. The dynamics of Eq. (2.11) is the equivalent of the usual rate equations for systems without environmental switching.

To sub-leading order, systems of this form, but without environmental switching, are described by stochastic differential equations of the form

$$\dot{x}(t) = v(x) + \sqrt{\frac{w(x)}{\Omega}}\eta(t), \tag{2.12}$$

where we have suppressed the obvious time dependence of x on the right-hand side. The dependence of the amplitude $w(x)$ on x indicates multiplicative noise, and $\eta(t)$ is Gaussian white noise of unit amplitude, i.e., $\langle \eta(t)\eta(t')\rangle = \delta(t-t')$. The term $v(x)$ represents deterministic drift. In a birth-death process with fixed birth rate b and death rate d one would have $v(x) = b - dx$, for example.

The equivalent of Eq. (2.12) for the model with environmental switching is given by the piecewise-diffusive process:

$$\dot{x}(t) = v_{\sigma(t)}(x) + \sqrt{\frac{w_{\sigma(t)}(x)}{\Omega}}\eta(t). \tag{2.13}$$

Equation (2.13) is similar to the outcome of the procedure described in Refs. [27, 58], where the system-size expansion was carried out for systems with periodically driven rates. The main difference is the fact that $\sigma(t)$ is now a stochastic process itself, whereas the external driving was deterministic in Ref. [27]. In the limit $\Omega \to \infty$ the noise $\eta(t)$ does not contribute, and we recover the PDMP dynamics of Eq. (2.11).

For the case of the linear model described above we have $v_\sigma(x) = b_\sigma - dx$ and $w_\sigma(x) = b_\sigma + dx$. These are the drift term and noise amplitude one would obtain from a standard Kramers–Moyal expansion at fixed environmental state σ.

In the spirit of the usual linear-noise approximation (LNA) we next write $x(t) = \phi(t) + \xi(t)/\sqrt{\Omega}$ and obtain

$$\begin{aligned} \dot{\phi}(t) &= v_{\sigma(t)}(\phi), \\ \dot{\xi}(t) &= v'_{\sigma(t)}(\phi)\xi(t) + \sqrt{w_{\sigma(t)}(\phi)}\eta(t). \end{aligned} \tag{2.14}$$

We have written $v'_\sigma = \mathrm{d}v_\sigma(\phi)/\mathrm{d}\phi$, and we have suppressed the time dependence of ϕ on the right-hand side.

From the LNA it is possible to proceed and to approximate the stationary distribution of the process, $\Pi^*(\xi, \phi, \sigma) = \Pi^*(\xi|\phi, \sigma)\Pi^*(\phi, \sigma)$. The distribution $\Pi^*(\phi, \sigma)$ is the stationary outcome of the PDMP, and it can be computed exactly, see Eqs. (2.8) for the linear birth-death model. The general case is discussed in the following section.

In the stationary regime the distribution of ξ will, in principle, depend on the state σ of the environment and on the variable ϕ. In order to proceed we now assume that the dependence on σ can be neglected, so that we write $\Pi^*(\xi|\phi, \sigma) \approx \Pi^*(\xi|\phi)$. This is an approximation, but it turns out to work well for all models we have tested. Making this assumption we write

$$\Pi^*(\xi, \phi, \sigma) \approx \Pi^*(\xi|\phi)\ \Pi^*(\phi, \sigma). \tag{2.15}$$

The distribution $\Pi^*(\xi|\phi)$ is Gaussian with mean zero, and with a variance which depends on ϕ and which can be obtained analytically as described in the next section. The resulting picture is illustrated in Fig. 2.4. A given realisation of the environmental process generates a realisation of the PDMP. The state of a finite population, subject to the same path of environmental states, will fluctuate about the PDMP trajectory, as indicated by the shading in Fig. 2.4.

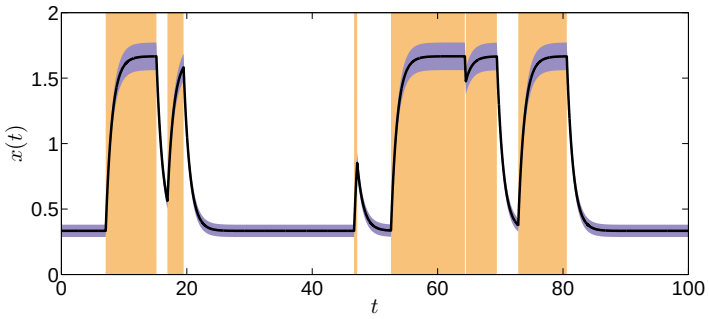

Figure 2.4: Sample path of the PDMP of the linear model ($\phi(t)$, solid line) and environmental state $\sigma(t)$ (background shading). The dynamics in the finite system for the same realisation of the environmental process will deviate from the PDMP. The standard deviation of the deviation is approximated by Eq. (2.36) as discussed below, and shown here as shading around the PDMP trajectory. Parameters are $b_0 = 1/3$, $b_1 = 5/3$, $d = 1$, $\lambda_1 = \lambda_0 = 1$ and $\Omega = 150$.

From these approximations the stationary distribution of $x = \phi + \Omega^{-1/2}\xi$ can then be estimated as

$$\Pi^*(x) = \sum_\sigma \int \mathrm{d}\phi\, \mathrm{d}\xi \left[\Pi^*(\xi|\phi)\Pi^*(\phi,\sigma)\delta(x - \phi - \Omega^{-1/2}\xi)\right]. \tag{2.16}$$

Returning to Fig. 2.1, we compare the stationary distribution of the linear model as obtained from Eq. (2.16) against the results of numerical simulations. The results from the theory are shown as solid lines, and the simulation data as histograms. We find that the approximation reproduces the numerical results to a good accuracy.

2.4 General formalism

2.4.1 Definition and master equation

The linear model discussed so far was deliberately simple and the main purpose of studying it was to develop a general intuition. In order to extend the method beyond the linear case, we now consider a more general model. This will introduce several new aspects to the problem.

As before, we restrict our discussion to the case of a single species and two environmental states. We write n for the number of individuals in the population, and $\sigma \in \{0, 1\}$ for the state of the environment. We use the notation $\lambda_1(n/\Omega)$ for the rate with which the environment switches from state 0 to state 1, and $\lambda_0(n/\Omega)$ for the rate

of switches in the opposite direction. Unlike in the previous sections, we now allow for an explicit dependence of these rates on the state of the population, $\lambda_\sigma = \lambda_\sigma(n/\Omega)$.

We assume that there are M possible reactions in the population, labelled $m = 1, \ldots, M$. Each reaction m occurs with rate $\Omega r_{m,\sigma}(n/\Omega)$ dependent on the current state of the environment and population. Any occurrence of a reaction of type m is taken to change the number of individuals in the population by S_m. These are the underlying stoichiometric coefficients. The propensity functions, $\Omega r_{m,\sigma}(n/\Omega)$, together with the stoichiometric coefficients completely define the dynamics of the population.

The master equation describing the time evolution of $P(n, \sigma)$ then reads

$$\begin{aligned} \frac{\mathrm{d}}{\mathrm{d}t}P(n,0) &= \mathcal{M}_0 P(n,0) - \lambda_1\left(\frac{n}{\Omega}\right)P(n,0) + \lambda_0\left(\frac{n}{\Omega}\right)P(n,1), \\ \frac{\mathrm{d}}{\mathrm{d}t}P(n,1) &= \mathcal{M}_1 P(n,1) + \lambda_1\left(\frac{n}{\Omega}\right)P(n,0) - \lambda_0\left(\frac{n}{\Omega}\right)P(n,1). \end{aligned} \tag{2.17}$$

The operators $\mathcal{M}_0$ and $\mathcal{M}_1$ are given by

$$\mathcal{M}_\sigma = \Omega \sum_{m=1}^{M} \left(\mathcal{E}^{-S_m} - 1\right) r_{m,\sigma}\left(\frac{n}{\Omega}\right). \tag{2.18}$$

The master equation can be expressed in terms of $\Pi(x, \sigma, t)$, the probability density of finding the random processes at x, σ at time t. The dynamics of the joint probability distribution can be approximated by

$$\begin{aligned} \partial_t \Pi(x,0) &= \mathcal{L}_0 \Pi(x,0) - \lambda_1(x)\Pi(x,0) + \lambda_0(x)\Pi(x,1), \\ \partial_t \Pi(x,1) &= \mathcal{L}_1 \Pi(x,1) + \lambda_1(x)\Pi(x,0) - \lambda_0(x)\Pi(x,1), \end{aligned} \tag{2.19}$$

where the Fokker–Planck operators $\mathcal{L}_0$ and $\mathcal{L}_1$ are given by

$$\mathcal{L}_\sigma = \sum_{m=1}^{M} \left(-S_m \partial_x + \frac{{S_m}^2}{2\Omega}\partial_x^2\right) r_{m,\sigma}(x). \tag{2.20}$$

As before we have truncated the expansion of the operators in powers of Ω^{-1} after the sub-leading terms. It follows we have

$$\mathcal{L}_\sigma = -\partial_x v_\sigma(x) + \frac{1}{2\Omega}\partial_x^2 w_\sigma(x), \tag{2.21}$$

where we have introduced

$$\begin{aligned} v_\sigma(x) &= \sum_{m=1}^{M} S_m r_{m,\sigma}(x), \\ w_\sigma(x) &= \sum_{m=1}^{M} S_m^2 r_{m,\sigma}(x). \end{aligned} \tag{2.22}$$

Again, the process described by Eqs. (2.19) contains multiplicative noise and it is difficult to solve these equations in general. In the next section, we begin by analysing the dynamics in the limit of an infinite population.

2.4.2 Leading-order approximation: piecewise-deterministic Markov process

We first analyse the process in the limit of infinite system size. Here, we outline the main steps of the analysis and give the central results. The details of the calculation can be found in Appendix 2.7.

As before we write ϕ instead of x in the limit of an infinite system, and we find the PDMP dynamics

$$\begin{aligned}\partial_t \Pi(\phi,0) &= -\partial_\phi\left[v_0(\phi)\Pi(\phi,0)\right] - \lambda_1(\phi)\Pi(\phi,0) + \lambda_0(\phi)\Pi(\phi,1),\\ \partial_t \Pi(\phi,1) &= -\partial_\phi\left[v_1(\phi)\Pi(\phi,1)\right] + \lambda_1(\phi)\Pi(\phi,0) - \lambda_0(\phi)\Pi(\phi,1).\end{aligned} \tag{2.23}$$

This indicates a flow of the form

$$\dot{\phi} = v_\sigma(\phi), \tag{2.24}$$

in between switches of the environment. These switches in turn occur with rates $\lambda_\sigma(\phi)$.

We now proceed by assuming that the deterministic flow in each of the environments is towards a unique fixed point, i.e., that there are points ϕ^*_σ for $\sigma \in \{0,1\}$ such that

$$v_\sigma(\phi^*_\sigma) = 0. \tag{2.25}$$

For the time being we assume that there is only one such fixed point per state; for a more general case see Section 2.5.3. We assume $\phi^*_0 < \phi^*_1$ without loss of generality. After a potential transient the PDMP will eventually be confined to the interval (ϕ^*_0, ϕ^*_1). Our assumption above (only one fixed point in each environmental state) implies that the v_σ do not change sign on this interval, $v_0(\phi) < 0$ and $v_1(\phi) > 0$ for $\phi \in (\phi^*_0, \phi^*_1)$: the flow is always towards fixed point ϕ^*_0 in state $\sigma = 0$, and towards ϕ^*_1 in state $\sigma = 1$, as also illustrated in Fig. 2.2.

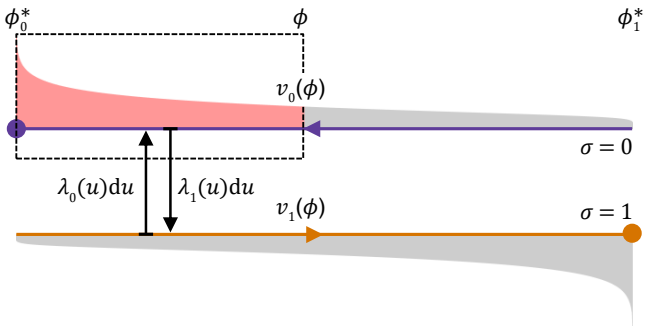

Figure 2.5: Illustration of the physical interpretation of the currents $J_\sigma(\phi)$ (see text).

To analyse the PDMP further, it is useful to introduce currents

$$\begin{aligned} J_0(\phi) &= v_0(\phi)\Pi(\phi,0) - \int_{\phi_0^*}^{\phi} [-\lambda_1(u)\Pi(u,0) + \lambda_0(u)\Pi(u,1)]\,\mathrm{d}u, \\ J_1(\phi) &= v_1(\phi)\Pi(\phi,1) - \int_{\phi_0^*}^{\phi} [+\lambda_1(u)\Pi(u,0) - \lambda_0(u)\Pi(u,1)]\,\mathrm{d}u. \end{aligned} \tag{2.26}$$

The physical interpretation of these currents is illustrated in Fig. 2.5. We focus on a domain (ϕ_0^*, ϕ), where $\phi_0^* \leq \phi \leq \phi_1^*$. The first term of the RHS of Eqs. (2.26) accounts for the probability flowing *out of* such a domain at location ϕ due to the Liouville flow in environmental state σ. The term containing the integral describes the *net flow* of probability out of the domain due to switching between the environmental states. Thus, the quantity $J_\sigma(\phi + \Delta\phi) - J_\sigma(\phi)$ represents the total amount of probability leaving the interval $(\phi, \phi + \Delta\phi)$ per unit time.

This leads to equations of continuity

$$\partial_t \Pi(\phi,\sigma) = -\partial_\phi J_\sigma(\phi). \tag{2.27}$$

In the stationary state the currents are divergence-free ($\partial_\phi J_\sigma^* = 0$). Using the zero-current boundary conditions at ϕ_0^* and ϕ_1^* we find $J_\sigma^*(\phi) \equiv 0$ throughout. Summing the two stationary currents, $J_0^*(\phi) + J_1^*(\phi) = 0$, we immediately find $\Pi^*(\phi,1) = -[v_0(\phi)/v_1(\phi)]\Pi^*(\phi,0)$, which allows one to replace $\Pi^*(\phi,1)$ in favour of $\Pi^*(\phi,0)$ (or vice versa) in the zero-current conditions. This results in two closed equations for $\Pi^*(\phi,0)$ and $\Pi^*(\phi,1)$ respectively. These can then be integrated directly, and we find

$$\begin{aligned} \Pi^*(\phi,0) &= \frac{\mathcal{N}}{-v_0(\phi)} h(\phi), \\ \Pi^*(\phi,1) &= \frac{\mathcal{N}}{v_1(\phi)} h(\phi), \end{aligned} \tag{2.28}$$

where $\mathcal{N}$ is a normalisation constant. The function $h(\phi)$ is given by

$$h(\phi) \equiv \exp\left[-\int^{\phi}\left(\frac{\lambda_1(u)}{v_0(u)}+\frac{\lambda_0(u)}{v_1(u)}\right)\,\mathrm{d}u\right]. \tag{2.29}$$

Further details of the calculation are given in Appendix 2.7.

Later we will need the stationary conditional probability $\Pi^*(\sigma|\phi)$—the stationary probability of having environmental state σ given the population has state ϕ. As discussed above we have $v_0(\phi)\Pi^*(\phi,0)+v_1(\phi)\Pi^*(\phi,1)=0$. Writing $\Pi^*(\phi,\sigma)=\Pi^*(\phi)\Pi^*(\sigma|\phi)$ and using $\Pi^*(0|\phi)+\Pi^*(1|\phi)=1$ in Eq. (2.28) leads to

$$\begin{aligned}\Pi^*(0|\phi) &= \frac{v_1(\phi)}{v_1(\phi)-v_0(\phi)},\\ \Pi^*(1|\phi) &= \frac{-v_0(\phi)}{v_1(\phi)-v_0(\phi)}.\end{aligned} \tag{2.30}$$

It is perhaps surprising that these conditional probabilities are independent of the switching rates λ_1 and λ_0.

2.4.3 Sub-leading order: linear-noise approximation

We now proceed by including contributions of intrinsic noise to sub-leading order. We focus on a time interval between switches of the environment, i.e., we assume σ is constant. During such time intervals the environmental noise has no effect, and the problem reduces to that of a conventional individual-based system with a fixed environment. Following established procedures we write $n/\Omega=\phi(t)+\Omega^{-1/2}\xi(t)$. The deterministic dynamics are given by $\dot{\phi}=v_\sigma(\phi)$. The outcome of a standard LNA can be expressed as a linear Langevin equation

$$\dot{\xi}(t)=v'_\sigma(\phi)\xi+\sqrt{w_\sigma(\phi)}\eta(t) \tag{2.31}$$

for fluctuations about $\phi(t)$, where

$$w_\sigma(\phi)=\sum_m S_m^2 r_{m,\sigma}(\phi). \tag{2.32}$$

These relations describe the evolution of the population (within the LNA) between switches of the environment. When a change of the environment occurs the variable $\sigma(t)$ changes at a discrete point in time, and the next such interval of constant σ begins.

Within the LNA the evolution of the probability to observe state ϕ, ξ, σ is described by the following set of equations

$$\begin{aligned}
\partial_t \Pi(\phi,\xi,0) = & -\partial_\phi \left[v_0(\phi)\Pi(\phi,\xi,0)\right] - v_0'(\phi)\,\partial_\xi\left[\xi\Pi(\phi,\xi,0)\right] + \frac{w_0(\phi)}{2}\partial_\xi^2\Pi(\phi,\xi,0) \\
& - \lambda_1(\phi)\Pi(\phi,\xi,0) + \lambda_0(\phi)\Pi(\phi,\xi,1), \\
\partial_t \Pi(\phi,\xi,1) = & -\partial_\phi \left[v_1(\phi)\Pi(\phi,\xi,1)\right] - v_1'(\phi)\,\partial_\xi\left[\xi\Pi(\phi,\xi,1)\right] + \frac{w_1(\phi)}{2}\partial_\xi^2\Pi(\phi,\xi,1) \\
& + \lambda_1(\phi)\Pi(\phi,\xi,0) - \lambda_0(\phi)\Pi(\phi,\xi,1).
\end{aligned} \tag{2.33}$$

While the expressions on the right-hand side look complicated, the different terms have a clear physical meaning. The Liouvillian terms $-\partial_\phi[v_\sigma(\phi)\Pi(\phi,\xi,\sigma)]$ describe the deterministic flow $[\dot{\phi} = v_\sigma(\phi)]$ between switches of the environment. The Fokker–Planck-like terms $-v_\sigma'(\phi)\partial_\xi\left[\xi\Pi(\phi,\xi,\sigma)\right] + w_\sigma(\phi)\partial_\xi^2\Pi(\phi,\xi,\sigma)/2$ capture the evolution of ξ within the LNA of Eq. (2.31). Finally, the terms proportional to $\lambda_\sigma(\phi)$ describe switching of the environment. Consistent with the expansion in the system-size Ω we have replaced $\lambda_\sigma(x)$ by $\lambda_\sigma(\phi)$, i.e., any dependence of the switching rates on the state of the population is taken to be on the state of the PDMP ϕ.

2.4.4 Stationary state within the linear-noise approximation

At stationarity the time derivatives on the LHS of Eqs. (2.33) vanish. Using asterisks as before to denote stationary distributions, and writing $\Pi^*(\phi,\xi,\sigma) = \Pi^*(\phi,\sigma)\Pi^*(\xi|\phi,\sigma)$, we find

$$\begin{aligned}
0 = & -\partial_\phi\left[v_0(\phi)\,\Pi^*(\phi,0)\,\Pi^*(\xi|\phi,0)\right] \\
& - \Pi^*(\phi,0)\,v_0'(\phi)\,\partial_\xi\left[\xi\Pi(\xi|\phi,0)\right] + \frac{1}{2}\Pi^*(\phi,0)\,w_0(\phi)\,\partial_\xi^2\Pi^*(\xi|\phi,0) \\
& - \partial_\phi\left[v_1(\phi)\,\Pi^*(\phi,1)\,\Pi^*(\xi|\phi,1)\right] \\
& - \Pi^*(\phi,1)\,v_1'(\phi)\,\partial_\xi\left[\xi\Pi(\xi|\phi,1)\right] + \frac{1}{2}\Pi^*(\phi,1)\,w_1(\phi)\,\partial_\xi^2\Pi^*(\xi|\phi,1)
\end{aligned} \tag{2.34}$$

from summing the two equations (2.33) at stationarity.

At this point we introduce a further approximation. We assume $\Pi^*(\xi|\phi,0) \approx \Pi^*(\xi|\phi,1)$, and simply write $\Pi^*(\xi|\phi)$ for either of these. This will be justified below.

Making this assumption leads to

$$0 = -\Big(\Pi^*(0|\phi)v_0'(\phi) + \Pi^*(1|\phi)v_1'(\phi)\Big)\frac{\partial}{\partial\xi}\xi\Pi^*(\xi|\phi) + \frac{1}{2}\Big(\Pi^*(0|\phi)w_0(\phi) + \Pi^*(1|\phi)w_1(\phi)\Big)\frac{\partial^2}{\partial\xi^2}\Pi^*(\xi|\phi), \tag{2.35}$$

where we have used the relation $v_0(\phi)\Pi^*(\phi,0)+v_1(\phi)\Pi^*(\phi,1)=0$, valid at stationarity, to show that the terms containing derivatives with respect to ϕ cancel out.

Eq. (2.35) resembles a stationary Fokker–Planck equation. The drift and diffusion coefficients are obtained from the v_σ' and w_σ, weighted by the likelihood to find the environment in each of its states when the PDMP is at ϕ.

Solving the stationary equation (2.35) is standard [4]; we find a Gaussian distribution, $\Pi^*(\xi|\phi)$, with zero mean and with variance

$$s^2(\phi) = -\frac{1}{2}\frac{\Pi^*(0|\phi)w_0(\phi) + \Pi^*(1|\phi)w_1(\phi)}{\Pi^*(0|\phi)v_0'(\phi) + \Pi^*(1|\phi)v_1'(\phi)}. \tag{2.36}$$

Using Eq. (2.30) this can be simplified to give

$$s^2(\phi) = \frac{1}{2}\frac{w_0(\phi)v_1(\phi) - w_1(\phi)v_0(\phi)}{v_0(\phi)v_1'(\phi) - v_1(\phi)v_0'(\phi)}. \tag{2.37}$$

We conclude this section with a brief comment on the approximation $\Pi^*(\xi|\phi,\sigma) \approx \Pi^*(\xi|\phi)$. In the fast-switching limit the approximation is plausible, the system switches between environmental states too fast for the variable ξ to equilibrate to a distribution specific to the environmental state. For this case, the approximation reproduces the result of Ref. [38]. In the limit of slow switching on the other hand the system spends most of its time near the fixed points ϕ_0^* and ϕ_1^*. Our approach then also recovers appropriate distributions of ξ. For example, when $\phi \approx \phi_0^*$ we have $v_0(\phi=\phi_0^*)=0$ and Eq. (2.37) hence reduces to $s^2(\phi_0^*) = -[w_0(\phi_0^*)/(2v_0'(\phi_0^*))]$. This is the stationary variance of the process $\dot\xi = -v_0'(\phi_0^*)\xi + \sqrt{w_0(\phi_0^*)}\eta$. A similar argument applies when $\phi \approx \phi_1^*$. Outside the limits of fast and slow switching, the quality of the approximation can be verified numerically. In Fig. 2.6 we illustrate this for a model with nonlinear dynamics (discussed in more detail in the next section). To test the validity of the above assumption we have implemented the following measurement protocol: We first generate a combined realisation of the environmental process and the PDMP, i.e., a realisation of the process defined by Eqs. (2.23). Subsequently we generate a realisation of the birth-death dynamics in a finite population for the same path of the environment.

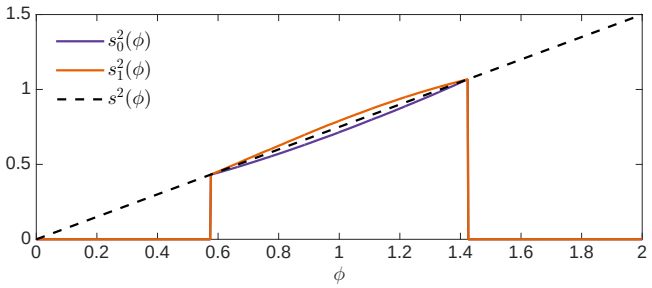

Figure 2.6: The variance of ξ, conditioned on the state ϕ of the PDMP and the state of the environment (see text for details). Results are shown for the dimerisation process of Section 2.5.1. Solid lines are $s_0^2(\phi)$ and $s_1^2(\phi)$ obtained from simulations (see text for definitions). The dashed line shows the approximation of Eq. (2.37). Parameters used are $b_0 = 0.667$, $b_1 = 4.048$, $d = 2$, $\lambda_1 = \lambda_0 = 1$ and $\Omega = 150$.

In the stationary state we then measure the variance of ξ conditioned on the state ϕ of the PDMP and on the environmental state σ. We denote this variance by $s_\sigma^2(\phi)$. This is then averaged over multiple realisations, and compared against the approximation of Eq. (2.37). The data in Fig. 2.6 shows that the approximation works well, with only slight deviations in the region away from the two fixed points ϕ_0^* and ϕ_1^*. For the linear model numerical results and the theoretical prediction are indistinguishable; in Appendix 2.10 we show the approximation is exact for the linear model.

2.5 Further Examples

2.5.1 Nonlinear reactions rates

In order to demonstrate the generality of our approach, we now proceed to a model system with nonlinear reaction rates. The system is identical to the one described in Eq. (2.2), except that the last reaction (removal of individuals) is replaced by

$$2\mathcal{P} \xrightarrow{d/\Omega} \varnothing. \tag{2.38}$$

The above notation indicates that this last reaction occurs with rate $dn(n-1)/(2\Omega)$, where n is the number of individuals in the system. The reaction can be interpreted as a dimerisation process, in which two particles of type $\mathcal{P}$ form a complex which is chemically inert and hence effectively removed. In addition to the switches between $\mathcal{G}_0$ and $\mathcal{G}_1$, this system is described by two reactions, with stoichiometric coefficients

and reaction rates

$$\begin{aligned} S_1 &= +1,\ r_{1,\sigma} = b_\sigma, \\ S_2 &= -2,\ r_{2,\sigma} = \frac{d}{2}x^2. \end{aligned} \tag{2.39}$$

We have written $x = n/\Omega$ as before. Using the notation of the preceding sections, we have the following drift and the diffusion terms

$$v_\sigma(x) = b_\sigma - x^2 d, \quad \text{and} \quad w_\sigma(x) = b_\sigma + 2x^2 d. \tag{2.40}$$

In the limit $\Omega \to \infty$, we obtain a PDMP with fixed points $\phi^*_\sigma = \sqrt{b_\sigma/d}$ for $\sigma = 0, 1$. As before we assume $b_0 < b_1$. The stationary distribution of the PDMP is found from Eq. (2.28),

$$\begin{aligned} \Pi^*(\phi, 0) &= \frac{\mathcal{N}}{\phi^2 - {\phi^*_0}^2} \left(\frac{\phi - \phi^*_0}{\phi^*_0 + \phi}\right)^{\frac{\lambda_1}{\sqrt{4b_0 d}}} \left(\frac{\phi^*_1 - \phi}{\phi^*_1 + \phi}\right)^{\frac{\lambda_0}{\sqrt{4b_1 d}}}, \\ \Pi^*(\phi, 1) &= \frac{\mathcal{N}}{{\phi^*_1}^2 - \phi^2} \left(\frac{\phi - \phi^*_0}{\phi^*_0 + \phi}\right)^{\frac{\lambda_1}{\sqrt{4b_0 d}}} \left(\frac{\phi^*_1 - \phi}{\phi^*_1 + \phi}\right)^{\frac{\lambda_0}{\sqrt{4b_1 d}}}, \end{aligned} \tag{2.41}$$

for $\phi \in (\phi^*_0, \phi^*_1)$, and where $\mathcal{N}$ is the usual normalisation constant.

From Eq. (2.37) finally we find $s^2(\phi) = 3\phi/4$, i.e.,

$$\Pi^*(\xi|\phi) = \sqrt{\frac{2}{3\pi\phi}} \exp\left(-\frac{2}{3\phi}\xi^2\right). \tag{2.42}$$

The stationary distribution $\Pi^*(x)$ is then obtained by numerically evaluating Eq. (2.16). Results are compared against simulation in Fig. 2.7, and we find convincing agreement between theoretical predictions and simulations. This confirms the validity of the assumptions and approximations made during the course of the analytical calculation.

2.5.2 System-dependent environmental transition rates

We now turn to another variation of the original linear model [Eqs. (2.2)]. For the dynamics within the population we use the same reactions and rates as in Eqs. (2.2), but we consider the case in which the rates with which the environment switches between states depends on the state of the population, i.e.,

$$\begin{aligned} \mathcal{G}_0 &\xrightarrow{\lambda_1(n/\Omega)} \mathcal{G}_1, \\ \mathcal{G}_1 &\xrightarrow{\lambda_0(n/\Omega)} \mathcal{G}_0, \end{aligned} \tag{2.43}$$

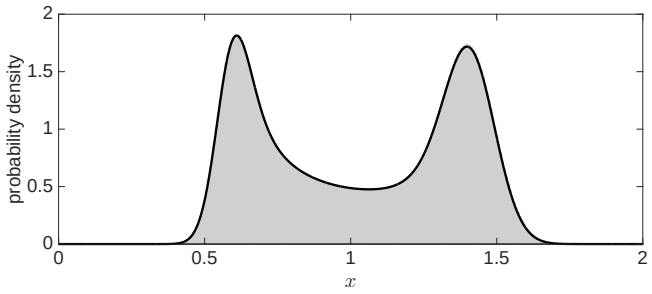

Figure 2.7: Stationary distribution for the nonlinear model of Sec. 2.5.1. The solid line is the theoretical prediction, and the histogram is data obtained from simulations using the Gillespie algorithm. Parameters are $b_0 = 0.667$, $b_1 = 4.048$, $d = 2$, $\lambda_1 = \lambda_0 = 1$ and $\Omega = 150$.

where we choose the linear form $\lambda_\sigma(n/\Omega) = \alpha_\sigma + \beta_\sigma(n/\Omega)$. The coefficients α_σ and β_σ are constants, chosen such that λ_σ remain non-negative.

The drift and diffusion terms of the dynamics within the population are

$$v_\sigma(x) = b_\sigma - xd, \quad \text{and} \quad w_\sigma(x) = b_\sigma + xd. \tag{2.44}$$

as before. The stationary distribution of the PDMP in the limit of infinite populations is obtained from Eqs. (2.28) as

$$\begin{aligned} \Pi^*(\phi,0) &= \mathcal{N} e^{\frac{\beta_0+\beta_1}{d}\phi} \frac{(\phi-\phi_0^*)^{\kappa_1}\,(\phi_1^*-\phi)^{\kappa_0}}{\phi-\phi_0^*}, \\ \Pi^*(\phi,1) &= \mathcal{N} e^{\frac{\beta_0+\beta_1}{d}\phi} \frac{(\phi-\phi_0^*)^{\kappa_1}\,(\phi_1^*-\phi)^{\kappa_0}}{\phi_1^*-\phi}, \end{aligned} \tag{2.45}$$

where the exponents κ_σ are given by

$$\kappa_\sigma = \frac{\alpha_\sigma}{d} + \frac{\beta_\sigma b_0}{d^2}. \tag{2.46}$$

The dynamics within the population is the same as in the linear model above, so evaluating Eq. (2.37) again leads to $s^2(\phi) = \phi$. The theoretical estimate of the stationary distribution $\Pi^*(x)$, finally, is again found from numerical integration of Eq. (2.16).

Fig. 2.8 shows a sample path of the dynamics and the stationary distribution for the choice $\lambda_1(x) = \lambda_0(x) = x$ (i.e., $\alpha_0 = \alpha_1 = 0$ and $\beta_0 = \beta_1 = 1$). In this case, transitions between states are more likely at higher concentrations of the system. Again, we find good agreement between the predicted distribution and the simulation results. It is important to note that the parameters we used in the figure are not special in any way: we have tested other choices of the parameter, and we find an agreement between simulations and theory of a similar quality.

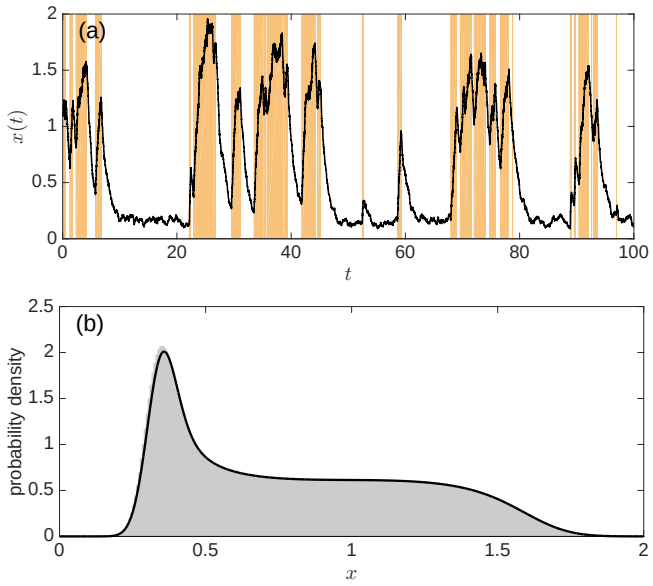

Figure 2.8: Model in which rates of environmental switching depends on the state of the population. Panel (a) shows a typical time course, as generated by the Gillespie algorithm. Panel (b) depicts the stationary distribution; the histogram is from simulations and the solid line represents the approximation from our theory. Model parameters are $\alpha_0 = \alpha_1 = 0, \beta_0 = \beta_1 = 1, b_0 = 1/3, b_1 = 5/3, d = 1$ and $\Omega = 150$.

2.5.3 Multiple fixed points

In the final example, we consider more complicated dynamics within the population such that there are multiple fixed points of the flows $v_\sigma(x)$. The switching between the two environmental states is taken to occur with constant rates λ_σ. Specifically, the population dynamics are now modelled by the following reactions

$$\begin{aligned} \mathcal{G}_\sigma &\xrightarrow{\Omega c_{1,\sigma}} \mathcal{G}_\sigma + \mathcal{P}, \\ \mathcal{G}_\sigma + \mathcal{P} &\xrightarrow{c_{2,\sigma}} \mathcal{G}_\sigma, \\ \mathcal{G}_\sigma + 2\mathcal{P} &\xrightarrow{c_{3,\sigma}/\Omega} \mathcal{G}_\sigma + 3\mathcal{P}, \\ \mathcal{G}_\sigma + 3\mathcal{P} &\xrightarrow{c_{4,\sigma}/\Omega^2} \mathcal{G}_\sigma + 2\mathcal{P}, \end{aligned} \tag{2.47}$$

with constant parameters $c_{i,\sigma} > 0$. The corresponding stoichiometric coefficients for the four reactions are

$$S_1 = S_3 = +1, \; S_2 = S_4 = -1, \tag{2.48}$$

and the propensities $r_{m,\sigma}(x)$ read

$$\begin{aligned} r_{1,\sigma}(x) &= c_{1,\sigma}, & r_{2,\sigma}(x) &= c_{2,\sigma}x, \\ r_{3,\sigma}(x) &= \frac{c_{3,\sigma}}{2}x^2, & r_{4,\sigma}(x) &= \frac{c_{4,\sigma}}{6}x^3. \end{aligned} \tag{2.49}$$

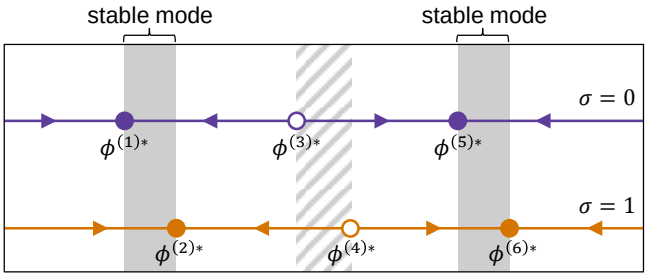

Figure 2.9: Illustration of the Liouville flow in the two environmental states $\sigma = 0, 1$ for the model in Sec. 2.5.3. Stable fixed points are shown as filled circles, and unstable fixed points as open circles. The shaded areas represent the two stable dynamic modes described in the text.

Additional details of the model and the numerical values of the parameters we used for our analysis can be found in Appendix 2.8.

Again, we first consider the PDMP, i.e., the limit $\Omega \to \infty$. For the parameters chosen for our analysis one finds three fixed points of the dynamics $\dot{\phi} = v_0(\phi)$, at $\phi^* \approx 0.20, 0.90$, and 1.6. We label these $\phi^{(1)*}, \phi^{(3)*}$, and $\phi^{(5)*}$. These fixed points are linearly stable, unstable, and stable respectively. In the environmental state $\sigma = 1$ we have fixed points $\phi^* \approx 0.4, 1.1$ and 1.8, labelled $\phi^{(2)*}, \phi^{(4)*}$,and $\phi^{(6)*}$(again stable, unstable, and stable respectively). This arrangement of fixed points is illustrated in Fig 2.9. The dynamics of the PDMP depend on the initial condition. If started between the fixed points $\phi^{(1)*}$ and $\phi^{(2)*}$, the system will be confined between these two values and follow a dynamics similar to that of the system in Sec. 2.5.1. Similarly, if the initial condition is between the two fixed points $\phi^{(5)*}$ and $\phi^{(6)*}$, the PDMP will operate in the interval between these two points. We will refer to these as the two 'stable modes' of the PDMP dynamics. For other initial conditions the PDMP will eventually reach one of these two stable modes as well, which one this is will depend on the starting point and on the exact path the environment takes.

If the system is finite, the dynamics are subject to intrinsic noise. Two representative trajectories are shown Fig. 2.10. Depending on initial conditions the system either remains close to the interval between $\phi^{(1)*}$ and $\phi^{(2)*}$ or near the interval between $\phi^{(5)*}$ and $\phi^{(6)*}$. Intrinsic noise will allow for excursions outside these intervals, similar to what was observed in Sec. 2.5.1. The finite system can traverse the region between $\phi^{(2)*}$ and $\phi^{(5)*}$, at least in principle, and move from one of the dynamic modes to the other. This is similar to escaping from a basin of attraction in systems with

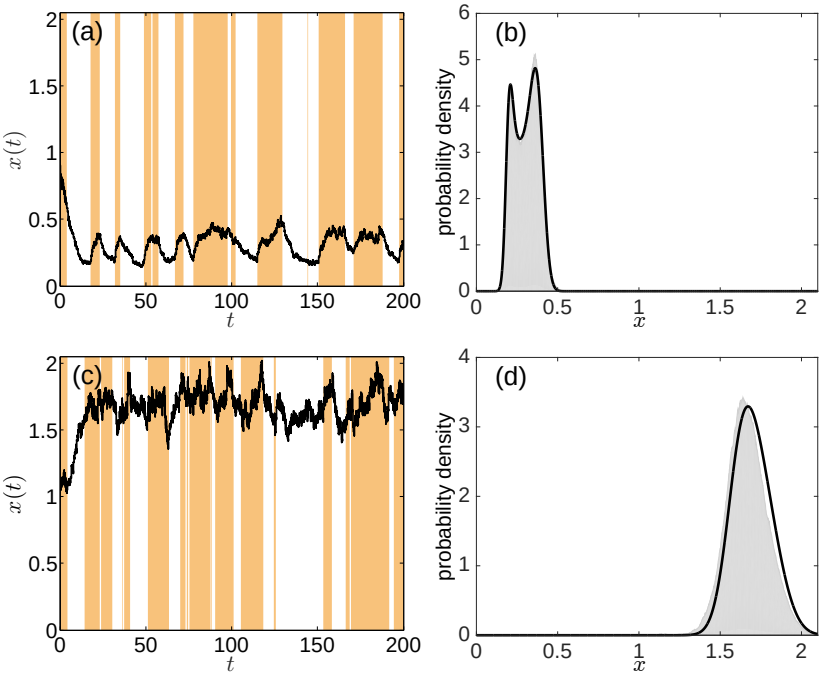

Figure 2.10: Representative realisations and quasi-stationary distributions for the model with described in Sec. 2.5.3. Panels (a) and (b) represent one dynamic mode and panels (c) and (d) represent the other. More precisely, panels (a) and (b) show the outcome when the initial condition is to the left of $\phi^{(3)*}$; panels (c) and (d) show a situation in which the dynamics is started to the right of $\phi^{(4)*}$. The histograms in panels (b) and (d) are from Gillespie simulations, and the solid lines are from the analytical approximation. Model parameters are $\lambda_1 = \lambda_0 = 0.2$ and $\Omega = 1000$, remaining parameters as described in Appendix 2.8.

constant environment. We generally expect that the rate with which this happens is exponentially suppressed in the noise strength. We will assume that such events are sufficiently rare so that they can be ignored for the purposes of our analysis.

The general approach we have developed can then be applied to the system in either of the two dynamic modes. Due to the complexity of the flow fields $v_\sigma(x)$, the relevant equations have to be evaluated numerically. In Fig. 2.10 we show the resulting predictions for the stationary distribution in either mode. As in the previous examples, comparison with data from numerical simulations shows very good agreement.

2.6 Conclusions

In summary, we have constructed a systematic approach with which to investigate the effects of demographic noise in systems subject to sudden random switches of reaction rates. We have focused on relatively simple birth-death processes of one single species and in which birth and death rates depend on both the state of the population and on the state of an external environment. The states of the environment follow a telegraph process, with transition rates which may depend on the state of the population. Previously existing approaches either disregard intrinsic fluctuations and only account for environmental noise, or they focus on cases in which there is a clear separation of time scales between the population dynamics and the dynamics of the environment. The former approach in particular leads to the well-established picture of so-called piecewise deterministic Markov processes. Our work systematically improves on this view; we take into account demographic fluctuations to leading order and carry out a system-size expansion and linear-noise approximation about the PDMP dynamics.

Using the linear-noise approximation, and retaining the discreteness of the environmental process, we then approximate the resulting stationary distribution of the population dynamics. We have tested the resulting theory on a number of model systems, both with linear and nonlinear reaction rates, situations in which environmental switching depends on the state of the population, and covering systems with single dynamic modes and cases where there are multiple attractors. In all cases we have tested, the approximation is in good agreement with results from simulations. In

particular no separation of time scales is required.

The technique we provide makes our understanding of processes involving both intrinsic and extrinsic noise more complete. While the existing PDMP description has been shown to be successful in many instances, it disregards intrinsic noise entirely. We are now in a position to describe the effects of demographic noise in systems with switching environments in the spirit of the van Kampen expansion. This allows us to investigate models subject to combinations of intrinsic and extrinsic noise, and in particular systems in which some degrees of freedom can be treated within a linear-noise approximation, while other variables remain fundamentally discrete. Such systems can be of relevance for example in the context of genetic switches, bacterial populations subject to varying external conditions, or to predator-prey dynamics. In order to make the method more applicable several extensions could in principle be considered in future work. This includes the case of multiple environmental states, systems with more than one species, or indeed environmental dynamics beyond simple telegraph processes. For the former two cases, there are inherent difficulties in finding the stationary distribution for the PDMP since the equivalent of Eq. (2.52) is not necessarily a first-order ODE, but rather a higher-order PDE. While the analysis presented herein considers small fluctuations from demographic noise, it has limited ability to handle phenomena driven by large demographic fluctuations such as fixation; in such cases approaches based on WKB methods may be more useful [25, 30, 59].

2.7 Appendix A: The stationary distribution of the PDMP

In this section we briefly discuss the calculation of the stationary distribution of the PDMP. Following on from Eq. (2.26), and writing $\partial_\phi J^*_\sigma(\phi) \equiv 0$ in the stationary state, we have $J^*_\sigma(\phi) \equiv 0$ throughout, using zero-current conditions at the boundaries. This leads to

$$\begin{aligned} J^*_0(\phi) &= v_0(\phi)\Pi^*(\phi,0) - \int_{\phi^*_0}^{\phi} \left[-\lambda_1(u)\Pi^*(u,0) + \lambda_0(u)\Pi^*(u,1)\right] \mathrm{d}u = 0, \\ J^*_1(\phi) &= v_1(\phi)\Pi^*(\phi,1) - \int_{\phi^*_0}^{\phi} \left[+\lambda_1(u)\Pi^*(u,0) - \lambda_0(u)\Pi^*(u,1)\right] \mathrm{d}u = 0. \end{aligned} \tag{2.50}$$

Summing the two stationary currents, $J_0^*(\phi) + J_1^*(\phi) = 0$, we immediately find $v_0(\phi)\Pi^*(\phi,0) + v_1(\phi)\Pi^*(\phi,1) = 0$ for all ϕ, i.e., $\Pi^*(\phi,1) = -\left[v_0(\phi)/v_1(\phi)\right]\Pi^*(\phi,0)$. Inserting this into the first equation of (2.50) gives

$$v_0(\phi)\Pi^*(\phi,0) + \int_{\phi_0^*}^{\phi}\left[\lambda_1(u)\Pi^*(u,0) + \lambda_0(u)\frac{v_0(\phi)}{v_1(\phi)}\Pi^*(u,0)\right]\mathrm{d}u = 0. \tag{2.51}$$

Differentiating with respect to ϕ one obtains

$$\rho_0'(\phi) + \left[\frac{\lambda_1(\phi)}{v_0(\phi)} + \frac{\lambda_0(\phi)}{v_1(\phi)}\right]\rho_0(\phi) = 0, \tag{2.52}$$

where we have introduced $\rho_0(\phi) \equiv v_0(\phi)\Pi^*(\phi,0)$, and where ρ_0' indicates a derivative with respect to ϕ. An analogous derivation shows that $\rho_1(\phi) \equiv v_1(\phi)\Pi^*(\phi,1)$ fulfills the same relation (we note that the expression in the square brackets in Eq. (2.52) is symmetric with respect to simultaneous exchanges $0 \leftrightarrow 1$).

Equation (2.52) and its analogue for $\rho_1(\phi)$ can directly be integrated and we find

$$\Pi^*(\phi,0) = \frac{\mathcal{N}_0}{v_0(\phi)}h(\phi), \qquad \Pi^*(\phi,1) = \frac{\mathcal{N}_1}{v_1(\phi)}h(\phi), \tag{2.53}$$

where

$$h(\phi) = \exp\left[-\int^{\phi}\mathrm{d}u\ \left(\frac{\lambda_1(u)}{v_0(u)} + \frac{\lambda_0(u)}{v_1(u)}\right)\right], \tag{2.54}$$

and where $\mathcal{N}_0$ and $\mathcal{N}_1$ are normalisation constants. Using again the relation $v_0(\phi)\Pi^*(\phi,0) + v_1(\phi)\Pi^*(\phi,1) = 0$, derived above, we conclude $\mathcal{N}_0 = -\mathcal{N}_1 \equiv -\mathcal{N}$, and so we have

$$\Pi^*(\phi,0) = \frac{\mathcal{N}}{-v_0(\phi)}h(\phi), \qquad \Pi^*(\phi,1) = \frac{\mathcal{N}}{v_1(\phi)}h(\phi). \tag{2.55}$$

Recalling that $v_0 < 0$ and $v_1 > 0$ throughout the domain of the PDMP, $\mathcal{N}$ is a positive constant, to be determined from the normalisation condition

$$\int_{\phi_0^*}^{\phi_1^*}\left[\Pi^*(\phi,0) + \Pi^*(\phi,1)\right]\mathrm{d}\phi = 1. \tag{2.56}$$

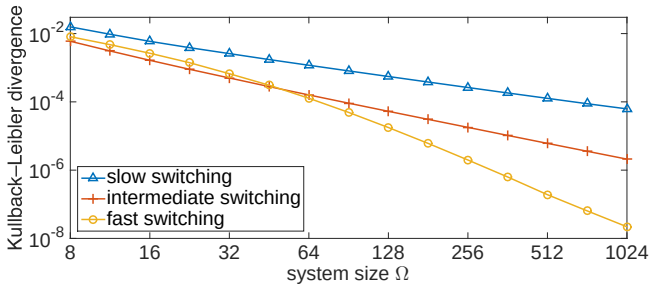

Figure 2.11: The Kullback-Leibler divergence between the true stationary distribution of the system and our approximation for the linear model. Each line shows a different parameter regime from Figure 2.1. The true stationary distribution is determined by fourth order Runge–Kutta integration of the master equation.

2.8 Appendix B: Further details of the model with multiple fixed points

For the model described in Sec. 2.5.3 the functions $v_\sigma(x)$ and $w_\sigma(x)$ as defined in Eq. (2.22) are given by

$$\begin{aligned} v_\sigma(x) &= c_{1,\sigma} - c_{2,\sigma}x + c_{3,\sigma}x^2 - c_{3,\sigma}x^4, \\ w_\sigma(x) &= c_{1,\sigma} + c_{2,\sigma}x + c_{3,\sigma}x^2 + c_{3,\sigma}x^4. \end{aligned} \tag{2.57}$$

The parameters chosen for the analysis in Sec. 2.5.3 are

$$\begin{aligned} c_{1,0} &= 0.11, \quad c_{1,1} = 0.31, \\ c_{2,0} &= 0.76, \quad c_{2,1} = 1.24, \\ c_{3,0} &= 2.14, \quad c_{3,1} = 2.60, \\ c_{4,0} &= 2.40, \quad c_{4,1} = 2.40. \end{aligned} \tag{2.58}$$

2.9 Appendix C: Accuracy of our approach

The accuracy of our approach can be characterised by computing the Kullback–Leibler divergence [60] between the true stationary distribution and our approximation. Figure 2.11 shows how the Kullback–Leibler divergence changes with system size for the linear model. Each line represents one of the parameter regimes displayed in Figure 2.1. Birth rates, death rates, and switching rates have been chosen such that Ω

is the average population of the system. The divergence decreases as the system size is increased, with relatively small system sizes having appreciably small divergences. Similar results are observed for the nonlinear and feedback models.

2.10 Appendix D: Approximation Eq. (2.15) is exact for the linear model

In this appendix we provide further support for approximation Eq. (2.15) by showing it is exact for the case of a linear model. Consider the case of a linear birth-death process with births and deaths occurring with per capita rates b_σ and d_σ, respectively, leading to functions $v(\phi) = b_\sigma - \phi d_\sigma$ and $w(\phi) = b_\sigma + \phi d_\sigma$. Making approximation Eq. (2.15) allowed us to write Eq. (2.37), which in this case would allow us to approximate the variance of process $\xi(t)$ for a given coordinate ϕ as $s^2(\phi) = \phi$.

Here we show that, after a transient time, the above gives the exact variance from demographic noise following the LNA for the linear model. To show this result, consider the linear Fokker–Planck equation describing the dynamics of process $\xi(t)$ in environmental state σ:

$$\frac{\partial}{\partial t}\Pi(\xi,t) = -v'_\sigma[\phi(t)]\frac{\partial}{\partial \xi}\Pi(\xi,t) + \frac{w_\sigma[\phi(t)]}{2}\frac{\partial^2}{\partial \xi^2}\Pi(\xi,t). \tag{2.59}$$

Substituting in the functions for the linear model, the change in variance $s^2(t)$ is then given by (see Ref. [2] pp. 258)

$$\frac{\mathrm{d}}{\mathrm{d}t}s^2 = -2d_\sigma s^2(t) + b_\sigma + \phi(t)d_\sigma. \tag{2.60}$$

Consider the change in the deviation of variance $s^2(t)$ from $\phi(t)$:

$$\frac{\mathrm{d}}{\mathrm{d}t}\left(s^2 - \phi\right) = -2d_\sigma\left[s^2(t) - \phi(t)\right], \tag{2.61}$$

where we have used Eq. (2.24). We see $s^2(t) \to \phi(t)$ as $t \to \infty$ in all environmental states.

2.11 Bibliography

[1] P. G. Hufton, Y. T. Lin, T. Galla, and A. J. McKane. Intrinsic noise in systems with switching environments. *Phys. Rev. E* **93**, 052119 (2016).

[2] N. G. van Kampen. *Stochastic Processes in Physics and Chemistry*. North-Holland, Amsterdam (2007).

[3] C. W. Gardiner. *Handbook of Stochastic Methods*. Springer-Verlag, Berlin (2004).

[4] H. Risken. *The Fokker–Planck Equation: Methods of Solution and Applications*. Springer-Verlag, Berlin (1989).

[5] M. J. Keeling and P. Rohani. *Modeling Infectious Diseases in Humans and Animals*. Princeton University Press, Princeton NJ (2008).

[6] C. J. Mode and C. K. Sleeman. *Stochastic Processes in Epidemiology: HIV/AIDS, Other Infectious Diseases, and Computers*. World Scientific, Singapore (2000).

[7] A. J. Black and A. J. McKane. Stochastic amplification in an epidemic model with seasonal forcing. *J. Theor. Biol.* **267**, 85 (2010).

[8] D. J. Wilkinson. *Stochastic Modelling for Systems Biology*. CRC Press, Boca Raton (2012).

[9] D. T. Gillespie. Stochastic simulation of chemical kinetics. *Annu. Rev. Phys. Chem.* **58**, 35 (2007).

[10] T. B. Kepler and T. C. Elston. Stochasticity in transcriptional regulation: origins, consequences, and mathematical representations. *Biophys. J.* **81**, 3116 (2001).

[11] A. M. Walczak, A. Mugler, and C. H. Wiggins. Analytic methods for modeling stochastic regulatory networks. In *Computational Modeling of Signaling Networks*, volume 880 of *Methods in Molecular Biology*, pages 273–322. Humana Press, New York (2012).

[12] V. Shahrezaei and P. S. Swain. Analytical distributions for stochastic gene expression. *Proc. Natl. Acad. Sci. U.S.A.* **105**, 17256 (2008).

[13] N. Kumar, T. Platini, and R. V. Kulkarni. Exact distributions for stochastic gene expression models with bursting and feedback. *Phys. Rev. Lett.* **113**, 268105 (2014).

[14] N. G. van Kampen. A power series expansion of the master equation. *Can. J. Phys.* **39**, 551 (1961).

[15] Y. T. Lin, H. Kim, and C. R. Doering. Features of fast living: on the weak selection for longevity in degenerate birth-death processes. *J. Stat. Phys.* **148**, 647 (2012).

[16] Y. T. Lin, H. Kim, and C. R. Doering. Demographic stochasticity and evolution of dispersion I. Spatially homogeneous environments. *J. Math. Biol.* **70**, 647 (2015).

[17] Y. T. Lin, H. Kim, and C. R. Doering. Demographic stochasticity and evolution of dispersion II: Spatially inhomogeneous environments. *J. Math. Biol.* **70**, 679 (2015).

[18] G. W. Constable and A. J. McKane. Models of Genetic Drift as Limiting Forms of the Lotka-Volterra Competition Model. *Phys. Rev. Lett.* **114**, 038101 (2015).

[19] O. Kogan, M. Khasin, B. Meerson, D. Schneider, and C. R. Myers. Two-strain competition in quasineutral stochastic disease dynamics. *Phys. Rev. E* **90**, 042149 (2014).

[20] T. Biancalani, D. Fanelli, and F. Di Patti. Stochastic Turing patterns in the Brusselator model. *Phys. Rev. E* **81**, 046215 (2010).

[21] T. Biancalani, T. Galla, and A. J. McKane. Stochastic waves in a Brusselator model with nonlocal interaction. *Phys. Rev. E* **84**, 026201 (2011).

[22] T. Butler and N. Goldenfeld. Fluctuation-driven Turing patterns. *Phys. Rev. E* **84**, 011112 (2011).

[23] S. Leibler and E. Kussell. Individual histories and selection in heterogeneous populations. *Proc. Natl. Acad. Sci. U.S.A.* **107**, 13183 (2010).

[24] C. Escudero and J. Á. Rodríguez. Persistence of instanton connections in chemical reactions with time-dependent rates. *Phys. Rev. E* **77**, 011130 (2008).

[25] M. Assaf, A. Kamenev, and B. Meerson. Population extinction in a time-modulated environment. *Phys. Rev. E* **78**, 041123 (2008).

[26] S. Schuler, T. Speck, C. Tietz, J. Wrachtrup, and U. Seifert. Experimental test of the fluctuation theorem for a driven two-level system with time-dependent rates. *Phys. Rev. Lett.* **94**, 180602 (2005).

[27] R. P. Boland, T. Galla, and A. J. McKane. Limit cycles, complex Floquet multipliers, and intrinsic noise. *Phys. Rev. E* **79**, 051131 (2009).

[28] A. Kamenev, B. Meerson, and B. Shklovskii. How Colored Environmental Noise Affects Population Extinction. *Phys. Rev. Lett.* **101**, 268103 (2008).

[29] M. Assaf, E. Roberts, Z. Luthey-Schulten, and N. Goldenfeld. Extrinsic Noise Driven Phenotype Switching in a Self-Regulating Gene. *Phys. Rev. Lett.* **111**, 058102 (2013).

[30] M. Assaf, M. Mobilia, and E. Roberts. Cooperation Dilemma in Finite Populations under Fluctuating Environments. *Phys. Rev. Lett.* **111**, 238101 (2013).

[31] E. Kussell, R. Kishony, N. Q. Balaban, and S. Leibler. Bacterial persistence a model of survival in changing environments. *Genetics* **169**, 1807 (2005).

[32] E. Kussell and S. Leibler. Phenotypic diversity, population growth, and information in fluctuating environments. *Science* **309**, 2075 (2005).

[33] M. Thattai and A. Van Oudenaarden. Intrinsic noise in gene regulatory networks. *Proc. Natl. Acad. Sci. U.S.A.* **98**, 8614 (2001).

[34] P. S. Swain, M. B. Elowitz, and E. D. Siggia. Intrinsic and extrinsic contributions to stochasticity in gene expression. *Proc. Natl. Acad. Sci. U.S.A.* **99**, 12795 (2002).

[35] F. Hayot and C. Jayaprakash. The linear noise approximation for molecular fluctuations within cells. *Phys. Biol.* **1**, 205 (2004).

[36] A. Bobrowski, T. Lipniacki, K. Pichór, and R. Rudnicki. Asymptotic behavior of distributions of mRNA and protein levels in a model of stochastic gene expression. *J. Math. Anal. Appl.* **333**, 753 (2007).

[37] M. S. Sherman and B. A. Cohen. A computational framework for analyzing stochasticity in gene expression. *PLoS Comput. Biol.* **10**, e1003596 (2014).

[38] P. Thomas, N. Popović, and R. Grima. Phenotypic switching in gene regulatory networks. *Proc. Natl. Acad. Sci. U.S.A.* **111**, 6994 (2014).

[39] A. Duncan, S. Liao, T. Vejchodskỳ, R. Erban, and R. Grima. Noise-induced multistability in chemical systems: Discrete versus continuum modeling. *Phys. Rev. E* **91**, 042111 (2015).

[40] P. Ashcroft, P. M. Altrock, and T. Galla. Fixation in finite populations evolving in fluctuating environments. *J. R. Soc. Interface* **11**, 20140663 (2014).

[41] Q. Luo and X. Mao. Stochastic population dynamics under regime switching. *J. Math. Anal. Appl.* **334**, 69 (2007).

[42] C. Zhu and G. Yin. On competitive Lotka–Volterra model in random environments. *J. Math. Anal. Appl.* **357**, 154 (2009).

[43] M. H. Davis. Piecewise-deterministic Markov processes: A general class of non-diffusion stochastic models. *J. Roy. Statist. Soc. Ser. B* **46**, 353 (1984).

[44] A. Faggionato, D. Gabrielli, and M. R. Crivellari. Non-equilibrium thermodynamics of piecewise deterministic Markov processes. *J. Stat. Phys.* **137**, 259 (2009).

[45] S. Zeiser, U. Franz, O. Wittich, and V. Liebscher. Simulation of genetic networks modelled by piecewise deterministic Markov processes. *IET Syst. Biol.* **2**, 113 (2008).

[46] S. Zeiser, U. Franz, and V. Liebscher. Autocatalytic genetic networks modeled by piecewise-deterministic Markov processes. *J. Math. Biol.* **60**, 207 (2010).

[47] J. Realpe-Gomez, T. Galla, and A. J. McKane. Demographic noise and piecewise deterministic Markov processes. *Phys. Rev. E* **86**, 011137 (2012).

[48] R. Grima, D. Schmidt, and T. Newman. Steady-state fluctuations of a genetic feedback loop: An exact solution. *J. Chem. Phys.* **137**, 035104 (2012).

[49] J. Peccoud and B. Ycart. Markovian modeling of gene-product synthesis. *Theor. Popul Biol.* **48**, 222 (1995).

[50] J. Hornos, D. Schultz, G. Innocentini, J. Wang, A. Walczak, J. Onuchic, and P. Wolynes. Self-regulating gene: an exact solution. *Phys. Rev. E* **72**, 051907 (2005).

[51] A. Raj, C. S. Peskin, D. Tranchina, D. Y. Vargas, and S. Tyagi. Stochastic mRNA synthesis in mammalian cells. *PLoS Biol.* **4**, e309 (2006).

[52] D. T. Gillespie. A general method for numerically simulating the stochastic time evolution of coupled chemical reactions. *J. Comput. Phys.* **22**, 403 (1976).

[53] D. T. Gillespie. Exact stochastic simulation of coupled chemical reactions. *J. Phys. Chem.* **81**, 2340 (1977).

[54] X. Mao and C. Yuan. *Stochastic Differential Equations with Markovian Switching.* Imperial College Press, London (2006).

[55] D. A. Potoyan and P. G. Wolynes. Dichotomous noise models of gene switches. *J. Chem. Phys.* **143**, 195101 (2015).

[56] I. Bena. Dichotomous Markov noise: exact results for out-of-equilibrium systems. *Int. J. Mod. Phys. B* **20**, 2825 (2006).

[57] K. Kitahara, W. Horsthemke, and R. Lefever. Coloured-noise-induced transitions: Exact results for external dichotomous Markovian noise. *Phys. Lett. A* **70**, 377 (1979).

[58] R. P. Boland, T. Galla, and A. J. McKane. How limit cycles and quasi-cycles are related in systems with intrinsic noise. *J. Stat. Mech: Theory Exp.* **2008**, P09001 (2008).

[59] M. Assaf, E. Roberts, and Z. Luthey-Schulten. Determining the Stability of Genetic Switches: Explicitly Accounting for mRNA Noise. *Phys. Rev. Lett.* **106**, 248102 (2011).

[60] S. Kullback. *Information theory and statistics.* Dover Publications Inc., Mineola NY (1968).

Chapter 3

Phenotypic switching of populations of cells in a stochastic environment

3.1 Preface

The contents of this chapter were previously published a paper in the Journal of Statistical Mechanics: Theory and Experiment in volume 2018, page 023501 in 2018 [1], which was authored by Peter G. Hufton[1], Yen Ting Lin[1,2] and Tobias Galla[1].

P.G.H.'s contribution includes the initial inception of the project, performing all calculations and analysis therein, coding simulations, producing all data and all figures, writing all sections of the paper, and responding to the reports of referees.

[1]Theoretical Physics, School of Physics and Astronomy, The University of Manchester, Manchester M13 9PL, United Kingdom

[2]Theoretical Division and Center for Nonlinear Studies, Los Alamos National Laboratory, Los Alamos, NM 87544, United States of America

Abstract

In biology phenotypic switching is a common bet-hedging strategy in the face of uncertain environmental conditions. Existing mathematical models often focus on periodically changing environments to determine the optimal phenotypic response. We focus on the case in which the environment switches randomly between discrete states. Starting from an individual-based model we derive stochastic differential equations to describe the dynamics, and obtain analytical expressions for the mean instantaneous growth rates based on the theory of piecewise-deterministic Markov processes. We show that optimal phenotypic responses are non-trivial for slow and intermediate environmental processes, and systematically compare the cases of periodic and random environments. The best response to random switching is more likely to be heterogeneity than in the case of deterministic periodic environments, net growth rates are globally higher under stochastic environmental dynamics. The combined system of environment and population of cells can be interpreted as a host-pathogen interaction, in which the host tries to choose environmental switching so as to minimise growth of the pathogen, and in which the pathogen employs a phenotypic switching optimised to increase its growth rate. We discuss the existence of Nash-like mutual best-response scenarios for such host-pathogen games.

3.2 Introduction

Outside of laboratory conditions, microbial cells are often subject to unpredictable adverse environmental changes. As a mechanism to survive such changes, we now understand that cells have evolved to switch stochastically between phenotypic states [2–6]. In contrast to more familiar forms of resistance caused by permanent genetic mutations, these switches are epigenetic in nature, reversible, and lead to heterogeneity in the population. Microbial cells have been shown to use this mechanism as a survival strategy to react to changing environments, for example induced by the administration of antibiotics or other short-term changes in environmental conditions [7, 8]. Due to

the continued interest in antibiotic resistance, understanding the use of phenotypic switching as a survival strategy is essential.

This paper focuses on modelling the dynamics of phenotypic switching in bacterial populations. Within such a population, variability from cell to cell can lead to a fitness advantage. A classic study by Bigger [9] suggests the existence of a subpopulation of bacterial cells more resistant to antibiotics than other members of the population; these more resilient cells are often referred to as 'persisters' [10–12]. The difference between 'normal' and 'persister' cells is phenotypic rather than genotypic. Consequently, a cell may switch back and forth between the normal and persister states, and a given population will contain subpopulations of both phenotypes simultaneously. This heterogeneity in the population constitutes a strategy to improve resistance to environmental stresses, a dynamic sometimes described as bet-hedging [13]. Biological systems use this form of risk-balancing against a number of different environmental stresses, including differences in temperature, concentrations of nutrients and toxins, or the state of a host immune response [7, 14–16]; Thattai *et al.* [17], for example, suggest a model considering the growth of cells in the urinary tract where the environment relates to the state of urination. The effects of environmental sources of noise on biochemical networks have been an important area of theoretical research, where it has been shown to modify switching rates [18–20] and induce bistability [21, 22]. Mathematical models of such bet-hedging strategies often focus on periodically varying environments, mainly to keep the analysis manageable. Examples can be found in Refs. [8, 14, 23–30]. To a lesser extent, bet-hedging has also been studied in stochastically varying environments [17, 31–36].

In this paper, we present a mathematical framework to model phenotypic switching as a mechanism of persistence in a fluctuating environment. We begin by considering an individual-based model, where possible 'reactions' include random birth and death events and stochastic phenotypic switching of individual cells, both in a periodically and stochastically changing environments. We use a recently-developed mathematical approach [37] to characterise the joint random processes and derive formulae for the fitnesses of the subpopulations and the overall growth rate. Further analysis shows that heterogeneity is advantageous for slowly switching environments, whereas homogeneity conveys a fitness advantage for quickly switching environments. By comparing our

results to the case of a periodic environment, we find that environmental stochasticity can, in principle, lead to strategies of phenotypic switching which are very different from those in periodic external environments.

The implications of our analysis are twofold. Firstly, the method advances the mathematical framework for analysing ecological models in random environments. It provides not only a more efficient computational scheme for studying growth dynamics than direct simulations, but also offers mechanistic insights into the problem. Secondly, the method can be used to investigate effective protocols of administering treatment, such as antibiotics to bacterial infection in a control-theoretic framework. We demonstrate both of these applications in idealised scenarios in the later sections of our paper. We also identify a scenario where the competition between the switching dynamics of a host environment and the phenotypic response of the pathogen constitute a game-theoretic scenario. Our analysis allows us to identify the optimal control strategy for the host and the optimal survival strategy for the pathogen. We show how this can result in mutual best responses, akin to what is known as Nash equilibria in game theory [38].

The remainder of the paper is organised as follows. In Sec. 3.3 we set up an individual-based model of phenotypic heterogeneity in a stochastic environment. We then approximate the dynamics of this model and obtain a solution for the average growth rate of the population of cells (Sec. 3.4). Using this solution, we analyse how the average growth rate changes with the parameters in Sec. 3.5. Specifically, we look into the optimum bet-hedging strategy for the bacteria to maximise its growth rate, and conversely the environmental switching strategy that best hinders the bacteria's growth rate. In Sec. 3.6 we summarise our results, and discuss possible directions for future work.

3.3 Model definitions

3.3.1 Individual-based model

We study an individual-based model of a well-mixed population of a species with phenotypic switching in a changing environment. Figure 3.1 (a) presents a summary of the model. We consider a simplified scenario of two phenotypes and two environmental

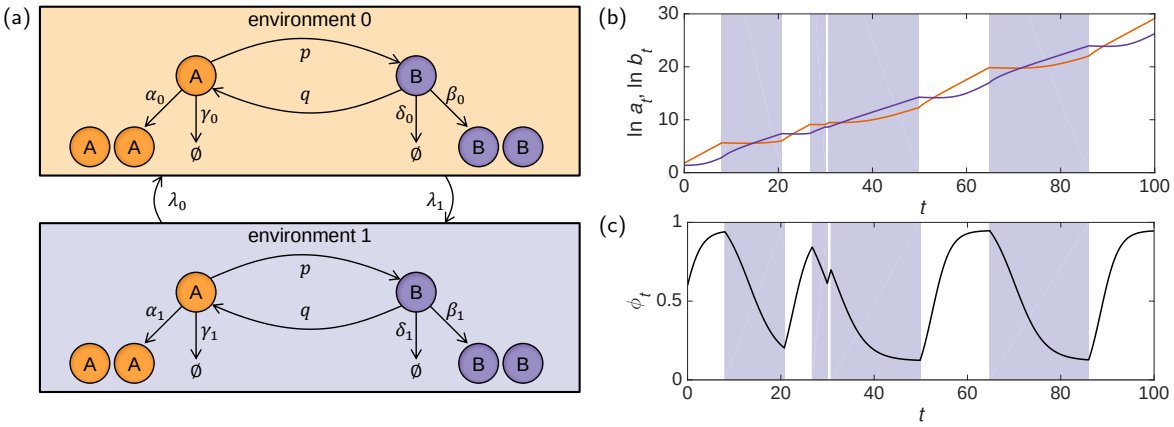

Figure 3.1: (a) Schematic overview of the model. Each cell can express either phenotype A or phenotype B, and switches from A to B with rate p, and vice versa with rate q. Cells of type A duplicate with rate α_σ and die with rate γ_σ, where $\sigma \in \{0, 1\}$ is the state of the environment. The rates for phenotype B are β_σ and δ_σ. The environment switches from state 0 to state 1 with rate λ_1, and vice versa with rate λ_0. The rates are such that the growth rate in environmental state 0 is higher for cells with phenotype A, and the growth rate in environmental state 1 is higher for cells with phenotype B ($\mu_0^A > \mu_0^B$, $\mu_1^A < \mu_1^B$). (b) A typical trajectory of the populations as a piecewise-deterministic Markov process (see text for details, phenotype A orange, phenotype B purple). The background shading indicates whether the environment is in state 0 (light) or state 1 (dark). The population of phenotype A is typically greater than that of phenotype B in environment 0 and vice versa in environment 1. (c) The corresponding trajectory of the proportion of the population expressing phenotype A. As the environment switches states the proportion of phenotype A alternately tends towards the two fixed points, ϕ_0^+ and ϕ_1^+, discussed in the text. Simulations use parameter set (b) (see text and Appendix 3.7). Environmental switching rates are $\lambda_1 = 0.10$, $\lambda_1 = 0.10$ and phenotypic switching rates are $p = 0.028$, $q = 0.043$.

states. Each cell in the population expresses either phenotype A or phenotype B, representing the 'normal' and 'persister' phenotypes, respectively. The birth and death dynamics of the phenotypes depend on an environmental state, which we label σ and which takes values 0 or 1. State 0 represents the 'growth state'; in this state external stresses on the population are absent and the normal phenotype outperforms the persister phenotype. State 1 on the other hand, is the 'stress state' and indicates that an external stress acts on the population. In this state, the persister phenotype outperforms the normal phenotype. This stress can for example be the presence of antibacterial agents, the absence of nutrients, unfavourable temperatures, or the state of a host immune response.

In our model individuals expressing phenotype A duplicate with rate α_σ and die with rate γ_σ. The corresponding rates for phenotype B are β_σ and δ_σ. We define the net growth rates $\mu_\sigma^A = \alpha_\sigma - \gamma_\sigma$ and $\mu_\sigma^B = \beta_\sigma - \delta_\sigma$. Cells expressing phenotype A are better suited to environment 0, whereas cells expressing phenotype B are better suited to environment 1. Specifically, parameters are chosen such that $\mu_0^A > \mu_0^B$ and $\mu_1^A < \mu_1^B$. Individuals switch between the two phenotypes stochastically [6]: individuals of phenotype A switch to phenotype B with rate p; switches in the opposite direction occur with rate q. The rates p and q constitute the 'switching strategy' of the population. These rates are assumed to be independent of the environment, i.e., cells switch between types A and B without sensing the state of the environment. The mathematical formalism we develop, however, does not rely on this assumption and can readily be extended to include environmental sensing, as considered in Refs. [17, 33, 39–42]. More specifically, all equations in this section can be modified to consider environmental sensing under the replacement of phenotypic switching rates p and q with environment-dependent quantities p_σ and q_σ.

We focus mainly on the case when the environmental switching follows a Markov process, i.e., the environmental process is memoryless. We also assume that the dynamics of the environment are external, in particular it is independent of the population. Switches from state $\sigma = 0$ to state $\sigma = 1$ occur with constant rate λ_1, and switches from 1 to 0 occur with constant rate λ_0. As a consequence, the lengths of the episodes spent in either environment are identically and independently distributed random variable sampled from exponential distributions with rate parameters λ_0 and λ_1,

respectively. Mathematically, the environment is described by an asymmetric random telegraph process [43].

In real-world systems the environmental switching process will often have memory and will not occur at constant rates. Instead, transitions of the environmental state will be more likely to occur at certain moments in time. In the extreme case of a laboratory setting they may be strictly prescribed by a definite experimental protocol. The case of strictly periodic switching between environmental states is regularly assumed in the literature, mostly for mathematical convenience. But, just like the Markovian case this is not entirely realistic either. The main motivation for comparing the cases of a Markovian environment on the one hand, and a strictly periodic environment on the other, is that these cases serve as two extremes; they delimit the regime of real-world controlled environmental switching statistics, and by studying the two extremes, we shed light on more realistic scenarios operating in-between.

In principle, the model described above could be simulated using the Gillespie algorithm [44]. In practice, this method is slow, in particular if the total population grows with time. Instead we therefore use a set of approximations which allow us to simulate the processes more efficiently, and also to obtain analytical results. Starting from the master equation for the model, we approximate the dynamics in the limit of a large but finite system size. This leads to a diffusion process with Markovian switching [45], or piecewise-diffusive process, and allows us to perform the so-called linear-noise approximation [46]. From this we obtain explicit expressions for the average growth rate of the population.

3.3.2 Diffusion process with Markovian switching and linear-noise approximation.

Since our model is Markovian, the evolution of the probabilities of the system being in a specific state is described by a master equation [43, 46, 47]. Except for a few special cases, however, there exists no analytical solution for a general master equation. We build on recent work [37,48,49] to approximate the dynamics of systems with switching environments, and perform a Kramers–Moyal expansion [43, 46, 47] in the limit of a large population of cells, but maintaining the discreteness of the environment. Further

details can be found in Appendix 3.8. The result of this expansion for our model is a set of two coupled Itō stochastic differential equations (SDEs) for the number of individuals a_t and b_t with phenotypes A and B, respectively. These equations are

$$\mathrm{d}a_t = \left(\mu_\sigma^A a_t - p a_t + q b_t\right)\mathrm{d}t + B_{\sigma 11}(a_t, b_t)\mathrm{d}W_t^{(1)} + B_{\sigma 12}(a_t, b_t)\mathrm{d}W_t^{(2)}, \tag{3.1a}$$

$$\mathrm{d}b_t = \left(\mu_\sigma^B b_t + p a_t - q b_t\right)\mathrm{d}t + B_{\sigma 21}(a_t, b_t)\mathrm{d}W_t^{(1)} + B_{\sigma 22}(a_t, b_t)\mathrm{d}W_t^{(2)}. \tag{3.1b}$$

In the limit of large populations, the formerly-discrete numbers of individuals a_t and b_t are approximated as continuous variables in Eqs. (3.1). The quantities $W_t^{(1)}$ and $W_t^{(2)}$ are independent Wiener processes (Brownian motion). The subscript t is used throughout this paper to indicate a random process. The coefficients $B_{\sigma ij}(a, b)$ characterise the strength of the demographic noise arising from the random birth-and-death process and the phenotypic switching events [43, 46]. We provide the exact forms of $B_{\sigma ij}$ in Appendix 3.8.

Equations (3.1) describe the random evolution of the population of bacteria *between* switching events of the environment [45]. In particular the quantities on the right-hand side with a subscript σ depend on the current state of the environment. For Markovian switching of the environment as described above, the environmental process σ_t is governed by the master equation

$$\frac{\mathrm{d}}{\mathrm{d}t}P_\sigma(t) = \lambda_\sigma P_{1-\sigma}(t) - \lambda_{1-\sigma}P_\sigma(t), \tag{3.2}$$

where $P_\sigma(t)$ denotes the probability that the environment is in state $\sigma \in \{0, 1\}$ at time t.

In our analysis, we also consider a periodic environment. In this case the state of the environment is a deterministic function given by

$$\sigma(t) = \begin{cases} 0 & \text{for} \quad 0 \le t' < \frac{1}{\lambda_1}, \\ 1 & \text{for} \quad \frac{1}{\lambda_1} \le t' < \frac{1}{\lambda_1} + \frac{1}{\lambda_0}, \end{cases} \tag{3.3}$$

and then repeated with period $T = 1/\lambda_0 + 1/\lambda_1$. This is chosen such that the duration of episodes spent in environments 0 and 1 respectively in the periodic case match the mean episode durations of the random environmental process.

The above equations provide us with a computational scheme for simulating trajectories of the system. For stochastically-switching environments, environmental switching times are generated randomly from an exponential distribution, using rate parameters λ_1 and λ_0 in environments 0 and 1, respectively.

Equations (3.1) are numerically integrated using the current σ until the next switching time is reached. When the prescribed switching time is reached, we switch environmental state and repeat the process. This procedure is more efficient than direct simulations of the individual-based system, especially for large populations. In particular the time to simulate Eqs. (3.1) does not increase with increasing population size, in contrast to the computing time required by the Gillespie algorithm.

By virtue of the central limit theorem, the strength of the demographic noise scales with the inverse square root of the total size of the population. Hence in the limit of large populations, the contribution of the diffusive terms in the SDEs [Eqs. (3.1)] becomes negligible. Ignoring the diffusive terms leads to a so-called piecewise-deterministic Markov process (PDMP) [50, 51],

$$\mathrm{d}a_t = \left(\mu_\sigma^A a_t - p a_t + q b_t\right) \mathrm{d}t, \tag{3.4a}$$

$$\mathrm{d}b_t = \left(\mu_\sigma^B b_t + p a_t - q b_t\right) \mathrm{d}t. \tag{3.4b}$$

This process evolves deterministically between stochastic environmental switching events, which occur at discrete times. This simplification allows for analytical solutions, and much of our further analysis will be carried out in this limit.

Figure 3.1 (b) shows a typical trajectory for both phenotypes and the environment using the PDMP method in a stochastically switching environment. The size of both populations increases approximately exponentially with time. This provides an *a posteriori* justification for our approximation to neglect intrinsic demographic noise. We note that the population of phenotype A tends to be larger in environmental state 0, and in state 1 phenotype B is usually more abundant, at least once enough time has passed since the last environmental switch.

3.4 Analysis

3.4.1 Stochastic differential equations for population size and composition

The model above is deceptively simple. By ignoring demographic noise, the population dynamics of Eq. (3.4) is a linear dynamical system, described by two coupled ordinary differential equations with Markovian switching. The standard technique to solve the dynamics of coupled linear ODEs is to find the eigenvalues and eigenvectors of the propagating matrix. Along the eigenvectors, growth or decay is exponential with rates equal to the corresponding eigenvalues. There are two subtleties in our particular case. First, when we have Markovian environmental switching, the time between environmental switches is random, and so the matrix describing the propagation of the population from the start of an episode to the end is also random. Second, the eigenvectors of the propagating matrix in one environment do not generally align with those in the other environmental state. As a result, the propagation of the population in the long run is described by products of a sequence of non-commuting random matrices. This makes further analysis difficult. Progress can however be made by introducing the processes

$$n_t = a_t + b_t, \tag{3.5a}$$

$$\phi_t = \frac{a_t}{a_t + b_t}. \tag{3.5b}$$

They describe the total number of individuals in the population, and the proportion of individuals of phenotype A, respectively. Together, the processes n_t and ϕ_t provide an alternative coordinate system for describing the state of the system; such coordinates have been used previously to describe competition in growing populations [52, 53]. With these definitions, Eqs. (3.1a) and (3.1b) become

$$\mathrm{d}n_t = n_t \left[\mu_\sigma^A \phi_t + \mu_\sigma^B (1-\phi_t)\right] \mathrm{d}t + n_t^{+\frac{1}{2}} C_{\sigma 11}(\phi_t)\mathrm{d}W_t^{(1)} + n_t^{+\frac{1}{2}} C_{\sigma 12}(\phi_t)\mathrm{d}W_t^{(2)}, \tag{3.6a}$$

$$\mathrm{d}\phi_t = \left[\Delta_\sigma \phi_t(1-\phi_t) - p\phi_t + q(1-\phi_t)\right] \mathrm{d}t + n_t^{-\frac{1}{2}} C_{\sigma 21}(\phi_t)\mathrm{d}W_t^{(1)} + n_t^{-\frac{1}{2}} C_{\sigma 22}(\phi_t)\mathrm{d}W_t^{(2)}, \tag{3.6b}$$

where $\Delta_\sigma = \mu_\sigma^A - \mu_\sigma^B$. Details of the coefficients $C_{\sigma ij}(\phi)$ are given in the Appendix 3.8.

Equation (3.6a) describes the growth of the total population; the average per capita growth rate is given by the expression in the square bracket. Equation (3.6b) describes the evolution of the proportion of cells expressing phenotype A.

Suppressing again the demographic noise leads to a PDMP description of n_t and ϕ_t, valid in the limit of a large system. The corresponding dynamics are given by Eqs. (3.6), with the noise terms $\mathrm{d}W_t^{(1)}$ and $\mathrm{d}W_t^{(2)}$ removed. Interestingly, in this limit the evolution of the fraction ϕ_t decouples from the evolution of the total population: the proportion of each phenotype in the population is independent of the size of the total population and follows the nonlinear logistic equation obtained from Eq. (3.6b). It is important to stress that the decoupling of the two processes is a consequence of the linearity of the model. More general dynamics will not have this property—for these models the dynamics of ϕ_t and the growth rate may depend on the population size n_t.

Nevertheless, our approach may still offer insight into cases with non-linear interactions, when the dynamics of ϕ_t do not decouple from n_t. For such cases, there will not necessarily be a single optimal phenotyptic switching strategy for all values of n_t, but rather different strategies which are optimal at different values. Therefore it makes sense to study the growth dynamics in a particular region of biological relevance, rather than for every value of n_t. A standard technique for analysing competition in laboratory experiments involves successive dilution steps of a population, in order to limit the population size to some region of biological interest and experimental practicability [54, 55]. The dynamics and growth rates are thus considered in this limited region of n_t only. For our mathematical framework we propose an analogous technique as a potential area of future research, namely to fix the population size at some specific n, and then to study the effective growth rate—the contents of the square bracket in Eq. (3.6a). This technique may also be compared to a birth-death model such as the Moran process, in which the population size is fixed through paired birth and death events [56].

3.4.2 Calculation of average growth rate

The right-hand side of Eq. (3.6a) shows that the instantaneous growth rate is given by

$$\mu_t \equiv \mu_\sigma^A \phi_t + \mu_\sigma^B (1 - \phi_t). \tag{3.7}$$

We are interested in computing the average growth rate of the system, which we write as $\mathrm{E}(\mu)$. This quantity can be understood as the instantaneous growth rate $\dot{n}/n$, averaged over many realisations of the random processes (after a transient time has passed). Since the process ϕ_t is ergodic, this ensemble average is equivalent to an average over a long time. Furthermore, it is easy to show that this average instantaneous growth rate is equivalent to the average rate of the exponential growth of the population over a long time, the so-called 'dominant Lyapunov exponent' [57]. To proceed, it is useful to first consider the average growth rate in a given environmental state σ, for which we write $\mathrm{E}(\mu|\sigma)$. This is the instantaneous growth rate averaged over all points in time at which the environment is in state σ. In order to compute this object and given Eq. (3.7) it is sufficient to know $\mathrm{E}(\phi|\sigma)$—the average value of ϕ in environmental state σ. In order to obtain this object, an average over intrinsic and environmental fluctuations is required. We note that these intrinsic fluctuations are represented in the stochastic differential equations Eqs. (3.6) by multiplicative noise. Further simplification can be achieved in the linear-noise approximation (LNA) [43, 46], valid also for large but finite populations. The LNA consists in replacing ϕ_t in the noise correlators (the coefficients $C_{\sigma ij}$) by the trajectory of the PDMP. In this limit, all fluctuations about the PDMP trajectory due to intrinsic noise will then be symmetrical, and so performing the average of ϕ with respect to intrinsic fluctuations is equivalent to considering the PDMP process only (see also Ref. [58]); the quantity $E(\phi|\sigma)$ then needs to be computed at as an average over the environmental process. Thus, for the remainder of the analysis we concentrate on the PDMP description of ϕ_t,

$$\mathrm{d}\phi_t = [\Delta_\sigma \phi_t (1 - \phi_t) - p\phi_t + q(1 - \phi_t)]\,\mathrm{d}t. \tag{3.8}$$

Figure 3.1 (c) shows a sample path of the PDMP for the proportion of the population with phenotype A, ϕ_t. The process tends towards two different fixed points depending on environmental state. An analysis of Eq. (3.8) shows that there are two

fixed points for each environmental state: one stable ϕ_σ^+, and one unstable ϕ_σ^-. These are given by

$$\phi_\sigma^\pm = \frac{\Delta_\sigma - p - q \pm \sqrt{(\Delta_\sigma - p - q)^2 + 4q\Delta_\sigma}}{2\Delta_\sigma}. \tag{3.9}$$

For our model, $\phi_1^+ < \phi_0^+$ since state 0 favours phenotype A and state 1 favours phenotype B. As the environment switches between states, the process ϕ_t alternates between tending towards these two stable fixed points. After sufficient time has passed, the process will be confined to the interval between the two stable fixed points (ϕ_1^+, ϕ_0^+).

Equation (3.8) describes a single-variable PDMP in a Markovian, two-state environment. Processes of this form have been the subject of recent studies, particularly in the context of gene regulatory networks [37, 48, 59, 60]. Reference [37] provides a general solution for the stationary probability density distribution $\Pi_\sigma^*(\phi)$ for such a process. In the context of the present model, we find

$$\Pi_0^*(\phi) = \tfrac{+\mathcal{N}}{\Delta_0} \left(\phi_0^+ - \phi\right)^{g-1} \left(\phi - \phi_0^-\right)^{-g-1} \left(\phi - \phi_1^+\right)^{h} \left(\phi_1^- - \phi\right)^{-h}, \tag{3.10a}$$

$$\Pi_1^*(\phi) = \tfrac{-\mathcal{N}}{\Delta_1} \left(\phi_0^+ - \phi\right)^{g} \left(\phi - \phi_0^-\right)^{-g} \left(\phi - \phi_1^+\right)^{h-1} \left(\phi_1^- - \phi\right)^{-h-1}, \tag{3.10b}$$

for $\phi \in (\phi_1^+, \phi_0^+)$. These densities are to be interpreted as follows: $\Pi_0^*(u)\mathrm{d}u$ is the probability to find the system in environmental state 0 and with $\phi \in (u, u + \mathrm{d}u]$ in the stationary state. A similar interpretation applies to $\Pi_1(\phi)$. The exponents g and h are given by

$$g = \frac{\lambda_1}{\Delta_0(\phi_0^+ - \phi_0^-)}, \qquad\qquad h = \frac{\lambda_0}{\Delta_1(\phi_1^+ - \phi_1^-)}, \tag{3.11}$$

and $\mathcal{N}$ is determined by normalisation, $\int_{\phi_1^+}^{\phi_0^+} \left[\Pi_0^*(\phi) + \Pi_1^*(\phi)\right] \mathrm{d}\phi = 1$.

Panels (a)–(f) in Figure 3.2 show the resulting stationary distributions for three different rates of environmental and phenotypic switching. In panels (a)–(c) we depict results for stochastic environmental dynamics, and in panels (d)–(f) the environment is periodic. The calculation of the stationary distribution for the periodic case is outlined in the Appendix 3.9. The orange line in each panel shows $\Pi_0^*(\phi)$ and the purple line shows $\Pi_1^*(\phi)$. As seen in the figure, the distributions are peaked near the two fixed points when environmental switching is slow [panels (a) and (d)]. At fast environmental switching rates, the system spends most of its time in the central region away from the fixed points [panels (c) and (f)].

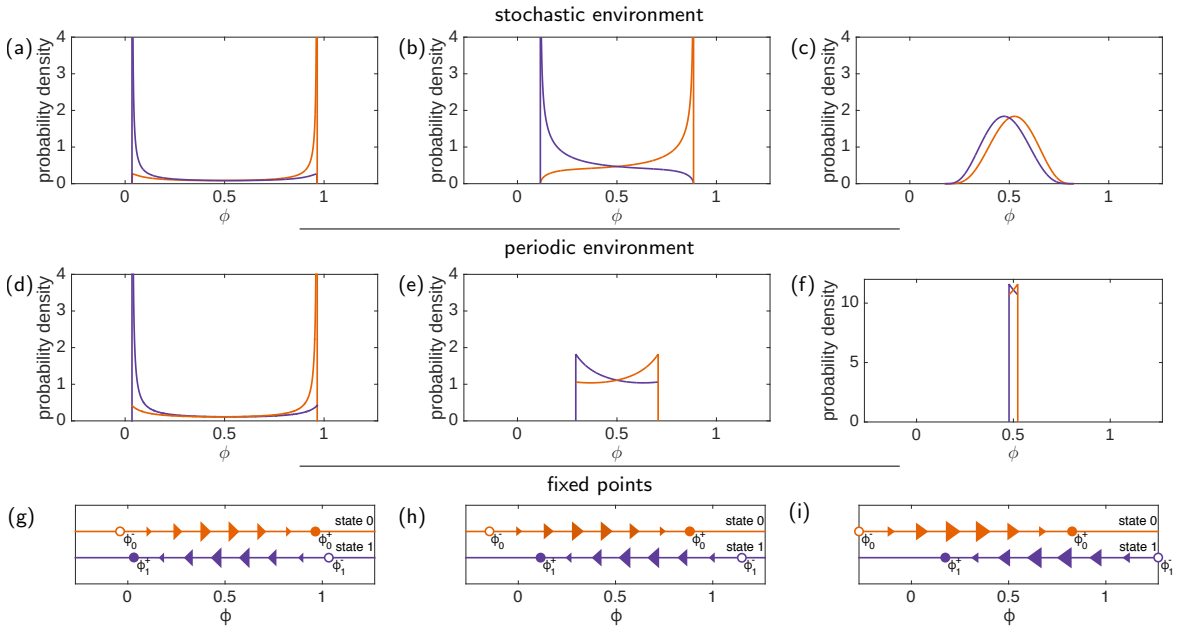

Figure 3.2: Panels (a), (b), and (c) show the stationary distributions of ϕ—the proportion of cell in phenotype A—for the case of a stochastic environment. These distributions are obtained from Eq. (3.10). From left to right, panels correspond to increasing environmental switching rates. The orange line shows $\Pi_0^*(\phi)$, and the purple line $\Pi_1^*(\phi)$ (see text for details). In the case of slow environment switching (a), the distribution is sharply peaked at the two fixed points whereas in the case of fast environmental switching (c) the distribution is peaked in the central region between the two fixed points. Panels (d), (e), and (f) show the stationary distributions for the case of a periodic environment. Panels (g), (h), and (i) depict the positions of stable and unstable fixed points and the direction of flow in each state. Parameters are from set (a) (see text and Appendix 3.7), along with: (a),(d), and (g) $\lambda_1, \lambda_0 = 0.10$, $p, q = 0.064$; (b),(e), and (h) $\lambda_1, \lambda_0 = 1.0$, $p, q = 0.24$; (c),(f), and (i) $\lambda_1, \lambda_0 = 10$, $p, q = 0.40$.

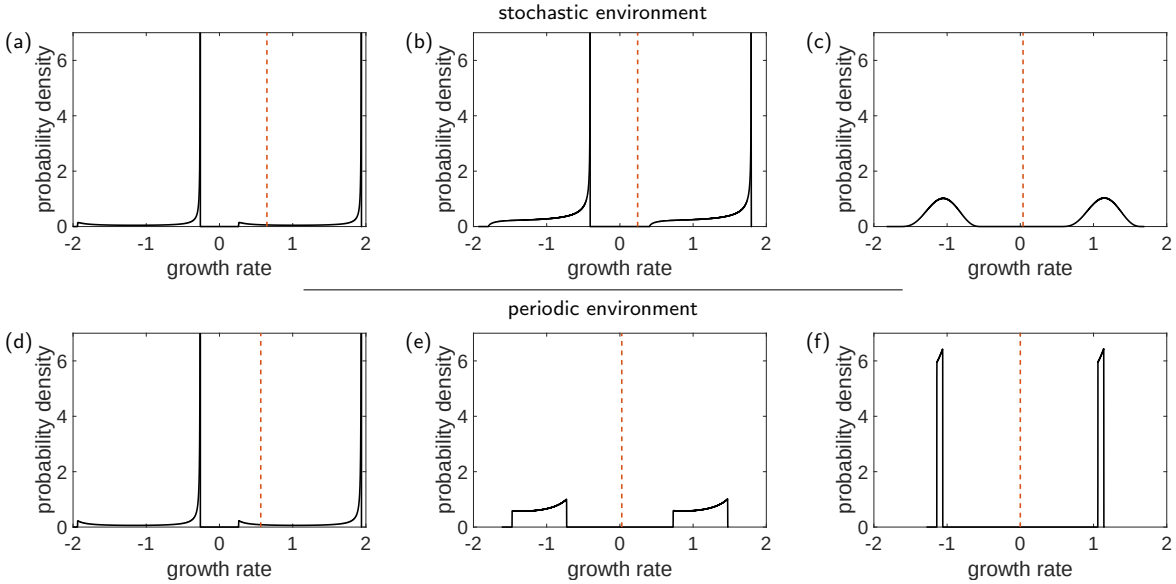

Figure 3.3: Distributions of the instantaneous growth rate for the case of stochastic environmental dynamics [panels (a), (b), and (c)], and periodic environment [panels (d), (e), and (f)]. Environmental switching rates increase from the panels on the left to those on the right. Each distribution consists of two distinct components, corresponding to the two environments. The dashed line indicates the average growth rate. Parameters are the same as in Fig. 3.2.

The distributions in Eqs. (3.10) can be used to calculate the probability density of growth rates via Eq. (3.7). For the case of stochastic environments these are shown in Fig. 3.3 (a–c). We proceed to study the fitness of a given phenotypic switching strategy (i.e., given switching rates p and q). To do this we focus on the average growth rate

$$\mathrm{E}\left(\mu\right) = P_0^* \mathrm{E}\left(\mu|0\right) + P_1^* \mathrm{E}\left(\mu|1\right), \tag{3.12}$$

where we have

$$\mathrm{E}\left(\mu|\sigma\right) = \mu_\sigma^A \mathrm{E}\left(\phi|\sigma\right) + \mu_\sigma^B \left[1 - \mathrm{E}\left(\phi|\sigma\right)\right], \tag{3.13}$$

and where P_σ^* is the probability of finding the environment in state σ in the stationary state. In the two-state system these are given by $P_0^* = \lambda_0/(\lambda_1 + \lambda_0)$ and $P_1^* = \lambda_1/(\lambda_1 + \lambda_0)$. The expectation value $\mathrm{E}\left(\phi|\sigma\right)$ is given by

$$\mathrm{E}\left(\phi|\sigma\right) = \int_{\phi_1^+}^{\phi_0^+} \frac{\phi \Pi_\sigma^*(\phi)}{P_\sigma^*} \, \mathrm{d}\phi. \tag{3.14}$$

Using Eqs. (3.10) we therefore have a closed integral equation for the average growth rate of the population. Evaluating Eq. (3.14) numerically, and substituting into Eq. (3.12) provides a very efficient way of calculating the average growth rate in

terms of the model parameters. Results for the mean growth rate are indicated as dashed vertical lines in Fig. 3.3. The analysis below is for phenotypic switching rates, p and q, which do not depend on the state of the environment. We note that the mathematical formalism applies to the case of environment-dependent switching rates as well; the calculation of the average growth rate can still be carried out if we replace p and q with environment-dependent phenotypic rates p_σ and q_σ. The dynamics are still reducible to a two-state PDMP for a single degree of freedom, and the stationary distribution can be obtained. Thus, the theory above provides an analytical formalism to investigate this case.

In the following section we use our solution to investigate the optimum switching strategy, i.e., the switching rates p, q which allows the cells to best proliferate. Conversely, we also identify the optimum environmental switching rates, i.e., the switching rates λ_0, λ_1 which best inhibit the growth of cells.

3.5 Results

In the context of our model, the biological strategy of bet-hedging refers to heterogeneity in the population to increase resilience against environmental changes, while at the same time maintaining the capability of growth. Specifically, we will quantify 'temporal' heterogeneity below—the extent to which both phenotypes are present over the course of time, but not necessarily simultaneously. For example, a population may largely consist of only one phenotype at any one time, but as the environment changes state, both phenotypes may be expressed in turn. Viewed over time such a population would be heterogeneous.

In our model, in the absence of external stress (state $\sigma = 0$), phenotype A has a higher fitness. On the other hand, not having any individuals of type B in the population is risky, as phenotype A is more susceptible to the stresses in environment $\sigma = 1$. The bet is hence hedged (the risk limited) by maintaining the capacity for a population of persister cells to establish itself should an external stress occur. The analysis in Sec. 3.4 provides the tools necessary to investigate the mechanics of bet-hedging. In particular, we have obtained an expression for the average growth rate, which can be evaluated numerically by a single integration. This significantly reduces

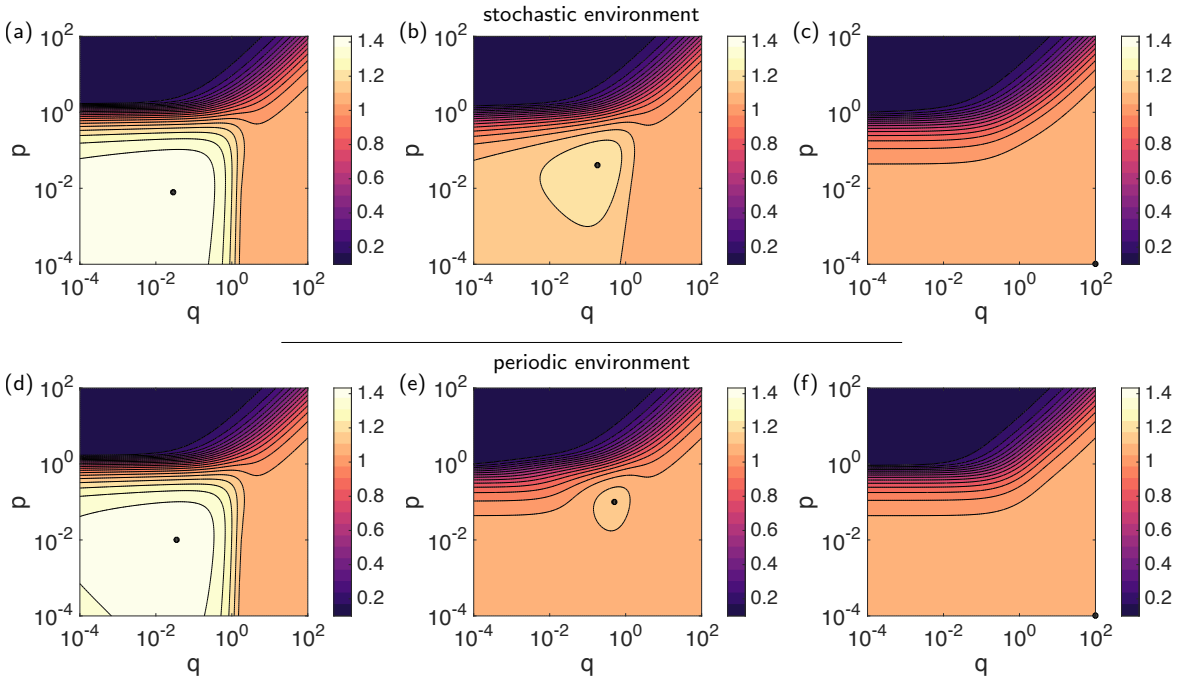

Figure 3.4: Heatmap plot of the average growth rates for different values of the phenotypic switching rates p and q. Panels (a), (b), and (c) show the case of a stochastic environment, and panels (d), (e), and (f) show that of a periodic environment. Environmental switching rates λ_1 and λ_0 increase from left [(a), (d)] to right [(c), (f)]. The black circle in each panel indicates the switching strategy which optimises the growth rate. When the environmental switching rates are slow, there is a non-trivial p and q maximising the growth rate. This means heterogeneity has a fitness advantage. When the environmental switching is fast, homogeneity is favoured. The stochastic case is found to have a higher growth rate than the periodic case for every value of p and q. Parameter set (a) (see Appendix 3.7) is used, along with: (a) and (d) $\lambda_1 = 0.010$, $\lambda_0 = 0.033$; (b) and (e) $\lambda_1 = 0.10$, $\lambda_0 = 0.33$; (c) and (f) $\lambda_1 = 1$, $\lambda_0 = 3.3$.

the computing time required to analyse the dynamics, in contrast to direct Monte Carlo simulation of the individual-based model [44]. This allows us to explore a wide range of parameter space to investigate bet-hedging strategies.

3.5.1 Optimal rate of phenotypic switching rate for stochastic environments

We first study the dependence of the average growth rate on phenotypic switching rates, for given environmental switching dynamics. We consider different regimes of environmental dynamics, ranging from slow to fast, relative to the time scale of the growth of the population.

Figure 3.4 shows how the average growth rate depends on the phenotypic switching

rates p and q. The parameters μ_σ^A and μ_σ^B, describing the growth rates of each phenotype, are fixed; panels (a), (b) and (c) correspond to regimes with increasingly fast environmental switching rates λ_0 and λ_1. When the environment switches relatively slowly, as in panels (a) and (b), there is a non-trivial phenotypic switching strategy which maximises the average growth rate, indicated by a black circle. When the environment switches very quickly, as in panel (c), the optimum strategy is found at the extremes of p and q, indicating that it is best for the population to express only a single phenotype [phenotype A in the case of Fig. 3.4 (c)]. These results are in agreement with previously reported work in similar systems [28, 61, 62]. In other words, when environmental changes are slow, heterogeneity conveys a fitness advantage, whereas homogeneity is more beneficial in the face of fast environmental changes.

This behaviour is further illustrated in Fig. 3.5 (a). Here, we show how the optimum phenotypic switching rates vary as we increase the environmental switching rates λ_0 and λ_1, but keeping their ratio λ_0/λ_1 fixed, (i.e., the relative amount of time spent in each environment). We identify three regimes. When the environmental switching is slow, the optimum switching strategy is achieved when the phenotypic switching rates match the environmental rates: $p = \lambda_1$ and $q = \lambda_0$.

For environmental switching in an intermediate regime, the optimum strategy involves phenotypic switching rates which are much slower than the environmental switching rates. When the environment switches very quickly, the optimum strategy is not to switch between phenotypes at all, as discussed above. Instead, it is best for the cells to keep expressing whichever phenotype is better on average. That is, always express phenotype A if $P_0^*\mu_0^A + P_1^*\mu_1^A < P_0^*\mu_0^B + P_1^*\mu_1^B$, and always phenotype B otherwise. The growth rate is then $P_0^*\mu_0^A + P_1^*\mu_1^A$, or $P_0^*\mu_0^B + P_1^*\mu_1^B$, respectively.

Our analytical findings for the regime of a slow environmental process are consistent with previous results by Thattai *et al.* [17], who studied both periodic and stochastic environments in numerical simulations. Results for periodically-switching environments can also be found in Refs. [28, 61]. Kussell and Leibler [33] report analytical results for randomly switching environments, using an approach based on maximising the average growth rate by minimising the transient time it takes a population to reach its environment-dependent quasi-stationary state.

Several quantitative measures of heterogeneity can in principle be considered. We

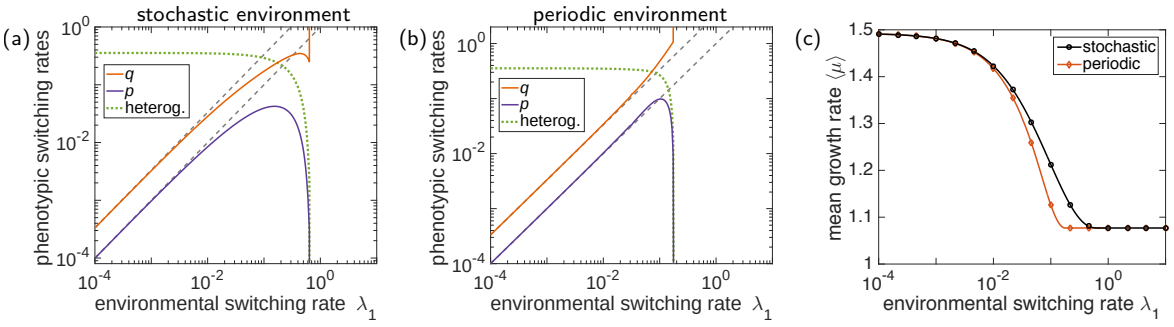

Figure 3.5: (a) The optimum phenotypic response as a function of environmental switching rates for a stochastic environment. The ratio of the environmental switching rates is fixed at $\lambda_0 = \frac{10}{3}\lambda_1$. The vertical axis shows the phenotypic switching rates p and q which maximise the average growth rate. The grey, dashed lines show the environmental switching rates λ_0 and λ_1 for comparison. When the environment switches slowly, the optimum strategy is given by matching the environmental rates: $p = \lambda_1, q = \lambda_0$. At faster environmental switching rates, the optimum strategy involves switching more slowly than the environment. At very fast environmental switching rates, the best strategy is to stay in one particular phenotype ($p \to 0$). (b) The optimum phenotypic as a function of environmental switching rates for a periodic environment. The periods the environments spends in state 0 and 1 have fixed durations, $1/\lambda_0$ and $1/\lambda_1$, respectively. At slow environmental switching rates, the optimum strategy is for the phenotypic switching rates to match the environment. At faster switching rates, the optimum strategy is to stay in a particular phenotype. For intermediate switching rates, phenotype switching rates slightly faster than the environment maximise the growth rate. The transition from heterogeneity to homogeneity occurs at slower environmental dynamics as in the stochastic case. The green dotted lines in panels (a) and (b) show the measure of temporal heterogeneity defined in the text. (c) Mean growth rate achieved by optimum choice of phenotypic switching rates p and q as we proportionally increase environmental switching rates. The markers indicate the results of Monte Carlo simulation of the PDMP and the periodic process. The mean growth rate in the case of stochastic environments is found to be universally larger than in periodic environments. Parameters μ_σ^A and μ_σ^B are as in the previous figures (set (a)).

focus on measuring 'temporal' heterogeneity, i.e., the extent to which both phenotypes exist over the course of time. To this end, we use a variation of Simpson's diversity index [63], and define heterogeneity as the probability that two cells selected at random from the population at two different times are of different phenotypes. Assuming that the individuals are sampled at two widely spread times, this probability is given by $2\langle\phi\rangle(1-\langle\phi\rangle)$. We have indicated this quantity in Fig. 3.5 (a) and (b). The data confirms that the population is heterogeneous for slow environmental switching, but homogeneous when the environmental dynamics are fast.

Our calculation of the mean growth rates and composition of the population allows us to address a related question concerning the dependence of phenotypic heterogeneity and the optimal phenotypic switching rate on the ratio of the two environments λ_0/λ_1. We summarise our findings here, rather than present the details. In the regime of very slow environmental switching, the optimum strategy involves phenotypic switching for all values of the ratio λ_0/λ_1. This is because enough time passes in each environmental episode for the population to reach and benefit from its optimising quasi-stationary distribution. In the intermediate-switching regime, however, if a much longer time is spent on average in one environment than in the other it becomes optimal to express only the phenotype which performs best in this more frequent environment.

3.5.2 Optimal rate of phenotypic switching rate for periodic environments

We perform a parallel study of the model with periodic environmental switching, described by Eq. (3.3). When the environment switches periodically and the infinite-population limit is taken, the dynamical system becomes deterministic. In the long run, the trajectory of $\phi(t)$ then converges to a limit cycle. In environment 0 phenotype A is favoured; $\phi(t)$ increases until it reaches a 'turning point' ϕ_{high} when the environment switches. Then, in environment 1 phenotype B is favoured; $\phi(t)$ decreases until turning point ϕ_{low}, at which point the environment returns to state 0. It is straightforward to numerically evaluate ϕ_{high} and ϕ_{low}. As the trajectory tends to a limit cycle, we can compute the stationary distribution, i.e., the probability density of finding the variable $\phi(t)$ at a given point in the interval $[\phi_{\text{low}}, \phi_{\text{high}}]$ at a randomly chosen time.

Further details of the mathematical method can be found in the Appendix 3.9.

A comparison between the distributions of ϕ for stochastic and periodic switching environments is presented in Fig. 3.2. This figure shows that the domain in which the distribution of ϕ is non-zero is larger in the case of stochastic switching than for periodic environments. The effect is less pronounced for slow switching than for fast switching. When the environment switches stochastically, it is possible for the duration of each episode in a fixed state σ to last longer than in the periodic case. As a result the trajectory of the PDMP can exceed the deterministic extremes ϕ_{low} and ϕ_{high} of the periodic case.

This difference has significant consequences for the growth rates and resulting phenotypic switching strategies. Figure 3.3 shows the distribution of growth rates for both cases. As one can see, these distributions are broader for the case of stochastic environments than for periodic environmental changes, especially for intermediate and fast switching. Figure 3.4 (d)–(f) shows the numerically computed average growth rate in periodically switching environments as a function of phenotypic switching rates p and q (and for given λ_0, λ_1). The growth rates for each p and q is generally lower than that of the system with stochastic environmental dynamics with the same parameters.

Similarly to Figure 3.5 (a), Figure 3.5 (b) shows the optimum phenotypic switching strategy, but for the case of a periodically switching environment. Superficially, the two figures look similar. In each we identify two extreme regimes of behaviour: (i) the limit of slow environmental switching where the optimum phenotypic strategy is to switch with the same rates as the environment, and (ii) the fast environmental regime where homogeneity is preferred. In the case of stochastic environmental dynamics, Figure 3.5 (a), an intermediate regime can be detected; this is however largely absent in the case of deterministic periodic environmental dynamics, where the transition between regimes (i) and (ii) is more abrupt [Figure 3.5 (b)]. A closer analysis reveals further differences between the cases of stochastic and periodic environments. For environmental dynamics at intermediate rates, i.e., between regimes (i) and (ii), the optimum phenotypic switching rates differ by as much as an order of magnitude between the stochastic and periodic cases. We also see that the stochastic case favours heterogeneity at much higher switching rates than the periodic case.

Figure 3.5 (c) shows how the average growth rates compare in the cases of a Markovian environment and a periodically switching environment when the optimum phenotypic strategy is in effect. Stochastic switching produces a growth rate that is universally larger than in the periodic switching case. We found the same result for all tested parameters and for all values of phenotypic switching; similar results were previously also reported in Ref. [17]. We note that even small differences in the growth rate can lead to significant differences in population size over long times, as the growth is exponential.

The explanation for this enhancement in growth rate is as follows: At any point in time, the instantaneous growth rate is given by Eq. (3.7). The distribution of ϕ hence directly translates into a distribution of μ, as illustrated in Figs. 3.2 and 3.3. The difference between the growth rates for stochastic and periodic environments is most pronounced in the intermediate switching regime; the distributions of ϕ in this regime are shown Figs. 3.2 (b) and (e), for the cases of stochastic and periodic environments respectively. Figs. 3.3 (b) and (e) show the corresponding distributions of growth rates. For periodic switching the distribution of ϕ is largely flat, with only minor peaks near the fixed points when the flow field in either environment is slow. Conversely, stochastic environmental dynamics permit long episodes of time spent in a particular environment. In such long episodes the variable ϕ will mostly reside near the relevant fixed point, generating the peaked behaviour seen in Fig. 3.2 (b). Recalling that phenotype A grows more quickly than B in environment 0 and vice versa in environment 1, we conclude that the system is well-adapted to the environmental state at each of these peaks. This leads to an overall enhanced growth rate, relative to the periodic case.

The case of Markovian switching and the case of periodic switching are two extreme descriptions of the environmental process; we might expect a real-world environment to change with dynamics somewhere in-between [17]. Our analysis suggests that, for an environment with dynamics between these two extremes, the average growth rate would fall somewhere in-between as well, and similarly for the optimum phenotypic switching rate.

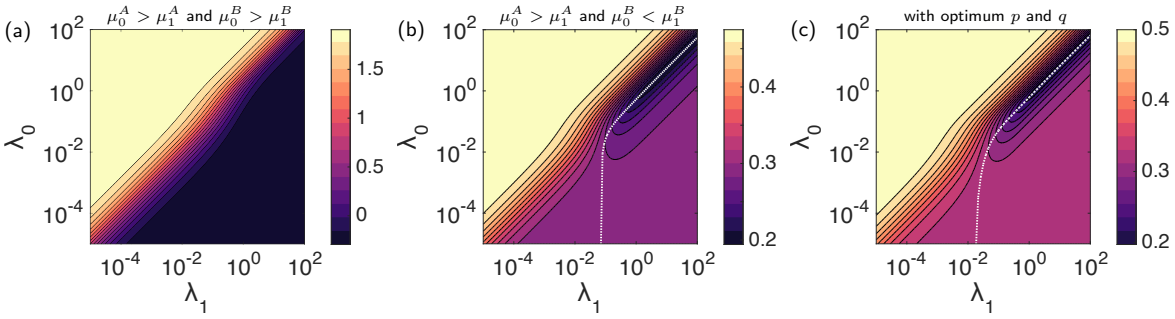

Figure 3.6: (a) Heatmap plot of the average growth rate as a function of λ_1 and λ_0 using parameter set (a) as in the previous figures. The phenotypic switching rates are $p = 0.1 = q = 0.1$. For these parameters the lowest growth rate is achieved when permanently in the stress state, $\lambda_0 = 0$. (b) The same quantity for parameter set (b), where $\mu_0^A > \mu_1^A$ and $\mu_0^B < \mu_1^B$. The phenotypic switching rates are fixed at $p = 0.0275$, $q = 0.0425$. The growth rate decreases as both switching rates are decreased in proportion. For a given λ_0 there is a non-trivial value of λ_1 which minimises the growth rate, shown here as a white line. It tend towards a straight line–a constant ratio which is given by Eq. (3.15): $\lambda_0/\lambda_1 = 0.557$ resulting in an average growth rate of $\langle\mu\rangle = 0.194$. (c) Heatmap plot for the *optimum* average growth rate as a function of the environmental switching rates: at each position on the graph the population of cells uses the optimum phenotypic switching strategy for the given environmental process. Parameters μ_σ^A and μ_σ^B as in panel (b). When the switching is sufficiently fast, there is a ratio of environmental switching rates which minimises the cell's best possible growth rate. This ratio is given by Eq. (3.16).

3.5.3 Optimal environmental switching strategy to inhibit population growth

The environmental switching dynamics can be used to model a host immune response [12, 17]. By switching between the two states, we assume the host aims to minimise the average growth rate of the population. In another application, the phenotypes can be wildtype bacteria and antibiotic-resistant strain, and the two environmental states represent the absence and presence of antibiotic treatment. The goal is then again to minimise growth, by varying the environmental protocol. Our analysis allows us to investigate the dependence of the growth rate on environmental switching rates λ_0 and λ_1. In this Section we investigate which environmental switching strategy best inhibits the growth of the population. The figures shown here are for stochastic environmental switching, however we found qualitatively similar results for periodic environments.

Figure 3.6 (a) and (b) show how the average growth rate changes if we vary the environmental switching rates for fixed phenotypic switching rates p and q. Each panel represents a different set of parameters. The case shown in Figure 3.6 (a) is a

representation of bacteria in which both phenotypes are disadvantaged by the presence of an antibacterial agent, but in which the persister phenotype is affected less by the external stress than the normal phenotype. Mathematically one has $\mu_0^A > \mu_1^A$, $\mu_0^B > \mu_1^B$, $\mu_0^A > \mu_0^B$, and $\mu_1^B > \mu_1^A$. Specifically, we use the parameter set used in previous studies [23], and we will refer to this as parameter set (a) in the text which follows; the numerical values can be found in the Appendix 3.7. Unsurprisingly, the average growth rate is minimised when the environment stays in environmental state 1 (i.e., $\lambda_0 = 0$), which can be seen as representing the antibiotic state. Another trend shown by our results is that proportionally increasing both environmental switching rates universally decreases the average growth rate. That is, proportionally faster switching rates better inhibit the growth of a population. This result has been found for all tested parameters, suggesting that the best way apply antibiotics may involve many short periods of antibiotic treatment.

The parameters used in Fig. 3.6 (b) differ from those in Fig. 3.6 (a) in that here $\mu_0^A > \mu_1^A$ and $\mu_0^B < \mu_1^B$. We use the parameters of Ref. [24], and will refer to this as parameter set (b) in the text which follows; numerical values are again given in Appendix 3.7. Here, phenotype A performs better in environment 0 than in environment 1, and phenotype B performs better in environment 1 in environment 0. In this case, the optimum environmental strategy involves non-trivial switching. The white line in panel Fig. 3.6 (b) indicates the optimum choice of λ_1, for given λ_0. When both λ_0 and λ_1 are large growth is minimised for a non-trivial ratio, λ_1/λ_0.

The limit of infinitely fast environmental switching can be characterised analytically. In this limit, the dynamics can be modelled using ordinary differential equations, using effective mean birth and death rates [64,65]. Minimising the growth rate in this limit leads to an equation describing the optimum environmental strategy to inhibit the growth of the population. The minimal growth rate is found when P_0^*, the probability of being in environmental state 0, is given by

$$P_0^* = \frac{-\Delta_1 + p - q}{\Delta_0 - \Delta_1} - \left(\frac{-pq}{(\mu_0^A - \mu_1^A)(\mu_0^B - \mu_1^B)} \right)^{1/2}. \tag{3.15}$$

The argument of the square root indicates a necessary condition (up to relabelling) for the existence of this optimum, $\mu_0^A > \mu_1^A$ and $\mu_0^B < \mu_1^B$. This explains why we have no non-trivial minimum in the fast-switching limit for the parameters used in Fig. 3.6 (a),

but there is one for the parameters used in Fig. 3.6 (b). The analytical optimum given by Eq. (3.15) agrees with the results shown in Fig. 3.6 (b).

3.5.4 Co-evolution of host and pathogen

The interplay between the growth-maximising strategy of the cells and the growth-minimising strategy of the environment provides an interesting scenario. Given a set of environmental switching rates, there can be phenotypic switching rates which maximise the average growth rate. Conversely, for given phenotypic switching rates, there can be non-trivial environmental switching rates which minimise the growth rate. This suggests the possibility of a combined set of rates, from which the growth rate cannot be increased by unilaterally changing p and q (the 'strategy' of the population), and from which the growth rate cannot be decreased by unilaterally changing λ_1 and λ_0 (the strategy of the hosting environment). From a game-theoretic perspective, neither player of the game (the population of cells and the immune system) can improve their performance by changing their strategy. This can be viewed as a Nash equilibrium [38].

For a given set of model parameters, μ_σ^A, μ_σ^B and given environmental switching rates, optimal phenotypic switching rates can be found by evaluating Eq. (3.12) for different values of p and q, and then identifying the maximum. This maximum can then be studied as a function of λ_0 and λ_1. For parameter set (a) the evolutionarily optimising strategy is found to be trivial: the environment stays in the stress state and the cell expresses the persister phenotype only, leading to an overall growth rate μ_1^B.

For parameter set (b), however, the results are less trivial, since each phenotypes prefers a different environment. Figure 3.6 (c) shows the average growth rate given optimal phenotypic switching in this case. This figure was constructed as follows: for each combination of λ_0 and λ_1 we found the values of p and q maximising the growth rate. The value of this maximum is then plotted in the figure. For each value of λ_1 the white line in the figure depicts the value of λ_0, which minimises this maximum achievable growth rate; from the point of view of the hosting environment this line shows the best choice of λ_0 for each λ_1. As before, the growth rate decreases as the environmental switching rates are increased proportionally. Hence, the environment's

best strategy is to switch states quickly, and with a choice of λ_0/λ_1 so that switching rates fall on the white line in Figure 3.6 (c).

As discussed in earlier sections the maximising phenotypic strategy in the limit of fast environments leads to homogeneity, i.e., it is best for the population to only express the phenotype does better in a (weighted) average over both environmental states. This gives a growth rate which is the greater of $P_0^*\mu_0^A + P_1^*\mu_1^A$ and $P_0^*\mu_0^B + P_1^*\mu_1^B$. Inspecting these expressions, one finds that changing the ratio of λ_0 and λ_1 increases one of the quantities and decreases the other. It follows that the greater of the two growth rates is minimised when both growth rates are equal. This the case when

$$\frac{\lambda_0}{\lambda_1} = -\frac{\Delta_1}{\Delta_0}. \tag{3.16}$$

This gives us the proportion of each environmental state which minimises the average growth rate in the limit of fast environmental switching, given an optimally switching population. This minimum optimum growth rate is given by

$$\langle\mu\rangle = \frac{\mu_1^B\mu_0^A - \mu_0^B\mu_1^A}{\mu_0^A + \mu_1^B - \mu_0^B - \mu_1^A}. \tag{3.17}$$

The phenotypic switching strategy of the cell cannot change to increase the growth rate. Similarly, if the environment assumes that the cell population will optimise its phenotypic switching strategy, the environment cannot move to minimise the growth rate. We remark that the final rate is independent of the phenotypic switching rates p and q, i.e., the environment's minimisation of the growth rate removes the effect of the phenotypic switching strategy altogether.

The analytical result from Eq. (3.16) agrees with the ratio given defined by the fast-switching asymptote of the white line in Fig. 3.6 (c). The minimum growth rate in this case is 0.197, which is significantly less than if the environmental states did not switch, which would result in growth rates 0.5 or 0.325, respectively, for the two environmental states.

3.6 Conclusions

In conclusion we have studied a stylised model of phenotypic switching strategies in the face of changing environments. We have focused on the role of time scales of

phenotypic and environmental switching for the growth of the population, and our analysis addresses in particular the case of stochastically switching environments.

In contrast to some existing work, our analysis starts from an explicit individual-based model of the population dynamics, defined by birth events, death events, and stochastic phenotypic switching. Our analysis then proceeds through the formulation of a piecewise-deterministic Markov process. This allows us to derive closed-form solutions for the resulting growth rates of the population for general environmental and phenotypic switching rates. Our work complements existing literature which, for mathematical convenience, has often concentrated on strictly periodic environmental dynamics. We systematically compare the cases of periodic versus stochastically switching external conditions. Our main results can be summarised as follows: (i) Using our theory, we demonstrated that the optimal phenotypic switching rates are equal to the rates of the environmental process ($p = \lambda_1, q = \lambda_0$) for slow stochastic environmental dynamics. This result was previously reported in simulations [17, 33]. For environmental dynamics in an intermediate regime the optimal switching rates are markedly lower than those of the environment. (ii) The optimal bet-hedging strategy of the bacterial population favours heterogeneity (both phenotypes present) in slow environments, but is replaced by a homogeneous strategy (one phenotype only) for fast switching. The transition between these regimes is sudden as the switching rates of the environmental process are increased. We find that stochastic environments favour heterogeneity over a larger range of environmental dynamics than a strictly periodic environment. (iii) Instantaneous growth rates are universally higher in the case of stochastic environments than in the periodic case. Our analysis shows that this due to the possibility to spend long periods of time in either environment when the environmental process is stochastic—a possibility that is absent for strictly periodic environments. (iv) The combined system of population and environment can be interpreted as the interaction between a hosting environment and a pathogen. The host tries to control environmental switching to minimise growth of the pathogen. The pathogen, on the other hand, attempts to maximise its growth rate by phenotypic switching with optimised rates. Our analysis shows that mutual best-response scenarios can be identified, in which neither the host nor the pathogen can improve by unilateral changes of their strategy. This is akin to the concept of Nash equilibria in

game theory.

In this paper, we developed a mathematical framework for the analysis of phenotypic switching in stochastic environments. More broadly, our work is applicable to ecological models of competition in dynamic random external conditions. Such problems are widespread in theoretical ecology, in predator-prey models effectively random environments could for example account for external shocks such as earthquakes and epidemics [66–68]. Our work can provide insights into the mechanics of such problems, and as a key contribution, the analytical computation of average growth rates allows one to dispense with costly Monte Carlo simulations.

We stress that the model we have focused on is stylised and could naturally be extended in many different ways to describe more realistic and complicated features. This may include models in which the dynamics of the environment are coupled to the state of the population of microbial species [35]. Further complications also occur when there are more than two environmental states. We have chosen the stylised scenario of a binary environment as it represents situations in which an external stress is either absent or present. A model with two environmental states and two phenotypes, each doing best in one of the two environments, is a minimal, but non-trivial baseline. While it is unsurprising that much of the existing literature has focused on this case, models with more environmental states have for example been studied in [33]. To obtain interesting scenarios it is then also necessary to introduce multiple phenotypes. While a detailed extension of our analysis to such cases is pending we expect many of the results to be qualitatively similar in this case. Several recent papers [69–71] consider the role of a continuous environment, and it would be interesting and challenging to establish the exact relation between these two approaches. We highlight this as a potential area for future research. We note in particular that environmental processes based on stochastic differential equations may lead to scenarios in which the environment spends significant time in intermediate states, a possibility that is excluded by construction in our model. It is not clear if, when, and how these differences affect the response of the population. The phenotypic switching rates themselves are treated as static in our model; this is an approximation as well, bacteria have been demonstrated to sense and adapt to external conditions [72, 73]. Incorporating this type of SOS response is another line of future work to make models of phenotypic switching more realistic.

The formalism we have presented can be applied to study such cases.

3.7 Appendix A: Model parameters

We consider the model for two different sets of parameters, $\mu_\sigma^{A,B}$. Parameter set (a) was previously used by Patra and Klumpp [23], and is shown in Table 3.1 (a). In this case, both phenotypes A and B perform better in environment 0 (no external stress) than in environment 1 (with external stress). The persister phenotype B grows more slowly state 0, but also decays less quickly in state 1. This model is a classic representation of bacteria in which both phenotypes are disadvantaged by the presence of an antibacterial agent, but in which the persister phenotype is affected less by the external stress than the normal phenotype. Mathematically one has $\mu_0^A > \mu_1^A$, $\mu_0^B > \mu_1^B$, $\mu_0^A > \mu_0^B$, and $\mu_1^B > \mu_1^A$.

The second set of parameters was previously used by Belete and Balázsi [24], see Table 3.1 (b). These parameters have different properties: phenotype B now performs better in environment 1 than it does in environment 0; i.e., $\mu_0^A > \mu_1^A$, $\mu_0^B < \mu_1^B$, $\mu_0^A > \mu_0^B$, and $\mu_1^B > \mu_1^A$.

(a)

μ_0^A	2.0 h^{-1}
μ_0^B	0.2 h^{-1}
μ_1^A	−2.0 h^{-1}
μ_1^B	−0.2 h^{-1}

(b)

μ_0^A	0.5000 h^{-1}
μ_0^B	0.0001 h^{-1}
μ_1^A	0.0001 h^{-1}
μ_1^B	0.3250 h^{-1}

Table 3.1: The two parameter sets: (a) from Ref. [23], and (b) from Ref. [24].

3.8 Appendix B: Derivation of diffusive process with Markovian switching

3.8.1 Kramers–Moyal expansion

The individual-based model describes the evolution of three random processes: the number of individuals with phenotype A (a_t), the number of individuals with phenotypes B (b_t), and the state of the environment ($\sigma_t \in \{0, 1\}$). The master equation describes the time evolution of the probability distribution of these random processes,

and is given by

$$\begin{aligned}\frac{\mathrm{d}}{\mathrm{d}t}P_{a,b,\sigma}(t) = &\left(\mathcal{E}_a^{-1}-1\right)\alpha_\sigma a P_{a,b,\sigma}(t)\\ &+\left(\mathcal{E}_b^{-1}-1\right)\beta_\sigma b P_{a,b,\sigma}(t)\\ &+\left(\mathcal{E}_a^{+1}-1\right)\gamma_\sigma a P_{a,b,\sigma}(t)\\ &+\left(\mathcal{E}_b^{+1}-1\right)\delta_\sigma b P_{a,b,\sigma}(t)\\ &+\left(\mathcal{E}_a^{+1}\mathcal{E}_b^{-1}-1\right)pa P_{a,b,\sigma}(t)\\ &+\left(\mathcal{E}_a^{-1}\mathcal{E}_b^{+1}-1\right)qb P_{a,b,\sigma}(t)\\ &+\lambda_\sigma P_{a,b,1-\sigma}(t)-\lambda_{1-\sigma}P_{a,b,\sigma}(t)\end{aligned} \tag{3.18}$$

where $P_{a,b,\sigma}(t)$ is the probability of random processes (a_t, b_t, σ_t) having values (a, b, σ) at time t.

For compactness, we suppress the explicit time dependence of the probability distribution. The notation $\mathcal{E}_a^{\pm}$ and $\mathcal{E}_a^{\pm}$ represents the step operators,

$$\begin{aligned}\mathcal{E}_a^{\pm}f(a,b) =& f\left(a\pm 1, b\right),\\ \mathcal{E}_b^{\pm}f(a,b) =& f\left(a, b\pm 1\right),\end{aligned}$$

where $f(a, b)$ is a generic function of a and b.

We proceed to approximate the master equation by means of a Kramers–Moyal expansion [34, 46], i.e., we replace the step operators by the first two non-trivial terms in their Taylor expansion. The variables a and b become continuous during this process, which is valid in the limit of large populations. Collecting terms up to order a^{-2} or b^{-2} and maintaining the discreteness of the environmental switching we find that the probability density $\Pi_\sigma(a, b)$ is governed by the following equation

$$\begin{aligned}\partial_t\Pi_\sigma(a,b) = &-\partial_a\left(\mu_\sigma^A a - pa + qb\right)\Pi_\sigma(a,b)\\ &-\partial_b\left(\mu_\sigma^B b + pa - qb\right)\Pi_\sigma(a,b)\\ &+\tfrac{1}{2}\partial_a^2\left(\alpha_\sigma a + \gamma_\sigma a + pa + qb\right)\Pi_\sigma(a,b)\\ &+\tfrac{1}{2}\partial_b^2\left(\beta_\sigma b + \delta_\sigma b + pa + qb\right)\Pi_\sigma(a,b)\\ &-\partial_a\partial_b\left(pa + qb\right)\Pi_\sigma(a,b)\\ &+\lambda_\sigma\Pi_{\sigma'}(a,b) - \lambda_{\sigma'}\Pi_\sigma(a,b).\end{aligned} \tag{3.19}$$

The first two terms on the right-hand side are the drift terms as found in the Fokker–Planck equation [47], describing the flow of probability along the a and b directions,

the next three terms describe diffusion, and the final two terms represent the random switching between the two environmental states. This Fokker–Planck equation has the diffusion matrix

$$D_\sigma = \begin{pmatrix} a\left(\alpha_\sigma + \gamma_\sigma\right) + pa + qb & -pa - qb \\ -pa - qb & b\left(\beta_\sigma + \delta_\sigma\right) + pa + qb \end{pmatrix}. \tag{3.20}$$

The process described by the Fokker–Planck equation can be equivalently formulated as a stochastic differential equation,

$$da_t = \left(\mu_\sigma^A a_t - pa + qb\right) \mathrm{d}t + B_{\sigma 11}(a_t, b_t)\mathrm{d}W_t^{(1)} + B_{\sigma 12}(a_t, b_t)\mathrm{d}W_t^{(2)}, \tag{3.21a}$$

$$\mathrm{d}b_t = \left(\mu_\sigma^B b_t + pa - qb\right) \mathrm{d}t + B_{\sigma 21}(a_t, b_t)\mathrm{d}W_t^{(1)} + B_{\sigma 22}(a_t, b_t)\mathrm{d}W_t^{(2)}, \tag{3.21b}$$

where the matrix B_σ fulfills $B_\sigma^2 = D_\sigma$. Specifically, we have

$$B_\sigma(a,b) = \frac{1}{r}\begin{pmatrix} a\left(\alpha_\sigma + \gamma_\sigma\right) + pa + qb + s & -pa - qb, \\ -pa - qb & b\left(\beta_\sigma + \delta_\sigma\right) + pa + qb + s, \end{pmatrix} \tag{3.22}$$

where we have introduced the shorthand

$$s = \left[ab\left(\alpha_\sigma + \gamma_\sigma\right)\left(\beta_\sigma + \delta_\sigma\right) + a\left(\alpha_\sigma + \gamma_\sigma\right)\left(pa + qb\right) + b\left(\beta_\sigma + \delta_\sigma\right)\left(pa + qb\right)\right]^{\frac{1}{2}}, \tag{3.23a}$$

$$r = \left[a\left(\alpha_\sigma + \gamma_\sigma\right) + b\left(\beta_\sigma + \delta_\sigma\right) + 2pa + 2qb + 2s\right]^{\frac{1}{2}}. \tag{3.23b}$$

The process σ_t remains discrete and is described by the master equation

$$\frac{\mathrm{d}}{\mathrm{d}t}P_\sigma = \lambda_\sigma P_{1-\sigma} - \lambda_{1-\sigma}P_\sigma. \tag{3.24}$$

3.8.2 Transformation of coordinates

We are able to make analytical progress by changing to relative coordinates. We introduce the random processes $n_t = a_t + b_t$ and $\phi_t = a_t/n_t$, describing the total population and fraction expressing phenotype A, respectively. Using Eq. (3.21) and applying the rules of Ito calculus we find

$$\begin{aligned} \mathrm{d}n_t = {} & n_t\left(\mu_\sigma^A\phi_t + \mu_\sigma^B(1-\phi_t)\right)\mathrm{d}t \\ & + n_t^{\frac{1}{2}}C_{\sigma 11}(\phi_t)\mathrm{d}W_t^{(1)} + n_t^{\frac{1}{2}}C_{\sigma 12}(\phi_t)\mathrm{d}W_t^{(2)} + \mathcal{O}(n^0), \end{aligned} \tag{3.25a}$$

$$\begin{aligned} \mathrm{d}\phi_t = {} & \left[\Delta_\sigma\phi_t(1-\phi_t) - p\phi_t + q(1-\phi_t)\right]\mathrm{d}t \\ & + n_t^{-\frac{1}{2}}C_{\sigma 21}(\phi_t)\mathrm{d}W_t^{(1)} + n_t^{-\frac{1}{2}}C_{\sigma 22}(\phi_t)\mathrm{d}W_t^{(2)} + \mathcal{O}(n^{-1}), \end{aligned} \tag{3.25b}$$

where the matrix elements of $C_\sigma(\phi)$ are given by

$$\begin{aligned}
C_{\sigma 11}(\phi) &= \frac{1}{r'}\left[\phi\left(\alpha_\sigma+\gamma_\sigma\right)+s'\right], \\
C_{\sigma 12}(\phi) &= \frac{1}{r'}\left[(1-\phi)\left(\beta_\sigma+\delta_\sigma\right)+s'\right], \\
C_{\sigma 21}(\phi) &= \frac{1}{r'}\left\{(1-\phi)\left[\phi\left(\alpha_\sigma+\gamma_\sigma\right)+s'\right]+p\phi+q(1-\phi)\right\}, \\
C_{\sigma 22}(\phi) &= \frac{1}{r'}\left\{-\phi\left[(1-\phi)\left(\beta_\sigma+\delta_\sigma\right)+s'\right]-p\phi-q(1-\phi)\right\}.
\end{aligned} \tag{3.26}$$

and where

$$\begin{aligned}
s' = &\Big\{\phi(1-\phi)\left(\alpha_\sigma+\gamma_\sigma\right)\left(\beta_\sigma+\delta_\sigma\right)+\phi\left(\alpha_\sigma+\gamma_\sigma\right)\left[p\phi-q(1-\phi)\right] \\
&+(1-\phi)\left(\beta_\sigma+\delta_\sigma\right)\left[p\phi+q(1-\phi)\right]\Big\}^{1/2}, \\
r' = &\left[\phi\left(\alpha_\sigma+\gamma_\sigma\right)+(1-\phi)\left(\beta_\sigma+\delta_\sigma\right)+2p\phi+2q(1-\phi)+2s'\right]^{1/2}.
\end{aligned} \tag{3.27}$$

3.9 Appendix C: Growth rate in periodic environments

In the periodic case the environment is described by Eq. (3.3). Neglecting intrinsic fluctuations the entire dynamical system becomes deterministic, and the evolution of ϕ is described by the ordinary differential equation

$$\frac{\mathrm{d}\phi}{\mathrm{d}t} = \Delta_{\sigma(t)}\phi(1-\phi) - p\phi + q(1-\phi). \tag{3.28}$$

In the long run, any trajectory of $\phi(t)$ converges to a limit cycle: in environmental state 0 phenotype A is favoured, and so $\phi(t)$ increases to a 'turning point' ϕ_{high} at which point the environment switches. In environmental state 1 phenotype B is favoured, so $\phi(t)$ decreases until another turning point ϕ_{low} at which point the environment switches again. The turning points ϕ_{low} and ϕ_{high} can be found by numerical integration of Eq. (3.28).

As the trajectory tends to a limit cycle, we can compute the resulting distribution for ϕ, i.e., the fraction of time $\phi(t)$ spends in a given interval during a cycle. This distribution is limited to the on the domain $[\phi_{\text{low}}, \phi_{\text{high}}]$. We let $T = 1/\lambda_1 + 1/\lambda_0$ be the period of the limit cycle. Since the time $\mathrm{d}t$ spent in a specific range $\mathrm{d}\phi$ is given by Eq. (3.28), we find

$$\Pi^*_\sigma(\phi) = \frac{1}{T}\frac{1}{\left|\Delta_\sigma\phi(1-\phi) - p\phi + q(1-\phi)\right|}, \tag{3.29}$$

for $\phi \in [\phi_{\text{low}}, \phi_{\text{high}}]$. These distributions are analogous to the stationary distributions when the environments switch stochastically. The remaining analysis the same as Eq. (3.13) onwards.

We remark another method of finding the average growth rate in periodically-switching environments involves finding the eigenvalues of a propagating matrix [24–26] (and additional analytical results become available when assuming small switching rates [23] and symmetric parameters [28]). The approach used here, however, produces a distribution of ϕ which is useful to compare with the stochastic case.

3.10 Bibliography

[1] P. G. Hufton, Y. T. Lin, and T. Galla. Phenotypic switching of populations of cells in a stochastic environment. *J. Stat. Mech. Theory Exp.* **2018**, 023501 (2018).

[2] C. Wiuff, R. Zappala, R. Regoes, K. Garner, F. Baquero, and B. Levin. Phenotypic tolerance: antibiotic enrichment of noninherited resistance in bacterial populations. *Antimicrob. Agents Chemother.* **49**, 1483 (2005).

[3] B. R. Levin and D. E. Rozen. Non-inherited antibiotic resistance. *Nature Rev. Microbiol.* **4**, 556 (2006).

[4] W. K. Smits, O. P. Kuipers, and J.-W. Veening. Phenotypic variation in bacteria: the role of feedback regulation. *Nature Rev. Microbiol.* **4**, 259 (2006).

[5] M. Leisner, K. Stingl, E. Frey, and B. Maier. Stochastic switching to competence. *Curr. Opin. Microbiol.* **11**, 553 (2008).

[6] P. J. Choi, L. Cai, K. Frieda, and X. S. Xie. A stochastic single-molecule event triggers phenotype switching of a bacterial cell. *Science* **322**, 442 (2008).

[7] K. Lewis. Persister cells, dormancy and infectious disease. *Nature Rev. Microbiol.* **5**, 48 (2007).

[8] N. Q. Balaban, J. Merrin, R. Chait, L. Kowalik, and S. Leibler. Bacterial persistence as a phenotypic switch. *Science* **305**, 1622 (2004).

[9] J. W. Bigger. Treatment of staphylococcal infections with penicillin by intermittent sterilisation. *Lancet* **244**, 497 (1944).

[10] N. Dhar and J. D. McKinney. Microbial phenotypic heterogeneity and antibiotic tolerance. *Curr. Opin. Microbiol.* **10**, 30 (2007).

[11] O. Gefen and N. Q. Balaban. The importance of being persistent: heterogeneity of bacterial populations under antibiotic stress. *FEMS Microbiol. Rev.* **33**, 704 (2009).

[12] P. B. Rainey, H. J. Beaumont, G. C. Ferguson, J. Gallie, C. Kost, E. Libby, and X.-X. Zhang. The evolutionary emergence of stochastic phenotype switching in bacteria. *Microb. Cell Fact.* **10**, 1 (2011).

[13] A. Grafen. Formal darwinism, the individual–as–maximizing–agent analogy and bet–hedging. *Proc. Natl. Acad. Sci. U.S.A.* **266**, 799 (1999).

[14] M. Acar, J. T. Mettetal, and A. van Oudenaarden. Stochastic switching as a survival strategy in fluctuating environments. *Nature Genet.* **40**, 471 (2008).

[15] B. Hallet. Playing Dr Jekyll and Mr Hyde: combined mechanisms of phase variation in bacteria. *Curr. Opin. Microbiol.* **4**, 570 (2001).

[16] L. Tuchscherr, E. Medina, M. Hussain, W. Völker, V. Heitmann, S. Niemann, D. Holzinger, J. Roth, R. A. Proctor, K. Becker, *et al.* Staphylococcus aureus phenotype switching: an effective bacterial strategy to escape host immune response and establish a chronic infection. *EMBO Mol. Med.* **3**, 129 (2011).

[17] M. Thattai and A. Van Oudenaarden. Stochastic gene expression in fluctuating environments. *Genetics* **167**, 523 (2004).

[18] V. Shahrezaei, J. F. Ollivier, and P. S. Swain. Colored extrinsic fluctuations and stochastic gene expression. *Mol. Syst. Biol.* **4**, 196 (2008).

[19] B. Hu, D. A. Kessler, W.-J. Rappel, and H. Levine. Effects of input noise on a simple biochemical switch. *Phys. Rev. Lett.* **107**, 148101 (2011).

[20] M. Leisner, J.-T. Kuhr, J. O. Rädler, E. Frey, and B. Maier. Kinetics of genetic switching into the state of bacterial competence. *Biophys. J* **96**, 1178 (2009).

[21] M. Samoilov, S. Plyasunov, and A. P. Arkin. Stochastic amplification and signaling in enzymatic futile cycles through noise-induced bistability with oscillations. *Proc. Natl. Acad. Sci. U.S.A.* **102**, 2310 (2005).

[22] G. Caravagna, G. Mauri, and A. d'Onofrio. The interplay of intrinsic and extrinsic bounded noises in biomolecular networks. *PLoS One* **8**, e51174 (2013).

[23] P. Patra and S. Klumpp. Emergence of phenotype switching through continuous and discontinuous evolutionary transitions. *Phys. Biol.* **12**, 046004 (2015).

[24] M. K. Belete and G. Balázsi. Optimality and adaptation of phenotypically switching cells in fluctuating environments. *Phys. Rev. E* **92**, 062716 (2015).

[25] M. Lachmann and E. Jablonka. The inheritance of phenotypes: an adaptation to fluctuating environments. *J. Theor. Biol.* **181**, 1 (1996).

[26] E. Kussell, R. Kishony, N. Q. Balaban, and S. Leibler. Bacterial persistence. *Genetics* **169**, 1807 (2005).

[27] S. Leibler and E. Kussell. Individual histories and selection in heterogeneous populations. *Proc. Natl. Acad. Sci. U.S.A.* **107**, 13183 (2010).

[28] B. Gaál, J. W. Pitchford, and A. J. Wood. Exact results for the evolution of stochastic switching in variable asymmetric environments. *Genetics* **184**, 1113 (2010).

[29] I. Lohmar and B. Meerson. Switching between phenotypes and population extinction. *Phys. Rev. E* **84**, 051901 (2011).

[30] P. Patra and S. Klumpp. Population dynamics of bacterial persistence. *PLoS One* **8**, e62814 (2013).

[31] R. Levins. *Evolution in Changing environments: some Theoretical Explorations.* Princeton University Press, Princeton NJ (1968).

[32] P. Haccou and Y. Iwasa. Optimal mixed strategies in stochastic environments. *Theor. Popul. Biol.* **47**, 212 (1995).

[33] E. Kussell and S. Leibler. Phenotypic diversity, population growth, and information in fluctuating environments. *Science* **309**, 2075 (2005).

[34] M. J. Gander, C. Mazza, and H. Rummler. Stochastic gene expression in switching environments. *J. Math. Biol.* **55**, 249 (2007).

[35] P. Visco, R. J. Allen, S. N. Majumdar, and M. R. Evans. Switching and growth for microbial populations in catastrophic responsive environments. *Biophys. J* **98**, 1099 (2010).

[36] D. Horvath and B. Brutovsky. Study of selected phenotype switching strategies in time varying environment. *Phys. Lett. A* **380**, 1267 (2016).

[37] P. G. Hufton, Y. T. Lin, T. Galla, and A. J. McKane. Intrinsic noise in systems with switching environments. *Phys. Rev. E* **93**, 052119 (2016).

[38] J. Nash. Non-cooperative games. *Ann. Math.* pages 286–295 (1951).

[39] M. C. Donaldson-Matasci, C. T. Bergstrom, and M. Lachmann. The fitness value of information. *Oikos* **119**, 219 (2010).

[40] O. Rivoire and S. Leibler. The value of information for populations in varying environments. *J. Stat. Phys.* **142**, 1124 (2011).

[41] R. Pugatch, N. Barkai, and T. Tlusty. Asymptotic cellular growth rate as the effective information utilization rate. *arXiv preprint arXiv:1308.0623* (2013).

[42] M. Ogura, M. Wakaiki, H. Rubin, and V. M. Preciado. Delayed bet-hedging resilience strategies under environmental fluctuations. *Phys. Rev. E* **95**, 052404 (2017).

[43] C. W. Gardiner. *Handbook of Stochastic Methods*. Springer-Verlag, Berlin (2004).

[44] D. T. Gillespie. Exact stochastic simulation of coupled chemical reactions. *J. Phys. Chem.* **81**, 2340 (1977).

[45] X. Mao and C. Yuan. *Stochastic differential equations with Markovian switching*. Imperial College Press, London (2006).

[46] N. G. van Kampen. *Stochastic Processes in Physics and Chemistry.* Elsevier, Amsterdam (2007).

[47] H. Risken. *The Fokker–Planck Equation: Methods of Solution and Applications.* Springer-Verlag, Berlin (1989).

[48] Y. T. Lin and C. R. Doering. Gene expression dynamics with stochastic bursts: Construction and exact results for a coarse-grained model. *Phys. Rev. E* **93**, 022409 (2016).

[49] Y. T. Lin and T. Galla. Bursting noise in gene expression dynamics: linking microscopic and mesoscopic models. *J. R. Soc. Interface* **13**, 20150772 (2016).

[50] M. H. Davis. Piecewise-deterministic Markov processes: A general class of non-diffusion stochastic models. *J. Roy. Statist. Soc. Ser. B* **46**, 353 (1984).

[51] A. Faggionato, D. Gabrielli, and M. R. Crivellari. Non-equilibrium thermodynamics of piecewise deterministic Markov processes. *J. Stat. Phys.* **137**, 259 (2009).

[52] A. Melbinger, J. Cremer, and E. Frey. Evolutionary game theory in growing populations. *Phys. Rev. Lett.* **105**, 178101 (2010).

[53] J. Cremer, A. Melbinger, and E. Frey. Evolutionary and population dynamics: A coupled approach. *Phys. Rev. E* **84**, 051921 (2011).

[54] S. Lechner, K. Lewis, and R. Bertram. Staphylococcus aureus persisters tolerant to bactericidal antibiotics. *J. Mol. Microbiol. Biotechnol.* **22**, 235 (2012).

[55] M. J. Wiser, N. Ribeck, and R. E. Lenski. Long-term dynamics of adaptation in asexual populations. *Science* **342**, 1364 (2013).

[56] P. A. P. Moran. *The statistical processes of evolutionary theory.* Clarendon Press, Oxford (1962).

[57] J. A. Metz, R. M. Nisbet, and S. A. Geritz. How should we define fitness for general ecological scenarios? *Trends. Ecol. Evol.* **7**, 198 (1992).

[58] B. S. Bayati. Deterministic analysis of extrinsic and intrinsic noise in an epidemiological model. *Phys. Rev. E* **93**, 052124 (2016).

[59] A. Crudu, A. Debussche, and O. Radulescu. Hybrid stochastic simplifications for multiscale gene networks. *BMC Syst. Biol.* **3**, 89 (2009).

[60] S. Zeiser, U. Franz, and V. Liebscher. Autocatalytic genetic networks modeled by piecewise-deterministic Markov processes. *J. Math. Biol.* **60**, 207 (2010).

[61] D. M. Wolf, V. V. Vazirani, and A. P. Arkin. Diversity in times of adversity: probabilistic strategies in microbial survival games. *J. Theor. Biol.* **234**, 227 (2005).

[62] M. Salathé, J. Van Cleve, and M. W. Feldman. Evolution of stochastic switching rates in asymmetric fitness landscapes. *Genetics* **182**, 1159 (2009).

[63] E. H. Simpson. Measurement of diversity. *Nature* (1949).

[64] E. L. Haseltine and J. B. Rawlings. Approximate simulation of coupled fast and slow reactions for stochastic chemical kinetics. *J. Chem. Phys.* **117**, 6959 (2002).

[65] C. V. Rao and A. P. Arkin. Stochastic chemical kinetics and the quasi-steady-state assumption: application to the Gillespie algorithm. *J. Chem. Phys.* **118**, 4999 (2003).

[66] Q. Luo and X. Mao. Stochastic population dynamics under regime switching. *J. Math. Anal. Appl.* **334**, 69 (2007).

[67] C. Zhu and G. Yin. On hybrid competitive Lotka–Volterra ecosystems. *Nonlinear Anal. Theory Methods Appl.* **71**, e1370 (2009).

[68] J. Bao, X. Mao, G. Yin, and C. Yuan. Competitive Lotka–Volterra population dynamics with jumps. *Nonlinear Anal. Theory Methods Appl.* **74**, 6601 (2011).

[69] M. Assaf, E. Roberts, Z. Luthey-Schulten, and N. Goldenfeld. Extrinsic noise driven phenotype switching in a self-regulating gene. *Phys. Rev. Lett.* **111**, 058102 (2013).

[70] E. Roberts, S. Be'er, C. Bohrer, R. Sharma, and M. Assaf. Dynamics of simple gene-network motifs subject to extrinsic fluctuations. *Phys. Rev. E* **92**, 062717 (2015).

[71] M. Assaf, M. Mobilia, and E. Roberts. Cooperation dilemma in finite populations under fluctuating environments. *Phys. Rev. Lett.* **111**, 238101 (2013).

[72] T. Dörr, K. Lewis, and M. Vulić. SOS response induces persistence to fluoroquinolones in Escherichia coli. *PLoS Genet.* **5**, e1000760 (2009).

[73] T. Dörr, M. Vulić, and K. Lewis. Ciprofloxacin causes persister formation by inducing the TisB toxin in Escherichia coli. *PLoS Biol.* **8**, e1000317 (2010).

Chapter 4

A stochastic and dynamical view of pluripotency in mouse embryonic stem cells

4.1 Preface

The contents of this chapter were previously published a paper in PLOS Computational Biology in volume 14, page 1 in 2018 [1], which was authored by Yen Ting Lin[1,2], Peter G. Hufton[1], Esther J. Lee[3], and Davit A. Potoyan[4,5]. All four authors share joint first authorship for this work.

It is important to note that the contents of this chapter arose from a collaboration between the theoretical physics department at the University of Manchester, and the biological physics and chemistry departments at Rice University, Houston, Texas. The major aim of this collaboration was to expound the use of the PDMP as an efficient tool for simulation and parameter exploration to audiences in more applied, biological areas. While the methods were mostly developed by P.G.H. and Y.T.L, the biological expertise came primarily from D.A.P. and E.J.L. P.G.H.'s contribution includes

[1]Theoretical Physics, School of Physics and Astronomy, The University of Manchester, Manchester M13 9PL, United Kingdom
[2]Theoretical Division and Center for Nonlinear Studies, Los Alamos National Laboratory, Los Alamos, NM 87544, United States of America
[3]Department of Bioengineering, Rice University, Houston, Texas, United States of America
[4]Department of Chemistry, Iowa State University, Ames, Iowa, United States of America
[5]Department of Chemistry and Center for Theoretical Biological Physics, Rice University, Houston, Texas, United States of America

developing the model (along with Y.T.L. and D.A.P.), performing mathematical analysis (along with Y.T.L.), jointly writing all sections of the paper (along with Y.T.L., E.J.L., and D.A.P.), and responding to referee reports (along with Y.T.L. and D.A.P.). Although the final data for Figs. 4.2–4.7 was obtained by Y.T.L., P.G.H. simultaneously developed independent code and performed simulations to (1) discover results and shape the direction of the paper, and (2) as a confirmation of the results produced by Y.T.L. This included Monte Carlo simulation of the individual-based model, the PDMP, and finding parameter sets which minimise the Hamming distance from experimental data.

Abstract

Pluripotent embryonic stem cells are of paramount importance for biomedical sciences because of their innate ability for self-renewal and differentiation into all major cell lines. The fateful decision to exit or remain in the pluripotent state is regulated by complex genetic regulatory networks. The rapid growth of single-cell sequencing data has greatly stimulated applications of statistical and machine-learning methods for inferring topologies of pluripotency-regulating genetic networks. The inferred network topologies, however, often only encode Boolean information while remaining silent about the roles of dynamics and molecular stochasticity inherent in gene expression. Herein we develop a framework for systematically extending Boolean-level network topologies into higher-resolution models of networks which explicitly account for the promoter architectures and gene state switching dynamics. We show the framework to be useful for disentangling the various contributions that gene switching, external signaling, and network topology make to the global heterogeneity and dynamics of transcription factor populations. We find the pluripotent state of the network to be a steady state which is robust to global variations of gene switching rates which we argue are a good proxy for epigenetic states of individual promoters. The temporal dynamics of exiting the pluripotent state, on the other hand, are significantly influenced by the rates of genetic switching which makes cells more responsive to changes in extracellular signals.

4.2 Author summary

In the embryonic stage mammalian cells are pluripotent: they have not yet committed to any specific cell type. The commitment to a cell type is controlled by pluripotency networks, the bio-molecular inventory of which is unsurprisingly complex, spanning a myriad of transcription factors, genes, and epigenetic factors. Thanks to advances in high-throughput sequencing and related computational tools for data analysis, we are beginning to unravel basic topological features of pluripotency networks. Networks

inferred from sequencing data are often cast in Boolean representations which specify the existence and nature of regulatory connections between pairs of biomolecules. While immensely useful, the Boolean networks remain silent about the stochasticity and dynamics of molecules that are indelible features of bio-molecular life inside cells. Understanding stochastic and dynamic features of pluripotency networks is crucial if one is to have a mechanistic understanding of cell fate determination rationalized in terms of fundamental physico-chemical processes. The computational framework proposed in this work offers a way of bridging the divide between Boolean networks and higher-resolution views of networks in a predictive and quantitative manner. The usefulness of the framework is demonstrated by reproducing a number of experimental trends and creating new insights about the stochastic and dynamical nature of pluripotency.

4.3 Introduction

Embryonic stem cells derived from mammalian blastocysts are pluripotent: they show an indefinite capacity for self-renewal and the ability to differentiate into every cell type constituting an adult organism [2–4]. The development of healthy tissues hinges on the ability of these pluripotent stem cells to make critical decisions determining when and into which kind of cells to differentiate in response to the environment. It is therefore unsurprising that fates of embryonic cells are decided through sophisticated biological computations by a tightly-integrated regulatory network consisting of genetic, epigenetic, and signaling layers [4].

The expression of genes is subject to intrinsic noise due to finite molecular copy numbers [5] and due to randomness in extracellular environment. Thus, while at the level of the organism development is often predictable, with a well-defined order of events, at the level of single cells fate determination is fundamentally stochastic [6, 7]. Indeed, many studies probing the transcription of pluripotency-regulating genes in single cells have found high variability in distributions of transcription factors and mRNA molecules [8–10].

Several hypotheses about the functional roles for the highly heterogeneous expression of pluripotency transcription factors (TFs) have been put forward. One idea

is that stochastic excursions in the population levels of transcription factors help by steering cells towards distinct states [11, 12]. A different hypothesis claims transcriptional noise to be advantageous by facilitating the exploration of the state space of a gene network such that, at any instant, a sub-population of cells is optimally primed to be responsive to differentiation signals [13]. The heterogeneity of populations of pluripotent cells has also raised some concerns that pluripotency is ill-defined at a single-cell level [13] and instead should be viewed as a macroscopic state emerging at the level of an ensemble of cells. A comprehensive physical picture of pluripotency at the single-cell level therefore remains unclear.

In this regard, the roles of modeling and computational approaches are seen as especially important for bridging the gap between our understanding of molecular dynamics of regulatory networks and phenotypic outcomes. A rapid growth in single-cell sequencing data has opened many avenues for carrying out statistical inferences of pluripotency-regulating genetic networks [14–16]. In vitro studies of mouse embryonic stem cells (mESC) in different culture conditions, in particular, have become an ideal model system for computationally inferring gene networks and exploring mechanistic issues surrounding pluripotency and lineage commitment [16]. In a *tour de force* study of mESCs by Dunn *et al.* [17], regulatory relationships between transcription factors were uncovered through analysis of pairwise correlations in gene expression. Using mean values of RNA-seq counts as constraints, a minimal network topology was derived showing a high degree of predictive power with respect to perturbations of the network, such as gene knockouts.

Network topologies in general, however, remain silent about the roles of molecular noise and dynamics in stem cell differentiation governed by stochastic biochemical reactions. Higher-resolution views may incorporate populations of TFs and logic describing the dynamics of production and of binding and unbinding. One has to ultimately test such a view using mass-action-based kinetics which integrate relevant molecular factors. The inclusion of such complications increases the number of parameters, and hence the likelihood of overfitting. The key challenge lies in finding the adequate resolution for the network which is able to be predictive and does not pose insurmountable computational burden.

In the present work, we outline a framework for extending Boolean-resolution

networks—a commonly derived product from high-throughput experimental results—into stochastic and dynamical models with microscopic resolution of promoter architecture and individual gene-switching events. The computational scheme utilizes static Boolean information about the network topology and uses novel analytical model reduction to increase the computational efficiency, allowing for extensive searches in the space of microscopic reaction rates. This framework is successfully applied to the network topology inferred by Dunn *et al.* [17] in order to build a mass-action-based stochastic dynamic model which is capable of describing both the discrete states of all the genes and the populations of transcription factors. Starting from minimal assumptions about the rates of various reactions, we find parameter regimes where a remarkable agreement with the experimental gene expression profiles [17] is achieved for all combinations of external signals. We show that average gene-expression levels in complex regulatory networks are not uniquely determined by gene-switching rates, which cautions about the limitations of mean expression data and suggests strategies of inference which utilize higher moments in distributions of transcription factors. Using single-cell experiments which have probed expression of pluripotency factors [8,9], we are able to argue that gene switching in pluripotent states happens primarily on the intermediate scale relative to the reactions of production and degradation (dilution). This regime better agrees with the diverse set of experiments available [8–10,17] and provides an explanation for the multimodality in distributions of transcription factors and burst-like expression dynamics for some genes.

In the second half of the paper, armed with a predictive and physically-motivated model of a pluripotency network, we explore the dynamics of lineage commitment driven by withdrawal of various well documented signals (LIF, 2i) for maintaining the naïve state of pluripotency. We find a number of non-trivial consequences of molecular noise and gene-switching dynamics. We show that global variations of gene-switching rates (which may mimic epigenetic changes) yield a significant leverage over stability, sensitivity and exiting dynamics of pluripotent states. We also show that the intermediate gene-switching regime generates higher sensitivity for the network when responding to external signals.

4.4 Results

4.4.1 Framework for deriving microscopic-resolution networks from experimentally inferred Boolean network topologies

In this Section we outline the steps for constructing higher-resolution regulatory networks with explicit promoter architecture, gene states, and transcription factor copy numbers, starting from experimentally-inferred Boolean network topologies. To illustrate the potential of our modeling framework we have chosen the most comprehensive Boolean network to date, which describes the regulation of pluripotency factors of mouse embryonic stem cells [17]. In the next subsection we describe how Boolean logic is converted into the molecular logic of promoter states via a set of simplifying assumptions. Once promoter logic is defined, in the second subsections we go on to define the resolution of protein to promoter interactions.

These assumptions lead to a set of chemical reactions describing transitions between gene states. In the third subsection we introduce the rules defining the production and degradation of transcription factors. In the fourth subsection we give an overview of the multi-scale simulation techniques appropriate for the simulation of stochastic switching of genetic states with a single-molecule-level resolution. In particular we contrast the rigorous-yet-computationally-inefficient individual-based model (IB) with a more efficient piecewise-deterministic Markov Process (PDMP) which we adopt and extensively validate in the present work.

4.4.2 Extending the Boolean logic to molecular logic

The Boolean model of Dunn *et al.* specifies twelve genes in the network. We use G_i to denote a gene and P_i to denote the corresponding functional TFs ($i \in \{1, 2, ..., 12\}$) in the following framework. The network topology (Fig. 4.1) contains static information about the types of interactions between pairs of genes. The interactions are classified as being either repressing or activating. To study the dynamics of complex genetic networks, one has to extend the Boolean-level description to account for the molecular logic of gene regulation. This molecular logic specifies the precise relation between the

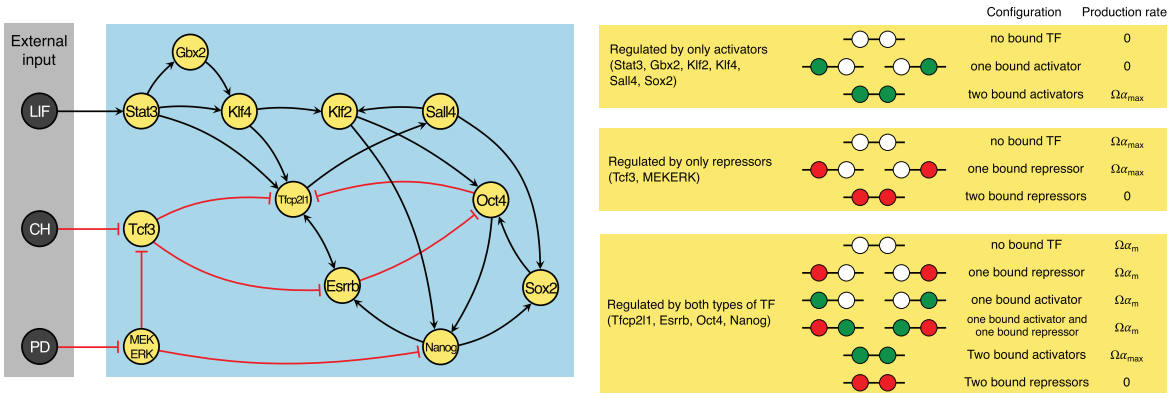

Figure 4.1: **Network topology and molecular logic**. The left panel shows a schematic diagram of the network topology, reproduced from Dunn *et al.* [17]. Each node corresponds to a given gene and their placement from left to right is chosen to indicate a trend of downstreamness from three external inputs. In our mechanistic model, each gene produces a unique transcription factor at a rate which depends on the binding state of its promoter site. These transcription factors then go on to bind and activate (black arrow) or repress (red bar) other genes. The three nodes on left correspond to extra-cellular signals, which are either absent or present. The right panel shows our assumed molecular logic of transcriptional regulation when there are $N = 2$ promoter sites per gene. Each circle is a binding site: it can be either empty (white), bound by an activator (green), or bound by a repressor (red). The right panel lists possible combinations of the promoter sites. Depending on the configuration of the promoter site, transcription factors are produced with rates 0, $\Omega\alpha_m$, and $\Omega\alpha_{\max}$, modeling the effects of cooperative binding.

binding of transcription factors to the promoters and the regulatory outcome in terms of gene activation or repression. In the case where the same sites can be bound to different transcription factors, the combinatorial nature of regulation can give rise to ambiguity in molecular logic. Indeed, even on the level of Boolean networks, the logic is ambiguous and many possible truth tables have to be enumerated in order to select an appropriate picture for the dependence of a gene on its regulating signals. Ideally, such ambiguities should be resolved by directly inferring regulatory logic. Alternatively, one could simulate different combinatorial possibilities until sufficient agreement with experiments is reached.

In our case, we assume a set of rules which applies to every gene in the network. This is a simplifying assumption, the justification for which is obtained *a posteriori*; networks with optimized parameters yield gene expression patterns consistent with the experiments. The fact that these simplifying assumptions work surprisingly well implies a dominance of the global network topology over the local details of molecular

regulatory logic of gene promoters.

For each gene, we assume a fixed number N of promoter sites. The genes which are only regulated by activators are always "OFF" unless N promoter sites are bound to activators. Similarly, the genes which are only regulated by repressors are always "ON" unless N promoter sites are bound to repressors. For those genes which are regulated by both activators and repressors, their activity is up-regulated to "ON" (resp. down-regulated to "OFF") only when N promoter sites are bound to activators (resp. repressors), otherwise they have a "MEDIUM" activity. These rules are illustrated quantitatively in the right panel of Fig. 4.1.

4.4.3 Binding and unbinding of transcription factors to promoter sites

From the topology, we know that each gene is regulated (activated or repressed) by a subset of TFs; we denote the subset of the TFs which regulates gene i by $S_i \in \{P_1, P_2, ..., P_{12}\}$. For example, the subset of the TFs which regulates the core gene Nanog is the set of transcription factors $\{\text{Klf2}, \text{Sox2}, \text{MEKERK}\}$ (see Fig. 4.1). The binding and unbinding of the transcription factors to the promoter sites of gene i can be summarized by the following binding and unbinding reactions:

$$\begin{aligned} G_i + P_j &\underset{k_{\text{off}}}{\overset{Nk_{\text{on}}\Omega^{-1}}{\rightleftharpoons}} G_iP_j && \text{for } P_j \in S_i, \quad \text{(first TF)} \\ &\vdots \\ G_iP_j \ldots P_k + P_l &\underset{Nk_{\text{off}}}{\overset{k_{\text{on}}\Omega^{-1}}{\rightleftharpoons}} G_iP_j \ldots P_kP_l && \text{for } P_l \in S_i, \quad \text{(final TF)} \end{aligned} \tag{4.1}$$

where the rates are written per the reactants, i.e., a given P_j binds to a given unbound promoter G_i with rate $Nk_{\text{on}}\Omega^{-1}$ etc. The "system size" parameter Ω has been introduced which sets the scale for a typical number of TFs in the system [5, 18] without loss of generality. The scaling of these switching reactions is chosen such that the time scale of gene switching is independent of Ω [19]. Notice that we have adopted the parallel-binding mechanism [20] which assumes the transcription factors bind to any of the unbound promoter sites independently with a rate constant k_{on}.

4.4.4 Production and degradation of transcription factors

Each gene G_i "produces" its own transcription factor P_i with a rate which depends on the promoter state of G_i. We use a one-step model of transcription [21] whereby transcription factors are produced via a unimolecular step. This approximation coarse grains several sequential intermediate reactions (polymerase recruitment, mRNA production, RNA splicing, etc.) into one effective step [22, 23]. This approximation has become popular in models of protein production [19, 24, 25]. All of the transcription factors are assumed to have finite lifetimes set by the rate of degradation, thus ensuring the existence of stable steady states with a finite number of molecules. The absolute time is set to be $\sim$1hr which is consistent with experimental measurements reported on the lifetimes of pluripotency transcription factors [26–29].

The reactions are

$$\begin{aligned} G_i &\xrightarrow{\Omega\alpha} G_i + P_i, \qquad \text{(TF production)} \\ P_i &\xrightarrow{\gamma} \varnothing. \qquad\quad \text{(TF degradation)} \end{aligned} \tag{4.2}$$

Here, the rate constant of the production of TFs ($\Omega\alpha$) depends on the promoter's configuration and is determined by the molecular logic defined previously. We further assume the production rate when the gene is "ON", "MEDIUM", and "OFF" to be $\Omega\alpha_{\max}$, $\Omega\alpha_m$, and 0 (see Fig. 4.1). These rates are taken to be identical among all the genes.

We note that one can adopt a view with a higher resolution of the network depending on the available experimental data and the nature of the question posed. The computational framework can readily incorporate in an explicit manner more steps, for instance to model the effects of cell cycle regulation, different epigenetic states, and binding of non-coding RNAs. Herein we consider the most simplified dynamical model which describes only the promoter configurations and the population dynamics of the transcription factors. This model aims to use the optimal resolution for capturing trends in gene expression while remaining feasible for efficient stochastic simulations. After converting the Boolean topology into a higher-resolution network of biochemical reactions, our next goal is to exhaustively sample a vast space of parameters in order to identify the optimal parameter regimes with which the model best reproduces experimental results.

4.4.5 Multi-scale simulation of complex genetic networks

Biochemical reactions in gene networks are of a fundamentally probabilistic nature; this demands a stochastic description of the kinetics. The conventional mean-field mass-action-based kinetics only describe the dynamical behavior in the thermodynamic limit, and ignore the stochastic effects which arise from the discreteness of the system. In our model, the system might be considered highly discrete, as there is only a single copy of each gene, and their discrete promoter states dictate the dynamics of the transcription factors. The most rigorous way to simulate such a reaction system is by numerically solving the chemical master equation which accounts for all possible states of the network down to the level of single molecules [5,21]. In high dimensions, i.e., when the number of species is large, this approach is not computationally efficient. Instead, kinetic Monte Carlo algorithms are the most straightforward way to generate sample paths of the stochastic process. We refer to the stochastic process modeling the reactions down to the single-molecule level with the well-mixed assumption as the individual-based model (IB).

The state of our individual-based model is characterized by the state of each gene's promoter sites—how many sites are bound to specific kinds of transcription factors—and the integer populations of the transcription factors. The rates at which the process stochastically transitions from one state to another are specified by the reactions Eqs. (4.1) and (4.2). Fully individual-based models, however, suffer from a steep scaling of computational time with the number of discrete system states. This fact renders them inefficient for simulating large gene networks, especially when it comes to scanning or exploring the parameter space.

A wide range of approximate schemes have been employed to simulate complex gene regulatory networks [30–32]. Most conventional approximations so far have been the size-expansion methods [33,34] which are known for being problematic when the molecular noise induced by discrete genetic switching becomes non-negligible [19, 35, 36]. On the other hand, for embryonic stem cell networks it is essential to account for the stochastic nature of genetic switching events which give rise to multimodality in the probability distributions of transcription factors populations. These local maxima in

the multidimensional probability distributions of a stochastic genetic network correspond to metastable states and are also known as local attractors which corresponding to distinct promoter configurations and hence likely also to distinct phenotypic states [37–39]. Theoretically a network with M independently functioning genes can generate up to $\sim 2^M$ distinct phenotypic states [40].

Thus, even if populations of all the other species are present in large quantities, the stochastic fluctuations caused by the genetic switches (due to stochastic binding-unbinding events of the transcriptional factors to a discrete number of promoter sites) between ON, MEDIUM, and OFF states cannot be ignored, unless the switching is operating in the extremely fast limit compared to any other reactions, known as the "adiabatic regime" [36, 40, 41]. In the other cases—the non-adiabatic regime—gene switching can completely dominate the dynamics in the network [36, 42]. Eukaryotic gene regulatory networks are often found in the intermediate regime where gene-switching events are dynamically interwoven with the rest of the reactions in the network and cannot be ignored [6, 43, 44]. Single-cell studies of mESCs in particular have shown bursty behavior in gene expression with sudden jumps in the levels of proteins resulting in multi-modal distributions of core transcription factors [8].

The sheer volume and complexity of information that is emerging from experiments on embryonic stem cells have motivated the application of a wide variety of modeling strategies for confronting the observed patterns of gene expression in ESCs [45, 46]. Some of the computational techniques used so far include Boolean networks [17,47–49], Hopfield neural networks [50–52], systems of coupled ordinary [53, 54] and stochastic differential equations [11, 55, 56] with Hill coefficients, agent-based models [57], individual-based models [44, 58, 59], and small noise approximations to individual-based models [60–62].

Many of the early computational models of embryonic stem cells focused on small fragments of pluripotency networks, typically involving bistable switches [11,53]. These early pioneering studies yielded many insights on stochastic decision making in regards to fate determination and self-renewal [45]. Relatively few studies have also looked at larger portions of regulatory networks while including a stochastic treatment of genetic switching dynamics by either carrying out individual-based simulations [44, 58] or small-noise approximations [60–63].

Because of the computationally-demanding nature of individual-based models and the restricted validity of small-noise approximations to the near-adiabatic gene switching, the full range of stochastic and dynamical regimes displayed by different gene-switching time-scales has remained unexplored. Additionally with very few exceptions [44], the kinetic parameters in many of the previous models have been not thoroughly explored or informed by data and have had to be selected from physical intuition alone. These limitations have now been overcome in the present work. Thanks to a series of recent developments in modeling of gene expression dynamics [19, 24, 25, 36, 64–66], a novel computational framework utilizing piecewise-deterministic Markov processes (PDMPs) [67] has emerged as a rigorous approximation to the fully individual-based model.

The idea behind the PDMP is simple: reactions with large number of molecules are evolved deterministically, while reactions with smaller numbers of molecules are propagated as discrete, random switching events. This approach treats discrete genetic switching events exactly, while assuming noise due to the finite nature of populations of transcription factors to be negligible in comparison. As shown in the subsequent sections, the assumptions underlying the PDMP approach turn out to be sound as we go on to obtain a nearly perfect quantitative agreement with full blown kinetic Monte Carlo schemes even for the case of the complex networks of mESCs operating in the intermediate gene-switching regime.

For the present study, we find that simulation of the PDMP is nearly $\mathcal{O}(10^3)$-fold faster at generating stochastic trajectories than conventional individual-based kinetic Monte Carlo techniques. This rigorous and rapid sampling of gene-switching events has not only allowed us to investigate the stochastic dynamics of the regulatory network at a longer time scale compared to conventional kinetic Monte Carlo methods, but also enabled us to explore a vast parameter space efficiently. We used the obtained information to inform our parameters in the microscopic-resolution models of mESCs. The mathematical details of the PDMP described in greater detail can be found in Sec 4.6.

4.4.6 In the pluripotent state the mean levels of gene expression are robust with respect to changes of gene state switching rates.

After converting the Boolean topology to a higher-resolution genetic network, we use the PDMP to efficiently explore the kinetic parameter regimes. This is done in order to: (i) identify the steady states for a particular set of parameters; (ii) obtain a set parameters that best reflects the experimental constrains; and (iii) study the response of the network to changes in gene-switching rates. The experimental data used for constraining rate coefficients are the binarized gene expression levels of pluripotency transcription factors under well-defined culture conditions consisting of different combinations of leukemia inhibitory factor (LIF), glycogen synthase kinase 3 (CH), and mitogen-activated protein kinase (PD). Identical culture conditions were used by Dunn *et al.* [17] to infer the original Boolean topology.

The optimization of rate coefficients is done by defining a uniform threshold η among all the TFs and with different external conditions; TFs whose population densities are higher than η are classified as expressed, while those below the threshold are not expressed. Then, we employ the Hamming distance (the number of discrepancies between the simulated and experimental profiles) as a cost-function for the optimization. The Hamming distance is minimized through multiple rounds of simulations where we vary the uniform threshold η and four free and non-dimensional model parameters (see Ssec. 4.6.3): the number of promoter sites per gene N, the rate constant of TFs binding to the promoter k_{on}, rate constant for a bound TF to dissociate from the promoter k_{off}, and the production rate α_m when the gene is in the "MEDIUM" state.

Through this procedure, we find that the binary expression patterns can be closely reproduced (minimal Hamming distance = 3) by the model when the number of the promoter sites $N \geq 2$. We remark that, given the small number of free parameters, this is a very small amount of deviation from the experimental results; the remaining deviations are likely to have been caused by the simplifications to the logic and dynamics in the construction of our individual-based model. The qualitative features for $N = 2, 3, \ldots 5$ cases were found to be similar (not shown). We here choose to

present the data for the simplest case $N = 2$. We note that various other forms of cooperativity, including cases when bound TF at the promoter recruits other TFs (either of its own kind or other type), can be readily incorporated into the current computational framework by changing the association rates k_{on} as promoter-state dependent. For simplicity, we only illustrate the most basic form of cooperativity in this pilot paper. We find for any given N there exists a "valley" in the remaining model parameter space $k_{\text{on}}, k_{\text{off}}, \alpha_m$, as illustrated in Fig. 4.2(A). The inferred parameter α_m is consistently low ($\lesssim 0.02$), meaning that the "MEDIUM" production rate is almost zero. This implies that the negative regulation of those genes which are regulated both by activators and repressors (Tfcp2l1, Esrrb, Nanog, and Oct4) in the model are technically fulfilled by inhibition (i.e., regulating TFs by blocking the promoter sites), instead of actually down-regulating the production activity. In addition, the valley suggests a relationship between k_{on} and k_{off}, where $k_{\text{on}} \approx 10 k_{\text{off}}$. This implies a certain asymmetric time scale between the binding and unbinding processes.

We chose three parameter sets in this valley of cost function, corresponding to three distinct dynamical regimes of binding and unbinding reactions between the TFs and the promoter sites: slow ($k_{\text{on}} = 3.2$, $k_{\text{off}} = 0.2$, $\alpha_m = 0.02$), intermediate ($k_{\text{on}} = 16$, $k_{\text{off}} = 1.5$, $\alpha_m = 0.01$), and fast ($k_{\text{on}} = 102$, $k_{\text{off}} = 10$, $\alpha_m = 0.005$) compared to the time scale of the TF dynamics. We remark that as we non-dimensionalize the model using the protein degradation rate γ (see Sec. 4.6.3), the time scale of the binding and unbinding are fast, intermediate, or slow *relative* to the time scale of the protein dynamics, also set by γ (see Eq. 4.3). All of the parameter sets successfully reproduce the experimental gene expression patterns (Fig. 4.2) corresponding to pluripotent and lineage committed cells.

The fact that the rate parameters of the network occupy finite regions and cover different regimes suggests that distinct gene expression profiles can tolerate some fluctuations in reaction rates. Such rate fluctuations, reflecting the effect of extrinsic noise, are inevitable in dynamic cellular environments of embryonic cells which experience frequent epigenetic and extracellular perturbations [16, 27, 68]. In a way, changes in gene-switching rates can be seen as a proxy for how global epigenetic changes govern the rates of transcription factor binding to target genomic regions.

From the methodology point of view, the absence of a unique regime of rates

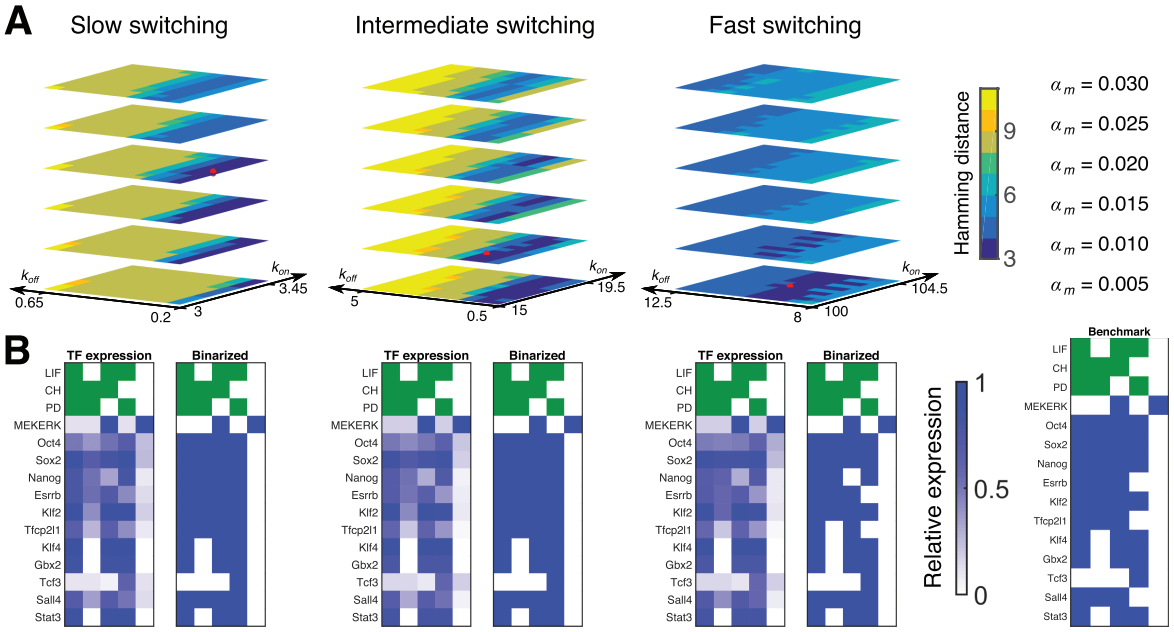

Figure 4.2: **PDMP stochastic simulations identify three genetic switching regimes that are consistent with experimental data.** When switching is slow, intermediate, or fast we find certain parameters which closely match the experimental results obtained by Dunn *et al.* [17]. The consistency of our model with experimental results is measured using a Hamming distance—a measure where one counts the number of discrepancies between the binary expression of each TF for both cases. (A) Shown are the identified regions in parameter regimes that minimize Hamming distance. There are three free parameters: the binding rate k_{on}, unbinding rate k_{off}, and basal transcription rate α_m. For slow switching, the parameters are $k_{\text{on}} = 3.2$, $k_{\text{off}} = 0.2$, $\alpha_m = 0.02$; for intermediate switching, $k_{\text{on}} = 16$, $k_{\text{off}} = 1.5$, $\alpha_m = 0.01$; for fast switching, $k_{\text{on}} = 102$, $k_{\text{off}} = 10$, $\alpha_m = 0.005$. The selected parameter sets are presented as red dots in the landscapes in the upper panel, hereby referred to as *the* slow, fast and intermediate parameter regimes. (B) Comparison of computed and discretized gene expression profiles (blue) with those of the experiments (Benchmark panel) [17]. External inputs are shown in green.

implies the following: inferring networks using only mean levels of gene expression (as is done for Boolean networks) may lead to the loss of valuable information contained in higher moments of distribution. Thus new approaches of inference need to be developed in order to account for broad distributions of transcription factors. For this reason, we look beyond the comparisons of mean expression levels and turn to comparing stationary distributions of transcription factors observed in experiments with the computationally generated distributions in three chosen parameter regimes identified in Fig. 4.2. We generate the stationary distributions of the TF concentrations in the model, with eight different environmental conditions, in the specified three parameter sets in Fig. 4.3. We observe qualitatively that in the "fast" parameter

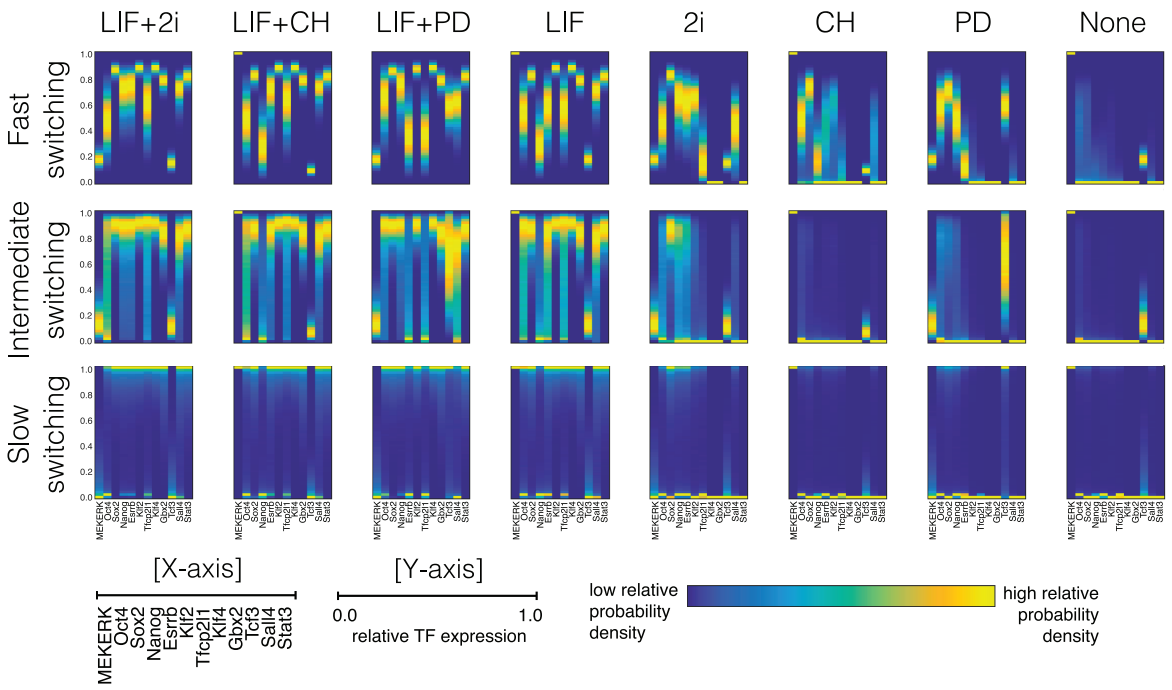

Figure 4.3: **Gene expression profiles of pluripotency factors predicted by PDMP simulations.** Each column corresponds to different external inputs, and each row corresponds to regimes of slow, intermediate, and fast gene switching. 2i refers to the dual inhibitor (PD+CH) external input. Parameters used are those identified in Fig. 4.2. More than 10^5 sample paths were used for generating each condition.

set the distribution of each TF is unimodal, and in the "slow" parameter set, the distribution of each TF is peaked near 0 and 1 in non-dimensional units. In the intermediate regime, on the other hand, with some environmental conditions, broader distributions of the gene expression are observed.

The pluripotent state of mESCs has been the subject of intense investigations by nucleic acid-based single-cell techniques such as RNA-seq, sm-FISH, qPCR and there is now extensive data on the steady-state distributions of RNA and transcription factors maintained under pluripotency-favoring culture conditions [8,9,69]. These experiments have revealed a heterogeneous nature of gene expression with many TFs, such as Nanog and Esrrb, having long-tailed or bimodal distributions (see for example Fig. 5a in Ref. [8]). Additionally, the single-cell stochastic trajectories of TFs have shown sharp, bursty transitions implying infrequent genetic-switching events [8]. Qualitatively, these experimental observations are more consistent with the intermediate regime of genetic switching as seen from Fig. 4.3, as in the case of slow switching nearly all of the transcription factors express bimodality and in the case of fast switching the expressions of all the factors are narrow and unimodal.

In Fig. 4.3, consistent with experiments, we also find that under LIF gene expression is more heterogeneous than under 2i, but also that the overall levels of expression are higher [8, 9]. In all three regimes of genetic switching supporting pluripotency (LIF+2i,LIF+PD, LIF+CH, LIF and 2i), core transcriptions factors such as Nanog, Oct4, Sox2 are highly expressed. The same factors are also repressed in conditions favoring differentiation (CH, PD and none) irrespective of gene-switching regime. In the next section, we show the routes and dynamics of lineage commitment from pluripotent states strongly depend on the level of noise in different gene-switching regimes.

Although the PDMP approach accurately captures the effects of genetic switching, it assumes demographic noise arising from finite populations to be negligible. To test the validity of this assumption and assess the contribution of different sources of noise in establishing the steady-state distribution of the pluripotent state, we carry out individual-based simulations for the intermediate switching regime of the network, Fig 4.4. In the individual-based model all reactions are treated stochastically thereby accounting for all of the sources of noise in the system. The resulting gene expression profiles follow closely those obtained by PDMP simulations, showing that the noise arising from stochastic switching events of promoter configuration accounts for the significant part of overall variability in the network. Trajectories of individual transcription factors show that indeed most of the variance in the molecular distributions are generated by genetic switching events which appear as abrupt stochastic jumps.

4.4.7 Dynamics of lineage commitment is significantly affected by the dynamical changes of individual gene-switching rates

We next ask how the steady-state gene expression patterns displayed by the gene network respond to extracellular perturbations in the form of the initiation or termination of pluripotency signals. Both dual inhibitor 2i (PD+CH) and Leukemia factor LIF based signaling have been shown to provide a stable environment for maintaining pluripotency of stem cells in vitro [4, 17]. Conversely, withdrawal of either LIF or 2i leads to irreversible lineage commitment after a 24-hour period. Despite a similar ability to guard pluripotent cells against lineage commitment, these factors deploy

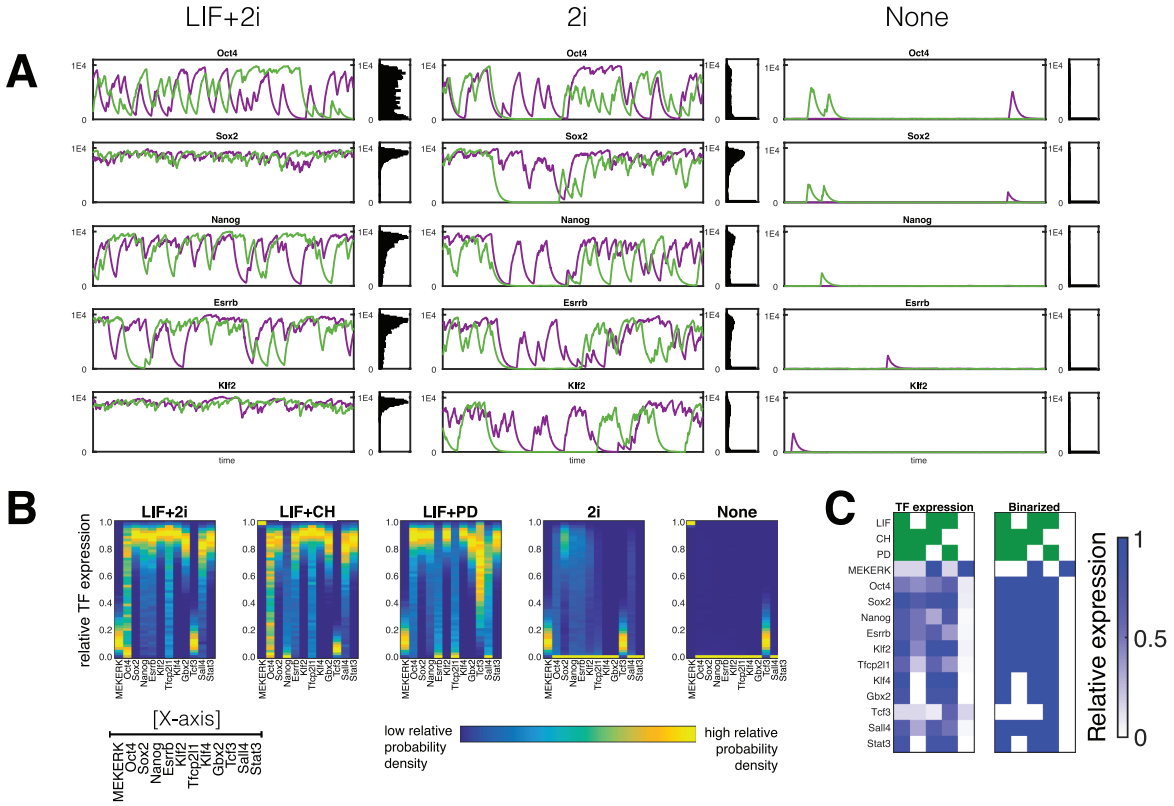

Figure 4.4: **Gene expression profiles of pluripotency factors predicted by individual-based simulations.** The intermediate switching regime is chosen to be presented as it is the regime which best captures the experimentally measured distributions [8,9]. (A) Shown are two representative trajectories and full distributions of select few transcription factors under three different conditions generated by individual-based simulations. Typical lifetime for pluripotency transcription factors [26–29] ($\sim$ 1 hr) is used for setting the absolute time-scale of simulations (B) Gene expression profile showing the near quantitative agreement with results of PDMP simulations shown in Fig. 4.3. (C) Gene expression profile of individual-based model, for comparison with the PDMP and experimental benchmark shown in Fig. 4.2.

different regulatory mechanisms reflected in distinct distributions of core TFs: Nanog, Oct4, and Sox2. As a result, stem cell differentiation by withdrawal of different signals proceeds via different routes. To gain a mechanistic understanding of how the interplay of signaling, molecular noise, and network architecture gives rise to the steady-state expression profiles, we study the dynamics of transitioning between the pluripotent and lineage committed states induced by rapid initiation and withdrawal of signaling conditions (LIF, CH, PD).

The temporal evolution of distributions of the TFs exiting (LIF/2i withdrawal) and entering (LIF/2i immersion) pluripotent states reveals rich, dynamical signatures of these transitions (Fig. 4.5). To reveal the role of stochasticity in these transitions, we

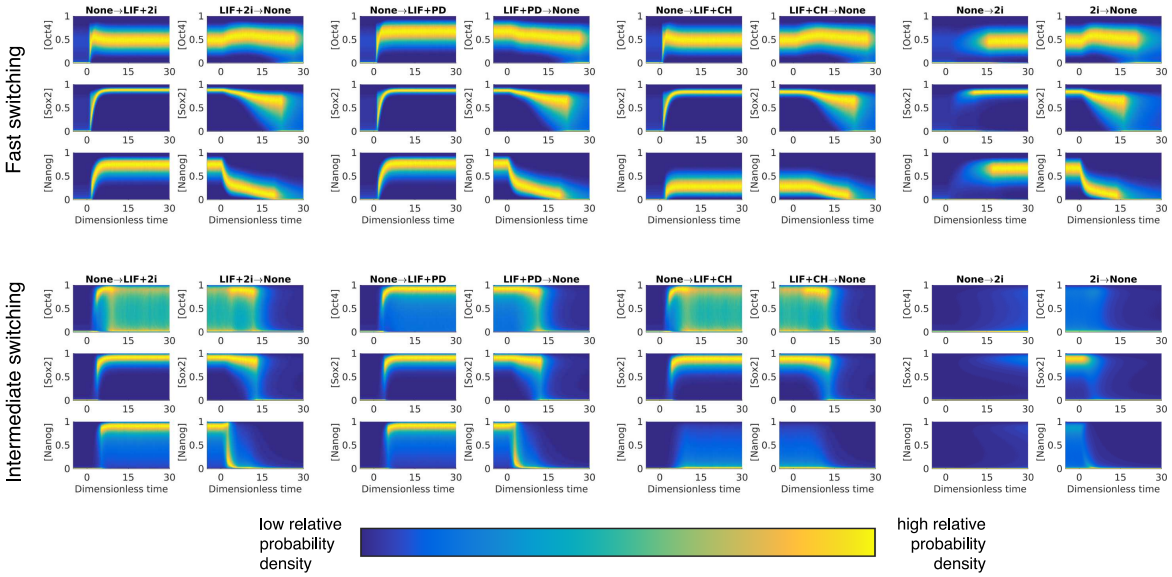

Figure 4.5: **The dynamical behavior of the distributions of transcription factor densities for the intermediate and fast switching regimes.** At time $t = 0$, the external inputs are changed. The plots show the evolution in probability density for a large ensemble (10^5) of PDMP sample paths. The times and populations are respectively rescaled by $1/\gamma$ and $\alpha_{\max}/\gamma$ (see Sec. 4.6.3). We assume the proteins are stable and so the their estimated half-life is of an order 8 hour [8]; in other words $\gamma \sim 1/8\ \mathrm{hr}^{-1}$, and the entire course of simulation ($t \in (0, 30)$) corresponds to physically 240 hours.

compare the intermediate regime—which is dominated by genetic switching—to the fast regime—in which transitions are largely governed by the network topology and the fluctuation of promoter configuration is almost-completely ignored. The irreversible nature of transitions manifests clearly in different routes exiting and entering the pluripotent state (transitions to and from the None state in Fig. 4.5).

In the intermediate regime of genetic switching rates, expression noise greatly facilitates transitions out of the pluripotent state by making the network more responsive to changes in environmental signaling. In contrast, in the fast-switching regime, upon withdrawal of pluripotency signals the downstream regulation happens on a much slower time scale with some factors remaining virtually unresponsive to changes of signaling. This signaling enhancement in the intermediate regime reveals the importance of molecular noise in making pluripotent states more sensitive to environmental conditions. There are qualitatively different patterns of re-entrance into pluripotent states upon LIF vs 2i addition, with LIF being much more efficient at reversing pluripotency compared to the 2i. The different potentials of signaling cultures for pluripotency

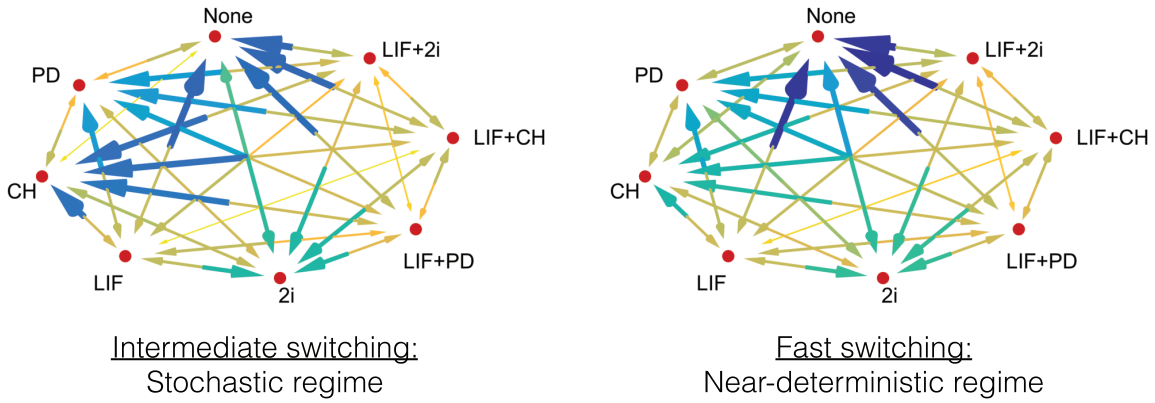

Figure 4.6: **Transition times between the stationary distributions of different external conditions.** A larger, darker arrow indicates that a given transition takes a longer time to converge to its stationary state. This time scale is measured by simulating a large ensemble (10^5) of PDMP sample paths to provide a simulated probability density and finding the Jensen–Shannon divergence [70, 71] between the instantaneous distribution of each TF and its final stationary distribution. The time for the each divergence to fall below a threshold ($:= 0.3$) is recorded, and we choose the largest of these as a quantification of the transition time. The numerical values can be found in Tables S1 and S2 in the Supporting Information.

reversal has been established in experiments [4] which have shown that in the later stages of commitment only the LIF is able to reverse lineage-primed cells back to their naive pluripotent states. The exit and re-entrance from pluripotency upon withdrawal and addition of LIF shows complex signatures of hysteresis and bifurcations. This suggests that there can be multiple pathways of entering or exiting pluripotency. The transition times for all signaling-induced changes of the steady states of the network are visualized on a kinetic diagram, Fig. 4.6. This figure shows an underlying structure to these transitions where conversion among pluripotent states takes place with lower "activation barriers" compared to transitions accompanying loss of pluripotency. In the intermediate-switching regime there is a clear time-scale separation between transitions which keep cells in pluripotent states and transitions out of pluripotent states. One may argue that such a time-scale separation between signals inducing differentiation and pluripotency allows embryonic cells to execute developmental decisions more faithfully. In the fast-switching regime this clear time scale separation is partially lost where only the loss of all three signals is separated from the rest of the transitions.

Detailed analysis of individual distributions and trajectories of transcription factors can be very informative due to their high information content. It is, however, not

immediately clear how changes in the expression of individual genes contribute to global changes corresponding to different phenotypic transitions. To reveal such global changes, we project stochastic trajectories of all transcription factors onto the first two eigenvectors obtained by principal component analysis (PCA) of the reference pluripotent steady state (LIF+2i). Most of the variance of transcription factors is well captured by the few principal components. The high-dimensional steady state of the cellular network can thus be conveniently projected onto a 2-dimensional subspace, allowing us to visualize the attractor states of the network as probability landscapes $\pi(PC_1, PC_2)$ which are often masked by heterogeneous distributions.

Comparing these probability landscapes with different gene-switching regimes reveals the distinct roles played by gene-switching-induced molecular noise and the deterministic network topology in guiding the transition out of the pluripotent states (Fig 4.7). The intermediate gene-switching regime, once again, appears to be the more viable regime underlying pluripotent states since the probability landscape shows up as a broad attractor with interconnected states. Going towards the limit of slow switching results in the fragmentation of the landscape into states separated by high barriers. This gene-switching-induced remodeling of attractors shows the potential for regulation via global epigenetic changes which are purported to act via silencing or activating entire sets of genes at once [16]. Thus one may view gene-switching rates as a proxy for genome-wide acetylation/methylation patterns which can dramatically alter the access of transcription factors to key target genomic sites. The sequential removal of pluripotency-inducing signals reveals a consistent change in the size of the attractor towards occupying smaller regions on the landscape. This argues for the physical state of the network corresponding to pluripotent states to be the one with maximal variance of regulatory transcription factors where lineage commitment is accompanied by their gradual constraining and repression. A similar idea which views pluripotency as a macrostate emerging from an ensemble of cells which try to maximizes the information entropy with respect to regulatory transcription factors has been postulated before [13, 72]. The analysis of the steady-state stochastic dynamics of the pluripotency network in this work appears in agreement with this view. Furthermore, we are able to suggest a microscopic origin of this entropic paradigm. By analyzing pairwise

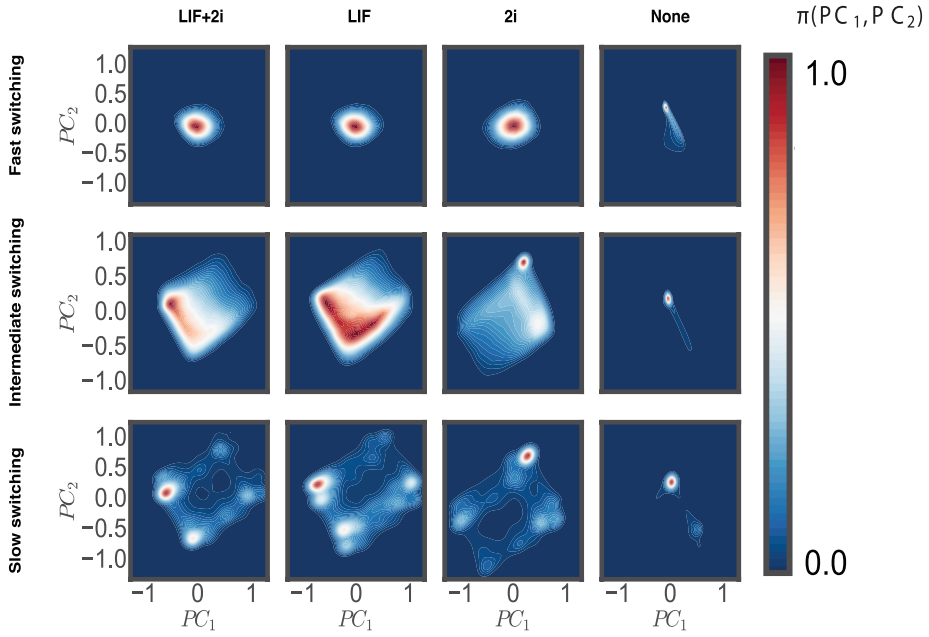

Figure 4.7: **Mapping the cellular attractors of the genetic network under different switching and signaling conditions.** We project PDMP-simulated gene expression distributions onto the first two principal components. The reference state for principal components was chosen to be the LIF+2i/intermediate switching.

correlations among different transcription factors we find that signals like LIF/2i create greater independence between the expression of core transcription factors, leading them to explore a larger range of values. Hence, removal of these signals leads to more constrained and interdependent patterns of gene expression for the same transcription factors which greatly diminishes overall variance.

4.5 Discussion

Experimental [17, 52, 73] and computational studies [55, 57, 74, 75] of embryonic stem cell networks have increasingly emphasized a systems-level perspective where pluripotency is a result of sophisticated biological computations done by a tightly-integrated set of genes, epigenetic and transcription factors [17, 76]. The rapid growth of gene-expression data on mESCs under many different *in vitro* conditions has enabled reliable inferences of the underlying topology of pluriptoency-regulating networks [17]. At the same time single-cell probes of gene expression in mESCs reveal significant heterogeneity and dynamism in bio-molecular populations[8, 9], suggesting that molecular

stochasticity and non-equilibrium processes could be playing a crucial role in regulating pluripotnecy and stem cell differentiation. Thus the schematic network topology models inferred from real data, while immensely useful, are not always sufficient for rationalizing the single-cell data, which is rich with stochastic and dynamical information. On the other hand, full chemical-master-equation-based stochastic simulations of complex ESC networks with complete bio-molecular inventory quickly become impractical, especially when making data-driven parameter searches and explorative simulations with a large number of external conditions.

In the present work we have developed a multi-scale computational scheme for converting experimentally-inferred Boolean topologies into quantitative and predictive models of networks with a microscopic resolution of gene-expression dynamics. The employed computational model is based on previously proposed hybrid stochastic dynamics approaches [19,24,25,36] in which the switching dynamics of individual genes are considered exactly while the rest of the biochemical reactions are approximated as deterministic processes. This hybrid-stochastic approach is approximately thousand fold faster than conventional kinetic Monte Carlo methods. This gain in computational speed allows us to simulate large scale gene regulatory networks of ESC under different culture conditions and gene-switching regimes. Thanks to rapid hybrid simulations we are able to use a standard optimization approach to exhaustively sample the space of rates and find the closest match with the experimental gene expression data collected different culturing environments [17]. The approximation introduced due to using the hybrid scheme is validated by showing excellent quantitative agreement of both steady states distributions and dynamical transition times with the fully stochastic simulations for the identified parameter sets. This agreement also shows that the switching events of genes—due to stochastic TFs binding to the promoter sites—is likely a dominant source of variance in transcription factor populations of ESC networks.

We find that the intermediate regime, in which the gene-switching rate is comparable to the other reaction rates in the network, is most consistent with single-cell measurements [8–10]. This result has also been pointed out by Sasai *et al.* [44] when exploring time scale hierarchy in stem cell networks with individual-based models and concluding that experimentally observed phenotypic heterogeneity likely originates

from promoter reorganization and genetic switching taking place on the comparable time-scale with the rest of the biochemical processes. In this intermediate-switching regime the transcription factors show bursty dynamics which lead to heterogeneous distributions with some showing long-tailed and bimodal features. Consistent with many experiments [8–10], our simulations show that the presence of LIF and 2i signals is crucial for maintaining the stability of pluripotent states, which in our model are defined as states with an up-regulated triad of pluripotency factors Nanog/Oct4/Sox2. Withdrawal of either LIF/2i initiates lineage commitment via a robust pattern of reduced expression of the Nanog/Oct4/Sox2 triad in the simulations.

To characterize the dynamics of lineage commitment, we have computed the transition times of going from pluripotent to differentiated steady states. We find that an intermediate regime of gene switching generates more heterogeneous distributions of transcription factors, which in turn makes the network more responsive to changes in signaling conditions. For instance, the response time to LIF/2i withdrawal is much faster in a more stochastic regime than in the more deterministic regime corresponding to faster gene switching time scales. Next, by carrying out principal component analysis on ensembles of gene expression profiles, we find a much simpler description of pluripotency and lineage commitment in terms of effective probability landscapes. As the signals safeguarding pluripotency are removed, these landscapes reveal a gradual narrowing of the steady-state attractor explored by the network. Thus, we see a hierarchical organization of differentiation landscapes where pluripotent states pose the largest attractor which is maintained through the extracellular signals and the molecular noise of gene switching.

Given the rapid rise of information from high throughput single-cell nucleic acid based techniques (RNA-seq, RNA-FISH, qPCR, etc.), we expect microscopic resolution models, such as reported in the present work, to play important roles in bridging the systems-level behavior of genetic networks with the underlying molecular-level processes of binding, reaction and diffusion.

4.6 Methods

4.6.1 Constructing the piecewise-deterministic Markov process (PDMP)

In the individual-based description of complex genetic networks studied in the present work, one models each individual reactive species as a Markov jump process. The underlying master equation governing the Markvoian evolution of the entire network is analytically intractable and in general even numerical simulations quickly become computational inefficient once dimensionality of the system becomes too high [77]. Specifically what contributed to this inefficiency is the population scale of transcription factors for which it is common to have values on the order of $\Omega = 10^4$ as is characteristic for biological cells. Thus the use of standard continuous-time Monte Carlo [18, 78] sampling techniques becomes unfeasible especially if one wants to sample the kinetic parameter regimes for finding optimal sets of rate coefficients.

Fortunately the latest efforts of modeling gene-expression dynamics [19, 24, 25, 36, 64, 65, 79] have lead to the emergence of a new class of techniques which are broadly based on using a piecewise-deterministic Markov process (PDMP) to approximate the individual-based model with a switching property. In this section, we briefly recapitulate the construction of the PDMP. A more thorough analysis can be found in the literature cited [19, 24, 25, 36, 64, 65, 79] .

A PDMP is a process such that, in between discrete random switching events, the evolution of the process is deterministic. To construct the deterministic evolution of the TF populations, starting from the chemical master equations, we performed a Kramers–Moyal expansion [77, 80] in the population of TFs while maintaining the discreteness of the genetic state; we keep only the first order of the expansion. The result is a standard Liouville equation governing the *deterministic flow* of the distribution. The joint probability distribution of our model converges to the deterministic flow in a given genetic state and in the thermodynamic limit $\Omega \to \infty$ [80]. With the PDMP approach, the demographic noise originating from random birth-death events are neglected, so that the population density $x_i(t)$ of each TF evolves according to

$$\frac{\mathrm{d}}{\mathrm{d}t} x_i(t) = \alpha_i - \gamma x_i(t), \tag{4.3}$$

where $\alpha_i \in \{0, \alpha_m, \alpha_{\max}\}$ is the production rate of the ith TF dependent on the ith gene's configuration of promoter sites. While the evolution of the TF population density is deterministic, the binding and unbinding events of the regulating TFs to their target genes are still stochastic and formulated according to Eq. (4.1).

We finally emphasize that the PDMP only retains the contribution of *switching noise* which arises from the discrete and stochastic binding and unbinding events between the TFs and the promoter sites, and ignores *demographic stochasticity* from the discrete production and degradation processes of the TFs.

4.6.2 Generating exact sample paths of the PDMP

To simulate the stochastic binding and unbinding statistics of the promoter sites, accurate waiting times must be generated. A waiting time exists for each possible stochastic transition; the smallest of these times tells us how long the system stays in the current configuration of promoter sites, and to which promoter configuration it transitions. In general, waiting times can be generated by mapping a uniform random variable to a random time using the survival function. Since in our case the transition rates are functions of dynamical state variables, this involves the numerical integration of survival functions describing each potential transition [64]. In our case, the simple form of Eq. 4.3 (and thus of the transition rates) allows us to improve upon this by generating waiting times without numerical integration, detailed in Appendix 4.7.

4.6.3 Non-dimensionalization of model parameters

Under the assumptions we proposed, there are initially six free model parameters: $\Omega\alpha_{\max}$ and $\Omega\alpha_m$ as the production rates when each of the genes has an "ON" or "MEDIUM" activity, γ as the protein degradation rate, N as the number of promoter sites, and lastly $k_{\text{on}}\Omega^{-1}$ and k_{off} as the binding and unbinding rates between the TFs and the promoter sties. We remark that the population scale Ω is fixed at 10^4.

Through suitable non-dimensionalization of the physical time and concentrations of the TFs, we reduce the number of parameters. As can be seen from the above formulation (Eq. 4.3), the time scale of the TF dynamics is set by the degradation rate γ. For stable proteins, the time scale of degradation is of the order of the times of the

cell cycle. We therefore choose the unit of physical time such that γ is 1. Similarly, the maximum concentration in the TF can achieve in Eq. 4.3 is $\alpha_{\max}/\gamma$. We can choose a unit for the concentrations of the chemical species such that $\alpha_{\max} = 1$, so the concentration of the TFs are always bounded in $(0, 1)$. After non-dimensionalization, the model ends up with four free parameters: $\alpha_m \in \{0, 1\}$ as the intermediate production rate of those genes which are regulated by both activators and repressors, k_{on}, k_{off} as the binding and unbinding rate of the TF to the promoter sites, and N as the number of promoter sites per gene.

4.6.4 Using the checkerboard diagram to infer the parameter regime

To narrow down the parameter regime, we match our model predictions to the experimental findings of Dunn *et al.* [17] in which the authors measured the TF expression under various combinations of external signals: LIF, CH, and PD. We aim to match the model prediction to a twelve-by-five "checkerboard diagram" which records the experimentally measured expression pattern presented in Fig. 4.2. To achieve this goal, we performed a sweep in a vast parameter space: $\alpha_m \in [0, 1]$, $k_{\text{on}}, k_{\text{off}} \in [0, 110]$, and $N = 1, 2, \ldots, 5$. For each parameter set, we simulated 10^3 PDMP sample paths for a time to sufficiently reflect the stationary state, and the average TF expression levels were recorded. Because of the non-dimensionalization, the expression level (the population density) of each TF is a real number in between 0 and 1. This results in a twelve-by-five real-valued matrix, which is binarized by a threshold. To find the optimal threshold, we use the number of discrepancies between the model prediction and the target matrix—the Hamming distance—as a quantitative measure. For each parameter set, an optimal threshold which minimizes the Hamming distance was then found computationally, and the minimal Hamming distance was recorded and plotted in Fig. 4.2 in the main text as a "landscape" of how good the model captures the experimental results. We found that for $N = 1$ and $N \geq 2$, the global minimal Hamming distance is 5 and 3 respectively. We chose $N = 2$ to present our follow-up analysis, as it incorporates the capacity of modeling cooperative binding which is often modeled phenomenologically. We find the Hamming distance can be constantly as

small as 3 in a vast region in the space of binding/unbinding rates when α_m is small ($\lesssim 0.02$). Therefore, in the manuscript we present the landscape of a fast switching regime $k_{\text{on}} \approx 100$, an intermediate regime $k_{\text{on}} \approx 15$ and a slow switching regime $k_{\text{on}} \approx 3$.

4.6.5 Validating the PDMP against the individual-based model

For the three selected parameter sets, 10^4 sample paths of a fully individual-based model were generated by standard kinetic Monte Carlo simulations—namely Gillespie's stochastic simulation algorithm (SSA) [18, 78]. The population scale Ω for each TF is set to be 10^4. A parallel analysis is carried out and the results are consistent with the predictions from using the PDMP. We report the results for the intermediate switching regime in Fig. 4.4.

4.6.6 Visualizing stochastic fluctuations in gene expression on low dimensional manifolds using principal component analysis (PCA)

While the joint probability distributions are measured by kinetic Monte Carlo sampling, the dimensionality of the dynamical system is very high: each TF has a real-valued density, so that even if we marginalize over the genetic states the probability density is a 12-dimensional object. Although Fig. 4.4 summarizes the marginal distributions of the real-valued TF density and contains rich information, it is desirable to visualize the results in a lower-dimensional space to draw qualitative conclusions. To achieve this goal, we perform the standard principal component analysis [81]. We chose a baseline external condition to be LIF+2i; the first two principal components were computed. For the rest of the external conditions, the joint probability distributions are projected onto the plane spanned by these principal components; the results are presented in Fig. 4.7.

4.6.7 Dynamical transitions between different external signals

To investigate dynamical transitions when the external driving conditions (whether LIF, CH, and PD are present) change, we prepare 10^5 independent sample paths with an initial external condition until the joint probability distribution converges to the stationary distribution. Then, the external condition is switched instantaneously to the second condition. We further evolve the dynamical system until stationarity for the second conditions is reached. The results are summarized in Fig. 4.5. To estimate the transition times between the stationary distributions with different external conditions, we measure the Jensen–Shannon distance of the marginal distribution of each TF density, at any given time during the transition to the final marginal distribution. We measure and report the first time when all 12 distances are below a threshold value of 0.3, presented in Fig. 4.6.

4.7 Appendix: Efficient generation of waiting times for genetic-switching events

Our approach requires the generation of accurate waiting times, which dictate how long the system stays in the current configuration of promoter sites, and to which promoter configuration it transitions. In our case the simple form of the PDMP, and consequently of the transition rates, allows us to generating waiting times without numerical integration of the survival function.

The TF density of a given type, with an initial condition x_0 at time 0, is described by

$$x(t) = \frac{\alpha}{\gamma} + \left(x_0 - \frac{\alpha}{\gamma}\right) \exp\left(-\gamma t\right). \tag{4.4}$$

We dropped the subscript i for brevity in this section. It follows that the survival function—the probability that the switching time is greater than time t—describing a genetic binding event is given by

$$\begin{aligned} S(t) &= \exp\left[-k_{\text{on}} \int_0^t x(t')\mathrm{d}t'\right] \\ &= \exp\left\{-\frac{k_{\text{on}}}{\gamma}\left[\alpha t - \left(x_0 - \frac{\alpha}{\gamma}\right)\left(e^{-\gamma t} - 1\right)\right]\right\}. \end{aligned} \tag{4.5}$$

To use the inverse method, one generates a random number $u \sim \mathrm{Unif}\,(0,1)$ and solves the equation $u = S(t)$ for t. The solution is a random binding time with the correct distribution.

When the density is monotonically decreasing ($x_0 > \alpha$), the procedure allows one to rigorously generate *exact* switching times [82]. This involves generating two independent random numbers u_1, $u_2 \sim \mathrm{Unif}\,(0,1)$ such that the random time of a binding event t is given by $t = \min(t_1, t_2)$ where

$$t_1 = \begin{cases} -\gamma\,(\log u_1)\,/\,(\alpha k_{\mathrm{on}}) & \text{if } \alpha \neq 0, \\ \infty & \text{if otherwise.} \end{cases} \tag{4.6a}$$

$$t_2 = \begin{cases} -\gamma \log\left\{(\log u_2)\,/\,[k_{\mathrm{on}}\,(x_0 - \alpha/\gamma)] + 1\right\} & \text{if } u_2 > \exp\left[-k_{\mathrm{on}}\,(x_0 - \alpha/\gamma)\right], \\ \infty & \text{if otherwise.} \end{cases} \tag{4.6b}$$

The case when the density is monotonically increasing $u = S(t)$ is not analytically solvable but can be solved numerically and with efficiency using the Newton–Raphson scheme. Using these two approaches together, the random waiting times for the next binding event of gene i can be efficiently generated.

The unbinding events are independent of the population of TFs. Since each bound TF on a promoter dissociate independently and identically with a rate k_{off}, the waiting time of each of the dissociating events is exponentially distributed ($\sim \exp\,(k_{\mathrm{off}})$) and can be efficiently generated [78].

At any given point in time and given the state of the system, we can use the above procedures to generate the random waiting times for binding or unbinding events. Before the first event (i.e., the binding or unbinding event with the minimal waiting times) takes place, the dynamics of TF evolve deterministically and all the promoter states remains constant. At the time of the earliest binding or unbinding event, the promoter state corresponding to this binding or unbinding event is updated, and new random waiting times are generated.

4.8 Bibliography

[1] Y. T. Lin, P. G. Hufton, E. J. Lee, and D. A. Potoyan. A stochastic and dynamical view of pluripotency in mouse embryonic stem cells. *PLOS Comput. Biol.* **14**, 1

(2018).

[2] M. Evans. Discovering pluripotency: 30 years of mouse embryonic stem cells. *Nat. Rev. Mol. Cell. Biol.* **12**, 680 (2011).

[3] C. E. Murry and G. Keller. Differentiation of embryonic stem cells to clinically relevant populations: lessons from embryonic development. *Cell* **132**, 661 (2008).

[4] G. Martello and A. Smith. The nature of embryonic stem cells. *Ann. Rev. Cell. Dev. Biol.* **30**, 647 (2014).

[5] N. G. Van Kampen. *Stochastic processes in physics and chemistry*, volume 1. Elsevier, Amsterdam (1992).

[6] O. Symmons and A. Raj. Whats Luck Got to Do with It: Single Cells, Multiple Fates, and Biological Nondeterminism. *Mol. cell.* **62**, 788 (2016).

[7] G. Balázsi, A. van Oudenaarden, and J. J. Collins. Cellular decision making and biological noise: from microbes to mammals. *Cell* **144**, 910 (2011).

[8] Z. S. Singer, J. Yong, J. Tischler, J. A. Hackett, A. Altinok, M. A. Surani, L. Cai, and M. B. Elowitz. Dynamic heterogeneity and DNA methylation in embryonic stem cells. *Mol. Cell.* **55**, 319 (2014).

[9] R. M. Kumar, P. Cahan, A. K. Shalek, R. Satija, A. J. DaleyKeyser, H. Li, J. Zhang, K. Pardee, D. Gennert, J. J. Trombetta, *et al.* Deconstructing transcriptional heterogeneity in pluripotent stem cells. *Nature* **516**, 56 (2014).

[10] M. A. Canham, A. A. Sharov, M. S. Ko, and J. M. Brickman. Functional heterogeneity of embryonic stem cells revealed through translational amplification of an early endodermal transcript. *PLoS Biol.* **8**, e1000379 (2010).

[11] T. Kalmar, C. Lim, P. Hayward, S. Muñoz-Descalzo, J. Nichols, J. Garcia-Ojalvo, and A. M. Arias. Regulated fluctuations in nanog expression mediate cell fate decisions in embryonic stem cells. *PLoS Biol.* **7**, e1000149 (2009).

[12] S. Masui, Y. Nakatake, Y. Toyooka, D. Shimosato, R. Yagi, K. Takahashi, H. Okochi, A. Okuda, R. Matoba, A. A. Sharov, *et al.* Pluripotency governed

by Sox2 via regulation of Oct3/4 expression in mouse embryonic stem cells. *Nat. Cell Biol.* **9**, 625 (2007).

[13] B. D. MacArthur and I. R. Lemischka. Statistical mechanics of pluripotency. *Cell* **154**, 484 (2013).

[14] J. Feigelman, S. Ganscha, S. Hastreiter, M. Schwarzfischer, A. Filipczyk, T. Schroeder, F. J. Theis, C. Marr, and M. Claassen. Analysis of Cell Lineage Trees by Exact Bayesian Inference Identifies Negative Autoregulation of Nanog in Mouse Embryonic Stem Cells. *Cell Sys.* **3**, 480 (2016).

[15] H. Xu, Y.-S. Ang, A. Sevilla, I. R. Lemischka, and A. Ma'ayan. Construction and validation of a regulatory network for pluripotency and self-renewal of mouse embryonic stem cells. *PLoS Comput. Biol.* **10**, e1003777 (2014).

[16] S. Semrau and A. van Oudenaarden. Studying lineage decision-making in vitro: emerging concepts and novel tools. *Ann. Rev. Cell. Dev. Biol.* **31**, 317 (2015).

[17] S.-J. Dunn, G. Martello, B. Yordanov, S. Emmott, and A. Smith. Defining an essential transcription factor program for naive pluripotency. *Science* **344**, 1156 (2014).

[18] D. T. Gillespie. Exact stochastic simulation of coupled chemical reactions. *J. Phys. Chem.* **81**, 2340 (1977).

[19] P. G. Hufton, Y. T. Lin, T. Galla, and A. J. McKane. Intrinsic noise in systems with switching environments. *Phys. Rev. E* **93**, 052119 (2016).

[20] J. N. Weiss. The Hill equation revisited: uses and misuses. *FASEB J.* **11**, 835 (1997).

[21] P. C. Bressloff. *Stochastic processes in cell biology*, volume 41. Springer, Berlin (2014).

[22] T. B. Kepler and T. C. Elston. Stochasticity in transcriptional regulation: origins, consequences, and mathematical representations. *Biophys. J.* **81**, 3116 (2001).

[23] J. Hornos, D. Schultz, G. Innocentini, J. Wang, A. Walczak, J. Onuchic, and P. Wolynes. Self-regulating gene: an exact solution. *Phys. Rev. E* **72**, 051907 (2005).

[24] Y. T. Lin and T. Galla. Bursting noise in gene expression dynamics: linking microscopic and mesoscopic models. *J. R. Soc. Interface* **13**, 20150772 (2016).

[25] Y. T. Lin and C. R. Doering. Gene expression dynamics with stochastic bursts: Construction and exact results for a coarse-grained model. *Phys. Rev. E* **93**, 022409 (2016).

[26] S. Ramakrishna, B. Suresh, K.-H. Lim, B.-H. Cha, S.-H. Lee, K.-S. Kim, and K.-H. Baek. PEST motif sequence regulating human NANOG for proteasomal degradation. *Stem. Cell. Dev.* **20**, 1511 (2011).

[27] M.-E. Torres-Padilla and I. Chambers. Transcription factor heterogeneity in pluripotent stem cells: a stochastic advantage. *Development* **141**, 2173 (2014).

[28] E. Abranches, E. Bekman, and D. Henrique. Generation and characterization of a novel mouse embryonic stem cell line with a dynamic reporter of Nanog expression. *PLoS One* **8**, e59928 (2013).

[29] M. Thomson, S. J. Liu, L.-N. Zou, Z. Smith, A. Meissner, and S. Ramanathan. Pluripotency circuit members mediate germ layer fate choice of embryonic stem cells. *Cell* **145**, 875 (2011).

[30] J. Goutsias and G. Jenkinson. Markovian dynamics on complex reaction networks. *Phys. Rep.* **529**, 199 (2013).

[31] N. Le Novère. Quantitative and logic modelling of molecular and gene networks. *Nature Rev. Genet.* **16**, 146 (2015).

[32] T. Szekely and K. Burrage. Stochastic simulation in systems biology. *Comput. Struct. Biotechnol. J.* **12**, 14 (2014).

[33] M. F. Weber and E. Frey. Master equations and the theory of stochastic path integrals. *Rep. Prog. Phys.* **80**, 046601 (2017).

[34] M. Assaf and B. Meerson. WKB theory of large deviations in stochastic populations. *J. Phys. A* **50**, 263001 (2017).

[35] E. Wallace, D. Gillespie, K. Sanft, and L. Petzold. Linear noise approximation is valid over limited times for any chemical system that is sufficiently large. *IET Syst. Biol.* **6**, 102 (2012).

[36] D. A. Potoyan and P. G. Wolynes. Dichotomous noise models of gene switches. *J. Chem. Phys.* **143**, 195101 (2015).

[37] S. Huang, G. Eichler, Y. Bar-Yam, and D. E. Ingber. Cell fates as high-dimensional attractor states of a complex gene regulatory network. *Phys. Rev. Lett.* **94**, 128701 (2005).

[38] H. Ge, H. Qian, and X. S. Xie. Stochastic phenotype transition of a single cell in an intermediate region of gene state switching. *Phys. Rev. Lett.* **114**, 078101 (2015).

[39] A. Lipshtat, A. Loinger, N. Q. Balaban, and O. Biham. Genetic toggle switch without cooperative binding. *Phys. Rev. Lett.* **96**, 188101 (2006).

[40] M. Sasai and P. G. Wolynes. Stochastic gene expression as a many-body problem. *Proc. Natl. Acad. Sci. U.S.A.* **100**, 2374 (2003).

[41] A. M. Walczak, J. N. Onuchic, and P. G. Wolynes. Absolute rate theories of epigenetic stability. *Proc. Natl. Acad. Sci. U.S.A.* **102**, 18926 (2005).

[42] H. Feng, B. Han, and J. Wang. Adiabatic and non-adiabatic non-equilibrium stochastic dynamics of single regulating genes. *J. Phys. Chem. B* **115**, 1254 (2010).

[43] T. L. Lenstra, J. Rodriguez, H. Chen, and D. R. Larson. Transcription Dynamics in Living Cells. *Ann. Rev. Biophys.* (2016).

[44] M. Sasai, Y. Kawabata, K. Makishi, K. Itoh, and T. P. Terada. Time scales in epigenetic dynamics and phenotypic heterogeneity of embryonic stem cells. *PLOS Comput. Biol.* **9**, e1003380 (2013).

[45] M. Herberg and I. Roeder. Computational modelling of embryonic stem-cell fate control. *Development* **142**, 2250 (2015).

[46] Q. Bian and P. Cahan. Computational tools for stem cell biology. *Trends Biotechnol.* **34**, 993 (2016).

[47] S. Okawa, S. Nicklas, S. Zickenrott, J. C. Schwamborn, and A. del Sol. A generalized gene-regulatory network model of stem cell differentiation for predicting lineage specifiers. *Stem Cell Reports* **7**, 307 (2016).

[48] A. Yachie-Kinoshita, K. Onishi, J. Ostblom, E. Posfai, J. Rossant, and P. W. Zandstra. Modeling signaling-dependent pluripotent cell states with boolean logic can predict cell fate transitions. *bioRxiv* page 115683 (2017).

[49] S.-J. Dunn, M. A. Li, E. Carbognin, A. G. Smith, and G. Martello. A common molecular logic determines embryonic stem cell self-renewal and reprogramming. *bioRxiv* page 200501 (2017).

[50] A. H. Lang, H. Li, J. J. Collins, and P. Mehta. Epigenetic landscapes explain partially reprogrammed cells and identify key reprogramming genes. *PLoS Comp. Biol.* **10**, e1003734 (2014).

[51] A. T. Fard, S. Srihari, J. C. Mar, and M. A. Ragan. Not just a colourful metaphor: modelling the landscape of cellular development using hopfield networks. *NPJ Syst. Biol. Appl.* **2**, 16001 (2016).

[52] S. Jang, S. Choubey, L. Furchtgott, L.-N. Zou, A. Doyle, V. Menon, E. B. Loew, A.-R. Krostag, R. A. Martinez, L. Madisen, *et al.* Dynamics of embryonic stem cell differentiation inferred from single-cell transcriptomics show a series of transitions through discrete cell states. *eLife* **6**, e20487 (2017).

[53] V. Chickarmane, C. Troein, U. A. Nuber, H. M. Sauro, and C. Peterson. Transcriptional dynamics of the embryonic stem cell switch. *PLoS Comput. Biol.* **2**, e123 (2006).

[54] V. Chickarmane and C. Peterson. A computational model for understanding stem cell, trophectoderm and endoderm lineage determination. *PLoS One* **3**, e3478 (2008).

[55] S. Godwin, D. Ward, E. Pedone, M. Homer, A. G. Fletcher, and L. Marucci. An extended model for culture-dependent heterogenous gene expression and proliferation dynamics in mouse embryonic stem cells. *NPJ Syst. Biol. Appl.* **3**, 19 (2017).

[56] M. Herberg, T. Kalkan, I. Glauche, A. Smith, and I. Roeder. A model-based analysis of culture-dependent phenotypes of mESCs. *PloS One* **9**, e92496 (2014).

[57] M. Herberg, I. Glauche, T. Zerjatke, M. Winzi, F. Buchholz, and I. Roeder. Dissecting mechanisms of mouse embryonic stem cells heterogeneity through a model-based analysis of transcription factor dynamics. *J. Roy. Soc. Int.* **13**, 20160167 (2016).

[58] C. Li and J. Wang. Quantifying Waddington landscapes and paths of non-adiabatic cell fate decisions for differentiation, reprogramming and transdifferentiation. *J. R. Soc. Interface* **10**, 20130787 (2013).

[59] V. Chickarmane, V. Olariu, and C. Peterson. Probing the role of stochasticity in a model of the embryonic stem cell–heterogeneous gene expression and reprogramming efficiency. *BMC Sys. Biol.* **6**, 98 (2012).

[60] J. Wang, K. Zhang, L. Xu, and E. Wang. Quantifying the Waddington landscape and biological paths for development and differentiation. *Proc. Natl. Acad. Sci. U.S.A.* **108**, 8257 (2011).

[61] B. Zhang and P. G. Wolynes. Stem cell differentiation as a many-body problem. *Proc. Natl. Acad. Sci. U.S.A.* **111**, 10185 (2014).

[62] P. Wang, C. Song, H. Zhang, Z. Wu, X.-J. Tian, and J. Xing. Epigenetic state network approach for describing cell phenotypic transitions. *Interface Focus* **4**, 20130068 (2014).

[63] H. Feng and J. Wang. A new mechanism of stem cell differentiation through slow binding/unbinding of regulators to genes. *Sci. Rep.* **2**, 550 (2012).

[64] S. Zeiser, U. Franz, O. Wittich, and V. Liebscher. Simulation of genetic networks modelled by piecewise deterministic Markov processes. *IET Syst. Biol.* **2**, 113 (2008).

[65] Y. T. Lin and N. E. Buchler. Efficient analysis of stochastic gene dynamics in the non-adiabatic regime using piecewise deterministic Markov processes. *ArXiv e-prints* (2017).

[66] U. Herbach, A. Bonnaffoux, T. Espinasse, and O. Gandrillon. Inferring gene regulatory networks from single-cell data: a mechanistic approach. *arXiv preprint arXiv:1705.03407* (2017).

[67] M. H. Davis. Piecewise-deterministic Markov processes: A general class of non-diffusion stochastic models. *J. Roy. Statist. Soc. Ser. B* **46**, 353 (1984).

[68] H. Ochiai, T. Sugawara, T. Sakuma, and T. Yamamoto. Stochastic promoter activation affects Nanog expression variability in mouse embryonic stem cells. *Sci. Rep.* **4**, 7125 (2014).

[69] A. M. Klein, L. Mazutis, I. Akartuna, N. Tallapragada, A. Veres, V. Li, L. Peshkin, D. A. Weitz, and M. W. Kirschner. Droplet barcoding for single-cell transcriptomics applied to embryonic stem cells. *Cell* **161**, 1187 (2015).

[70] J. Lin. Divergence measures based on the Shannon entropy. *IEEE Trans. Inf. Theory* **37**, 145 (1991).

[71] D. M. Endres and J. E. Schindelin. A new metric for probability distributions. *IEEE Trans. Inf. Theory* **49**, 1858 (2003).

[72] S. J. Ridden, H. H. Chang, K. C. Zygalakis, and B. D. MacArthur. Entropy, ergodicity, and stem cell multipotency. *Phys. Rev. Lett.* **115**, 208103 (2015).

[73] A. Filipczyk, C. Marr, S. Hastreiter, J. Feigelman, M. Schwarzfischer, P. S. Hoppe, D. Loeffler, K. D. Kokkaliaris, M. Endele, B. Schauberger, *et al.* Network plasticity of pluripotency transcription factors in embryonic stem cells. *Nat. Cell Biol.* **17**, 1235 (2015).

[74] L. Marucci. Nanog Dynamics in Mouse Embryonic Stem Cells: Results from Systems Biology Approaches. *Stem Cells Int.* **2017** (2017).

[75] S. Kontogeorgaki, R. Sanchez-Garcia, R. Ewing, K. Zygalakis, and B. D. MacArthur. Noise-processing by signaling networks. *bioRxiv* page 075366 (2016).

[76] B. D. MacArthur, A. Ma'ayan, and I. R. Lemischka. Systems biology of stem cell fate and cellular reprogramming. *Nat. Rev. Mol. Cell. Biology* **10**, 672 (2009).

[77] C. W. Gardiner *et al. Handbook of stochastic methods*, volume 3. Springer, Berlin (1985).

[78] R. Schwartz. *Biological modeling and simulation: a survey of practical models, algorithms, and numerical methods*. MIT Press, Cambridge MA (2008).

[79] S. Zeiser, U. Franz, and V. Liebscher. Autocatalytic genetic networks modeled by piecewise-deterministic Markov processes. *J. Math. Biol.* **60**, 207 (2010).

[80] T. G. Kurtz. Solutions of ordinary differential equations as limits of pure jump Markov processes. *J. Appl. Probab.* **7**, 49 (1970).

[81] I. Jolliffe. *Principal component analysis*. Wiley Online Library, Hoboken NJ (2002).

[82] P. Bokes, J. R. King, A. T. Wood, and M. Loose. Transcriptional bursting diversifies the behaviour of a toggle switch: hybrid simulation of stochastic gene expression. *Bull. Math. Biol.* **75**, 351 (2013).

Chapter 5

Model reduction methods for classical stochastic systems with fast-switching environments: reduced master equations, stochastic differential equations, and applications

5.1 Preface

The contents of this chapter constitute a submitted manuscript, which has been made public on arXiv [1]. The manuscript was authored by Peter G. Hufton[1], Yen Ting Lin[1,2] and Tobias Galla[1]. All authors contributed to this work equally.

P.G.H.'s contribution includes the initial inception of the project, performing all calculations and analysis therein, coding simulations, producing the data for all figures (except Figs. 5.3, 5.6, and 5.7), finalising all figures, and writing all sections of the paper alongside Y.T.L. and T.G.

[1]Theoretical Physics, School of Physics and Astronomy, The University of Manchester, Manchester M13 9PL, United Kingdom

[2]Theoretical Division and Center for Nonlinear Studies, Los Alamos National Laboratory, Los Alamos, NM 87544, United States of America

Abstract

We study classical stochastic systems with discrete states, coupled to switching external environments. For fast environmental processes we derive reduced dynamics for the system itself, focusing on corrections to the adiabatic limit of infinite time scale separation. In some cases, this leads to master equations with negative transition 'rates' or bursting events. We devise a simulation algorithm in discrete time to unravel these master equations into sample paths, and provide an interpretation of bursting events. Focusing on stochastic population dynamics coupled to external environments, we discuss a series of approximation schemes combining expansions in the inverse switching rate of the environment, and a Kramers–Moyal expansion in the inverse size of the population. This places the different approximations in relation to existing work on piecewise-deterministic and piecewise-diffusive Markov processes. We apply the model reduction methods to different examples including systems in biology and a model of crack propagation.

5.2 Introduction

Physical and biological systems can never be fully isolated from their environment. This includes the dynamics of microbes in time-varying external conditions (e.g., antibiotic treatment) [2–5], or protein production in gene regulatory networks, influenced by the stochastic binding and unbinding of promoters [6–10]. Other examples can be found in models of evolutionary dynamics [11–14], the spread of diseases [15], and in ecology and population dynamics [16–19]. Many of models of these phenomena contain two types of randomness: one intrinsic to the system itself, and another generated by the noise in the environmental dynamics. Applications of systems coupled to stochastic external environments go as far as reliability analysis and crack propagation in materials, where environmental states correspond to different strains due to external loading [20–25]. The study of open quantum systems defines an entire area of research [26–28].

These examples share a common structure: there is the system proper and the environment, and a coupling between them; this interaction can act either in one way or in both directions. In such situations it is often not possible (or desirable) to track and analyse in detail the dynamics of the system *and* that of the environment. Instead the focus is on deriving reduced dynamics for the system itself, which in some way account for the influence of the environment on the system. Work on open quantum systems for example focuses on understanding the dynamics of reduced density matrices after integrating out the environment [26–28].

Existing work on open classical systems includes those described by stochastic differential equations (SDEs) coupled to continuous environments [11, 29–31], and deterministic models with discrete external noise [32–34]. A specific case of Brownian particles, subject to random external gating is considered in Ref. [35]. In chemical or biological systems the quasi-steady-state approximation or related adiabatic reduction techniques can be used to eliminate fast reactions [36, 37].

In this paper we consider open stochastic systems with discrete states. While some of our theory is applicable more generally, we mostly focus on populations of interacting 'individuals'. We will often use the words 'system' and 'population' synonymously. Examples we have in mind are chemical reaction system with discrete molecules, or populations in biological systems, composed of members of different species. For a fixed environment, such a system is described by a (classical) master equation defined by the transition rates between its discrete states. These transitions are typically events in which particles are produced or removed from the population, or in which a particle of one type is converted into another type. In biological populations they can represent birth or death events. We are interested in cases in which such a population is coupled to an external environment, which also takes discrete states. The environmental states in turn affect the transition rates within the population.

Our aim is to study the reduced dynamics of such systems after the environmental dynamics are integrated out. In particular we focus on the limit in which the environmental dynamics are fast compared to those of the population, but where the separation of time scales is not infinite. We show how reduced master equations can be derived systematically; interestingly negative transition 'rates' can emerge in these reduced dynamics. This is similar to what is observed in the theory of open quantum

systems [27,38,39], but there are also key differences. We provide an approximation at the level of sample paths in discrete-time, and comment on different numerical schemes to address master equations with negative rates. We also describe in more detail how expansions in the inverse time scale of the environmental dynamics can be combined with expansions in the inverse system size of the population. These are effectively weak-noise expansions for the extrinsic and intrinsic stochasticity of the problem. Finally we apply the formalism to a number of examples ranging from gene regulatory networks to crack propagation in materials.

Our aim is to study the reduced dynamics of such systems after the environmental dynamics are integrated out. In particular we focus on the limit in which the environmental dynamics are fast compared to those of the population, but where the separation of time scales is not infinite. We show how reduced master equations can be derived systematically; interestingly negative transition 'rates' can emerge in these reduced dynamics. This is similar to what is observed in the theory of open quantum systems [27, 38, 39], but there are also key differences. We provide an approximation at the level of sample paths in discrete-time, and comment on different numerical schemes to address master equations with negative rates. A main result of this chapter is a detailed description of how expansions in the inverse time scale of the environmental dynamics can be combined with expansions in the inverse system size of the population. These are effectively weak-noise expansions for the extrinsic and intrinsic stochasticity of the problem, which in many cases facilitate analytical results or more efficient simulation. Finally we apply the formalism to a number of examples ranging from gene regulatory networks to crack propagation in materials.

The remainder of the paper is organised as follows. In Sec. 5.3 we introduce the type of model we address, a classical stochastic system with discrete states coupled to an external environment, also with discrete states. In Sec. 5.4 we present the detailed mathematics used for the analysis and derive an effective master equation in the limit of fast time scales of the environmental switching; specifically, our analysis includes next-order corrections to the adiabatic limit of infinitely fast environments. We illustrate this using a set of simple examples. In Sec. 5.5 we use this general result to show how master equations with negative transition 'rates' arise, and comment on their interpretation and on a numerical scheme to sample its statistics at ensemble

level. Sec. 5.7 describes the effective dynamics on the level of sample paths, and provides more insight into reduced master equations with negative 'rates'. In Sec. 5.8 we combine expansions in the inverse size of the population with that in the time scale of the switching dynamics, and provide a systematic classification of the different resulting model reduction schemes. We discuss a set of applications in Sec. 5.9, before we summarise and present our conclusions in Sec. 5.10.

5.3 General definitions

5.3.1 Model

We focus on a classical system with discrete states, labelled ℓ, which is coupled to an environment also taking discrete states, which we label σ. The system and the environment evolve in continuous time. The dynamics of the system itself depend on the current state of the environment. The environment in turn switches between its states, with transition rates which can depend on the state ℓ of the system. The combined dynamics of system and environment are then governed by the master equation

$$\frac{\mathrm{d}}{\mathrm{d}t}p(\ell,\sigma,t) = \mathcal{M}_\sigma p(\ell,\sigma,t) + \lambda \sum_{\sigma'} A_{\sigma'\to\sigma}(\ell) p(\ell,\sigma',t), \tag{5.1}$$

where $p(\ell,\sigma,t)$ is the joint probability of finding the system in state ℓ and the environment in state σ at time t. The object $\mathcal{M}_\sigma$ is an operator, and determines how the state of the system can change when the environment is in state σ. More specifically, the effect of the operator can be written in the form

$$\mathcal{M}_\sigma p(\ell,\sigma,t) \equiv \sum_{\ell'} R^{(\sigma)}_{\ell'\to\ell} p(\ell',\sigma,t). \tag{5.2}$$

The matrix element $R^{(\sigma)}_{\ell'\to\ell}$ describes the rate at which the system transitions from state ℓ' to state ℓ when the environment is in state σ. For a chemical reaction system, the types of allowed transitions are specified by the stoichiometric coefficients; together with associated reaction rates these determine the transition matrix. In the context of population dynamics the matrix $R^{(\sigma)}_{\ell'\to\ell}$ is defined by the underlying birth and death processes (e.g., see Refs. [40, 41]).

The second term in Eq. (5.1), proportional to λ, characterises the environmental switching. The rate with which the environment transitions from state σ to state

σ' is $\lambda A_{\sigma\to\sigma'}(\ell)$. In the most general setup, these can depend on the state ℓ of the system. We write $\lambda\mathbf{A}(\ell)$ for the corresponding transition matrix. The pre-factor $\lambda > 0$ has been introduced to parametrise the time scale of the environment, relative to the internal dynamics of the population. Large values of $\lambda \gg 1$ indicate a fast environmental process. To fix the diagonal elements of both transition matrices, we use the convention $R^{(\sigma)}_{\ell\to\ell} = -\sum_{\ell'\neq\ell} R^{(\sigma)}_{\ell\to\ell'}$, and $A_{\sigma\to\sigma}(\ell) = -\sum_{\sigma'\neq\sigma} A_{\sigma\to\sigma'}(\ell)$.

5.3.2 Simplification in the adiabatic limit

We first consider the so-called 'adiabatic' limit of infinitely fast environmental switching, $\lambda \to \infty$. In this limit we find from Eq. (5.1)

$$\sum_{\sigma'} A_{\sigma'\to\sigma}(\ell) p(\ell,\sigma',t) = 0, \tag{5.3}$$

for all ℓ. We introduce the notation $\Pi(\ell,t) = \sum_\sigma p(\ell,\sigma,t)$ for the marginal of the probability distribution after integrating out the environment. We also write the joint distribution in terms of this marginal and a conditional probability: $p(\ell,\sigma,t) = \rho(\sigma|\ell,t)\Pi(\ell,t)$. Substituting this into Eq. (5.3) we find

$$\sum_{\sigma'} A_{\sigma'\to\sigma}(\ell) \rho^*(\sigma'|\ell) = 0, \tag{5.4}$$

for all ℓ, for the stationary distribution of the environment conditioned on the state of the system. We label this stationary distribution by an asterisk. In the adiabatic limit we then have

$$p(\ell,\sigma,t) = \rho^*(\sigma|\ell)\Pi(\ell,t). \tag{5.5}$$

We will use this relation as a starting point for further analysis; in this context we also obtain the reduced dynamics for $\Pi(\ell,t)$ in the adiabatic limit.

5.4 Analysis for fast but finite environments

5.4.1 General formalism

Our next aim is to derive reduced dynamics in the limit of fast environmental switching, but keeping the time-scale separation finite (i.e., λ large, but finite). Specifically, the objective is to derive a closed equation for the time-evolution of the distribution of

states $\Pi(\ell, t)$. This is done, in essence, by performing an expansion of the joint master equation for system and environment in powers of the time-scale separation λ^{-1}. We then retain the leading and sub-leading terms, and integrate out the environment. The algebraic steps are similar to those in Ref. [32], in which the authors work in the context of piecewise-deterministic Markov processes. We carry out the calculation starting from a system with discrete states ℓ. As we will see below, this leads to interesting features of the reduced dynamics, not necessarily seen for continuous states.

To separate leading-order terms from sub-leading contributions we start with the decomposition

$$p(\ell, \sigma, t) = \rho^*(\sigma|\ell)\Pi(\ell, t) + \frac{1}{\lambda} w_\sigma(\ell, t). \tag{5.6}$$

The sub-leading order term $w_\sigma(\ell, t)$ describes deviations from the adiabatic limit [Eq. (5.5)], due to a finite time scale of the environment. While the first term in Eq. (5.6) is the first term in an asymptotic expansion in λ^{-1}, we remark that $w_\sigma(\ell, t)$ is inclusive of all higher-order terms. Because of normalisation, this ansatz requires $\sum_\sigma w_\sigma(\ell, t) = 0$, for all ℓ. We proceed by inserting Eq. (5.6) into Eq. (5.1), and obtain

$$\begin{aligned}\rho^*(\sigma|\ell)\frac{\mathrm{d}}{\mathrm{d}t}\Pi(\ell, t) + \frac{1}{\lambda}\frac{\mathrm{d}}{\mathrm{d}t} w_\sigma(\ell, t) = \mathcal{M}_\sigma\left[\rho^*(\sigma|\ell)\Pi(\ell, t)\right] + \sum_{\sigma'} A_{\sigma'\to\sigma}(\ell) w_{\sigma'}(\ell, t) \\ + \frac{1}{\lambda}\mathcal{M}_\sigma w_\sigma(\ell, t),\end{aligned} \tag{5.7}$$

where one further term has been eliminated using Eq. (5.4). Next, we sum over the environmental states σ for each ℓ. We find

$$\frac{\mathrm{d}}{\mathrm{d}t}\Pi(\ell, t) = \sum_\sigma \mathcal{M}_\sigma\left[\rho^*(\sigma|\ell)\Pi(\ell, t)\right] + \frac{1}{\lambda}\sum_\sigma \mathcal{M}_\sigma w_\sigma(\ell, t). \tag{5.8}$$

Once the $w_\sigma(\ell, t)$ are expressed in terms of $\Pi(\ell, t)$, this equation describes the time-evolution of $\Pi(\ell, t)$, valid to sub-leading order in λ^{-1}.

To find the $w_\sigma(\ell, t)$ we collect the terms of order $(1/\lambda)^0$ in Eq. (5.7),

$$\sum_{\sigma'} A_{\sigma'\to\sigma}(\ell) w_{\sigma'}(\ell, t) = \rho^*(\sigma|\ell)\sum_{\sigma'} \mathcal{M}_{\sigma'}\left[\rho^*(\sigma'|\ell)\Pi(\ell, t)\right] - \mathcal{M}_\sigma\left[\rho^*(\sigma|\ell)\Pi(\ell, t)\right], \tag{5.9}$$

where we have used Eq. (5.8) to further simplify the result. Effectively, we have disregarded terms of order λ^{-1} in Eq. (5.7). This procedure indicates that the $w_\sigma(\ell, t)$ are to be obtained as the solution of Eq. (5.9), subject to $\sum_\sigma w_\sigma(\ell, t) = 0$ for all ℓ and t. The truncation of higher order terms leads to an error in Eq. (5.9) of order λ^{-1}. We

note that in specific cases master equations for the system can be obtained in closed form without truncation (examples can be found in Refs. [42, 43]). These usually rely on specific properties of the model at hand, such as linearity. Eqs. (5.8) and (5.9), while constituting an approximation to sub-leading order in λ^{-1}, hold more generally; we have not made significant restrictions on the dynamics of the system (i.e., on the operators $\mathcal{M}_\sigma$).

5.4.2 Switching dynamics independent of state of the system with two environmental states

We now make a simplifying assumption, and consider the case in which the environmental switching dynamics are independent of the state of the population; that is to say, the transition rate matrix $A_{\sigma\to\sigma'}$ does not depend on ℓ. In this case, the stationary distribution of the environment in the adiabatic limit is independent of the state of population, i.e., $\rho^*(\sigma|\ell) = \rho^*_\sigma$. The more general case is discussed further in Appendix 5.11 and below in Sec. 5.9.

In this simplified case the dynamics in the adiabatic limit are given by

$$\frac{\mathrm{d}}{\mathrm{d}t}\Pi(\ell,t) = \mathcal{M}_{\mathrm{avg}}\Pi(\ell,t), \tag{5.10}$$

where $\mathcal{M}_{\mathrm{avg}} = \sum_{\sigma'} \rho^*_{\sigma'}\mathcal{M}_{\sigma'}$ is an effective, average operator. Equation (5.10) is obtained from Eq. (5.8) by sending $\lambda \to \infty$, and using $\rho^*(\sigma|\ell) = \rho^*_\sigma$.

Equation (5.9), on the other hand, reduces to

$$\sum_{\sigma'} A_{\sigma'\to\sigma} w_{\sigma'}(\ell,t) = \rho^*_\sigma \left[\mathcal{M}_{\mathrm{avg}} - \mathcal{M}_\sigma\right]\Pi(\ell,t). \tag{5.11}$$

This relation indicates a balance of the form $\sum_{\sigma'} A_{\sigma'\to\sigma} w_{\sigma'}(\ell,t) + [\mathcal{M}_\sigma - \mathcal{M}_{\mathrm{avg}}]\,\rho^*_\sigma\Pi(\ell,t) = 0$. To understand this in more detail, we recall that $w_\sigma(\ell,t)$ describes the next-order deviation of the solution of Eq. (5.1) from the adiabatic limit when the environmental switching is finite [Eq. (5.6)]. When the environment is in state σ, the first term in the above balance relation is the influx of probability into state ℓ induced by these deviations and due to the environmental switching. Secondly, for finite environmental switching, the dynamics of the population are governed not by $\mathcal{M}_{\mathrm{avg}}$, but by $\mathcal{M}_\sigma$ when the environment is in state σ. The second term in the above relation reflects this; self-consistency of the ansatz requires that these contributions balance.

While the above procedure applies to an arbitrary number of discrete environmental states, it is useful to look at the case of two states, which we label $\sigma = 0$ and $\sigma = 1$. We then have $w_0(\ell, t) = -w_1(\ell, t)$ for all ℓ and t. To shorten the notation, we write k_0 and k_1 for the switching rates $A_{1\to 0}$ and $A_{0\to 1}$ respectively. In the adiabatic limit, the probabilities of finding the environment in each of its two states are then given by

$$\rho_0^* = \frac{k_0}{k_0 + k_1}, \qquad \rho_1^* = \frac{k_1}{k_0 + k_1}. \tag{5.12}$$

From Eq. (5.11) one obtains

$$w_\sigma(\ell, t) = \frac{k_\sigma}{(k_0 + k_1)^2} \left[\mathcal{M}_\sigma - \mathcal{M}_{\text{avg}}\right] \Pi(\ell, t). \tag{5.13}$$

Substituting in Eq. (5.8) and simplifying, we arrive at

$$\frac{\mathrm{d}}{\mathrm{d}t}\Pi(\ell, t) = \mathcal{M}_{\text{avg}}\Pi(\ell, t) + \frac{1}{2}\frac{\theta^2}{\lambda}(\mathcal{M}_0 - \mathcal{M}_1)^2\Pi(\ell, t), \tag{5.14}$$

where we have introduced the constant

$$\theta^2 = \frac{2k_0k_1}{(k_0 + k_1)^3}. \tag{5.15}$$

For systems with two environmental states and with population-independent environmental switching, Eq. (5.14) is a general result approximating the dynamics in the limit of fast switching. It captures the time-evolution of $\Pi(\ell, t)$ up to and including sub-leading terms in λ^{-1}. We will refer to this equation (and its analogue for more complicated setups) as a reduced master equation. An expression similar to Eq. (5.14) was derived in Ref. [32] for systems with continuous states. We note that $(\mathcal{M}_0 - \mathcal{M}_1)^2 = (\mathcal{M}_0^2 - 1) + (\mathcal{M}_1^2 - 1) - (\mathcal{M}_0\mathcal{M}_1 - 1) - (\mathcal{M}_1\mathcal{M}_0 - 1)$, indicating that Eq. (5.14) preserves total probability, i.e., $\frac{\mathrm{d}}{\mathrm{d}t}\sum_\ell \Pi(\ell, t) = 0$.

We will next illustrate this result in the context of two simple, but instructive examples.

5.4.3 Basic example

We consider a population of discrete individuals who all belong to a single species. The state of the population is specified by the number n of individuals. Discrete events involve the removal (death) of existing individuals ($n \to n - 1$), or the production (birth) of new individuals ($n \to n + 1$). In this first example we assume that the per

capita death rate δ does not depend on the state of the environment. The birth rate, however, does: it is $\Omega\beta_0$ in environmental state $\sigma = 0$, and $\Omega\beta_1$ in environmental state $\sigma = 1$. The scale parameter $\Omega > 0$ sets the typical number of particles; see also the next paragraph. This simple setup is widely used as an elementary model of protein production controlled by the state of a gene [6, 10, 44–46].

For this model, the operator $\mathcal{M}_\sigma$ can be written as

$$\mathcal{M}_\sigma = \Omega\beta_\sigma(\mathcal{E}^{-1} - 1) + \delta(\mathcal{E} - 1)n, \tag{5.16}$$

where we have introduced the raising operator $\mathcal{E}$, defined by its action on a function of n: $\mathcal{E}f(n) = f(n + 1)$. Operators act on everything to their right. We find

$$\mathcal{M}_{\text{avg}} = \Omega\beta_{\text{avg}}(\mathcal{E}^{-1} - 1) + \delta(\mathcal{E} - 1)n, \tag{5.17}$$

where $\beta_{\text{avg}} = (k_0\beta_0 + k_1\beta_1)/(k_0 + k_1)$. This operator describes the dynamics in the limit of infinitely fast switching ($\lambda \to \infty$). The resulting birth rate, $\Omega\beta_{\text{avg}}$, is the weighted average of the birth rates in the two environments. The total rate with which deaths occur in the population is δn. These rates balance when $n = (\beta_{\text{avg}}/\delta)\Omega$. It is in this sense that Ω sets the typical scale for the population size.

Inserting the expression for $\mathcal{M}_\sigma$ into Eq. (5.14) and reorganising terms we find

$$\begin{aligned}\frac{\mathrm{d}}{\mathrm{d}t}\Pi(n) = {} & \delta(\mathcal{E} - 1)n\Pi(n) \\ & + \left[\Omega\beta_{\text{avg}} - \frac{\Omega^2\theta^2}{\lambda}(\beta_0 - \beta_1)^2\right](\mathcal{E}^{-1} - 1)\Pi(n) \\ & + \frac{1}{2}\frac{\Omega^2\theta^2}{\lambda}(\beta_0 - \beta_1)^2\left[\mathcal{E}^{-2} - 1\right]\Pi(n),\end{aligned} \tag{5.18}$$

where we have suppressed the explicit dependence of $\Pi(n)$ on time. This equation captures terms up to (and including) order λ^{-1}; higher-order terms have been discarded.

Each term in the reduced master equation can be seen as describing a particular reaction (or type of event) in the population. The first term on the right-hand side (RHS) of Eq. (5.18) describes death events which occur with per capita rate δ. These events occur in either of the two environments, and appear in the reduced dynamics unaltered. The second term indicates birth events occurring with a rate $\beta_{\text{eff}} \equiv \Omega\beta_{\text{avg}} - (\Omega^2\theta^2/\lambda)(\beta_0 - \beta_1)^2$. The reduced dynamics are derived for $\lambda \gg 1$, and we will always assume that λ is large enough so that effective rates such as β_{eff} are non-negative.

The third term on the right-hand side of Eq. (5.18) describes events in which *two* individuals are created at the same time. This occurs with rate $\frac{1}{2}(\Omega^2\theta^2/\lambda)(\beta_0-\beta_1)^2$; we note that this rate is proportional to λ^{-1}. Such events are not part of the original dynamics in either environment (neither $\mathcal{M}_0$ nor $\mathcal{M}_1$ contain events of this type). They come about due to the fast switching with large, but finite time scale separation, and indicate 'bursting' behaviour. This is discussed in more detail in Sections 5.5 and 5.7. We stress that this type of bursting is different from that discussed for example in Refs. [47–50]; there, bursting in protein production is due to short-lived mRNA as a source of protein.

For further illustration, we briefly consider a second, albeit similar, example. We assume now that the birth rate is equal in the two environments ($\beta_0=\beta_1\equiv\beta$), but that there are different death rates, δ_0 and δ_1. We find

$$\begin{aligned}\frac{\mathrm{d}}{\mathrm{d}t}\Pi(n) &= \Omega\beta(\mathcal{E}^{-1}-1)\Pi(n)\\ &\quad+(\mathcal{E}-1)[\delta_{\mathrm{avg}}-\frac{\theta^2}{\lambda}(\delta_0-\delta_1)^2(2n-1)]n\Pi(n)\\ &\quad+\frac{1}{2}\frac{\theta^2}{\lambda}(\delta_0-\delta_1)^2\left[\mathcal{E}^2-1\right]n(n-1)\Pi(n)\end{aligned}\tag{5.19}$$

for the reduced dynamics. Again we note bursting behaviour, the last term in Eq. (5.19) describes 'double death' events, which are not present in the original dynamics. The factor $n(n-1)$ ensures that such events can only occur when there are at least two individuals in the population.

5.5 Several species and reduced master equations with negative transition rates

5.5.1 Model

We next consider an example in which there are two types of particles, labelled A and B. This is still a relatively simple setup, but it will help reveal a number of interesting features which can emerge in the reduced dynamics.

Particles of either type are removed with constant per capita rates γ and δ, respectively, and are created with rates $\Omega\alpha_\sigma$ and $\Omega\beta_\sigma$. These production rates depend on the state of the environment, as indicated by the subscript. The population takes

states $\ell = (n_A, n_B)$, where n_A is the number of particles of type A, and n_B the number of particles of type B. We then have operators

$$\begin{aligned}\mathcal{M}_\sigma = &\Omega\alpha_\sigma(\mathcal{E}_A^{-1} - 1) + \gamma(\mathcal{E}_A - 1)n_A \\ &+ \Omega\beta_\sigma(\mathcal{E}_B^{-1} - 1) + \delta(\mathcal{E}_B - 1)n_B,\end{aligned} \tag{5.20}$$

where $\mathcal{E}_A f(n_A, n_B) = f(n_A + 1, n_B)$, and similarly for $\mathcal{E}_B$. The switching between environmental states is the same as in the previous section. Using Eq. (5.14) we find, to sub-leading order in λ^{-1},

$$\begin{aligned}\frac{\mathrm{d}}{\mathrm{d}t}\Pi = &\gamma(\mathcal{E}_A - 1)n_A\Pi + \delta(\mathcal{E}_B - 1)n_B\Pi \\ &+ \Omega\alpha_{\text{eff}}(\mathcal{E}_A^{-1} - 1)\Pi + \Omega\beta_{\text{eff}}(\mathcal{E}_B^{-1} - 1)\Pi \\ &+ \frac{\Omega^2\theta^2}{2\lambda}(\Delta\alpha)^2(\mathcal{E}_A^{-2} - 1)\Pi \\ &+ \frac{\Omega^2\theta^2}{2\lambda}(\Delta\beta)^2(\mathcal{E}_B^{-2} - 1)\Pi \\ &+ \frac{\Omega^2\theta^2}{\lambda}\Delta\alpha\Delta\beta(\mathcal{E}_A^{-1}\mathcal{E}_B^{-1} - 1)\Pi,\end{aligned} \tag{5.21}$$

where $\Delta\alpha \equiv \alpha_0 - \alpha_1$ and $\Delta\beta \equiv \beta_0 - \beta_1$, and where

$$\begin{aligned}\alpha_{\text{eff}} &= \alpha_{\text{avg}} - \frac{\Omega\theta^2}{\lambda}(\Delta\alpha)^2 - \frac{\Omega\theta^2}{\lambda}\Delta\alpha\Delta\beta, \\ \beta_{\text{eff}} &= \beta_{\text{avg}} - \frac{\Omega\theta^2}{\lambda}(\Delta\beta)^2 - \frac{\Omega\theta^2}{\lambda}\Delta\alpha\Delta\beta.\end{aligned} \tag{5.22}$$

The quantity α_{avg} is defined as above, and similar for β_{avg}. We have suppressed the explicit dependence of Π on n_A, n_B and t to keep the notation compact.

Again, we can interpret the reduced master equation as a set of reactions. The first two terms on the RHS of Eq. (5.21) describe particle removal, present already in the original model, and independent of the state of the environment. The terms in the second line are single-birth reactions, as appeared originally in the model, but now with effective birth rates in the reduced dynamics as indicated in Eq. (5.22). Similar to the example in the previous Section, the effective rates α_{eff} and β_{eff} are non-negative, provided the switching is fast enough. Given that the reduced dynamics are derived in the limit $\lambda \gg 1$, we always assume that the time-scale separation λ is large enough so that $\alpha_{\text{eff}}, \beta_{\text{eff}} \geq 0$.

The remaining terms in Eq. (5.21) represent reactions which are not present in the original model; they arise from the effects of integrating out the environment. These

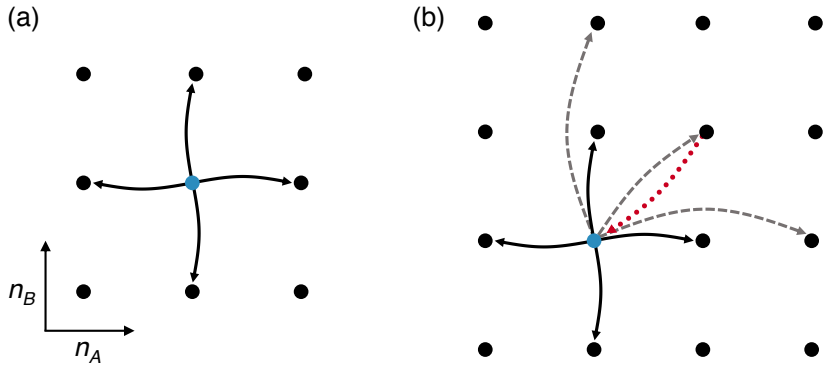

Figure 5.1: Illustration of the possible reactions for (a) the model described by equations (5.20), and (b) the approximation to the model described by Eq. (5.21). In the original model the next event can take the population from (n_A, n_B) to four possible destinations: $(n_A \pm 1, n_B), (n_A, n_B \pm 1)$. The bursting reactions in the reduced model lead to further states which can be reached, indicated by grey dashed arrows; these are $(n_A + 2, n_B), (n_A, n_B + 2), (n_A + 1, n_B + 1)$. For certain choices of parameters the transition to $(n_A + 1, n_B + 1)$ can have a negative 'rate'. In this case the flow of probability is from $(n_A + 1, n_B + 1)$ to (n_A, n_B) as indicated by the red dotted arrow; see Sec. 5.5.3 for details.

terms represent 'bursting' reactions; they describe events in which two particles of type A are produced simultaneously, or two particles of type B, or one of either type. This is illustrated in Fig. 5.1. Panel (a) is a schematic showing the four states that the population can reach from a given state in the next event in the original model. Panel (b) shows that the reduced dynamics allow three additional destinations (indicated by grey dashed arrows). The rates of the first two bursting reactions in Eq. (5.21) are proportional to $(\Delta\alpha)^2$ and $(\Delta\beta)^2$, and are always positive [lines three and four on the right-hand side of Eq. (5.21)]. The rate of the third bursting reaction [last term on RHS of Eq. (5.21)] is positive only if $\Delta\alpha$ and $\Delta\beta$ have the same sign. If $\Delta\alpha\Delta\beta < 0$, this reaction will have a negative (pseudo-) rate, no matter how large the time scale separation λ. In this case, it is not immediately clear how to proceed with the interpretation of Eq. (5.21). We will return to this below in Sec. 5.5.3, after we first briefly consider the case $\Delta\alpha\Delta\beta > 0$.

5.5.2 Positive correlation between the species

In the case $\Delta\alpha\Delta\beta > 0$, the correlations between n_A and n_B are positive. There is one state of the environment which favours both species, i.e., they each have a higher birth rate in this environmental state than in the other. All rates in Eq. (5.21) are positive

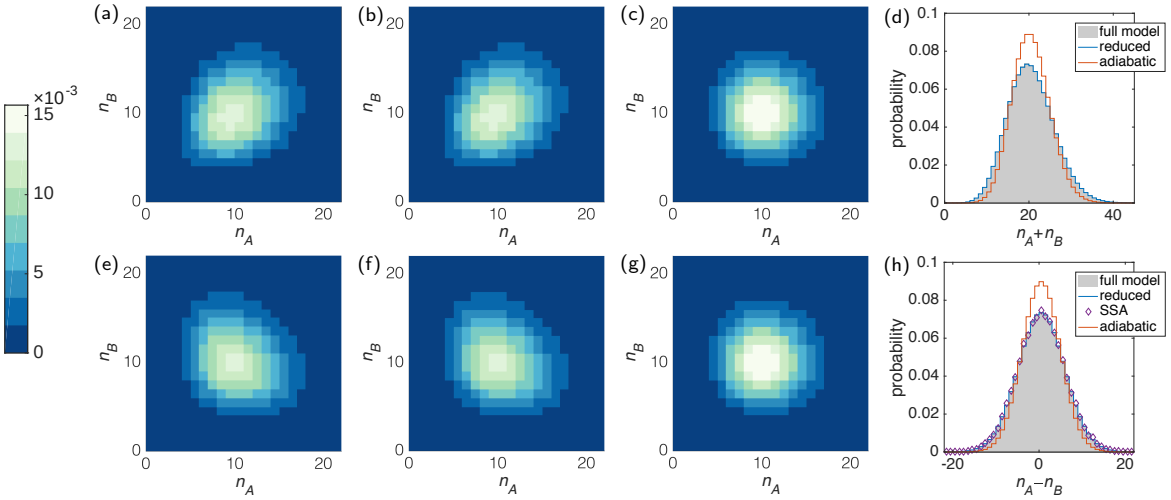

Figure 5.2: Stationary distribution of the model defined in Sec. 5.5.1 [see Eqs. (5.20)]. The upper panels are for $\Delta\alpha\Delta\beta > 0$, the lower row for $\Delta\alpha\Delta\beta < 0$. The distributions are obtained by numerical integration of: (a,e) the full master equation with explicit environment, (b,f) the reduced master Eq. (5.21), and (c,g) the adiabatic approximation; (d) shows the marginal distribution of $n_A + n_B$; panel (h) shows $n_A - n_B$. Markers labelled 'SSA' in panel (h) are from the stochastic simulation algorithm (SSA) described in Sec. 5.6.2. Parameters are $\alpha_0 = 0, \alpha_1 = 1, \beta_0 = 0, \beta_1 = 1$ in the upper row, and $\alpha_0 = 0, \alpha_1 = 1, \beta_0 = 1, \beta_1 = 0$ in the lower row. Remaining parameters are $\Omega = 20, \lambda = 20, k_0 = k_1 = 1$.

(provided λ is sufficiently large, so that $\alpha_{\text{eff}}, \beta_{\text{eff}} \geq 0$), and mathematically there is then a clear and unique way of interpreting this equation as a continuous-time Markov process. The events described by the various terms are then as above: single deaths, single births and bursting reactions in which two particles are produced. The notion of sample paths is well-defined; they can be generated using the standard Gillespie algorithm [51, 52].

Some support for the validity of the reduced master equation is given in Fig. 5.2, panels (a)–(c). In panel (a) we show the stationary distribution obtained from numerically integrating the full master equation Eq. (5.1), i.e., from the full dynamics of population and environment. Panel (b) shows the corresponding distribution from numerical integration of the reduced master equation (5.21). In panel (c) we have taken the adiabatic limit $\lambda \to \infty$. In each case the numerical integration is carried out using a Runge–Kutta scheme (RK4). The reduced dynamics capture the correlations between n_A, n_B in the original model; this correlation is no longer seen in the adiabatic approximation. Panel (d) shows the marginal distribution for the quantity $n_A + n_B$ to allow better comparison.

5.5.3 Anti-correlations and negative transition rates

For cases in which $\Delta\alpha$ and $\Delta\beta$ have opposite signs, the interpretation of Eq. (5.21) presents an interesting feature. In this situation the (pseudo-) rate of the last reaction $(\Omega^2\theta^2/\lambda)\Delta\alpha\Delta\beta$ is negative, irrespective of the value of λ. The interpretation of this term is then not clear *a priori*, and Eq. (5.21) is not a master equation in the usual sense. We will nevertheless refer to it as the reduced master equation, quotation marks or a prefix 'pseudo-' are implied. Similarly, we will continue to speak of rates, even if these are negative.

In order to better understand a master equation with negative rates, we focus on a pair of states, which we label ℓ and ℓ', and on a single reaction of type $\ell \to \ell'$ occurring with a rate $R_{\ell\to\ell'}$. In the specific example above one would have $\ell = (n_A, n_B)$ and $\ell' = (n_A + 1, n_B + 1)$. The corresponding terms in the master equation are then

$$\frac{\mathrm{d}}{\mathrm{d}t}\Pi(\ell,t) = -R_{\ell\to\ell'}\Pi(\ell,t), \tag{5.23a}$$

$$\frac{\mathrm{d}}{\mathrm{d}t}\Pi(\ell',t) = R_{\ell\to\ell'}\Pi(\ell,t). \tag{5.23b}$$

In conventional cases the rate is positive, $R_{\ell\to\ell'} > 0$. The master equation then describes a non-negative probability flow $R_{\ell\to\ell'}\,\Pi(\ell)$ from ℓ to ℓ' (we suppress the time dependence of $\Pi(\ell)$ for convenience).

For $R_{\ell\to\ell'} < 0$, the flow of probability per unit time in Eqs. (5.23) is $|R_{\ell\to\ell'}|\,\Pi(\ell) \geq 0$ from ℓ' to ℓ. This is not a standard Markovian situation: the flow is directed from ℓ' to ℓ, but proportional to the probability already present at ℓ. Furthermore, the magnitude of this flow does not depend on $\Pi(\ell')$. In making this argument, we have assumed $\Pi(\ell) \geq 0$. This assumption is not always justified in master equations with negative rates. However the above argument holds more generally: a negative value of $R_{\ell\to\ell'}\,\Pi(\ell)$ indicates a positive probability flux $|R_{\ell\to\ell'}\,\Pi(\ell)|$ from ℓ' to ℓ. Similar structures with negative rates are found in open quantum systems, and an approach renormalising master equations of this type has been proposed for example in Refs. [38, 39]. We illustrate this using Eqs. (5.23), assuming again $R_{\ell\to\ell'} < 0$. For $\Pi(\ell') > 0$ one defines the renormalised transition rate

$$T_{\ell'\to\ell}(t) \equiv \frac{\Pi(\ell,t)}{\Pi(\ell',t)}\,|R_{\ell\to\ell'}|\,. \tag{5.24}$$

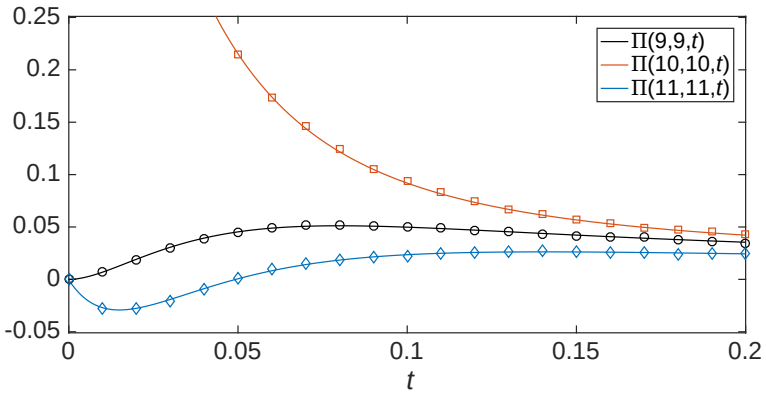

Figure 5.3: Time evolution of several entries $\Pi(n_A, n_B, t)$ for the example defined in Sec. 5.5.1. The solid lines show results from integrating the reduced master equation (5.21), starting from a delta-distribution $\Pi(n_A, n_B, t = 0) = \delta_{n_A,10}\delta_{n_B,10}$. Markers are from the numerical simulation scheme described in Sec. 5.6.1. Model parameters are $\alpha_0 = 0, \alpha_1 = 1, \beta_0 = 1, \beta_1 = 0$, $\Omega = 20, \lambda = 20, k_0 = k_1 = 1$.

The master equation (5.23) can be then written as

$$\frac{\mathrm{d}}{\mathrm{d}t}\Pi(\ell, t) = T_{\ell'\to\ell}(t)\Pi(\ell', t), \tag{5.25a}$$

$$\frac{\mathrm{d}}{\mathrm{d}t}\Pi(\ell', t) = -T_{\ell'\to\ell}(t)\Pi(\ell', t). \tag{5.25b}$$

Equations (5.25), then, resemble a more traditional master equation, and $T_{\ell'\to\ell}$ is the rate for transitions from ℓ' to ℓ. However, this rate depends on the probability distribution Π, in particular $T_{\ell'\to\ell}$ is a function of $\Pi(\ell)$. This indicates non-Markovian properties [27, 38, 39].

5.5.4 Lack of positivity in initial transients

Numerically integrating the reduced master equation (5.21), we find transient regimes of negative (pseudo-) probabilities. For example, if the initial condition is chosen as a delta-peak concentrated on one state $\ell = (n_A, n_B)$, the numerical solution for $\Pi(n_A + 1, n_B + 1)$ is negative for a limited time as shown in Fig. 5.3. We analyse this further in Fig. 5.4, where we show the duration t^* of the initial transient in which negative probabilities are accumulated. The data suggests that this time window is limited to a duration of order λ^{-1}.

While we have not attempted to establish formal conditions under which Eq. (5.21) preserves positivity, we note that negative transients have been observed before in reduced dynamics for open classical and quantum systems [53–56]. Indeed, it is not

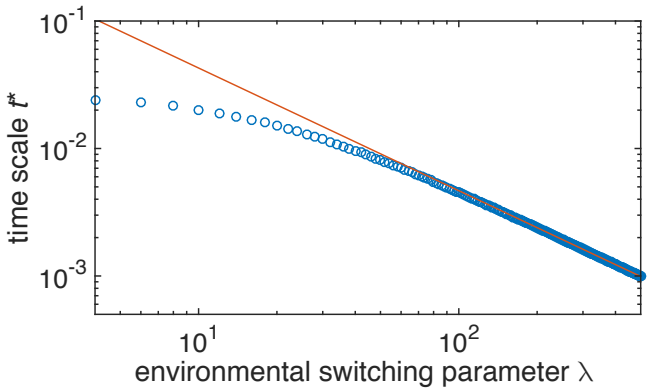

Figure 5.4: Time scale t^* over which negative probabilities are accumulated. Specifically, t^* is the time at which the sum of all negative entries in Π has maximal magnitude; data is from numerical integration of Eq. (5.21). The solid line is a guide and corresponds to $t^* \propto 1/\lambda$. Parameters and initial condition are the same as Fig. 5.3.

surprising that Eq. (5.21) should become unphysical on short time scales. The typical time between switches of the environmental state is of order λ^{-1}, and the reduced dynamics were derived by integrating out the fast environmental dynamics. We cannot expect Eq. (5.21) to resolve the physics of the problem on time scales shorter than order λ^{-1}, as then the detailed mechanics of the environment become important.

We have verified that the appearance of transient negative solutions can be cured by first integrating the full master equation describing the population and the environment for a short period of time, and then subsequently changing to the reduced master equation (5.21). Alternatively, the reduced dynamics can be started from 'slipped' initial conditions [53, 55].

Focusing on long times, we find that the stationary distribution obtained from numerical integration of Eq. (5.21) for $\Delta\alpha\Delta\beta < 0$ captures the negative correlation of n_A and n_B in the original dynamics. This can be seen in Fig. 5.2(e) and (f). Working in the adiabatic limit, however, produces significant deviations [panels (g) and (h)].

For the general reduced master equation [i.e., the analogue of Eq. (5.21) for a general model], we have not attempted to establish formal conditions where all rates remain positive. We remark that positivity in the probabilities is preserved for all initial conditions only if all rates are positive. When negative rates are included, negative probabilities exist transiently; negative transients have been observed before in reduced dynamics for open classical and quantum systems [53–56]. In a classical setting, the appearance of negative transients has been observed previously when truncating

Kramers–Moyal expansions at $n \geq 3$ terms; for such a truncation, positivity is violated over short times as shown by Pawula's theorem. This does not, however, imply that such expansions are of no use; rather, the $n \geq 3$ truncations of the Kramers–Moyal expansion can produce better agreement with true probability distributions than the traditional Fokker–Planck $n = 2$ truncation [57]. It is not surprising that Eq. (5.21) should become unphysical on short time scales. The typical time between switches of the environmental state is of order λ^{-1}, and the reduced dynamics were derived by integrating out the fast environmental dynamics. We cannot expect Eq. (5.21) to resolve the physics of the problem on time scales shorter than order λ^{-1}, as then the detailed mechanics of the environment become important.

5.6 Numerical approaches to a master equation with negative rates

5.6.1 Distribution-level simulation

The time-dependent solution $\Pi(\ell, t)$ can be obtained by direct numerical integration of the reduced master equation, for example using a Runge–Kutta scheme. However for large state spaces this approach can become slow. The technique described in this Section can, in some cases, provide a faster alternative.

We consider a large number M of discrete units of probability, $1/M$. At each point in time the state of the simulation is defined by the 'occupation numbers' N_ℓ for all states ℓ; some of the N_ℓ may be negative. One has $\sum_\ell N_\ell = M$. The algorithms proceeds along the following steps:

1. For given occupation numbers N_ℓ at time t, make a list of all possible reactions, labelled by index γ. Each reaction has a site of origin, ℓ_γ, a destination site, ℓ'_γ, and rate $r_\gamma = R_{\ell_\gamma \to \ell'_\gamma} N_{\ell_\gamma}$. Some of the r_γ may be negative.
2. Draw a random number τ from an exponential distribution with parameter $\sum_\gamma |r_\gamma|$.
3. Pick a reaction from the list created in 1. The probability to pick γ is $|r_\gamma| / \sum_{\gamma'} |r_{\gamma'}|$.
4. If $r_\gamma > 0$ increase $N_{\ell'_\gamma}$ by one and reduce N_{ℓ_γ} by one. If $r_\gamma < 0$ reduce $N_{\ell'_\gamma}$ by one and increase N_{ℓ_γ} by one.

5. Increment time by τ, and go to 1.

The process in step 4 allows occupation numbers to go negative. The typical time step of this scheme is given by $1/\sum_\gamma |r_\gamma|$, and reaction γ is triggered with probability $|r_\gamma|/(\sum_{\gamma'} |r_{\gamma'}|)$. Thus $|r_\gamma|$ reactions of type γ are triggered per unit time. The sign convention in step 4 ensures correct sampling of the reduced master equation.

We tested this procedure for the example given by Eq. (5.21). Results are shown in Fig. 5.3; there is near perfect agreement between the Monte Carlo procedure and direct numerical integration of the reduced master equation.

We stress that this algorithm does not generate sample paths for the reduced master equation. This motivates us to ask whether the notion of a sample path is valid for a master equation involving negative transition rates.

5.6.2 'Path-level' simulation

As discussed in Sec. 5.5.2 the reduced master equation (5.21) defines a Markovian process for $\Delta\alpha\Delta\beta > 0$. All rates in the reduced master equation are non-negative, and sample paths can be simulated using the conventional Gillespie method [51, 52]. The solution of Eq. (5.21) can be recovered from the statistics of a large ensemble of such realisations.

In Sec. 5.5.4 we have seen that reduced master equations with negative rates can—for certain initial conditions—lead to negative transient solutions. These can be delivered by the ensemble-level algorithm in Sec. 5.6.1. A simulation generating sample paths cannot capture these negative (pseudo-) probabilities.

However, this does not preclude a meaningful notion of sample paths in situations where the reduced master equation is started from an initial distribution which avoids subsequent negative transients. For example, one could focus on the stationary state of Eq. (5.21).

A stochastic simulation algorithm was discussed in Ref. [39] for non-Markovian jumps in quantum systems. This method simulates processes defined by quantum master equations with temporarily negative decay rates. Realisations are generated by combining non-Markovian quantum jumps with the deterministic evolution of quantum states between jumps [38]. The central idea is to represent the solution of the master equation by an ensemble of sample paths, which are generated *in parallel*. In contrast

with standard methods [51, 52] these paths are correlated with each other. Here, we show this method fails to produce sample paths which are representative of the full model.

In order to test the principles of this approach we have adapted it to the case of the classical master equation

$$\frac{\mathrm{d}}{\mathrm{d}t}\Pi(\ell,t)=\sum_{\ell'}R_{\ell'\to\ell}\Pi(\ell',t), \tag{5.26}$$

where some of the rates $R_{\ell'\to\ell}$ may be negative. The algorithm uses Eqs. (5.24) and (5.25) to convert reactions with negative rates into reactions in the opposite direction, and with positive renormalised rates. In order to do this we need the entries of the probability distribution, $\Pi(\ell)$ and $\Pi(\ell')$, see Eq. (5.24). These in turn are estimated from the ensemble of sample paths. In this way, the trajectories are correlated with each other, because the evolution of a single sample path depends on the ensemble [38, 39].

We index each trajectory individually, so that we can follow the time evolution of each sample path. At each point in time the ensemble is specified by the state of each of the sample paths. We write N_ℓ for the number of sample paths in state ℓ. To keep the notation compact we suppress the time dependence of N_ℓ. One has $\sum_\ell N_\ell = M$ at all times, where M is the size of the ensemble.

Before we detail the algorithm we describe the construction of a matrix $\mathbf{S}$ with elements $S_{\ell\to\ell'}$ which give the rate of a reaction $\ell\to\ell'$ to occur *in the ensemble*. The matrix is needed frequently in the algorithm, and is constructed as follows: (i) start with $S_{\ell\to\ell'}=0$ for all ℓ,ℓ'; (ii) for all reactions $\ell\to\ell'$ with positive rate $R_{\ell\to\ell'}$ increase $S_{\ell\to\ell'}$ by $R_{\ell\to\ell'}$; (iii) for reactions with negative rate $R_{\ell\to\ell'}$ and $N_{\ell'}>0$ construct $T_{\ell'\to\ell}$ as in Eq. (5.24), where $N_\ell/N_{\ell'}$ is used as a proxy for $\Pi(\ell)/\Pi(\ell')$. If $N_{\ell'}=0$ set $T_{\ell'\to\ell}=0$. Increase $S_{\ell'\to\ell}$ by $T_{\ell'\to\ell}$; (iv) finally, for all pairs ℓ,ℓ' multiply $S_{\ell\to\ell'}$ by N_ℓ. For a given master equation (i.e., a given matrix $\mathbf{R}$) the matrix $\mathbf{S}$ is a function of the current state of the ensemble, i.e., of the $\{N_\ell\}$. All entries $S_{\ell\to\ell'}$ $(\ell\neq\ell')$ are non-negative. The diagonal elements are zero. The element $S_{\ell\to\ell'}$ indicates the rate for a reaction $\ell\to\ell'$ to occur, given the current state of the ensemble. One has $S_{\ell\to\ell'}=0$ if no sample path in the ensemble is in state ℓ. We also note that the total rate for a reaction of any type to happen, $\sum_{\ell\neq\ell'}S_{\ell\to\ell'}$, scales linearly with M. This guarantees

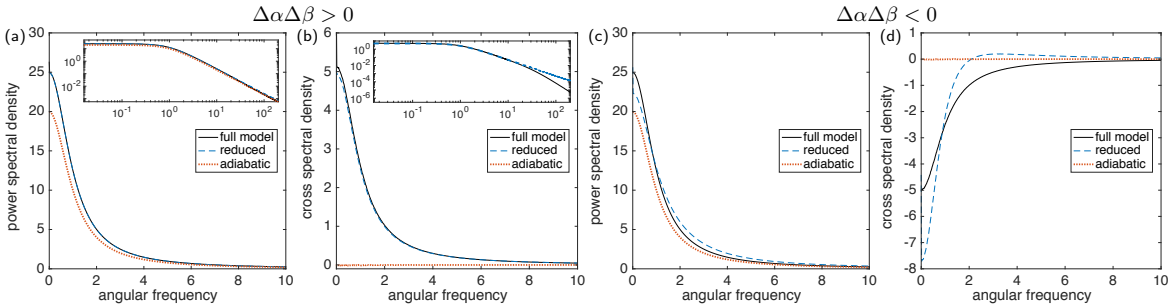

Figure 5.5: Spectra of fluctuations for the model defined in Sec. 5.5.1. Panels (a) and (b) are for $\Delta\alpha\Delta\beta > 0$; (c) and (d) for $\Delta\alpha\Delta\beta < 0$. We show the power spectral density $S_{AA}(\omega)$ in (a) and (c), and the cross spectral density $S_{AB}(\omega)$ in (b) and (d); the insets show the same quantities on a logarithmic scale. Parameters: $\alpha_0 = 0, \alpha_1 = 1$, $\lambda k_0 = \lambda k_1 = 20, \Omega = 20$ in all panels; $\beta_0 = 0, \beta_1 = 1$ in (a,b); $\beta_0 = 1, \beta_1 = 0$ in (c,d).

that each time step in the procedure below is of order M^{-1}, or in other words, that order M reactions occur per unit time.

The algorithm proceeds as follows:

1. Given the current state of the ensemble compute the matrix $\mathbf{S}$ as described above.
2. Draw a random time increment τ from an exponential distribution with parameter $s = \sum_{\ell,\ell'} S_{\ell\to\ell'}$.
3. Randomly select an origin ℓ and a destination ℓ' with a probability weighted by $S_{\ell\to\ell'}$ (i.e., the probability that ℓ is picked as an origin and ℓ' as a destination is $S_{\ell\to\ell'}/s$).
4. Randomly (with equal probabilities) pick one of the sample paths currently in state ℓ and change its state to ℓ'.
5. Increment time by τ and go to step 1.

We note that this algorithm does not allow for any state ℓ to ever have a negative occupancy N_ℓ. Furthermore, if all $R_{\ell\to\ell'}$ are non-negative the simulation reduces to the standard Gillespie algorithm [51,52]. In this case the sample paths remain uncorrelated from each other.

To test the algorithm we use the example in Eq. (5.21). The algorithm captures the stationary distribution accurately, as illustrated by the markers in Fig. 5.2 (h). Next, we test whether the simulation reproduces dynamical properties of the sample paths of the full model.

To this end, we define the power spectral density $S_{AA}(\omega) = \langle|\hat{n}_A(\omega)|^2\rangle$, where $\hat{n}_A(\omega)$ is the Fourier transform of the random process $n_A(t)$. Similarly, we also look at

the cross power spectral density $S_{AB}(\omega) = \left\langle n_A^\dagger(\omega) n_B(\omega) \right\rangle$ (the superscript † denotes complex conjugation). These are the Fourier transforms of the autocorrelation and cross-correlation functions respectively. Figure 5.5 shows these quantities, measured in the regime when $\Pi(n_A, n_B)$ has reached the stationary state, and averaged over a large ensemble of trajectories.

Panels (a) and (b) serve as a benchmark, and show the case $\Delta\alpha\Delta\beta > 0$ when all rates in the reduced master equation are positive. Thus the above simulation scheme reduces to the standard Gillespie method. As seen in the figure the power and cross spectra $S_{AA}(\omega)$ and $S_{AB}(\omega)$ obtained from simulating paths of the reduced master equation agree well with those from simulations of the full model, at least at sufficiently low frequencies ω. At larger frequencies deviations are seen, this is particularly visible for the cross spectrum; see the inset of panel (b). These deviations between reduced and the full model are not surprising; the reduced model does not resolve the mechanics of the environment on short time scales. Spectra obtained from sample paths of the master equation in the adiabatic limit show significant deviations from those of the full model; we note in particular that the cross spectrum $S_{AB}(\omega)$ vanishes [dotted red line in Fig. 5.5 (b)]; see also Appendix 5.12.1 for further analysis.

Results for the case with negative rates in the reduced master equation are shown in panels (c) and (d) of Fig. 5.5. We find marked differences between the spectra generated from the reduced master equation with the above algorithm and those of sample paths of the full model. This is particularly noticeable in the cross spectrum in panel (d). Further details can also be found in Appendix 5.12.2.

We conclude that the trajectories generated by the above simulation algorithm do not represent sample paths of the full model when the reduced master equation contains negative rates. Our findings invite the question whether algorithms of this type [38, 39] provide a faithful representation of the full dynamics of open quantum systems and their environment. It would be interesting to compare the structure of the reduced dynamics in the classical and quantum cases, and to relate our observations to the quantum regression theorem [58].

5.7 An intuition to our expansion on the level of sample paths

In Sec. 5.4.1 we derived the general formalism for approximating the dynamics of a system coupled to a fast-switching environment. We found this resulted in an effective reduced master equation, which can describe 'bursting' events not present in the dynamics of the original model. From a physical perspective, however, it is not obvious how such bursting events can arise as a consequence of the coupling to a fast environment when such events do not occur in any (fixed) state of the environment. In this section we look at this problem from viewpoint of single trajectories of the full model in discrete time, in order to provide intuition to this result. Taking this view also allows us to develop a method to use the reduced dynamics to approximate sample paths of the full model in discrete time; using a time step larger than λ^{-1} we avoid the issues highlighted in the previous section.

5.7.1 Effective time-averaged reaction rates

We focus again on the two-species example given in Sec. 5.5. An interpretation of the terms in Eq. (5.21) can be obtained by looking at one sample path of the full model (population and environment) for a time interval $I \equiv [t_0, t_0 + \Delta t]$. We focus on the birth reactions. If the production rate $\Omega\alpha$ of particles of type A were constant in time, the number of birth events in the interval would be a Poissonian random variable with parameter $\Omega\alpha\Delta t$, and similarly for particles of type B (see also Ref. [59]). In the present model, the production rates are not constant in time as they depend on the state of the environment. For a given trajectory of the environment we introduce the quantity

$$\overline{\alpha} = \frac{1}{\Delta t}\int_{t_0}^{t_0+\Delta t} \mathrm{d}t' \; \alpha_{\sigma(t')}, \tag{5.27}$$

and a similar definition for $\overline{\beta}$; the quantities $\Omega\overline{\alpha}$ and $\Omega\overline{\beta}$ are time-averaged production rates in the time interval I.

The number of production events of particles of type A in I can then be expected to be Poissonian with parameter $\Omega\overline{\alpha}\Delta t$, and similarly for B. We note that $\overline{\alpha}$ and $\overline{\beta}$ are random variables when Δt is finite, as they depend on the random path of the

environment, $\sigma(t')$, $t' \in I$. The quantities $\overline{\alpha}$ and $\overline{\beta}$ will in general be correlated, as they derive from the same realisation of the environment. The main principle of the calculation that follows is to approximate $\overline{\alpha}$ and $\overline{\beta}$ as correlated Gaussian random variables, while capturing their first and second moments. This Gaussian approximation is justified provided that there is a large number of switches of the environment during the time interval I, i.e., when $\lambda\Delta t \gg 1$.

5.7.2 Averaging out the environmental process

Correlations of the environmental process decay on time scales proportional to λ^{-1}. This means that the environment is in its stationary distribution, except for a short period of order λ^{-1} at the beginning. For $\lambda\Delta t \gg 1$ this period constitutes a negligibly small fraction of the time interval, and the distribution of $\sigma(t')$ can hence be assumed to be the stationary one at all times t' during the interval. Writing $\langle \ldots \rangle$ for averages over the environmental process we have $\langle \overline{\alpha} \rangle = \alpha_{\rm avg}$ and $\langle \overline{\beta} \rangle = \beta_{\rm avg}$.

Moving on to the second moments we find

$$\begin{aligned} \langle \overline{\alpha}^2 \rangle &= (\Delta t)^{-2} \int_I \int_I \mathrm{d}t\, \mathrm{d}t' \left\langle \alpha_{\sigma(t)} \alpha_{\sigma(t')} \right\rangle , \\ &= (\Delta t)^{-2} \sum_{\sigma\sigma'} \alpha_\sigma \alpha_{\sigma'} \\ &\quad \times \int_I \int_I \mathrm{d}t\ \mathrm{d}t' \rho[\sigma, \min(t,t')]\ \rho\left(\sigma', |t-t'| \,\middle|\, \sigma\right), \end{aligned} \tag{5.28}$$

where $\rho[\sigma, \min(t,t')]$ is the probability distribution of σ at the earlier of the two times t and t'. It is given by the stationary distribution of the environment, $\rho[\sigma, \min(t,t')] = \rho^*_\sigma$, with ρ^*_σ as in Eq. (5.12). The notation $\rho(\sigma', \tau|\sigma)$ in Eq. (5.28) indicates the probability of finding the environment in state σ' if τ units of time earlier it was in state σ ($\tau > 0$). These can be obtained straightforwardly from the asymmetric telegraph process for the environment, $\rho(0, \tau|0) = \rho^*_0 \left[1 + \frac{k_1}{k_0} e^{-\lambda(k_0+k_1)\tau}\right]$, and $\rho(0, \tau|1) = \rho^*_0 \left[1 - e^{-\lambda(k_0+k_1)\tau}\right]$. Using this in Eq. (5.28) we find

$$\begin{aligned} \langle \overline{\alpha}^2 \rangle = \alpha^2_{\rm avg} + \Bigg[&\frac{2}{\lambda(k_0+k_1)\Delta t} + \frac{2}{\lambda^2 (k_0+k_1)^2 \Delta t^2} \\ &\times \left(e^{-\lambda(k_0+k_1)\Delta t} - 1\right) \Bigg] \frac{k_0 k_1}{(k_0+k_1)^2} (\alpha_0 - \alpha_1)^2. \end{aligned} \tag{5.29}$$

For $\lambda\Delta t \gg 1$ the first term in the square bracket dominates relative to the second, so

we can approximate

$$\left\langle \overline{\alpha}^2 \right\rangle - \alpha_{\rm avg}^2 \approx \frac{\theta^2}{\lambda \Delta t} (\Delta\alpha)^2, \tag{5.30a}$$

with $\theta^2 = 2k_0k_1/(k_0+k_1)^3$ as before [see Eq. (5.15)]. Following similar steps one finds

$$\left\langle \overline{\beta}^2 \right\rangle - \beta_{\rm avg}^2 \approx \frac{\theta^2}{\lambda \Delta t} (\Delta\beta)^2, \tag{5.30b}$$

$$\left\langle \overline{\alpha}\overline{\beta} \right\rangle - \alpha_{\rm avg}\beta_{\rm avg} \approx \frac{\theta^2}{\lambda \Delta t} \Delta\alpha\Delta\beta. \tag{5.30c}$$

We therefore approximate the joint probability distribution of $\bar{\alpha}$ and $\bar{\beta}$ in the fast switching limit as a bivariate normal distribution with these parameters.

5.7.3 Resulting event statistics

The probability that exactly m_A production events for species A occur during the time interval Δt, and m_B for species B, is given by

$$\mathrm{P}(m_A, m_B) = \left\langle e^{-\Delta t \Omega \left(\overline{\alpha}+\overline{\beta}\right)} \frac{(\Delta t \Omega \overline{\alpha})^{m_A}}{m_A!} \frac{(\Delta t \Omega \overline{\beta})^{m_B}}{m_B!} \right\rangle_{\overline{\alpha},\overline{\beta}}, \tag{5.31}$$

resulting from Poissonian statistics for given $\overline{\alpha}, \overline{\beta}$, subsequently averaged over the Gaussian distribution for $\overline{\alpha}$ and $\overline{\beta}$ (this average is indicated as $\langle \ldots \rangle_{\overline{\alpha},\overline{\beta}}$). Expanding in powers of Δt, and carrying out the Gaussian average we find

$$\begin{aligned}
\mathrm{P}(m_A{=}1, m_B{=}0) &= \Delta t \Omega \left[\alpha_{\rm avg} - \tfrac{\Omega\theta^2}{\lambda}(\Delta\alpha)^2 - \tfrac{\Omega\theta^2}{\lambda}\Delta\alpha\Delta\beta \right] \\
&\quad - \Delta t^2 \Omega^2 (\alpha_{\rm avg}^2 + \beta_{\rm avg}^2), \\
\mathrm{P}(m_A{=}0, m_B{=}1) &= \Delta t \Omega \left[\beta_{\rm avg} - \tfrac{\Omega\theta^2}{\lambda}(\Delta\beta)^2 - \tfrac{\Omega\theta^2}{\lambda}\Delta\alpha\Delta\beta \right] \\
&\quad - \Delta t^2 \Omega^2 (\alpha_{\rm avg}^2 + \beta_{\rm avg}^2), \\
\mathrm{P}(m_A{=}2, m_B{=}0) &= \tfrac{1}{2}\Delta t \tfrac{\Omega^2\theta^2}{\lambda}(\Delta\alpha)^2 + \tfrac{1}{2}\Delta t^2 \Omega^2 \alpha_{\rm avg}^2, \\
\mathrm{P}(m_A{=}0, m_B{=}2) &= \tfrac{1}{2}\Delta t \tfrac{\Omega\theta^2}{\lambda}(\Delta\beta)^2 + \tfrac{1}{2}\Delta t^2 \Omega^2 \beta_{\rm avg}^2, \\
\mathrm{P}(m_A{=}1, m_B{=}1) &= \tfrac{\Omega^2\theta^2}{\lambda}\Delta t \Delta\alpha\Delta\beta + \Delta t^2 \Omega^2 \alpha_{\rm avg}\beta_{\rm avg},
\end{aligned} \tag{5.32}$$

where we have ignored higher-order terms (those which go like Δt^3 or $\Delta t^2/\lambda$). Larger numbers of production events ($m_A + m_B \geq 3$) do not contribute at this order.

It is tempting to consider the limit of infinitesimally small Δt, and to use the first-order terms in Δt in Eq. (5.32) to construct reaction rates. If one does so, one recovers the rates exactly as they appear in the reduced master equation (5.21); for

example one would infer a rate of $\frac{1}{2}(\Omega^2\theta^2/\lambda)(\Delta\alpha)^2$ for events in which two particles of type A are produced and none of type B ($m_A = 2, m_B = 0$). The rate of an event in which one A and one B are produced simultaneously would be $(\Omega^2\theta^2/\lambda)\Delta\alpha\Delta\beta$, which is negative if $\Delta\alpha\Delta\beta < 0$.

However, taking the limit $\Delta t \to 0$ at fixed λ is not compatible with the assumption that a large number of environmental switching events occur in a given time-step, i.e., $\lambda\Delta t \gg 1$. To illustrate this further we carried out simulations of the full model of population and environment, and measured how many birth events of either particle type occur in a given time interval Δt. Specifically we focus on the probability $P(m_A = 1, m_B = 1)$ of seeing exactly one birth event of type A and one birth event of type B during such a time interval; note that in the full model these births occur in two separate events. The lines in Fig. 5.6 show the predictions of Eqs. (5.32), results from simulations of the full model are shown as markers. We first notice that simulations deviate from the results of Eqs. (5.32) at large values of Δt. This is to be expected as Eqs. (5.32) are derived neglecting higher-order terms in Δt. Simulations and the above expressions agree to good accuracy at intermediate values of the time step; we write Δt_* for the lower end of this range, and Δt^* for the upper end. As seen in Fig. 5.6, the lower threshold Δt_* decreases as the switching of the environment becomes faster (i.e., λ is increased). The reduction of the threshold is in-line with the requirement $\lambda\Delta t \gg 1$ for the theoretical analysis above. As seen in the figure the results of Eqs. (5.32) are largely determined by the term of order Δt^2 when they match simulations of the full model (the slope of the simulation data in the log-log plot of Fig. 5.6 is then approximately two). This term, $\Delta t^2\Omega^2\alpha_{\rm avg}\beta_{\rm avg}$, is positive, irrespective of the sign of $\Delta\alpha\Delta\beta$. At low values of $\Delta t \lesssim \Delta t_*$, we observe systematic deviations between simulations of the full model and the expressions in Eqs. (5.32). For the case $\Delta\alpha\Delta\beta < 0$ it is obvious that this must occur: at small Δt, Eqs. (5.32) predict $\mathrm{P}(m_A = 1, m_B = 1) \approx (\Omega^2\theta^2/\lambda)\Delta t\Delta\alpha\Delta\beta < 0$, whereas $P(m_A = 1, m_B = 1)$ is non-negative in simulations by definition. Deviations at small time steps are also seen in the left-hand panel of Fig. 5.6, the expression in Eqs. (5.32) shows a cross-over to linear scaling in Δt, whereas simulation results scale approximately as Δt^2.

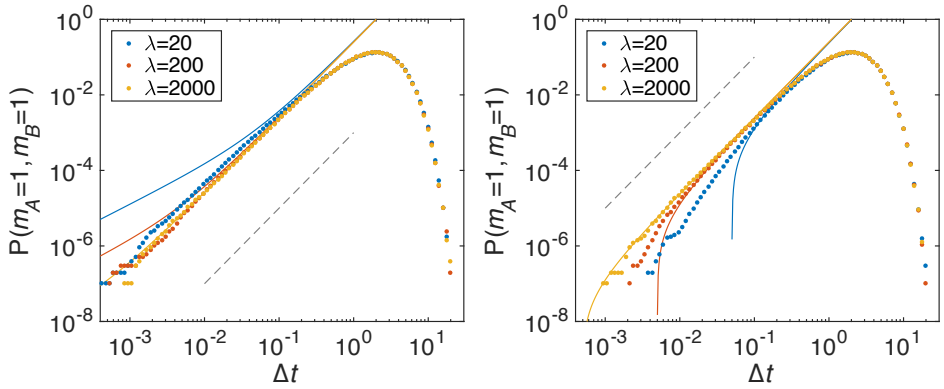

Figure 5.6: Probability of seeing $m_A = 1, m_B = 1$ in a given time interval of duration Δt. Circles show the results of simulation of the full model (population and environment); full lines show Eq. (5.32). The dashed line shows a slope of 2 for comparison. Data is shown for different values of λ, all other model parameters are as in the earlier figures. Left: $\Delta\alpha\Delta\beta > 0$, right: $\Delta\alpha\Delta\beta < 0$.

5.7.4 Simulation procedure for discrete-time sample paths

The analysis of the previous section is based on a discretisation of time into intervals of length Δt. In the limit of fast switching of the environment it then assumes that the time-averaged birth rates $\Omega\overline{\alpha}$ and $\Omega\overline{\beta}$ are Gaussian random variables with statistics given in Eqs. (5.30). We will now use this interpretation to define an algorithm with which to approximate sample paths of the full model in discrete time. We note that $\overline{\alpha}$ and $\overline{\beta}$ can take negative values in this Gaussian approximation. This issue arises irrespective of the sign of $\Delta\alpha\Delta\beta$ and is separate from the problem of negative rates in the reduced master equation. The probability for $\overline{\alpha}$ and/or $\overline{\beta}$ to be negative is exponentially suppressed in $\lambda\Delta t$, as the mean of the Gaussian distribution, $(\alpha_{\rm avg}, \beta_{\rm avg})$, does not depend on λ or Δt, and the covariance matrix is of order $(\lambda\Delta t)^{-1}$ [Eq. (5.30)]. As the switching of the environment becomes faster the distributions of $\overline{\alpha}$ and $\overline{\beta}$ become increasingly peaked around their mean. For the purposes of the numerical scheme we truncate the distribution at zero.

The algorithm uses ideas from the τ-leaping variant of the Gillespie algorithm [59], and proceeds as follows:

1. Assume the simulation has reached time t and that the current particle numbers are n_A and n_B. Draw correlated Gaussian random numbers $\overline{\alpha}$ and $\overline{\beta}$, from a distribution with $\langle\overline{\alpha}\rangle = \alpha_{\rm avg}$, and $\langle\overline{\beta}\rangle = \beta_{\rm avg}$, and with second moments as in Eqs. (5.30). If $\overline{\alpha} < 0$ set $\overline{\alpha} = 0$ and similar for $\overline{\beta}$.

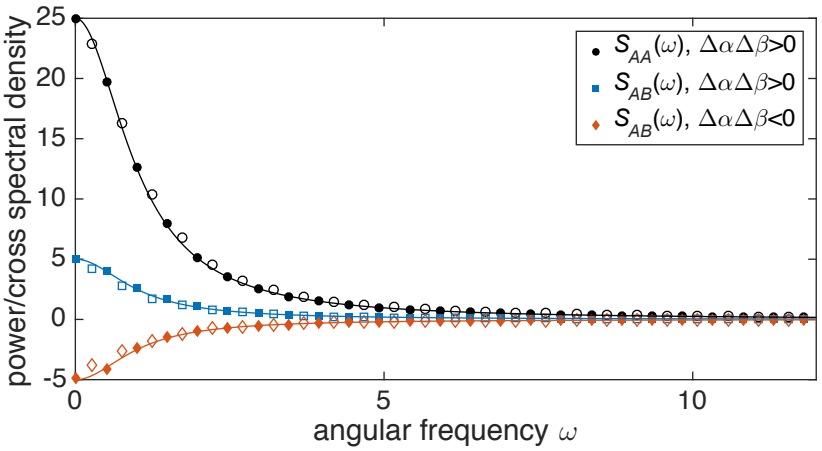

Figure 5.7: Spectra of fluctuations from direct simulations of the full model (filled symbols), and using the discrete-time algorithm in Sec. 5.7.4 (open symbols). The model is the same as in previous figures ($k_0 = k_1 = 1, \Omega = 20, \lambda = 20, \alpha_0 = 0, \alpha_1 = 1$, $\Delta t = 0.1$). Solid lines show the power spectrum/cross spectrum obtained from the linear-noise approximation of the reduced dynamics, Eq. (5.59).

2. Using the $\overline{\alpha}$ and $\overline{\beta}$ just generated, draw independent integer random numbers m_A and m_B from Poissonian distributions with parameters $\Omega\overline{\alpha}\Delta t$ and $\Omega\overline{\beta}\Delta t$, respectively.
3. For the death processes draw Poissonian random variables m'_A and m'_B from Poissonian distributions with parameters $\gamma n_A \Delta t$ and $\delta n_B \Delta t$ respectively.
4. Update the particle numbers to $n_A + m_A - m'_A$ and $n_B + m_B - m'_B$, respectively (if this results in $n_A < 0$ set $n_A = 0$, and similar for n_B).
5. Increment time by Δt and go to 1.

We have introduced a cutoff procedure in step 4 of the algorithm, in order to prevent particle numbers from going negative. This is necessary due to the discrete-time nature of the process, and well-known in the context of τ-leaping [59]. In particular this is not related to the appearance of negative rates in the reduced master equation, and applies in the case $\Delta\alpha\Delta\beta > 0$ as well.

We have carried out simulations using this algorithm for both cases $\Delta\alpha\Delta\beta > 0$ and $\Delta\alpha\Delta\beta < 0$. As shown in Fig. 5.7 the resulting spectra of fluctuations are in agreement with those of the full model, at least to reasonable approximation. In particular the cross spectrum $S_{AB}(\omega)$ comes out negative in the anti-correlated case. We attribute remaining discrepancies to the discretisation of time and the assumptions of Gaussian effective birth rates.

It is important to stress that agreement with the full model requires a careful choice

of the time step Δt. On the one hand, one needs $\Delta t \gtrsim 1/\lambda$, otherwise it is not justified to replace $\overline{\alpha}$ and $\overline{\beta}$ by Gaussian random variables. On the other hand, the so-called 'leap condition' for τ-leaping must be fulfilled [59], that is, the time step Δt must not be long enough for the population to change significantly in one step. More precisely the changes in particle numbers must remain of order Ω^0 in each step.

5.8 Expansion in system size

In the previous Sections we started from a microscopic process in a population of discrete individuals, subject to a randomly switching environment. We then carried out an expansion in the limit of fast environmental switching. We discussed different levels of coarse graining: the switching of the environment was either kept in its original form (full model), treated as fast but not infinitely so (reduced master equation), or the adiabatic limit of infinitely fast switching was taken (master equation with effective, average rates). So far we have considered discrete populations; its intrinsic stochastic dynamics, due to production and removal events, were not approximated.

Another approximation method for Markov jump processes with small jump sizes involves carrying out an asymptotic expansion in powers of the inverse population size. In the context of large populations, and without the complication of environmental switching, this typically is achieved by performing either the Kramers–Moyal expansion or van Kampen's system-size expansion [60, 61]. These techniques are commonly used in a number of applications of population dynamics; they have recently been extended to the case of jump processes in switching environments [62–64]. Following such an expansion, the state of the population is continuous and, for a fixed environmental state, described by a stochastic or ordinary differential equation. Alternative approaches, based on the WKB method, have been pursued for example in Refs. [9, 11, 17, 30, 31, 65]. These approaches, however, do not provide a description of the population which is dynamical.

The purpose of this Section is to combine Kramers–Moyal-type expansions with an expansion in the time scale separation between environment and population. This leads to different dynamical levels of description depending on how the environmental switching and the discreteness and intrinsic stochasticity of the population are treated.

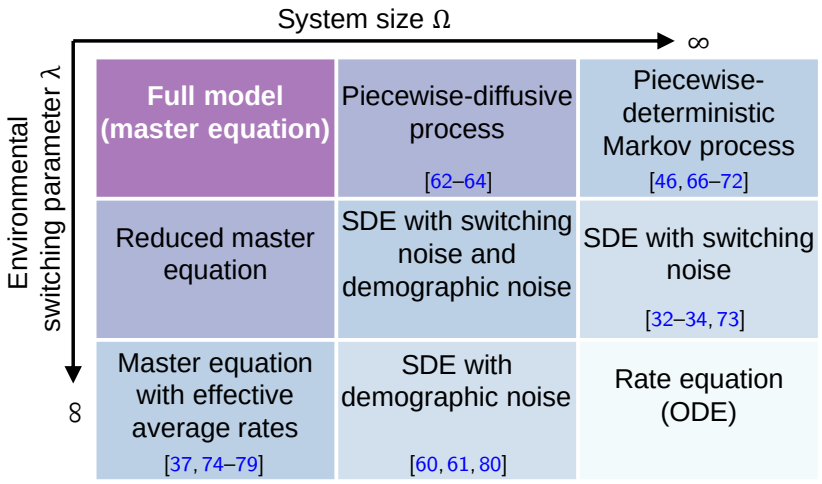

Figure 5.8: Schematic overview of the different model-reduction schemes for populations coupled to external environments with discrete states. Each column and row corresponds to a successive layer of approximation.

Studying these different levels of approximation is also useful to put our results of the previous Sections into the context with existing work [32–34, 37, 46, 62–64, 66–79]. We will first give a general overview, and then consider a specific example.

5.8.1 Overview

A schematic overview is given in Fig. 5.8. Broadly speaking the overall picture involves expansions in the inverse switching time scale (λ^{-1}) and/or the inverse typical size of the population (Ω^{-1}). The parameters λ and Ω correspond to the vertical and horizontal directions in Fig. 5.8. In the upper row we perform no expansion in λ^{-1} (i.e, we keep all terms), in the middle row we assume $\lambda \gg 1$ but finite (keeping leading and sub-leading terms), and in the lower row the adiabatic limit has been taken ($\lambda \to \infty$), i.e., the noise due to the environmental switching is discarded altogether. The left-hand column describes models with a discrete population (arbitrary Ω), in the middle column we assume $\Omega \gg 1$, but finite, and in the right-hand column the limit $\Omega \to \infty$ has been taken, i.e., all intrinsic noise in the population is disregarded. We now discuss the relation between the different levels of approximation in more detail.

Expansion in environmental time scale

In the previous Sections we have focused on the left-hand column of Fig. 5.8. The upper left box is the full microscopic model, involving a discrete population of typical size Ω,

and an environmental process associated with a switching time scale set by λ. This full model is defined by the master equation (5.1). Expanding to sub-leading order in λ^{-1}, but keeping Ω fixed and general, one obtains the reduced master equation (5.8). Here, we restrict the discussion to processes in which the environmental switching is independent of the state of the population; the more general case is discussed briefly in Appendix 5.11. In the case of only two environmental states the reduced master equation is given by Eq. (5.14). It describes the process with bursting as discussed in Sec. 5.4.3.

The limit $\lambda \to \infty$ is the adiabatic limit; restricting the master equation to leading-order terms in λ^{-1} produces a process described by the master equation

$$\frac{\mathrm{d}}{\mathrm{d}t}\Pi(\ell, t) = \mathcal{M}_{\mathrm{avg}}\Pi(\ell, t). \tag{5.33}$$

For the case of two environmental states this can be obtained from Eq. (5.14), but the general form is applicable for multiple environmental states as well. Eq. (5.33) describes a process with the same types of reactions as the original dynamics, but with rates that are weighted averages over the stationary distribution of the environmental states. This is the lower left-hand box in Fig. 5.8. This is conceptually similar to the quasi-steady-state approximation [36, 37, 74–76, 79], in which the fast-reacting species are regarded as constant at values obtained from an appropriate weighted average. Another approach to approximating environmental noise in the fast-switching limit involves assuming a large number of environmental states, so that the environment may be approximated as continuous [81, 82].

Expansion in powers of inverse system size

In a different approach one can first approximate the intrinsic noise for large system size ($\Omega \gg 1$), starting from the full model (environment and population), without any expansion in the environmental switching time scale. This is done by carrying out a Kramers–Moyal expansion on the dynamics of the population, while simultaneously maintaining the discrete environmental states [64]. This corresponds to travelling horizontally along the first row of Fig. 5.8.

If sub-leading order terms in powers of the inverse system size are retained, one obtains piecewise-diffusive dynamics [62–64, 83], corresponding to the middle box in

the first row of Fig. 5.8. Between switches of the environmental state, the population is then described by a stochastic differential equation. The process is described by

$$\frac{\partial}{\partial t}p_\sigma(\mathbf{x},t) = \mathcal{F}_\sigma p_\sigma(\mathbf{x},t) + \lambda \sum_{\sigma'} A_{\sigma'\to\sigma} p_\sigma(\mathbf{x},t), \tag{5.34}$$

where $p_\sigma(\mathbf{x},t)$ is a probability density over continuous states $\mathbf{x}$, obtained from discrete states ℓ in the limit of large Ω (see Sec. 5.8.2 for a specific example). The $\mathcal{F}_\sigma$ are Fokker–Planck operators obtained from a Kramers–Moyal expansion on $\mathcal{M}_\sigma$.

Combined expansion

Starting from the piecewise-diffusive process [upper row, middle in Fig. 5.8, Eq. (5.34)] one can follow the same steps as in Sec. 5.4.1 and consider the limit of fast but not infinitely fast environmental switching. In Fig. 5.8 this means working down the central column. We simultaneously consider the limit of large Ω and the limit of large λ. In taking these limits we assume that the ratio Ω/λ remains finite, this will become more clear in the example discussed below (Sec. 5.8.2). For the case of two environmental states, the result can be read off from Eq. (5.14) simply replacing $\mathcal{M}_\sigma$ by $\mathcal{F}_\sigma$, i.e.,

$$\frac{\partial}{\partial t}\Pi(\mathbf{x},t) = \mathcal{F}_{\text{avg}}\Pi(\mathbf{x},t) + \frac{1}{2}\frac{\theta^2}{\lambda}(\mathcal{F}_0 - \mathcal{F}_1)^2\Pi(\mathbf{x},t). \tag{5.35}$$

An interpretation of Eq. (5.35) in terms of a stochastic differential equation can be obtained by expanding the term $(\mathcal{F}_0 - \mathcal{F}_1)^2$ further and keeping only terms to order $1/\Omega$. This stochastic differential equation contains two different sources of Gaussian noise, one representing demographic noise and the other the stochasticity of the environmental switching.

Finally, we could also take the adiabatic limit $\lambda \to \infty$; this leads to $\frac{\partial}{\partial t}\Pi(\mathbf{x},t) = \mathcal{F}_{\text{avg}}\Pi(\mathbf{x},t)$. In this limit the noise due to the environmental process has been eliminated entirely, and the resulting SDE contains only Gaussian noise coming from the intrinsic fluctuations in the population.

Piecewise-deterministic process

Finally, we can also take the limit of an infinite population $\Omega \to \infty$ first, keeping λ general. Thus, we neglect intrinsic fluctuations altogether. This is achieved by retaining only the leading-order term in the Kramers–Moyal expansion of the population. In

each fixed environment the dynamics of the population are then described by an ordinary differential equation. This constitutes what is known as a piecewise-deterministic Markov process (PDMP) [66, 67]. In Fig. 5.8 this is the right-hand box in the upper row. Mathematically, the PDMP is described by

$$\frac{\partial}{\partial t}p_\sigma(\mathbf{x},t) = \mathcal{L}_\sigma p_\sigma(\mathbf{x},t) + \lambda \sum_{\sigma'} A_{\sigma'\to\sigma} p_\sigma(\mathbf{x},t), \tag{5.36}$$

with Liouville operators $\mathcal{L}_\sigma$; they are first-order differential operators which describe the deterministic drift of the system in a given environmental state.

We can now use the PDMP as a starting point, and work down the right-hand column of Fig. 5.8, following the same steps as in Sec. 5.4.1, replacing $\mathcal{M}_\sigma$ by $\mathcal{L}_\sigma$. For two environmental states and keeping terms of order λ^{-1}, the result is analogous to Eq. (5.14). One finds

$$\frac{\partial}{\partial t}\Pi(\mathbf{x},t) = \mathcal{L}_{\text{avg}}\Pi(\mathbf{x},t) + \frac{1}{2}\frac{\theta^2}{\lambda}(\mathcal{L}_0 - \mathcal{L}_1)^2\Pi(\mathbf{x},t). \tag{5.37}$$

This is a Fokker–Planck equation and corresponds to an SDE in which Gaussian noise reflects the effects of the fast-switching environment. This result was previously reported in Ref. [32].

A further approximation to the dynamics would again involve taking the adiabatic limit: this is equivalent to ignoring the final term in Eq. (5.37). The resulting Liouville equation corresponds to an ODE description of the system. Its dynamics is then governed by a rate equation, where the reaction rates are weighted averages over the different environmental states. In such an approximation all stochasticity, both intrinsic and environmental, has been eliminated. This is the lower entry in the right-hand column of Fig. 5.8.

5.8.2 Example

We now focus on one of the single-species models in Sec. 5.4.3. The purpose of this basic example is purely illustrative; specific applications will be discussed in Sec. 5.9. Particles are produced at constant rate β, and they are removed with per capita rates δ_σ in environments $\sigma \in \{0, 1\}$. We have

$$\mathcal{M}_\sigma = \beta\Omega(\mathcal{E}^{-1} - 1) + \delta_\sigma(\mathcal{E} - 1)n, \tag{5.38}$$

where n is the number of particles in the population. Keeping the system-size parameter Ω fixed, and taking the limit of large but finite λ, one obtains Eq. (5.19). This corresponds to the middle box in the left-hand column of Fig. 5.8. Taking $\lambda \to \infty$ one has

$$\frac{\mathrm{d}}{\mathrm{d}t}\Pi(n,t) = \Omega\beta(\mathcal{E}^{-1}-1)\Pi(n,t) + (\mathcal{E}-1)\delta_{\mathrm{avg}} n \Pi(n,t), \tag{5.39}$$

where $\delta_{\mathrm{avg}} = (k_0\delta_0 + k_1\delta_1)/(k_0+k_1)$; this is the master equation with effective average rates (lower box on the left in Fig. 5.8).

Next, writing $x = n/\Omega$, and starting again from the full model of population and environment, we carry out a Kramers–Moyal expansion first (keeping terms up to sub-leading order in $1/\Omega$). One has the Fokker–Planck operators

$$\begin{aligned}
\mathcal{F}_0 &= \beta\left(-\partial_x + \frac{1}{2\Omega}\partial_x^2\right) + \delta_0\left(\partial_x + \frac{1}{2\Omega}\partial_x^2\right)x, \\
\mathcal{F}_1 &= \beta\left(-\partial_x + \frac{1}{2\Omega}\partial_x^2\right) + \delta_1\left(\partial_x + \frac{1}{2\Omega}\partial_x^2\right)x.
\end{aligned} \tag{5.40}$$

These operators together with Eq. (5.34) describe a piecewise-diffusive process (upper row, central column in Fig. 5.8); in a given environmental state the dynamics are described by an Ito SDE

$$\dot{x} = \beta - \delta_{\sigma(t)}x + \sqrt{\frac{\beta + \delta_{\sigma(t)}x}{\Omega}}\eta(t), \tag{5.41}$$

where $\eta(t)$ is Gaussian white noise of unit variance.

Further approximating the piecewise-diffusive process in the limit of fast environmental switching, we can insert the explicit form of $\mathcal{F}_\sigma$ into Eq. (5.35) to give

$$\begin{aligned}
\frac{\partial}{\partial t}\Pi(x,t) &= -\partial_x\left\{\left[\beta - \delta_{\mathrm{avg}}x + \frac{1}{2}g_{\mathrm{e}}\partial_x g_{\mathrm{e}}\right]\Pi(x,t)\right\} \\
&\quad + \frac{1}{2}\partial_x^2\left\{\left[g_{\mathrm{i}}^2 + g_{\mathrm{e}}^2\right]\Pi(x,t)\right\},
\end{aligned} \tag{5.42}$$

where $\Delta = \delta_0 - \delta_1$, and

$$g_{\mathrm{i}}(x)^2 = \frac{1}{\Omega}\left(\beta + \delta_{\mathrm{avg}}x\right), \tag{5.43}$$

$$g_{\mathrm{e}}(x)^2 = \frac{\theta^2}{\lambda}\Delta^2 x^2. \tag{5.44}$$

The subscript 'i' indicates intrinsic stochasticity (demographic noise), and 'e' labels the contribution to the noise from environmental switching. We note that $g_{\mathrm{i}}(x)^2 \propto \Omega^{-1}$, and $g(x)_{\mathrm{e}}^2 \propto \lambda^{-1}$. It is interesting to note that the same Fokker–Planck equation is

obtained by a direct Kramers–Moyal expansion of Eq. (5.19). Details can be found in Appendix 5.13.1. The contribution $g_e \partial_x g_e/2$ to the drift term in Eq. (5.42) is of order λ^{-1}, and it can safely be neglected to the order we are working at (see also Ref. [32]). Equation (5.42) then describes an Ito SDE of the form

$$\dot{x} = \beta - \delta_{\rm avg} x + g_{\rm i}(x)\eta_{\rm i}(t) + g_{\rm e}(x)\eta_{\rm e}(t), \tag{5.45}$$

in which $\eta_{\rm i}(t)$ and $\eta_{\rm e}(t)$ are independent Gaussian processes of unit variance, and with no correlations in time. The SDE (5.45), corresponds to the central box in Fig. 5.8.

Equation (5.42) can be used as a starting point for further approximations. In the case of infinitely fast switching, $\lambda \to \infty$, the term $g_{\rm e}(x)$ can be neglected, and one finds

$$\begin{aligned} \frac{\partial}{\partial t}\Pi(x,t) = & -\partial_x \left[(\beta - \delta_{\rm avg} x)\,\Pi(x,t)\right] \\ & + \frac{1}{2\Omega}\partial_x^2 \left[(\beta + \delta_{\rm avg} x)\,\Pi(x,t)\right]. \end{aligned} \tag{5.46}$$

We note that this relation can also be obtained by direct Kramers–Moyal expansion of Eq. (5.39). Only the Gaussian noise from the intrinsic stochasticity then remains in the SDE (5.45). This is the lower box in the central column of Fig. 5.8.

In the case of an infinite population $\Omega \to \infty$, Eq. (5.42) turns into

$$\begin{aligned} \frac{\partial}{\partial t}\Pi(x,t) = & -\partial_x \left[(\beta - \delta_{\rm avg} x)\,\Pi(x,t)\right] \\ & + \frac{\theta^2}{2\lambda}\Delta^2 \partial_x^2 \left[x^2 \Pi(x,t)\right], \end{aligned} \tag{5.47}$$

so that the noise term containing $g_{\rm i}(x)$ is no longer present in the SDE (5.45). This is the centre box in the right-hand column of Fig. 5.8. Equation (5.47) can also be found from Eq. (5.37) upon using $\mathcal{L}_\sigma \Pi(x) = -\partial_x(\beta - \delta_\sigma x)\Pi(x)$, see Appendix 5.13.2.

If all stochasticity is ignored altogether ($\lambda \to \infty$ and $\Omega \to \infty$) one has $g_{\rm i} = g_{\rm e} = 0$. In our example one then finds the rate equation

$$\dot{x} = \beta - \delta_{\rm avg} x. \tag{5.48}$$

This corresponds to the lower box in the right-hand column of Fig. 5.8.

5.8.3 Linear-noise approximation

In order to obtain analytical results, for example approximations to the stationary distribution and power spectral density of fluctuations, an additional step—the linear

noise approximation (LNA)—can be taken in Eq. (5.45). The LNA simplifies an SDE with multiplicative noise into one with additive noise, and is applicable when the noise is sufficiently small [61], i.e., in our case $\lambda \gg 1$ and $\Omega \gg 1$.

The stochastic differential equation (5.45) is of the form

$$\dot{x} = v_{\mathrm{avg}}(x) + g_{\mathrm{i}}(x)\eta_i(t) + g_{\mathrm{e}}(x)\eta_e(t), \tag{5.49}$$

where $v_{\mathrm{avg}}(x) = \beta - \delta_{\mathrm{avg}}x$, and where $g_{\mathrm{i}} = \mathcal{O}(\Omega^{-1/2})$ and $g_{\mathrm{e}} = \mathcal{O}(\lambda^{-1/2})$. The LNA can then be carried out using the ansatz

$$x(t) = x_{\mathrm{avg}}(t) + \Omega^{-1/2}\xi_{\mathrm{i}}(t) + \lambda^{-1/2}\xi_{\mathrm{e}}(t), \tag{5.50}$$

where $x_{\mathrm{avg}}(t)$ is a deterministic function to be determined self-consistently; the quantities $\xi_{\mathrm{i}}(t)$ and $\xi_{\mathrm{i}}(t)$ are each stochastic processes describing the deviations due to intrinsic and extrinsic noise, respectively. Inserting into Eq. (5.49), expanding in powers of $\Omega^{-1/2}$ and $\lambda^{-1/2}$ one obtains $\dot{x}_{\mathrm{avg}} = v_{\mathrm{avg}}(x_{\mathrm{avg}})$ from the lowest-order terms, and

$$\begin{aligned} \dot{\xi}_{\mathrm{i}} &= v'_{\mathrm{avg}}\left(x_{\mathrm{avg}}\right)\xi_{\mathrm{i}} + \Omega^{1/2} g_{\mathrm{i}}\left(x_{\mathrm{avg}}\right)\eta_i(t), \\ \dot{\xi}_{\mathrm{e}} &= v'_{\mathrm{avg}}\left(x_{\mathrm{avg}}\right)\xi_{\mathrm{e}} + \lambda^{1/2} g_{\mathrm{e}}\left(x_{\mathrm{avg}}\right)\eta_e(t), \end{aligned} \tag{5.51}$$

for the sub-leading order terms, where $v'_{\mathrm{avg}} = \mathrm{d}v_{\mathrm{avg}}/\mathrm{d}x$. We note that the arguments of both g_{i} and g_{e} are now given by x_{avg}, so that the multiplicative noise in Eq. (5.49) has been turned into additive noise. Introducing $\zeta(t) = \Omega^{-1/2}\xi_{\mathrm{i}}(t) + \lambda^{-1/2}\xi_{\mathrm{e}}(t)$ describing the total amount of deviation caused by both sources of noise, we can write this more compactly as $x(t) = x_{\mathrm{avg}}(t) + \zeta(t)$, with

$$\dot{\zeta} = v'(x_{\mathrm{avg}})\zeta + \left[g_{\mathrm{i}}(x_{\mathrm{avg}})^2 + g_{\mathrm{e}}(x_{\mathrm{avg}})^2\right]^{1/2}\eta(t), \tag{5.52}$$

where the two Gaussian processes have been combined, so that the stochasticity is described by a single white noise Gaussian process $\eta(t)$. In the above example we have $\dot{x}_{\mathrm{avg}} = \beta - \delta_{\mathrm{avg}}x_{\mathrm{avg}}$, and

$$\dot{\zeta} = -\delta_{\mathrm{avg}}\zeta + \left[\frac{\beta + \delta_{\mathrm{avg}}x_{\mathrm{avg}}}{\Omega} + \frac{\theta^2}{\lambda}\left(x_{\mathrm{avg}}\Delta\right)^2\right]^{1/2}\eta(t). \tag{5.53}$$

5.8.4 Analytical approximation for power spectra

We now return to the model with two species defined in Eq. (5.20). Carrying out a Kramers–Moyal expansion of the reduced master equation Eq. (5.21) we arrive at the

following stochastic differential equations for $x_A = n_A/\Omega$ and $x_B = n_B/\Omega$

$$\begin{aligned} \dot{x}_A &= \alpha_{\text{avg}} - \gamma x_A + \eta_A(t), \\ \dot{x}_B &= \beta_{\text{avg}} - \delta x_B + \eta_B(t). \end{aligned} \tag{5.54}$$

For compactness, we have absorbed the diffusion coefficients (describing both intrinsic and extrinsic noise) into the white noise terms η_A and η_B, so that they have the following covariance matrix:

$$\begin{aligned} \langle \eta_A(t)\eta_A(t')\rangle &= \left(\frac{\alpha_{\text{avg}} + \gamma x_A}{\Omega} + \frac{\theta^2}{\lambda}(\Delta\alpha)^2\right)\delta(t-t'), \\ \langle \eta_B(t)\eta_B(t')\rangle &= \left(\frac{\beta_{\text{avg}} + \delta x_B}{\Omega} + \frac{\theta^2}{\lambda}(\Delta\beta)^2\right)\delta(t-t'), \\ \langle \eta_A(t)\eta_B(t')\rangle &= \frac{\theta^2}{\lambda}\Delta\alpha\Delta\beta\delta(t-t'), \end{aligned} \tag{5.55}$$

see also Appendix 5.13.3.

To simplify matters we now restrict the discussion to the case $\gamma = \delta$ and $\alpha_{\text{avg}} = \beta_{\text{avg}}$ (the latter does not imply $\Delta\alpha = \Delta\beta$). In the long run the deterministic trajectory converges to the fixed point given by $x_A^* = x_B^* = \alpha_{\text{avg}}/\gamma$. Applying the LNA at this fixed point, we find

$$\begin{aligned} \dot{\zeta}_A &= -\gamma\zeta_A + \eta_A(t), \\ \dot{\zeta}_B &= -\gamma\zeta_B + \eta_B(t), \end{aligned} \tag{5.56}$$

where

$$\begin{aligned} \langle \eta_A(t)\eta_A(t')\rangle &= \left(\frac{2\alpha_{\text{avg}}}{\Omega} + \frac{\theta^2}{\lambda}(\Delta\alpha)^2\right)\delta(t-t'), \\ \langle \eta_B(t)\eta_B(t')\rangle &= \left(\frac{2\alpha_{\text{avg}}}{\Omega} + \frac{\theta^2}{\lambda}(\Delta\beta)^2\right)\delta(t-t'), \\ \langle \eta_A(t)\eta_A(t')\rangle &= \frac{\theta^2}{\lambda}\Delta\alpha\Delta\beta\delta(t-t'). \end{aligned} \tag{5.57}$$

In order to find the power spectral density of fluctuations, we perform a Fourier transform and obtain

$$\begin{aligned} \langle \zeta_A(\omega)\zeta_A^*(\omega')\rangle &= \delta(\omega+\omega')\Omega^{-2}S_{AA}(\omega), \\ \langle \zeta_A(\omega)\zeta_B^*(\omega')\rangle &= \delta(\omega+\omega')\Omega^{-2}S_{AB}(\omega), \end{aligned} \tag{5.58}$$

with

$$\begin{aligned} S_{AA}(\omega) &= \Omega^2\frac{\frac{2\alpha_{\text{avg}}}{\Omega} + \frac{\theta^2}{\lambda}(\Delta\alpha)^2}{\gamma^2+\omega^2}, \\ S_{AB}(\omega) &= \Omega^2\frac{\frac{\theta^2}{\lambda}\Delta\alpha\Delta\beta}{\gamma^2+\omega^2}. \end{aligned} \tag{5.59}$$

This result matches well with the results of Gillespie simulating the full model (for $\Omega = 20$, $\lambda = 20$). A comparison is shown in Fig. 5.7. In the adiabatic limit ($\lambda \to \infty$) Eq. (5.59) reduces to

$$\begin{aligned} S_{AA}(\omega) &= \Omega \frac{2\alpha_{\text{avg}}}{\gamma^2 + \omega^2}, \\ S_{AB}(\omega) &= 0, \end{aligned} \tag{5.60}$$

confirming again the absence of correlations between n_A and n_B in the limit of infinitely fast environments.

5.9 Further applications

In this Section we will apply the formalism we have developed to a series of specific examples.

5.9.1 Model of protein production

Motivation and model definitions

The dynamics of gene expression are inherently noisy [8,84], and stochastic approaches are hence most appropriate to model such processes. They also frequently exhibit a separation of time scales, see e.g. Refs. [47,79,85,86]. Here, we consider a commonly-used model which describes two essential steps for gene expression, the transcription into mRNA and the translation into protein [5,8,67,87–90]. The model describes a single gene G, which can be in two different states, labelled 'on' ($\sigma = 1$) and 'off' ($\sigma = 0$). The gene switches between these states with rates k_0 and k_1, respectively. In each state, mRNA molecules are produced with a rate Ωb_σ; they decay with rate d. The presence of mRNA also leads to the production of protein molecules; this occurs with rate β (per mRNA molecule). Protein molecules finally decay with rate δ. The model can be summarised by the following reactions

$$\begin{gathered} G_{\text{off}} \underset{\lambda k_0}{\overset{\lambda k_1}{\rightleftharpoons}} G_{\text{on}}, \quad \emptyset \xrightarrow{\Omega b_\sigma} M, \quad M \xrightarrow{d} \emptyset, \\ M \xrightarrow{\beta} M + P, \quad P \xrightarrow{\delta} \emptyset, \end{gathered} \tag{5.61}$$

where M and P refer to mRNA and protein molecules, respectively.

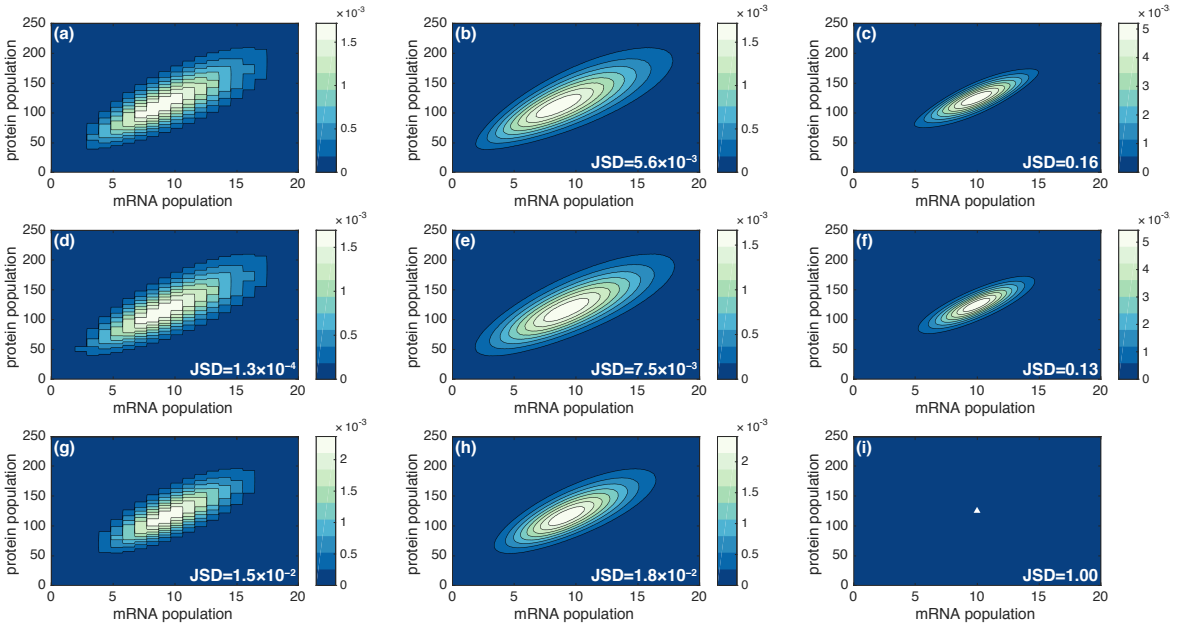

Figure 5.9: The stationary probability distribution of the populations of mRNA and protein molecules for the model in Sec. 5.9.1. Data is from Monte Carlo simulations of each different level of approximation in Fig. 5.8: (a) full model; (b) piecewise-diffusive process; (c) piecewise-deterministic Markov process; (d) reduced master equation with bursting; (e) SDE with switching noise and demographic noise; (f) SDE with switching noise; (g) master equation with average rates; (h) SDE with demographic noise; and (i) rate equation (▲ represents a delta peak). Parameters: $\Omega = 20, b_0 = 0, b_1 = 1, d = 1, \beta = 25, \delta = 2$, and $\lambda = 10, k_0 = k_1 = 1$.

Comparison of different approximation schemes

We proceed to consider the full model, and each of the eight levels of approximation in Fig. 5.8. The reduced master equation for large λ can be derived following the procedure outlined in Sec. 5.4. The details of this are very similar to the example in Sec. 5.4.3; we do not report them in full. The reduced master equation describes a set of effective reactions in which mRNA molecules are made in bursts of sizes one or two. We stress again that the origin of this type of bursting is different from the one discussed in Refs. [47–50]. These effective reactions can then be simulated by the standard Gillespie method, because the reduced master equation for this model does not contain negative rates.

Similarly, for the adiabatic limit $\lambda \to \infty$, effective production rates are obtained by replacing the rates b_σ in Eq. (5.61) by their weighted average, b_{avg}. This can then be used in the Gillespie simulation.

For large but finite Ω, the piecewise-diffusive process for this model is given by

$$\begin{aligned} \dot{m} &= \left(b_{\sigma(t)} - dm\right) + \Omega^{-1/2}\sqrt{b_{\sigma(t)} + dm}\;\eta^{\mathrm{m}}(t) \\ \dot{p} &= (\beta m - \delta p) + \Omega^{-1/2}\sqrt{\beta m + \delta p}\;\eta^{\mathrm{p}}(t), \end{aligned} \tag{5.62}$$

where Ωm and Ωp are the numbers of mRNA molecules and protein molecules, respectively, and where $\sigma(t)$ is the stochastic trajectory of the switching process for the gene; $\eta^{\mathrm{m}}(t)$ and $\eta^{\mathrm{m}}(t)$ are independent Gaussian white noise processes. For both Ω and λ large but finite we find the following description in terms of stochastic differential equations (corresponding to the central box in Fig. 5.8):

$$\begin{aligned} \dot{m} &= (b_{\mathrm{avg}} - dm) + \left[g_{\mathrm{i}}^{\mathrm{m}}(m,p)^2 + g_{\mathrm{e}}^{\mathrm{m}}(m,p)^2\right]^{1/2}\eta^{\mathrm{m}}(t), \\ \dot{p} &= (\beta m - \delta p) + g_{\mathrm{i}}^{\mathrm{p}}(m,p)\eta^{\mathrm{p}}(t), \end{aligned} \tag{5.63}$$

where

$$\begin{aligned} g_{\mathrm{i}}^{\mathrm{m}}(m,p) &= \Omega^{-1/2}\sqrt{b_{\mathrm{avg}} + dm}, \\ g_{\mathrm{e}}^{\mathrm{m}}(m,p) &= \lambda^{-1/2}\sqrt{\frac{2k_1k_0\left(b_0 - b_1\right)^2}{\left(k_0 + k_1\right)^3}}, \\ g_{\mathrm{i}}^{\mathrm{p}}(m,p) &= \Omega^{-1/2}\sqrt{\beta m + \delta p}. \end{aligned} \tag{5.64}$$

From these it is straightforward to obtain the remaining approximations in Fig. 5.8, by either sending the amplitude of the environmental noise $g_{\mathrm{e}}^{\mathrm{m}}$ to zero, or that of the intrinsic noise ($g_{\mathrm{i}}^{\mathrm{p}}$, and $g_{\mathrm{i}}^{\mathrm{m}}$), or both.

Figure 5.9 shows the stationary distributions obtained from Monte Carlo simulations of the full model and the eight different approximations. The arrangement in the figure corresponds to that in Fig. 5.8. We remark that the population remains discrete for the panels in the left-hand column, while expanding in powers of the system size (middle and right column) leads to continuous populations. In each panel we indicate a numerical estimate for the Jensen–Shannon divergence (JSD) of the respective stationary distribution relative to that of the full model in panel (a) [91].

The data in Fig. 5.9 shows that the successive approximations in powers of the system size and the switching rates reduce the accuracy in reproducing the full individual-based model. The JSD generally increases as one moves down or to the right in Fig. 5.9. For this model and parameter set, the only exception is the approximation in panel (f) which shows a smaller JSD than that in panel (c). This is due to the following effect. The full model in panel (a) can explore arbitrary numbers of mRNA and protein

molecules. The stationary distribution of the PDMP in panel (c) however has bounded support, because intrinsic noise is discarded. The distribution in panel (f) does not include effects of intrinsic noise either, but the environmental stochasticity has been approximated by Gaussian noise, restoring an unbounded support. This leads to the seemingly better agreement of (f) with the full model.

We are not necessarily proposing all eight approximations in Figs. 5.8 and 5.9 as starting points for further analysis or simulation. For instance, it is not easy to find analytical descriptions for the stationary distribution of the piecewise diffusive description in panel (b), and the piecewise deterministic model in panel (c). This is only feasible for simple models, see also our earlier work [64]. The SDE in panel (e) on the other hand (i.e., approximating both intrinsic and extrinsic randomness as Gaussian noise) allows for the stationary distribution, among other things, to be approximated analytically; following a linearisation of the noise terms (LNA) in Eq. (5.63), the resulting distribution is a bivariate Gaussian. At this level of approximation the stationary distribution can be obtained analytically. In this respect, approximation (e) can be seen as a useful trade-off between accuracy and practical analytical results in our limit of interest, at least for the unimodal distribution of the current model. We will also discuss the SDE as a starting point for efficient simulations in the context of the next example.

5.9.2 Bimodal genetic switch

Model

The simple model of protein production in the previous section shows a unimodal distribution. Pluripotent stem cells have the ability to differentiate into several possible cell types [46, 92, 93]; the basic features of the networks of genes, transcription factors and epigenetic variables leading to these cell-fate decisions are a current focus of research [84, 94–96]. Several hypotheses exist about the mechanisms leading to cell differentiation; among these it has been proposed that excursions of the genetic circuit into different areas of state space might contribute to steering cells towards distinct

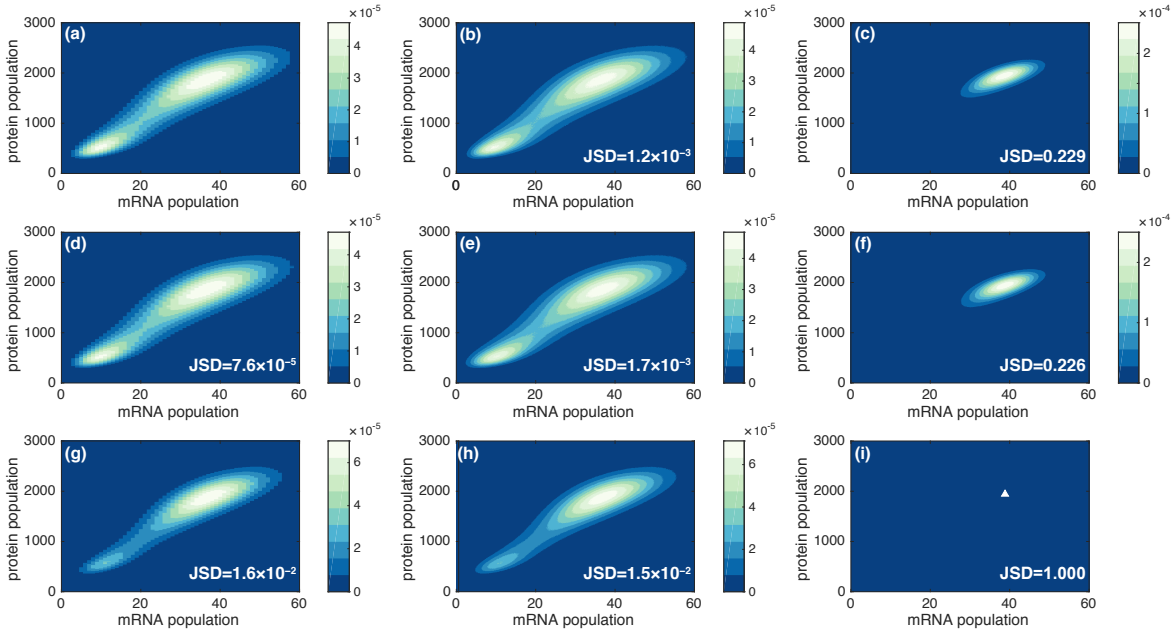

Figure 5.10: Stationary probability distribution of the populations of mRNA and protein molecules for the full model in Sec. 5.9.2, and the eight levels of model reduction in Fig. 5.8: (a) full model; (b) piecewise-diffusive process; (c) piecewise-deterministic Markov process; (d) reduced master equation; (e) SDE with switching noise and demographic noise; (f) SDE with switching noise; (g) master equation with average rates; (h) SDE with demographic noise; and (i) rate equation (▲ represents a delta peak). Parameters: $N = 2, \Omega = 50, b_0 = b_1 = 1, b_2 = 20, d = 9.2, \beta = 50, \delta = 1, k_- = 0.025, k_+ = 1$ and $\lambda = 1250$.

differentiated states [92, 93]. Bimodal distributions are observed in a variety of biological switches [30, 47, 97–99]. In this Section we discuss a stylised model of processes leading to bimodal distributions; the difference to the model in the previous Section is that this extended model admits a multi-modal stationary distribution. In the context of the above hypothesis, these different peaks would lead to distinct differentiated states.

The model describes a single gene G, with a promoter site which can bind to a total of up to N molecules of protein. Each protein molecule binds with a rate $\lambda k_+/\Omega$, and unbinds with a rate k_-. Binding and unbinding are sequential [100]. Depending on the current state of the gene (i.e., the number of bound proteins, $\sigma = 0, 1, \ldots, N$), mRNA molecules are produced with rate Ωb_σ. As in the previous section mRNA in turn decays with (per capita) rate d; mRNA leads to the production of protein molecules with a rate β per mRNA molecule. Protein molecules finally decay with rate δ. The

model can be summarised by the following reactions

$$\begin{aligned} G_\sigma + P &\underset{\lambda k_-}{\overset{\lambda k_+/\Omega}{\rightleftharpoons}} G_{\sigma+1}, \quad \text{for } \sigma < N \\ G_\sigma &\xrightarrow{\Omega b_\sigma} G_\sigma + M, \\ M \xrightarrow{d} \emptyset, \qquad M &\xrightarrow{\beta} M + P, \qquad P \xrightarrow{\delta} \emptyset. \end{aligned} \tag{5.65}$$

where M and P refer to molecules of mRNA and protein, respectively.

Mathematically, the two main differences compared to the model in the previous section are the following: (i) the environment (the gene) can take more than two states ($\sigma = 0, 1, \ldots, N$); (ii) the overall rate with which switches from state σ to $\sigma + 1$ occur ($\sigma < N$) depends on the number of protein. Each protein molecule contributes $\lambda k_+/\Omega$ to the switching rate; the total rate of switching from state $\sigma < N$ to $\sigma+1$ is $\lambda k_+ N_p/\Omega$, if the number of proteins is N_p. This means that the environmental switching depends on the state of the population.

Different architectures of the genetic switching and associated mRNA-production rates are discussed in the literature, e.g., [72, 94–96, 101]. We focus on $N = 2$, i.e., there are three possible enviromental states, $\sigma = 0, 1, 2$. We also assume that mRNA molecules are produced with a common basal rate in gene states $\sigma = 0, 1$, i.e. we set $b_0 = b_1$. When the maximum of $N = 2$ proteins are bound to the gene mRNA is produced with the activated rate Ωb_2, where $b_2 > b_0$ [46].

Comparison of the different approximation schemes

As in the previous model we test the eight different approximations in Fig. 5.8. In order to derive the reduced master equation, we need to go beyond the formalism of Sec. 5.4.2, as the environmental switching depends on the state of the population of mRNA and proteins. The construction therefore starts from Eqs. (5.8) and (5.9), with three environmental states $\sigma \in \{0, 1, 2\}$. The calculation leading to the reduced master equation for this model is tedious, but straightforward. The expression for the reduced master equation is lengthy, and given in Appendix 5.14.1.

For large but finite Ω, the piecewise-diffusive process for this model is as in Eq. (5.62);

the only difference is in the dynamics governing $\sigma(t)$. The approximation corresponding to the central box in Fig. 5.8 is given by the stochastic differential equations

$$\begin{aligned} \dot{m} &= (b_{\text{avg}}(p) - dm) + \left[g_{\text{i}}^{\text{m}}(m,p)^2 + g_{\text{e}}^{\text{m}}(m,p)^2\right]^{1/2} \eta^{\text{m}}(t), \\ \dot{p} &= (\beta m - \delta p) + g_{\text{i}}^{\text{p}}(m,p)\eta^{\text{p}}(t), \end{aligned} \tag{5.66}$$

where

$$\begin{aligned} b_{\text{avg}}(p) &= \frac{b_0 k_-^2 + b_0 k_- k_+ p + b_2 k_+^2 p^2}{k_-^2 + k_- k_+ p + k_+^2 p^2}, \\ g_{\text{e}}^{\text{m}}(m,p) &= \sqrt{\frac{2k_- k_+^2 p^2 \left[k_-^2 + 3k_- k_+ p + k_+^2 p^2\right]}{\lambda \left(k_-^2 + k_- k_+ p + k_+^2 p^2\right)^3} (b_2 - b_0)^2}, \\ g_{\text{i}}^{\text{m}}(m,p) &= \Omega^{-1/2} \sqrt{b_{\text{avg}}(p) + dm}, \\ g_{\text{i}}^{\text{p}}(m,p) &= \Omega^{-1/2} \sqrt{\beta m + \delta p}. \end{aligned} \tag{5.67}$$

Again it is straightforward to obtain the approximations (f), (h) and (i), by either sending the amplitude of the intrinsic noise (g_{i}^{m} and g_{i}^{p}) to zero, or of the environmental noise (g_{e}^{m}), or that of both.

Figure 5.10 shows the stationary distributions obtained for the full model, and for the different approximations. All data is from direct simulations, except (d) which is discussed further below. As before, the arrangement corresponds to that in the schematic of Fig. 5.8, and for each approximation we report the JSD relative to the stationary distribution of the full model in panel (a). The JSD in panel (f) is lower than that in (d) for the same reason as in the previous section. A similar effect is seen comparing (h) and (g). The figure also demonstrates the bimodal structure of the stationary distribution is induced by the intrinsic noise; it is present in each panel in the left-hand and centre columns, but in none of the panels in the right-hand column. While the model is stylised and not intended to directly model a particular biological system Fig. 5.10 demonstrates that analyses of this type may help to establish the origin of relevant biological features—in this case bimodality linked to pluripotency and cell-fate decision making is due to intrinsic rather than extrinsic noise.

On a technical note, we add that approximation (d), the reduced master equation, does not in itself define a Markovian process for this model, due to the appearance of negative rates (see Appendix 5.14.1). We have generated the data for the stationary distribution of the reduced master equation in two different ways. One is direct

numerical integration of the reduced master equation, this leads to a JSD relative to the distribution for the full model of approximately 7.6×10^{-5}. The second method consists of Gillespie simulations of an approximation to the reduced master equation (5.105), in which sub-leading terms of order Ω^2/λ are kept, but those of order Ω/λ are discarded; specifically, we have set $\varpi_1 = \varpi_2 = 0$ in Eq. (5.105) for the purpose of these simulations. This leads to a Markovian process, and sample paths can hence be generated using the standard Gillespie algorithm. The JSD for the stationary distribution obtained in this way from that of the full model is found to be approximately 9.1×10^{-5}. Visually, the results from the two methods are indistinguishable, and their JSD from each other is approximately 1.3×10^{-5}, almost an order of magnitude lower than the JSD of either of the two from the stationary distribution of the full model.

Other approaches to such systems are based on the WKB method [9,11,17,30,31]; while these approaches do not rely on a particular regime of λ, they have several differences from the approach outlined above: (i) The main purpose of the WKB-based methods is to compute stationary or quasi-stationary distributions. While some dynamical properties can be derived from this (e.g., mean first passage times [30]), the approach is not in itself a dynamic approach, i.e., it does not compute time-dependent quantities. In particular this method does not allow access to two-time objects such as correlation functions (or equivalently spectra of fluctuations). (ii) The WKB-based approaches are based on the limit of large population size. The reduced master equation [results shown in Fig. 5.10 (d)] and the master equation in the adiabatic limit [Fig. 5.10 (g)] make no such assumption. (iii) These methods are dependent on the existence of stable fixed points of the underlying deterministic limiting dynamics [e.g., Eq. (1) in Ref. [30]]. The quasi-stationary distributions computed by the WKB-based methods centre around such stable fixed points. Our model reduction approaches make no assumptions regarding the fixed-point structure of the limiting deterministic dynamics. In Fig. 5.10 we see multi-modality in the probability distributions even though the deterministic dynamics [i.e., the dynamics given by Eq. (5.66) after setting the noise strengths to zero] include only a single fixed point.

Efficient simulations and required computing time

Although in the previous two examples we have carried out all eight different approximations, we remark that some prove more useful than others in terms of providing an efficient simulation scheme for specific applications. The purpose of collating data from the different levels of model reduction in Figs. 5.9 and 5.10 was to give an illustration of the schematic Fig. 5.8 in the context of two concrete examples.

The approximation as an SDE [panel (e) in Figs. 5.8, 5.9 and 5.10] provides a good starting point for simulations of systems with intrinsic noise of small and moderate amplitude, and fast-switching environments. The SDE is an approximation, but it retains both intrinsic and extrinsic noise. In the context of simpler models, we have already used the SDE to carry out further mathematical analysis using the LNA (see Sec. 5.8.4). To further illustrate the possible advantages of the approximation as a SDE, we have investigated the amount of computing time needed to carry out simulations of the full model in Eq. (5.65), and of the SDE (5.66). Broadly speaking, the number of environmental switching events per unit time in the full model can be expected to scale as λ, and the number of events in the population per unit time grows as Ω. One would therefore expect the computing time required to generate a given number of sample paths for the full model up to a specified end time to grow when λ or Ω are increased. This is confirmed in Table 5.1. As seen in Table 5.1 the time required to generate sample paths of the SDE (5.66) is independent of λ and Ω, as these only enter in the noise strength. These results indicate that simulations of the SDE can be carried out more efficiently than those of the full model, especially when either the environmental switching is fast, or the typical population size large, or both. This is also the regime in which the SDE approximation becomes increasingly accurate.

5.9.3 Genetic network with multiple genes

A related model, as considered in Ref. [10], involves N identical promoter genes, $G^{(i)}$ ($i = 1, \ldots, N$), which can each be in their 'on' or 'off' states, and switch between these independently. This is different from the model in the previous section where a single gene can bind up to N molecules of protein. The N genes operate 'in parallel'; for the dynamics of the population only the total number of genes in each state

λ	Ω	computation time (s) for full model	computation time (s) for SDE with switching and demographic noise
500	50	62.4	34.3
1000	50	74.0	34.4
1500	50	85.0	34.4
2000	50	93.2	34.4
1250	20	40.4	34.5
1250	40	67.4	34.7
1250	60	95.7	34.4
1250	80	123.2	34.3

Table 5.1: Comparison of the simulation time of the full model Eq. (5.65) and the SDE (5.66). The Gillespie algorithm and Euler–Maruyama method ($\mathrm{d}t = 5 \times 10^{-3}$) are used, respectively, to simulate the system up to time 10^4. While the simulation time of the full model increases with λ and Ω, the simulation time for the SDE is independent of λ and Ω.

matters. As a consequence, there are $N+1$ different environmental states describing the configuration of the genes. We use the number of genes in the 'on' state to label these states, $\sigma \in \{0, \ldots, N\}$. We leave out the mRNA dynamics, and focus only on protein production and decay. We assume that each gene in its 'on' state contributes Ωb_1 to the total production rate, and each gene in its 'off' state contributes Ωb_0. As before the parameter Ω controls the typical size of the population of protein molecules. We then have $\Omega b_\sigma = (N-\sigma)\Omega b_0 + \sigma \Omega b_1$ for the total production rate. The model is defined by the reactions

$$\begin{aligned} G_{\mathrm{off}}^{(i)} &\xrightarrow{\Omega b_0} G_{\mathrm{off}}^{(i)} + \mathrm{P}, \qquad G_{\mathrm{off}}^{(i)} \underset{\lambda k_0}{\overset{\lambda k_1}{\rightleftharpoons}} G_{\mathrm{on}}^{(i)}, \\ G_{\mathrm{on}}^{(i)} &\xrightarrow{\Omega b_1} G_{\mathrm{on}}^{(i)} + \mathrm{P}, \qquad P \xrightarrow{\delta} \emptyset, \end{aligned} \tag{5.68}$$

where the reactions for different genes $i = 1, \ldots, N$ run independently. The SDE description of the model in the limit of large but finite Ω and λ is of the form

$$\dot{p} = N b_{\mathrm{avg}} - \delta p + \left[g_{\mathrm{i}}(p)^2 + g_{\mathrm{e}}(p)^2 \right]^{1/2} \eta(t), \tag{5.69}$$

where each gene contributes an average rate of production $b_{\mathrm{avg}} = (b_0 k_0 + b_1 k_1)/(k_0 + k_1)$. The contribution to the noise from intrinsic fluctuations has amplitude

$$g_{\mathrm{i}}(p)^2 = \frac{1}{\Omega} \left(N b_{\mathrm{avg}} + \delta p \right). \tag{5.70}$$

The environmental noise comes from the switching between the $N+1$ gene configurations; each gene switches between its on and off states independently. Following

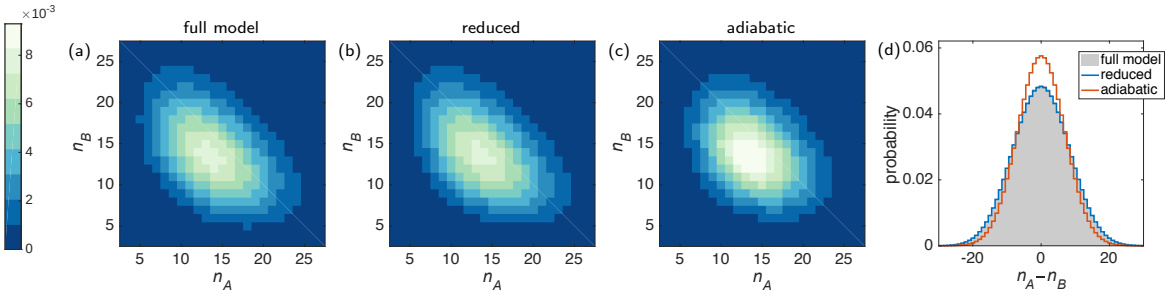

Figure 5.11: Stationary distribution for the genetic circuit with exclusive binding (Sec. 5.9.4) from numerical integration of (a) the full master equation with explicit environment, (b) the reduced master equation Eq. (5.108), and (c) the adiabatic approximation which considers average rates. Panel (d) shows the marginal distribution of $n_A - n_B$ in order to compare the three distributions. Parameters $\Omega\alpha_1 = 20$, $\Omega\alpha_0 = 0$, $\lambda\kappa_0 = \Omega\lambda\kappa_1 = 20$.

the earlier examples, one expects a contribution $2k_0k_1(b_0 - b_1)^2/[\lambda(k_0 + k_1)^3]$ to the variance of the environmental noise from each gene, so that the total variance is

$$g_e(p)^2 = \frac{2Nk_1k_0\,(b_0 - b_1)^2}{\lambda\,(k_0 + k_1)^3}. \tag{5.71}$$

We note that the relative fluctuations of the total production rate [i.e., the ratio $g_e(p)/(Nb_{\text{avg}})$] scales as $N^{-1/2}$.

Mathematically, the transition rate matrix for the $N + 1$ environmental states may be written as the tridiagonal matrix

$$\begin{aligned} A_{\sigma\to\sigma-1} &= \lambda k_0\sigma, && \text{for } \sigma \geq 1, \\ A_{\sigma\to\sigma+1} &= \lambda k_1(N - \sigma), && \text{for } \sigma \leq N - 1, \\ A_{\sigma\to\sigma\pm j} &= 0, && \text{for } j \geq 2, \end{aligned} \tag{5.72}$$

together with the convention $A_{\sigma\to\sigma} = -A_{\sigma\to\sigma-1} - A_{\sigma\to\sigma+1}$. The formalism of Sec. 5.4 can then be applied, but becomes algebraically tedious. Using numerical algebra packages we have verified Eq. (5.71) up to $N = 100$.

5.9.4 Genetic circuit with exclusive binding

Next, we consider a circuit with exclusive promoter binding [102, 103]. The model describes two genes G^A and G^B, and two corresponding proteins P^A and P^B. Proteins P^A and P^B bind to genes of the opposing type, G^B and G^A, respectively, with (per capita) rates $\lambda\kappa_1/\Omega$ and $\lambda\mu_1/\Omega$. They unbind from these promoters with rates $\lambda\kappa_0$ and $\lambda\mu_0$. These binding and unbinding reactions can be summarised as follows:

$$\begin{aligned} G^A_{\text{unbnd.}} + G^B_{\text{unbnd.}} &\underset{\lambda\kappa_0}{\overset{n_B\lambda\kappa_1/\Omega}{\rightleftharpoons}} G^A_{\text{bnd.}} + G^B_{\text{unbnd.}}, \\ G^A_{\text{unbnd.}} + G^B_{\text{unbnd.}} &\underset{\lambda\mu_0}{\overset{n_A\lambda\mu_1/\Omega}{\rightleftharpoons}} G^A_{\text{unbnd.}} + G^B_{\text{bnd.}}, \end{aligned} \tag{5.73}$$

where the subscripts 'bnd.' and 'unbnd.' indicate whether the gene is bound to a protein or unbound, respectively, and where n_A and n_B are the numbers of molecules of proteins of type A and B. In this model either gene G^A or gene G^B can be bound, but not both simultaneously. This is due to spatial considerations of the binding process: owing to the proteins size and the proximity of the genes, the binding of a particular protein blocks the other protein from binding [102, 103]. When gene G^A is bound, proteins of type A are produced with rate $\Omega\alpha_0$, and when it is unbound they are produced with rate $\Omega\alpha_1$. Similarly when gene G^B is bound, proteins of type B are produced with rate $\Omega\beta_0$, and when it is unbound they are produced with rate $\Omega\beta_1$. To summarise, the protein production rates in the three gene configurations are as follows:

	production rate P^A	production rate P^B
G^A, G^B unbound:	$\Omega\alpha_1$	$\Omega\beta_1$
G^A bound:	$\Omega\alpha_0$	$\Omega\beta_1$
G^B bound:	$\Omega\alpha_1$	$\Omega\beta_0$.

In this model one protein inhibits the expression of the other, i.e., $\alpha_0 < \alpha_1$ and $\beta_0 < \beta_1$. Additionally, protein A degrades with rate γ and protein B with rate δ.

In this model the birth rates of the two types of proteins are not independent; rather, they are connected through the state of the environment (the binding status of the two genes). Furthermore, when production of one protein is inhibited (for example protein A when G^A is bound), the other protein is expressed with a higher rate (G^B unbound). This is an example of a model of the kind considered in Sec. 5.5 where we showed how anti-correlations lead to negative rates in the reduced master equation. The reduced master equation for this model is lengthy, we present it in Appendix 5.14.2.

Figure 5.11 shows the results for the stationary distribution obtained from numerical integration of this reduced master equation; we also show the stationary distributions of the full model and of the adiabatic approximation. As seen in panel (d) of the figure the reduced master equation reproduces the stationary distribution of the full model with greater accuracy than the adiabatic approximation.

5.9.5 Staged switching of the environment

In many situations the switching between environmental states is not purely Markovian. Periodic switching between environmental states has been considered in experimental and theoretical studies of bacterial populations; for example the presence or absence of antibiotic treatment according to a periodic protocol. As a bet-hedging strategy, the bacteria respond to time-dependent external stresses with phenotypic heterogeneity [7, 83, 104–106]. In this context it is therefore important to be able to study stochastic populations coupled to environments described by a non-Markovian process.

In this Section we consider an example in which there are two distinct environmental conditions, labelled 0 and 1. In contrast with the previous examples, each of these conditions consists of several identical, internal states (or stages), which are traversed in sequence. Similar setups have been used to model dynamics which fall between the purely periodic and purely Markovian limits, see e.g. Refs. [7, 107, 108].

The model is illustrated in Fig. 5.12(a). There are N environmental states which correspond to environmental condition 0, and M states that correspond to environmental condition 1. States in condition 0 transition to the next state with rate $\lambda k_1 N$, and states corresponding to condition 1 transition to the next state with rate $\lambda k_0 M$. The environment cycles through all states in order, as indicated in the figure.

In this way, the time spent in condition 0 before switching to 1 is $\Gamma(N, \lambda N k_1)$-distributed, and similarly the time spent in condition 1 follows a $\Gamma(M, \lambda M k_0)$ distribution. Independent of N and M, the environment spends an average time $(\lambda k_1)^{-1}$ in condition 0 before it switches to 1, and then an average time $(\lambda k_0)^{-1}$ in condition 1 before it switches back to condition 0. Increasing the number of states N and M leads to an increased regularity of time spent in each condition. The limit $N, M \to \infty$ in particular corresponds to periodic switching between the two conditions.

For simplicity we disregard intrinsic noise in this example and focus on a piecewise-deterministic process. We assume that the dynamics are given by $\dot{x} = v_0(x)$ if the environment is in condition 0, and by $\dot{x} = v_1(x)$ if it is in condition 1. Based on the formalism of Sec. 5.4, we use a symbolic algebra package to solve Eq. (5.9), where the operator $\mathcal{M}_\sigma$ is substituted by the Liouville operator $\mathcal{L}_\sigma = -\partial_x v_\sigma(x)$. We use this to derive an SDE in the limit of fast but finite environmental dynamics. We find

$$\dot{x} = v_{\text{avg}}(x) + g_{\text{e}}(x)\eta(t), \tag{5.74}$$

where $\eta(t)$ is white Gaussian noise, and where the drift and diffusion terms are given by

$$\begin{aligned} v_{\text{avg}}(x) &= \frac{k_0 v_0(x) + k_1 v_1(x)}{k_0 + k_1}, \\ g_{\text{e}}(x) &= \lambda^{-1/2} \sqrt{\frac{k_1 k_0 (N+M) \left[v_0(x) - v_1(x)\right]^2}{NM \left(k_1 + k_0\right)^3}}. \end{aligned} \tag{5.75}$$

We have not attempted to formally prove this for general N and M; rather, we tested this result for a range of combinations $N, M < 150$ and found it to be true for all tested values.

In Fig. 5.12(b) we use a specific example, where the drift is $v_0(x) = b_0 - x$ and $v_1(x) = b_1 - x$; this choice corresponds to the protein production model considered in Sec. 5.4.3. In this figure we compare the stationary distributions obtained from simulation of the PDMP with the stationary distribution obtained analytically from solving the one-dimensional Fokker–Planck equation for Eq. (5.74). We show this data for different choices of N and M in Fig. 5.12(b), restricting to $N = M$ for simplicity.

Similarly, we compare the variance of the stationary distributions from the PDMP and the SDE in Fig. 5.12(c). The parameters λ, k_1, and k_0 are kept fixed; we focus again on the case $N = M$, and vary this number of internal states. Analytical results from the SDE and numerical simulation of the PDMP agree well for $N, M < 100$, but there are deviations when $N = M$ becomes large. This is due to fact that the PDMP tends to a deterministic limit cycle; this limit cycles leads to a finite variance of the corresponding distribution, indicated by the dashed line of Fig. 5.12(c)]. These limit cycle dynamics are not captured by the SDE.

The model as described above is only defined for integer values of N and M. However, the distribution of waiting times in either environmental condition can be

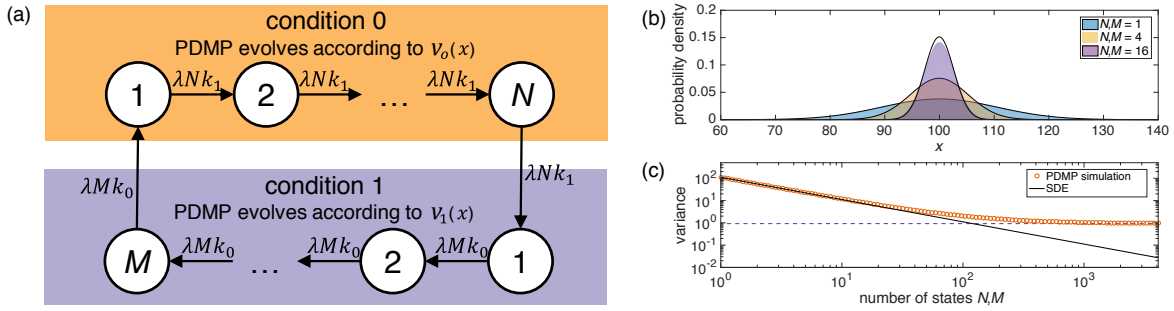

Figure 5.12: *Schematic and statistics for a model with staged switching of the environment.* (a) Schematic illustrating an environment with two distinct conditions, with N and M identical stages, respectively. (b) Stationary distribution for different values of $N = M$. Histograms show results of simulations, lines are from the theory described in the text. (c) Variance of the stationary distribution as a function of N (again for the case $N = M$). The black line shows the results of the theory, orange circles are from simulations of the piecewise-deterministic Markov process. Parameters N and M have been generalised to include non-integer values, by considering gamma-distributed waiting-time distributions in the two conditions (see text). Dashed line shows the variance of the limit cycle obtained in the limit of a periodic environment. Parameters: $b_0 = 100/3$ and $b_1 = 500/3$, $\lambda k_0 = \lambda k_1 = 20$.

generalised to the case of gamma distributions with non-integer shape parameters. The interpretation as a series of internal states within conditions $\sigma = 0$ and $\sigma = 1$ then no longer holds, but simulations of the model can still be carried out, drawing waiting times directly from the appropriate gamma distributions. The SDE (5.75) remains unaltered, and it provides an accurate description of the dynamics of the model also when N and M are not integers. This can be seen in Fig. 5.12(c), where many of the markers (circles) correspond to simulations for non-integer values of N and M.

5.9.6 Reliability analysis and crack propagation

The formalism we have developed can also be applied to the calculation of time-to-failure in models of industrial systems. One of the challenges in this field is to capture features of real-world systems in tractable mathematical models. In this context, many authors have used piecewise-deterministic processes with Markovian external environments. These models incorporate discrete environmental effects such as different modes of operation, external stresses or loads [23–25]. In these applications there is often a clear separation of time scales, the environmental switching is a much faster process than the degradation of the system. For example a piece of material may be subject to mechanical load which changes several times a day or hour, and the

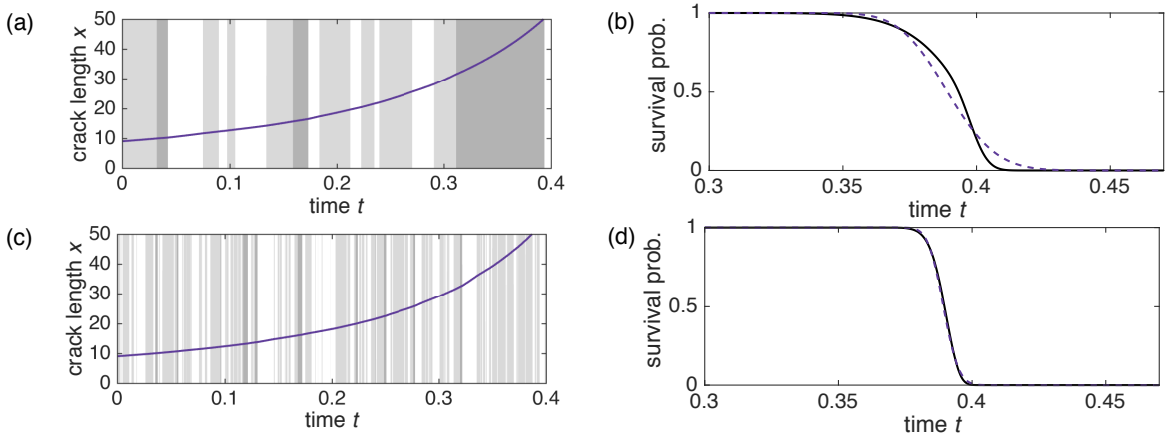

Figure 5.13: Panel (a): Sample path of the model of crack growth (Sec. 5.9.6). Background shading indicates the state of the environment, with states 0, 1 and 2 shown progressively darker. Panel (b): survival probability as a function of time. The black line shows results from Monte Carlo simulations, the dashed line is the prediction of Eq. (5.82). Panels (c) and (d) show the same quantities for tenfold increased switching rates. Model parameters are given in the text.

degradation of the material occurs over months or years.

Specifically, we consider the example of fatigue crack growth; this is an engineering problem describing the growth in the length of a crack in a mechanical component. One such model uses a piecewise-deterministic Markov process to describe the growth of the length of a crack [20–22, 109] as follows,

$$\dot{x} = x^b \times v_{\sigma(t)}, \tag{5.76}$$

where x is the crack length, the exponent $b > 0$ is a constant, and where as before $\sigma(t)$ represents the state of the environment at time t. The factor v_σ takes into account that the crack grows faster in some environments than in others. Transitions from state σ to σ' occur with rate $\lambda A_{\sigma\to\sigma'}$.

Given an initial length x_0, we are interested in the time it takes to reach the threshold length $x = L$; this is when the component is deemed unreliable. We use the formalism of the earlier sections to approximate the PDMP as an SDE in the limit of fast (but not infinitely fast) environmental switching ($\lambda \gg 1$). We then find the first-passage time of this SDE through the threshold value. While diffusive processes have been used as starting points in models of reliability [110, 111], we systematically reduce the PDMP to an effective stochastic differential equation.

In the simplest case of two environmental states (and writing $A_{0\to1} = k_1, A_{1\to0} = k_0$

as before), Eq. (5.76) can be approximated as by the SDE

$$\dot{x} = x^b v_{\text{avg}} + g\, x^b \eta(t), \tag{5.77}$$

where

$$v_{\text{avg}} = \frac{k_0 v_0 + k_1 v_1}{k_0 + k_1}, \qquad g^2 = \frac{2k_0 k_1 (v_0 - v_1)^2}{\lambda (k_0 + k_1)^3}. \tag{5.78}$$

Higher-order terms in λ^{-1} have been discarded. For the special case of exponential growth, $b = 1$, the SDE approximation turns into geometric Brownian motion. In a different context this has been implemented in Ref. [32]. We proceed to find the first-passage time of the process in Eq. (5.77) through the threshold L. This can be done following Ref. [112], but with a modification allowing for $b \neq 1$. As a first step we apply the transformation

$$y = \begin{cases} \ln x & b = 1, \\ \frac{x^{1-b}-1}{1-b} & b \neq 1. \end{cases} \tag{5.79}$$

The SDE (5.77) can then be written

$$\dot{y} = v_{\text{avg}} + g\, \eta(t). \tag{5.80}$$

For such a process, the distribution of first passage times through a given threshold is known [112]. Returning to the original variables, we obtain the probability density $Q(x_0, t)$ of first-passage times of the process Eq. (5.77) through L, if started at position x_0 at time $t = 0$. For $b = 1$ one finds

$$Q(x_0, t) = \frac{|\ln(L/x_0)|}{gt(2\pi t)^{1/2}} \exp\left(-\frac{\left[\ln(L/x_0) - (v_{\text{avg}} - \frac{g^2}{2})t\right]^2}{2g^2 t} \right), \tag{5.81}$$

and for $b \neq 1$ one has

$$Q(x_0, t) = \frac{1}{gt(2\pi t)^{1/2}} \left| \frac{L^{1-b} - x_0^{1-b}}{1-b} \right| \frac{-\left[(L^{1-b} - x_0^{1-b})/(1-b) - (v_{\text{avg}} - \frac{g^2}{2})t\right]^2}{2g^2 t}. \tag{5.82}$$

This approach can be extended to models with more than two environmental states, leading to modifications in the noise strength g. We demonstrate this with a numerical example. We use the parameters suggested in Ref. [109], in particular $b = 1.5$, and

$$\lambda \mathbf{A} = \begin{bmatrix} -40 & 40 & 0 \\ 54 & -60 & 6 \\ 20 & 0 & -20 \end{bmatrix}, \quad v = \begin{bmatrix} 1.0 \\ 0.9 \\ 1.2 \end{bmatrix}.$$

The initial crack length is $x_0 = 9$, and we use $L = 50$ as the threshold for the onset of failure. Compared to Ref. [109] we have rescaled time. Implementing our theory shows that the process can be approximated by the SDE (5.77) where $v_{\text{avg}} = 69/70$ and $g^2 = 141/274400$. This is obtained from solving Eq. (5.9) with a numerical algebra package, again substituting the operator $\mathcal{M}_\sigma$ with the appropriate Liouville operator. Figure 5.13(a) shows a sample path of the PDMP generated by Monte Carlo simulation, while the background indicates the state of the environment. Figure 5.13(b) shows the probability that a given component is still reliable at time t. The black line is obtained through Monte Carlo simulations, whereas the dashed line is the prediction of Eq. (5.82). For the specified parameters, the two lines show agreement. Increasing the switching rate [Fig. 5.13(d)] strengthens this agreement.

5.10 Conclusions

We have developed methods for the reduction and approximation of the dynamics of discrete stochastic systems coupled external environments with a finite number of discrete states. Our analysis focuses on the limit in which the environmental dynamics are fast relative to that of the system, but where the time scale separation is not necessarily infinite. In particular, we have derived reduced dynamics for the open system, capturing next-order corrections to the adiabatic limit.

The model reduction leads to master equations with bursting, and—in some cases—with negative transition 'rates'. Our analysis shows that negative (pseudo-) probabilities can arise from such non-Markov-process reduced dynamics, and it suggests that these negative transients only occur on time scales shorter than than that of the environment. The reduced dynamics—obtained by coarse graining the environmental process—does not resolve the physics of the problem on such fine time scales. The occurrence of bursting reactions can be understood further by looking at the time evolution of individual sample paths of system and environment over a finite time interval. This leads to a discrete-time approximation for the dynamics of the open system. The path of the environment in one time step can be approximated by Gaussian random variables; bursting in the system results from fluctuations of this discrete-time Gaussian process.

We find that trajectories obtained using a simulation algorithms adapted from open quantum systems to the classical case do not reproduce statistical features of sample paths of the full model of system and environment. This suggests further work on the relation of full and reduced dynamics in the quantum context. We note one potentially important difference between the classical and the quantum cases; the origin of non-Markovianity in open quantum systems is often attributed to a two-way exchange of information between the system and the environment [27, 28]. This mechanism is not available in some of the examples we have looked at, even though these models still lead to negative rates in the reduced dynamics (Sec. 5.5).

We placed our reduction schemes in the context of existing work on piecewise-deterministic Markov processes, and piecewise-diffusive processes. In particular we study combined expansions in the relative time-scale of the environment and/or the strength of the intrinsic noise. This provides a more complete picture of different approximations for systems with intrinsic noise and environmental fluctuations. We also introduced a scheme approximating such a process as a SDE, capturing both switching and demographic noise. We expect this tool to facilitate efficient simulation of open systems.

We have demonstrated how these results can be used to study a number of problems in different areas. In particular, the reduction schemes we have proposed allow for an approximation of the open system in terms of stochastic differential equations. The approximation is valid when populations are large and the environmental process fast. In this situation simulations of the full dynamics of the population and the environment are particularly costly. The stochastic differential equation approximates both the intrinsic and the extrinsic randomness as Gaussian noise, and it can be used to carry out simulations more efficiently. As we have shown, it also allows for analytical progress in some cases. We have used the different approximation schemes for a varied set of applications, including models of genetic circuits, cases in which the switching between external conditions is non-Markovian, and a model of crack propagation. These applications are only a selected set of examples of situations in which switching environments play a role. We expect that the model-reduction schemes we have developed will be of use for further open classical systems in biology and the physical sciences, and in other disciplines. In Sec. 5.8 we have related the

different approximations to each other, and to existing work. This may help to select the most appropriate approximation method for specific applications.

Our work raises a number of questions for future work. For example, it would be interesting to study in more detail the analogies and differences between non-Markovian reduced dynamics for open quantum systems and for classical systems coupled to fast environments. As a first step, one might focus on classical systems in which the dynamics of the environment depends on the state of the system itself (such as in the examples in Secs. 5.9.2 and 5.9.3), and try to characterise the mathematical structure of the resulting reduced dynamics, and the information flow between system and environment. We also note that we have found non-Markovian features in the reduced dynamics at sub-leading order only when the system itself has discrete states, but not when the population is described by a piecewise diffusive or piecewise deterministic process. Based on the Pawula theorem [60,80] we expect unphysical terms in the latter cases when the expansion is truncated at higher-orders. Further work is required to understand in more detail how these features non-Markovian features emerge in the combined coarse graining process for the population and the environment. A separate further line of research might focus on systems in which the environment takes continuous states (see e.g. Ref. [11,30,31]), and the comparison with the discrete case.

5.11 Appendix A: State-dependent environmental process

In this Section of the Appendix we briefly consider the case in which the transition matrix for the environmental process depends on the state of the system proper, i.e., $A_{\sigma\to\sigma'} = A_{\sigma\to\sigma'}(\ell)$. From Eq. (5.8) we have

$$\frac{\mathrm{d}}{\mathrm{d}t}\Pi(\ell,t) = \sum_{\sigma} \mathcal{M}_{\sigma}\left[\rho^{*}(\sigma|\ell)\Pi(\ell,t)\right] + \frac{1}{\lambda}\sum_{\sigma}\mathcal{M}_{\sigma}w_{\sigma}(\ell,t), \tag{5.83}$$

and from Eq. (5.9)

$$\sum_{\sigma'} A_{\sigma'\to\sigma}(\ell)w_{\sigma'}(\ell,t) = \rho^{*}(\sigma|\ell)\sum_{\sigma'}\mathcal{M}_{\sigma'}\left[\rho^{*}(\sigma'|\ell)\Pi(\ell,t)\right] - \mathcal{M}_{\sigma}\left[\rho^{*}(\sigma|\ell)\Pi(\ell,t)\right]. \tag{5.84}$$

This serves as a starting point for the further analysis.

5.11.1 Adiabatic limit

It is useful to define the following operators, acting on functions $f(\ell)$,

$$\widehat{\mathcal{M}}_\sigma f(\ell) = \mathcal{M}_\sigma[\rho^*(\sigma|\ell) f(\ell)], \tag{5.85}$$

where the right-hand side indicates that the operator $\mathcal{M}_\sigma$ acts on the object inside the square bracket. In the adiabatic limit one finds [by sending $\lambda \to \infty$ in Eq. (5.83)]

$$\frac{\mathrm{d}}{\mathrm{d}t}\Pi(\ell, t) = \widehat{\mathcal{M}}_{\mathrm{avg}}\Pi(\ell, t), \tag{5.86}$$

where we now have

$$\mathcal{M}_{\mathrm{avg}} = \sum_\sigma \widehat{\mathcal{M}}_\sigma. \tag{5.87}$$

Example

To illustrate the principle we use a population with n individuals of a single species, and a birth reaction with rate $b_\sigma(n)$. We then have $\mathcal{M}_\sigma = [\mathcal{E}^{-1} - 1]b_\sigma(n)$. We find

$$\mathcal{M}_{\mathrm{avg}}\Pi(n, t) = [\mathcal{E}^{-1} - 1]b_{\mathrm{avg}}(n)\Pi(n, t), \tag{5.88}$$

where

$$b_{\mathrm{avg}}(n) = \sum_\sigma \rho^*(\sigma|n) b_\sigma(n). \tag{5.89}$$

We note that $b_{\mathrm{avg}}(n)$ carries a dependence on n, even if $b_\sigma(n)$ is itself independent of n.

5.11.2 Next-order contribution

In order to address the sub-leading term in $1/\lambda$, we focus on the case of two environmental states, with switching rates $A_{1\to 0}(\ell) = k_0(\ell)$ and $A_{0\to 1}(\ell) = k_1(\ell)$. In this case we have $\rho^*(0|\ell) = k_0(\ell)/[k_0(\ell) + k_1(\ell)]$, and $\rho^*(1|\ell) = k_1(\ell)/[k_0(\ell) + k_1(\ell)]$. From Eq. (5.84) one then finds

$$w_0(\ell, t) = -w_1(\ell, t) = \frac{1}{k_0(\ell) + k_1(\ell)} \left[\rho^*(1|\ell)\widehat{\mathcal{M}}_0 - \rho^*(0|\ell)\widehat{\mathcal{M}}_1\right] \Pi(\ell, t). \tag{5.90}$$

Inserting into Eq. (5.83) we have

$$\frac{\mathrm{d}}{\mathrm{d}t}\Pi(\ell, t) = \mathcal{M}_{\mathrm{avg}}\Pi(\ell) + \frac{1}{\lambda}(\mathcal{M}_0 - \mathcal{M}_1)\frac{1}{k_0(\ell) + k_1(\ell)} \left[\rho^*(1|\ell)\widehat{\mathcal{M}}_0 - \rho^*(0|\ell)\widehat{\mathcal{M}}_1\right] \Pi(\ell, t), \tag{5.91}$$

which can be written as

$$\frac{\mathrm{d}}{\mathrm{d}t}\Pi(\ell,t) = \mathcal{M}_{\mathrm{avg}}\Pi(\ell) + \frac{1}{\lambda}\left[\widehat{\mathcal{M}}_0\rho^*(0|\ell)^{-1} - \widehat{\mathcal{M}}_1\rho^*(1|\ell)^{-1}\right]\frac{1}{k_0(\ell)+k_1(\ell)} \times \left[\rho^*(1|\ell)\widehat{\mathcal{M}}_0 - \rho^*(0|\ell)\widehat{\mathcal{M}}_1\right]\Pi(\ell,t). \tag{5.92}$$

While this object is quite lengthy, it formally describes the reduced dynamics to subleading order in $1/\lambda$, and can be used for further analysis. The next steps would then depend on the nature of the specific example at hand.

5.12 Appendix B: Further remarks relating to power spectra in Sec. 5.6.2

5.12.1 Cross spectra in adiabatic limit

We find in simulations of the model in Sec. 5.5.1 that the cross spectrum $S_{AB}(\omega)$ vanishes in the adiabatic limit (see Fig. 5.5). This can be understood by inspecting the master equation in the adiabatic limit [obtained from Eq. (5.21) by sending $\lambda \to \infty$],

$$\frac{\mathrm{d}}{\mathrm{d}t}\Pi = \gamma(\mathcal{E}_A - 1)n_A\Pi + \delta(\mathcal{E}_B - 1)n_B\Pi + \Omega\alpha_{\mathrm{avg}}(\mathcal{E}_A^{-1} - 1)\Pi + \Omega\beta_{\mathrm{avg}}(\mathcal{E}_B^{-1} - 1)\Pi. \tag{5.93}$$

No reaction in this equation involves both types of particles; hence there are no correlations between n_A and n_B, leading to $S_{AB}(\omega) = 0$.

5.12.2 Indepence of $S_{AA}(\omega)$ from $\Delta\beta$

We focus on the power spectral density $S_{AA}(\omega)$ of the dynamics defined by Eq. (5.21). Since $S_{AA}(\omega)$ is a feature only of the dynamics of species A, we can integrate out the variable n_B in Eq. (5.21). We obtain the following equation for the marginal distribution $\Pi_A(n_A)$:

$$\frac{\mathrm{d}}{\mathrm{d}t}\Pi_A(n_A) = \gamma(\mathcal{E}_a - 1)n_A\Pi_A(n_A) + \Omega\left[\alpha_{\mathrm{avg}} - \frac{\Omega\theta^2}{\lambda}(\Delta\alpha)^2\right](\mathcal{E}_a^{-1} - 1)\Pi_A(n_A) + \frac{\Omega^2\theta^2}{2\lambda}(\Delta\alpha)^2(\mathcal{E}_a^{-2} - 1)\Pi_A(n_A). \tag{5.94}$$

In particular, all terms proportional to $\Delta\alpha\Delta\beta$ have cancelled out, so that Eq. (5.94) should apply to both cases, $\Delta\alpha\Delta\beta > 0$ and $\Delta\alpha\Delta\beta < 0$. Thus, one would expect the power spectral density $S_{AA}(\omega)$ to be independent of the choice of $\Delta\beta$ (all other parameters kept fixed). This in turn indicates that the spectra $S_{AA}(\omega)$ in panels (a) and (c) of Fig. 5.5 should come out as identical, if the modified Gillespie algorithm is a valid method of generating sample paths of the reduced master equation (5.21). At sufficiently low frequencies one would also expect these spectra to agree with those obtained from simulating the full model. The observations in Fig. 5.5 indicate that (i) the spectra $S_{AA}(\omega)$ for the reduced model for $\Delta\alpha\Delta\beta > 0$ and $\Delta\alpha\Delta\beta < 0$ are markedly different from each other [compare panels (a) and (c)]; (ii) for $\Delta\alpha\Delta\beta > 0$, the spectrum $S_{AA}(\omega)$ from the reduced model agrees to a good approximation with that from the full model in the low-frequency range [panel (a)]. For $\Delta\alpha\Delta\beta < 0$, these findings suggest a problem in approximating sample paths of the full model from the reduced master equation, using the renormalisation technique.

5.13 Appendix C: Kramers–Moyal expansion

5.13.1 Kramers–Moyal expansion of reduced master equation

In this Appendix we carry out a direct Kramers–Moyal expansion of the reduced master equation (5.19). This master equation can be written as

$$\frac{\mathrm{d}}{\mathrm{d}t}\Pi(n,t) = \Omega\beta(\mathcal{E}^{-1}-1)\Pi(n) + (\mathcal{E}-1)\delta_{\mathrm{eff}}n\Pi(n,t) + \frac{1}{2}\frac{\theta^2}{\lambda}\Delta^2\left[\mathcal{E}^2-1\right]n(n-1)\Pi(n,t), \tag{5.95}$$

where $\Delta = \delta_0 - \delta_1$, and

$$\delta_{\mathrm{eff}} = \delta_{\mathrm{avg}} - \frac{1}{2}\frac{\theta^2}{\lambda}\Delta^2(2n-1). \tag{5.96}$$

To carry out the expansion we write $\mathcal{E}^2 = 1 + \frac{2}{\Omega}\partial_x + \frac{2}{\Omega^2}\partial_x^2 + \ldots$, and obtain (writing $x = n/\Omega$)

$$\begin{aligned}\frac{\partial}{\partial t}\Pi(x) = \beta\left(-\partial_x + \frac{1}{2\Omega}\partial_x^2\right)\Pi(x) + \left(\partial_x + \frac{1}{2\Omega}\partial_x^2\right)\delta_{\mathrm{eff}}x\Pi(x) \\ + \frac{1}{2}\frac{\theta^2}{\lambda}\Omega\Delta^2\left(2\partial_x + \frac{2}{\Omega}\partial_x^2\right)x\left(x - \frac{1}{\Omega}\right)\Pi(x),\end{aligned} \tag{5.97}$$

where neglected terms are of order $1/\Omega^2$ or of order $\frac{\theta^2}{\lambda}/\Omega \propto 1/(\lambda\Omega)$. There will be further terms in Eq (5.97) which can be neglected at the order we are working at. Next we collect terms

$$\frac{\partial}{\partial t}\Pi(x) = -\partial_x\left\{\left[\beta - \delta_{\rm eff}x - \frac{\theta^2}{\lambda}\Omega\Delta^2 x\left(x-\frac{1}{\Omega}\right)\right]\Pi(x)\right\} + \frac{1}{2\Omega}\partial_x^2\left\{\left[\beta + \delta_{\rm eff}x + 2\frac{\theta^2}{\lambda}\Omega\Delta^2x^2\right]\Pi(x)\right\}, \tag{5.98}$$

where another term of order $1/(\lambda\Omega)$ has been dropped. Now we use $\delta_{\rm eff} = \delta_{\rm avg} - \frac{1}{2}\frac{\theta^2}{\lambda}\Omega\Delta^2\left(2x - \frac{1}{\Omega}\right)$, and find

$$\frac{\partial}{\partial t}\Pi(x) = -\partial_x\left\{\left[\beta - \delta_{\rm avg}x + \frac{1}{2}\frac{\theta^2}{\lambda}\Omega\Delta^2 x\left(2x-\frac{1}{\Omega}\right) - \frac{\theta^2}{\lambda}\Omega\Delta^2 x\left(x-\frac{1}{\Omega}\right)\right]\Pi(x)\right\} + \frac{1}{2\Omega}\partial_x^2\left\{\left[\beta + \delta_{\rm avg}x - \frac{\theta^2}{\lambda}\Omega\Delta^2x^2 + 2\frac{\theta^2}{\lambda}\Omega\Delta^2x^2\right]\Pi(x)\right\}, \tag{5.99}$$

where yet another term of order $1/(\lambda\Omega)$ has been dropped. This is the same as

$$\frac{\partial}{\partial t}\Pi(x) = -\partial_x\left\{\left[\beta - \delta_{\rm avg}x + \frac{1}{2}\frac{\theta^2}{\lambda}\Delta^2 x\right]\Pi(x)\right\} + \frac{1}{2}\partial_x^2\left\{\left[\frac{1}{\Omega}(\beta+\delta_{\rm avg}x) + \frac{\theta^2}{\lambda}\Delta^2x^2\right]\Pi(x)\right\}, \tag{5.100}$$

i.e., we recover Eq. (5.42).

5.13.2 Reduced Liouville equation

Using $\mathcal{L}_\sigma\Pi(x) = -\partial_x(\beta - \delta_\sigma x)\Pi(x)$ in Eq. (5.37) gives

$$\frac{\partial}{\partial t}\Pi = -\partial_x(\beta - \delta_{\rm avg}x)\Pi(x) + \frac{1}{2}\frac{\theta^2}{\lambda}\Delta^2\partial_x x\partial_x\Pi(x). \tag{5.101}$$

Next we use $\partial_x\left(x\partial_x x\Pi(x)\right) = \partial_x^2\left(x^2\Pi\right) - \partial_x\left(x\Pi\right)$ to write this as

$$\frac{\partial}{\partial t}\Pi = -\partial_x\left(\beta - \delta_{\rm avg}x + \frac{1}{2}\frac{\theta^2}{\lambda}\Delta^2 x\right)\Pi(x) + \frac{1}{2}\frac{\theta^2}{\lambda}\Delta^2\partial_x^2[x^2\Pi(x)]. \tag{5.102}$$

This is Eq. (5.47).

5.13.3 Kramers–Moyal expansion for two-species model

Carrying out the Kramers–Moyal expansion on Eq. (5.21) we find

$$\begin{aligned}\frac{\partial}{\partial t}\Pi(x) = &\gamma\left(\partial_x + \frac{1}{2\Omega}\partial_x^2\right) x\Pi + \delta\left(\partial_y + \frac{1}{2\Omega}\partial_y^2\right) y\Pi \\ &+ \alpha_{\text{eff}}\left(-\partial_x + \frac{1}{2\Omega}\partial_x^2\right)\Pi + \beta_{\text{eff}}\left(-\partial_y + \frac{1}{2\Omega}\partial_y^2\right)\Pi \\ &+ \frac{\Omega\theta^2}{2\lambda}(\Delta\alpha)^2\left(-2\partial_x + \frac{2}{\Omega}\partial_x^2\right)\Pi(t) + \frac{\Omega\frac{\theta^2}{\lambda}}{2}(\Delta\beta)^2\left(-2\partial_y + \frac{2}{\Omega}\partial_y^2\right)\Pi \\ &+ \frac{\Omega\theta^2}{\lambda}\Delta\alpha\Delta\beta\left(-\partial_x - \partial_y + \frac{1}{2\Omega}\partial_x^2 + \frac{1}{2\Omega}\partial_y^2 + \frac{1}{\Omega}\partial_x\partial_y\right)\Pi. \end{aligned} \tag{5.103}$$

Using Eq. (5.22), this simplifies to

$$\begin{aligned}\frac{\partial}{\partial t}\Pi(x) = &-\partial_x\left(\alpha_{\text{avg}} - \gamma x\right)\Pi - \partial_y\left(\beta_{\text{avg}} - \delta y\right)\Pi \\ &+ \frac{1}{2}\partial_x^2\left(\frac{\alpha_{\text{avg}} + \gamma x}{\Omega} + \frac{\theta^2}{\lambda}\Delta\alpha^2\right)\Pi + \frac{1}{2}\partial_y^2\left(\frac{\beta_{\text{avg}} + \delta y}{\Omega} + \frac{\theta^2}{\lambda}\Delta\beta^2\right)\Pi \\ &+ \partial_x\partial_y\left(\frac{\theta^2}{\lambda}\Delta\alpha\Delta\beta\right)\Pi, \end{aligned} \tag{5.104}$$

which describes the dynamics of the stochastic differential equations in Eqs. (5.54,5.55).

5.14 Appendix D: Applications—Further details

5.14.1 Reduced master equation for bi-stable genetic circuit

In this Appendix we report the reduced master equation for the model described in Sec. 5.9.2. The reduced master equation is obtained starting from Eq. (5.8), where the $w_\sigma(\ell)$ are determined from (5.9). We do not report the full calculation; it is laborious,

but ultimately straightforward. The final result for the reduced master equation reads:

$$\begin{aligned}
&\frac{\mathrm{d}}{\mathrm{d}t}\Pi(N_p,N_m,t)\\
=\;&(\mathcal{E}_m^{-1}-1)\left\{\Omega\beta_{\rm avg}(N_p)-\frac{1}{\lambda}\Omega^2(\beta_2-\beta_0)^2\frac{1}{k_-}\frac{2\psi^2}{(1+\psi+\psi^2)^3}[\psi^2+3\psi+1]\right\}\Pi\\
&+(\mathcal{E}_m-1)[\delta_m N_m\Pi]\\
&+(\mathcal{E}_p^{-1}-1)[\alpha N_m+\varpi_1]\Pi\\
&+(\mathcal{E}_p-1)[\delta_p N_p+\varpi_2]\Pi\\
&+(\mathcal{E}_m^{-2}-1)\left[\frac{1}{\lambda}\Omega^2(\beta_2-\beta_0)^2\frac{1}{k_-}\frac{\psi^2}{(1+\psi+\psi^2)^3}\left[\psi^2+3\psi+1\right]\Pi\right]\\
&+(\mathcal{E}_m^{-1}\mathcal{E}_p^{-1}-1)(-\varpi_1\Pi)\\
&+(\mathcal{E}_m^{-1}\mathcal{E}_p-1)(-\varpi_2\Pi),
\end{aligned}\tag{5.105}$$

where we have introduced the following short-hand ($\sigma=0,1,2$),

$$\begin{aligned}
\psi(N_p)&=\frac{k_+N_p}{\Omega k_-},\\
\rho^*_\sigma(N_p)&=\frac{\psi(N_p)^{\sigma-1}}{1+\psi(N_p)+\psi(N_p)^2},\\
\Delta_\sigma(N_p)&=\rho^*_\sigma(N_p+1)-\rho^*_\sigma(N_p),\\
\beta_{\rm avg}(N_p)&=\sum_\sigma\rho^*_\sigma(N_p)\beta_\sigma,\\
\varpi_1&=\frac{1}{\lambda}\Omega(\beta_2-\beta_0)\frac{1}{k_-}\left\{[\rho^*_0(N_p+1)+\rho^*_1(N_p+1)]\Delta_2-\rho^*_1(N_p+1)\Delta_0\right\}\alpha N_m.\\
\varpi_2&=\frac{1}{\lambda}\Omega(\beta_2-\beta_0)\frac{1}{k_-}\{\rho^*_1(N_p-1)\Delta_0(N_p-1)\\
&\quad-[\rho^*_0(N_p-1)+\rho^*_1(N_p-1)]\Delta_2(N_p-1)\}\delta_pN_p.
\end{aligned}\tag{5.106}$$

We note that $\varpi_1>0$, irrespective of the choice of λ, so that the rate of the penultimate reaction in Eq. (5.105) is negative. The rates of all other reactions are non-negative, provided λ is large enough (all other parameters fixed).

5.14.2 Gene circuit with exclusive binding

In this Appendix we report the reduced master equation for the gene circuit with exclusive binding, discussed in Sec. 5.9.4. Labelling the states G^A and G^B not occupied, only G^A occupied, and only G^B occupied as $\sigma=0,1$, and 2, respectively, we have the transition matrix elements

$$A_{0\to1}=n_A\mu_1/\Omega,\quad A_{0\to2}=n_B\kappa_1/\Omega,\quad A_{1\to0}=\kappa_0,\quad A_{2\to0}=\mu_0,\tag{5.107}$$

where all other off-diagonal entries are zero, and the diagonal elements follow from the convention $\sum_{\sigma'} A_{\sigma\to\sigma'} = 0$. For the purposes of the numerical analysis we make the simplification $\alpha_0 = \beta_0, \alpha_1 = \beta_1$, and $\kappa_0 = \mu_0, \kappa_1 = \mu_1$, as well as $\gamma = \delta$. The reduced master equation in the limit of large but finite λ is then obtained as

$$\begin{aligned}
\frac{\mathrm{d}}{\mathrm{d}t}P_{n_A,n_B}(t) = \quad & \left(\mathcal{E}_A^{-1}-1\right)\left\{\Omega\frac{n_B\alpha_1\tilde{\kappa}_1+\alpha_0(\kappa_0+n_A\tilde{\kappa}_1)}{\kappa_0+(n_A+n_B)\tilde{\kappa}_1}-\frac{\Omega^2}{\lambda}\frac{2n_B\kappa_0\tilde{\kappa}_1(\alpha_0-\alpha_1)^2}{\left[\kappa_0+(n_A+n_B)\tilde{\kappa}_1\right]^3}\right\}P_{n_A,n_B}(t)\\
& + \left(\mathcal{E}_B^{-1}-1\right)\left\{\Omega\frac{n_A\alpha_1\tilde{\kappa}_1+\alpha_0(\kappa_0+n_B\tilde{\kappa}_1)}{\kappa_0+(n_A+n_B)\tilde{\kappa}_1}-\frac{\Omega^2}{\lambda}\frac{2n_A\kappa_0\tilde{\kappa}_1(\alpha_0-\alpha_1)^2}{\left[\kappa_0+(n_A+n_B)\tilde{\kappa}_1\right]^3}\right\}P_{n_A,n_B}(t)\\
& + \left(\mathcal{E}_A^{-2}-1\right)\frac{\Omega^2}{\lambda}\frac{n_B\tilde{\kappa}_1\left[\kappa_0^2+2n_A\kappa_0\tilde{\kappa}_1+n_A(n_A+n_B)\tilde{\kappa}_1^2\right](\alpha_0-\alpha_1)^2}{\kappa_0\left[\kappa_0+(n_A+n_B)\tilde{\kappa}_1\right]^3}P_{n_A,n_B}(t)\\
& - \left(\mathcal{E}_A^{-1}\mathcal{E}_B^{-1}-1\right)\frac{\Omega^2}{\lambda}\frac{2n_An_B\tilde{\kappa}_1^2\left[2\kappa_0+(n_A+n_B)\tilde{\kappa}_1\right](\alpha_0-\alpha_1)^2}{\kappa_0\left[\kappa_0+(n_A+n_B)\tilde{\kappa}_1\right]^3}P_{n_A,n_B}(t)\\
& + \left(\mathcal{E}_B^{-2}-1\right)\frac{\Omega^2}{\lambda}\frac{n_A\tilde{\kappa}_1\left[\kappa_0^2+2n_B\kappa_0\tilde{\kappa}_1+n_B(n_A+n_B)\tilde{\kappa}_1^2\right](\alpha_0-\alpha_1)^2}{\kappa_0\left[\kappa_0+(n_A+n_B)\tilde{\kappa}_1\right]^3}P_{n_A,n_B}(t)\\
& + \gamma(\mathcal{E}_A^{+1}-1)n_AP_{n_A,n_B}(t)+\gamma(\mathcal{E}_B^{+1}-1)n_BP_{n_A,n_B}(t),
\end{aligned} \tag{5.108}$$

where $\tilde{\kappa}_1$ has been introduced as shorthand for κ_1/Ω. We have discarded terms of order Ω/λ.

5.15 Bibliography

[1] P. G. Hufton, Y. T. Lin, and T. Galla. Model reduction methods for classical stochastic systems with fast-switching environments: reduced master equations, stochastic differential equations, and applications. *arXiv preprint arXiv:1803.02941* (2018).

[2] E. Kussell, R. Kishony, N. Q. Balaban, and S. Leibler. Bacterial persistence. *Genetics* **169**, 1807 (2005).

[3] E. Kussell and S. Leibler. Phenotypic diversity, population growth, and information in fluctuating environments. *Science* **309**, 2075 (2005).

[4] S. Leibler and E. Kussell. Individual histories and selection in heterogeneous populations. *Proc. Natl. Acad. Sci. U.S.A.* **107**, 13183 (2010).

[5] P. Thomas, N. Popović, and R. Grima. Phenotypic switching in gene regulatory networks. *Proc. Natl. Acad. Sci. U.S.A.* **111**, 6994 (2014).

[6] T. B. Kepler and T. C. Elston. Stochasticity in transcriptional regulation: origins, consequences, and mathematical representations. *Biophys. J.* **81**, 3116 (2001).

[7] M. Thattai and A. Van Oudenaarden. Stochastic gene expression in fluctuating environments. *Genetics* **167**, 523 (2004).

[8] P. S. Swain, M. B. Elowitz, and E. D. Siggia. Intrinsic and extrinsic contributions to stochasticity in gene expression. *Proc. Natl. Acad. Sci. U.S.A.* **99**, 12795 (2002).

[9] M. Assaf, E. Roberts, Z. Luthey-Schulten, and N. Goldenfeld. Extrinsic Noise Driven Phenotype Switching in a Self-Regulating Gene. *Phys. Rev. Lett.* **111**, 058102 (2013).

[10] A. Duncan, S. Liao, T. Vejchodskỳ, R. Erban, and R. Grima. Noise-induced multistability in chemical systems: Discrete versus continuum modeling. *Phys. Rev. E* **91**, 042111 (2015).

[11] M. Assaf, M. Mobilia, and E. Roberts. Cooperation Dilemma in Finite Populations under Fluctuating Environments. *Phys. Rev. Lett.* **111**, 238101 (2013).

[12] P. Ashcroft, P. M. Altrock, and T. Galla. Fixation in finite populations evolving in fluctuating environments. *J. R. Soc. Interface* **11**, 20140663 (2014).

[13] K. Wienand, E. Frey, and M. Mobilia. Evolution of a Fluctuating Population in a Randomly Switching Environment. *Phys. Rev. Lett.* **119**, 158301 (2017).

[14] R. West, M. Mobilia, and A. M. Rucklidge. Survival behavior in the cyclic Lotka-Volterra model with a randomly switching reaction rate. *Phys. Rev. E* **97**, 022406 (2018).

[15] A. J. Black and A. J. McKane. Stochastic amplification in an epidemic model with seasonal forcing. *J. Theor. Biol.* **267**, 85 (2010).

[16] C. Escudero and J. Á. Rodríguez. Persistence of instanton connections in chemical reactions with time-dependent rates. *Phys. Rev. E* **77**, 011130 (2008).

[17] M. Assaf, A. Kamenev, and B. Meerson. Population extinction in a time-modulated environment. *Phys. Rev. E* **78**, 041123 (2008).

[18] Q. Luo and X. Mao. Stochastic population dynamics under regime switching. *J. Math. Anal. Appl.* **334**, 69 (2007).

[19] C. Zhu and G. Yin. On competitive Lotka–Volterra model in random environments. *J. Math. Anal. Appl.* **357**, 154 (2009).

[20] J. Chiquet and N. Limnios. A method to compute the transition function of a piecewise deterministic Markov process with application to reliability. *Stat. Probab. Lett.* **78**, 1397 (2008).

[21] J. Chiquet, M. Eid, and N. Limnios. Modelling and estimating the reliability of stochastic dynamical systems with Markovian switching. *Rel. Eng. & Syst. Safety* **93**, 1801 (2008).

[22] J. Chiquet, N. Limnios, and M. Eid. Piecewise deterministic Markov processes applied to fatigue crack growth modelling. *J. Stat. Plan. Inf.* **139**, 1657 (2009).

[23] A. Lorton, M. Fouladirad, and A. Grall. A methodology for probabilistic model-based prognosis. *Eur. J. Oper. Res.* **225**, 443 (2013).

[24] H. Zhang, F. Dufour, Y. Dutuit, and K. Gonzalez. Piecewise deterministic Markov processes and dynamic reliability. *Proc. Inst. Mech. Eng., Part O: J. Risk and Reliab.* **222**, 545 (2008).

[25] A. Lorton, M. Fouladirad, and A. Grall. Computation of remaining useful life on a physic-based model and impact of a prognosis on the maintenance process. *Proc. Inst. Mech. Eng., Part O: J. Risk and Reliab* **227**, 434 (2013).

[26] H.-P. Breuer and F. Petruccione. *The theory of open quantum systems.* Oxford University Press, Great Clarendon Street, Oxford (2002).

[27] H.-P. Breuer, E.-M. Laine, J. Piilo, and B. Vacchini. Colloquium: Non-Markovian dynamics in open quantum systems. *Rev. Mod. Phys.* **88**, 021002 (2016).

[28] I. de Vega and D. Alonso. Dynamics of non-Markovian open quantum systems. *Rev. Mod. Phys.* **89**, 015001 (2017).

[29] P. C. Bressloff. Stochastic Fokker-Planck equation in random environments. *Phys. Rev. E.* **94**, 1 (2016).

[30] M. Assaf, E. Roberts, and Z. Luthey-Schulten. Determining the Stability of Genetic Switches: Explicitly Accounting for mRNA Noise. *Phys. Rev. Lett.* **106**, 248102 (2011).

[31] E. Roberts, S. Be'er, C. Bohrer, R. Sharma, and M. Assaf. Dynamics of simple gene-network motifs subject to extrinsic fluctuations. *Phys. Rev. E* **92**, 062717 (2015).

[32] P. C. Bressloff and J. M. Newby. Path integrals and large deviations in stochastic hybrid systems. *Phys. Rev. E* **89** (2014).

[33] P. C. Bressloff. Stochastic Liouville equation for particles driven by dichotomous environmental noise. *Phy. Rev. E* **95**, 012124 (2017).

[34] P. C. Bressloff. Feynman-Kac formula for stochastic hybrid systems. *Phys. Rev. E* **95**, 012138 (2017).

[35] P. C. Bressloff. Stochastically gated local and occupation times of a Brownian particle. *Phys. Rev. E* **95**, 012130 (2017).

[36] J. Bowen, A. Acrivos, and A. Oppenheim. Singular perturbation refinement to quasi-steady state approximation in chemical kinetics. *Chem. Eng. Sci.* **18**, 177 (1963).

[37] L. A. Segel and M. Slemrod. The quasi-steady-state assumption: a case study in perturbation. *SIAM Rev.* **31**, 446 (1989).

[38] H.-P. Breuer and J. Piilo. Stochastic jump processes for non-Markovian quantum dynamics. *EPL* **85**, 50004 (2009).

[39] J. Piilo, S. Maniscalco, K. Härkönen, and K.-A. Suominen. Non-Markovian Quantum Jumps. *Phys. Rev. Lett.* **100**, 180402 (2008).

[40] W. Ewens. *Mathematical Population Genetics 1.* Springer-Verlag, New York NY (2004).

[41] A. Traulsen and C. Hauert. *Stochastic Evolutionary Game Dynamics*, pages 25–61. Wiley-VCH, Weinheim (2010).

[42] J. M. Sancho and M. San Miguel. Theory of external two-state Markov noise in the presence of internal fluctuations. *J. Stat. Phys.* **37**, 151 (1984).

[43] E. Hernández-García, L. Pesquera, M. A. Rodríguez, and M. San Miguel. Random walk in dynamically disordered chains: Poisson white noise disorder. *J. Stat. Phys.* **55**, 1027 (1989).

[44] S. Zeiser, U. Franz, and V. Liebscher. Autocatalytic genetic networks modeled by piecewise-deterministic Markov processes. *J. Math. Biol.* **60**, 207 (2010).

[45] R. Grima, D. R. Schmidt, and T. J. Newman. Steady-state fluctuations of a genetic feedback loop: An exact solution. *J. Chem. Phys.* **137**, 035104 (2012).

[46] Y. T. Lin, P. G. Hufton, E. J. Lee, and D. A. Potoyan. A stochastic and dynamical view of pluripotency in mouse embryonic stem cells. *PLOS Comp. Biol.* **14**, 1 (2018).

[47] N. Friedman, L. Cai, and X. S. Xie. Linking Stochastic Dynamics to Population Distribution: An Analytical Framework of Gene Expression. *Phys. Rev. Lett.* **97**, 168302 (2006).

[48] V. Shahrezaei and P. S. Swain. Analytical distributions for stochastic gene expression. *Proc. Natl. Acad. Sci. U.S.A.* **105**, 17256 (2008).

[49] Y. T. Lin and C. R. Doering. Gene expression dynamics with stochastic bursts: Construction and exact results for a coarse-grained model. *Phys. Rev. E* **93**, 022409 (2016).

[50] Y. T. Lin and T. Galla. Bursting noise in gene expression dynamics: linking microscopic and mesoscopic models. *J. R. Soc. Interface.* **13**, 20150772 (2016).

[51] D. T. Gillespie. A general method for numerically simulating the stochastic time evolution of coupled chemical reactions. *J. Comp. Phys.* **22**, 403 (1976).

[52] D. T. Gillespie. Exact stochastic simulation of coupled chemical reactions. *J. Chem. Phys.* **81**, 2340 (1977).

[53] A. Suárez, R. Silbey, and I. Oppenheim. Memory effects in the relaxation of quantum open systems. *J. Chem. Phys.* **97**, 5101 (1992).

[54] P. Pechukas. Reduced Dynamics Need Not Be Completely Positive. *Phys. Rev. Lett.* **73**, 1060 (1994).

[55] S. Gnutzmann and F. Haake. Positivity violation and initial slips in open systems. *Z. Phys. B* **101**, 263 (1996).

[56] F. Benatti, R. Floreanini, and M. Piani. Nonpositive evolutions in open system dynamics. *Phys. Rev. A* **67**, 042110 (2003).

[57] H. Risken and H. Vollmer. On the application of truncated generalized Fokker-Planck equations. *Z. Phys. B* **35**, 313 (1979).

[58] G. Guarnieri, A. Smirne, and B. Vacchini. Quantum regression theorem and non-Markovianity of quantum dynamics. *Phys. Rev. A* **90**, 022110 (2014).

[59] D. T. Gillespie. Approximate accelerated stochastic simulation of chemically reacting systems. *J. Chem. Phys.* **115**, 1716 (2001).

[60] C. W. Gardiner. *Handbook of Stochastic Methods*. Springer-Verlag, Berlin (2004).

[61] N. G. van Kampen. *Stochastic Processes in Physics and Chemistry.* North-Holland, Amsterdam (2007).

[62] X. Mao and C. Yuan. *Stochastic differential equations with Markovian switching.* World Scientific, Singapore (2006).

[63] D. A. Potoyan and P. G. Wolynes. Dichotomous noise models of gene switches. *J. Chem. Phys.* **143**, 195101 (2015).

[64] P. G. Hufton, Y. T. Lin, T. Galla, and A. J. McKane. Intrinsic noise in systems with switching environments. *Phys. Rev. E* **93**, 052119 (2016).

[65] A. Kamenev, B. Meerson, and B. Shklovskii. How Colored Environmental Noise Affects Population Extinction. *Phys. Rev. Lett.* **101**, 268103 (2008).

[66] M. H. Davis. Piecewise-deterministic Markov processes: A general class of non-diffusion stochastic models. *J. Roy. Statist. Soc. Ser. B* **46**, 353 (1984).

[67] S. Zeiser, U. Franz, O. Wittich, and V. Liebscher. Simulation of genetic networks modelled by piecewise deterministic Markov processes. *IET Sys. Biol.* **2**, 113 (2008).

[68] H. Ge, H. Qian, and X. S. Xie. Stochastic phenotype transition of a single cell in an intermediate region of gene state switching. *Phys. Rev. Lett.* **114**, 078101 (2015).

[69] C. Jia. Simplification of Markov chains with infinite state space and the mathematical theory of random gene expression bursts. *Phys. Rev. E* **96**, 032402 (2017).

[70] C. Jia, M. Q. Zhang, and H. Qian. Emergent Lévy behavior in single-cell stochastic gene expression. *Phys. Rev. E* **96**, 040402 (2017).

[71] U. Herbach, A. Bonnaffoux, T. Espinasse, and O. Gandrillon. Inferring gene regulatory networks from single-cell data: a mechanistic approach. *BMC Syst. Biol.* **11**, 105 (2017).

[72] Y. T. Lin and N. E. Buchler. Efficient analysis of stochastic gene dynamics in the non-adiabatic regime using piecewise deterministic Markov processes. *J. Roy. Soc. Interface* **15** (2018).

[73] J. M. Newby and P. C. Bressloff. Quasi-steady State Reduction of Molecular Motor-Based Models of Directed Intermittent Search. *Bull. Math. Biol.* **72**, 1840 (2010).

[74] E. L. Haseltine and J. B. Rawlings. Approximate simulation of coupled fast and slow reactions for stochastic chemical kinetics. *J. Chem. Phys.* **117**, 6959 (2002).

[75] C. V. Rao and A. P. Arkin. Stochastic chemical kinetics and the quasi-steady-state assumption: application to the Gillespie algorithm. *J. Chem. Phys.* **118**, 4999 (2003).

[76] J. Goutsias. Quasiequilibrium approximation of fast reaction kinetics in stochastic biochemical systems. *J. Chem. Phys.* **122**, 184102 (2005).

[77] H. Qian, P.-Z. Shi, and J. Xing. Stochastic bifurcation, slow fluctuations, and bistability as an origin of biochemical complexity. *Phys. Chem. Chem. Phys.* **11**, 4861 (2009).

[78] C. D. Pahlajani, P. J. Atzberger, and M. Khammash. Stochastic reduction method for biological chemical kinetics using time-scale separation. *J. Theor. Biol.* **272**, 96 (2011).

[79] J. Kim, K. Josic, and M. R. Bennett. The Validity of Quasi-Steady-State Approximations in Discrete Stochastic Simulations. *Biophys. J.* **107**, 783 (2014).

[80] H. Risken. *The Fokker–Planck Equation: Methods of Solution and Applications.* Springer-Verlag, Berlin (1989).

[81] P. Thomas, A. V. Straube, and R. Grima. The slow-scale linear noise approximation: an accurate, reduced stochastic description of biochemical networks under timescale separation conditions. *BMC Syst. Biol.* **6**, 39 (2012).

[82] P. Thomas, R. Grima, and A. V. Straube. Rigorous elimination of fast stochastic variables from the linear noise approximation using projection operators. *Phys. Rev. E* **86**, 041110 (2012).

[83] P. G. Hufton, Y. T. Lin, and T. Galla. Phenotypic switching of populations of cells in a stochastic environment. *J. Stat. Mech.* **2018**, 023501 (2018).

[84] L. Cai, N. Friedman, and X. S. Xie. Stochastic protein expression in individual cells at the single molecule level. *Nature* **440**, 358 EP (2006).

[85] J. M. G. Vilar, H. Y. Kueh, N. Barkai, and S. Leibler. Mechanisms of noise-resistance in genetic oscillators. *Proc. Natl. Acad. Sci. U.S.A.* **99**, 5988 (2002).

[86] L. S. Weinberger, J. C. Burnett, J. E. Toettcher, A. P. Arkin, and D. V. Schaffer. *Cell* **122**, 169 (2005).

[87] M. Thattai and A. Van Oudenaarden. Intrinsic noise in gene regulatory networks. *Proc. Natl. Acad. Sci. U.S.A.* **98**, 8614 (2001).

[88] T. Lipniacki, P. Paszek, A. Marciniak-Czochra, A. R. Brasier, and M. Kimmel. Transcriptional stochasticity in gene expression. *J. Theor. Biol.* **238**, 348 (2006).

[89] A. Bobrowski, T. Lipniacki, K. Pichór, and R. Rudnicki. Asymptotic behavior of distributions of mRNA and protein levels in a model of stochastic gene expression. *J. Math. Anal. Appl.* **333**, 753 (2007).

[90] M. S. Sherman and B. A. Cohen. A computational framework for analyzing stochasticity in gene expression. *PLoS Comput. Biol.* **10**, e1003596 (2014).

[91] J. Lin. Divergence Measures Based on the Shannon Entropy. *IEEE Trans. Inf. Theor.* **37**, 145 (2006).

[92] S. Masui, Y. Nakatake, Y. Toyooka, D. Shimosato, R. Yagi, K. Takahashi, H. Okochi, A. Okuda, R. Matoba, A. A. Sharov, M. S. H. Ko, and H. Niwa. Pluripotency governed by Sox2 via regulation of Oct3/4 expression in mouse embryonic stem cells. *Nat. Cell Biol.* **9**, 625 EP (2007).

[93] T. Kalmar, C. Lim, P. Hayward, S. Muoz-Descalzo, J. Nichols, J. Garcia-Ojalvo, and A. Martinez Arias. Regulated Fluctuations in Nanog Expression Mediate Cell Fate Decisions in Embryonic Stem Cells. *PLOS Biol.* **7**, 1 (2009).

[94] N. E. Buchler, U. Gerland, and T. Hwa. On schemes of combinatorial transcription logic. *Proc. Natl. Acad. Sci. U.S.A.* **100**, 5136 (2003).

[95] B. Munsky, Z. Fox, and G. Neuert. Integrating single-molecule experiments and discrete stochastic models to understand heterogeneous gene transcription dynamics. *Methods* **85**, 12 (2015).

[96] M. Gómez-Schiavon, L.-F. Chen, A. E. West, and N. E. Buchler. BayFish: Bayesian inference of transcription dynamics from population snapshots of single-molecule RNA FISH in single cells. *Genome Biol.* **18**, 164 (2017).

[97] T. S. Gardner, C. R. Cantor, and J. J. Collins. Construction of a genetic toggle switch in Escherichia coli. *Nature* **403**, 339 (2000).

[98] D. M. Roma, R. A. O'Flanagan, A. E. Ruckenstein, A. M. Sengupta, and R. Mukhopadhyay. Optimal path to epigenetic switching. *Phys. Rev. E* **71**, 011902 (2005).

[99] E. Roberts, A. Magis, J. O. Ortiz, W. Baumeister, and Z. Luthey-Schulten. Noise contributions in an inducible genetic switch: a whole-cell simulation study. *PLoS Comput. Biol.* **7**, e1002010 (2011).

[100] J. N. Weiss. The Hill equation revisited: uses and misuses. *FASEB J.* **11**, 835 (1997).

[101] S. Karapetyan and N. E. Buchler. Role of DNA binding sites and slow unbinding kinetics in titration-based oscillators. *Phys. Rev. E* **92**, 062712 (2015).

[102] A. Lipshtat, A. Loinger, N. Q. Balaban, and O. Biham. Genetic toggle switch without cooperative binding. *Phys. Rev. Lett.* **96**, 188101 (2006).

[103] P. B. Warren and P. R. ten Wolde. Chemical models of genetic toggle switches. *J. Phys. Chem. B* **109**, 6812 (2005).

[104] M. Acar, J. T. Mettetal, and A. Van Oudenaarden. Stochastic switching as a survival strategy in fluctuating environments. *Nature Genet.* **40**, 471 (2008).

[105] O. Gefen and N. Q. Balaban. The importance of being persistent: heterogeneity of bacterial populations under antibiotic stress. *FEMS Microbiol. Rev.* **33**, 704 (2009).

[106] P. Patra and S. Klumpp. Emergence of phenotype switching through continuous and discontinuous evolutionary transitions. *Phys. Biol.* **12**, 046004 (2015).

[107] E. A. Korobkova, T. Emonet, H. Park, and P. Cluzel. Hidden stochastic nature of a single bacterial motor. *Phys. Rev. Lett.* **96**, 058105 (2006).

[108] A. J. Black, A. J. McKane, A. Nunes, and A. Parisi. Stochastic fluctuations in the susceptible-infective-recovered model with distributed infectious periods. *Phys. Rev. E* **80**, 021922 (2009).

[109] J. Chiquet and N. Limnios. Estimating stochastic dynamical systems driven by a continuous-time jump Markov process. *Method. Comput. Appl. Probab.* **8**, 431 (2006).

[110] Y. Lin and J. Yang. A stochastic theory of fatigue crack propagation. *AIAA journal* **23**, 117 (1985).

[111] B. Spencer Jr and J. Tang. Markov process model for fatigue crack growth. *J. Eng. Mech.* **114**, 2134 (1988).

[112] R. Capocelli and L. Ricciardi. A diffusion model for population growth in random environment. *Theor. Pop. Biol.* **5**, 28 (1974).

Chapter 6

Calculating normal tissue complication probabilities and probabilities of complication-free tumour control from stochastic models of population dynamics

6.1 Preface

The contents of this chapter constitute a submitted manuscript, which has been made public on arXiv [1]. The manuscript was authored by Peter G. Hufton[1], Elizabeth Buckingham-Jeffery[2], and Tobias Galla[1].

P.G.H.'s contribution includes developing the idea for the project, performing all calculations and analysis therein, coding and executing all simulations used for the figures (Fig. 6.5 was coded in partnership with E.B.-J.), and writing all sections of the paper in partnership with E.B.-J. and T.G.

[1]Theoretical Physics, School of Physics and Astronomy, The University of Manchester, Manchester M13 9PL, United Kingdom
[2]School of Mathematics, The University of Manchester, Manchester M13 9PL, United Kingdom

Abstract

We use a stochastic birth-death model for a population of cells to estimate the normal tissue complication probability (NTCP) under a particular radiotherapy protocol. We specifically allow for interaction between cells, via a nonlinear logistic growth model. To capture some of the effects of intrinsic noise in the population we develop several approximations of NTCP, using Kramers–Moyal expansion techniques. These approaches provide an approximation to the first and second moments of a general first-passage time problem in the limit of large, but finite populations. We use this method to study NTCP in a simple model of normal cells and in a model of normal and damaged cells. We also study a combined model of normal tissue cells and tumour cells. Based on existing methods to calculate tumour control probabilities, and our procedure to approximate NTCP, we estimate the probability of complication free tumour control.

6.2 Introduction

When giving a dose of radiation to a tumour it is likely that the surrounding healthy tissue will also be damaged. A radiotherapy treatment protocol aims to provide enough radiation to the tumour to control the cancer whilst not causing excessive side-effects by damaging surrounding tissue. To this end, a protocol must find a balance between maximising the tumour control probability (TCP) and minimising the normal tissue complication probability (NTCP). Normal tissue complications (NTCs) encompass a wide variety of problems ranging in severity from increased urinary frequency from the treatment of prostate cancers [2, 3] to severe neurological complications such as myelitis from the treatment of neck cancers [4] and organ failure [2].

There are numerous models of TCP and NTCP in the literature. Broadly, the term 'model' is used to describe two different types of mathematical approaches to characterising these probabilities. The first is statistical: based on cohorts of patients statistical models are developed to identify factors contributing to the TCP and the NTCP. This is then used to find mathematical expressions which allow one to estimate

the TCP or NTCP of a patient with given characteristics and for given radiation protocols [5, 6]. The focus of our work is not on this type of model. Instead, we concentrate on the second type of modelling approach, which seeks to compute TCP and NTCP 'bottom-up' from mechanistic principles of the population dynamics of tumour or normal cells [7,8]. These models are often stylised, but the key characteristic they all share is that they describe the dynamics of cell division and death. Many of these models are intrinsically stochastic. Mitosis and cell death are random events in such models, and the precise outcome is therefore uncertain; the tumour may or may not be controlled, and NTCs can arise, but do not have to. The aim of this line of research is to obtain, for a given model of the population dynamics of cells and a given radiation protocol, the TCP and NTCP. The word 'obtain' includes by computer simulation of the population, or by direct mathematical computation when this is possible. While simulations are sometimes viable, the mathematical route, when it is available, is generally preferable as explicit formulae provide an efficient way of evaluating TCP or NTCP, often much faster than simulation. Not all types of population dynamics can be treated mathematically exactly however. In such cases approximations have to be made in the mathematical calculation of TCP and NTCP.

TCP from a stochastic birth-death model has previously been described by Zaider and Minerbo [8]; subsequent work includes [9–11]. The generating function methods used, however, are limited to problems considering the extinction of all cells and where the dynamics are linear, and so are not directly applicable to NTCP. A stochastic birth-death model of normal tissue cells was described by Stocks *et al.* [12], but their mathematical calculation of NTCP ultimately does not take into account intrinsic stochasticity in the population. We extend this analysis and capture features of intrinsic noise in the calculation of NTCP. We use a stochastic birth-death model of normal tissue cells where cell death rates are affected by the dose and timing of radiotherapy. NTCP can be seen as the cumulative distribution function of the first-passage time of this stochastic birth-death process through a boundary; NTC sets in when the number of functional cells falls below a certain threshold. We obtain estimates of NTCP by approximating the distribution of first-passage times.

One may ask whether the inclusion of intrinsic noise is necessary in modelling NTCP. Hanin and Zaider [7] argue that deterministic approaches might be sufficient,

due to the high numbers of cells involved. However we note that the size of the population may vary depending on context. For example, the model could describe a functional subunit (FSU) of an organ, rather than the entire organ [6, 13, 14]. NTCP would then not necessarily indicate the probability that an organ fails, but instead that such a subunit no longer fulfils its function. For instance, Niemierko and Goitein consider a kidney split into 10^7 FSUs, where each FSU contains 10^4 cells [6]. In such circumstances noise in the population (i.e., within a FSU) may become relevant. Intrinsic stochasticity may also be important in the context of stem cells, especially if they are present in relatively small numbers [15–18]. It is also interesting to note that some of the statistical models mentioned above assume a normal distribution of NTC onset, see e.g., the model proposed by Lyman in Ref. [5]. The resulting NTCP then takes the form of an error function, i.e., the integral of a Gaussian distribution, similar to what we find from our approximations. It is important to note though that the origin of stochasticity may be different, as discussed in more detail in our conclusions.

Mathematically, our main result is intuitive. We find that, for a sufficiently large population, the distribution of first-passage times through the threshold at which an NTC sets in is approximately normal. The variance of this normal distribution decreases proportionally to the size of the population. The deterministic result for NTCP by Stocks *et al.* [12] is recovered in the limit of infinite population size (NTCP as approximated by Stocks *et al.* was either zero or one).

While our approximation is relatively crude, the mathematical simplicity of our result is a strength. Using our method to predict NTCP does not require extensive numerical calculations. In some examples closed-form expressions can be obtained, in other cases a small set of ordinary differential equations (ODEs) needs to be solved numerically, which can be done much more efficiently than integrating forward a potentially high-dimensional master equation. Since the linear-noise approximation (LNA), on which our approach is based, is ubiquitous in statistical physics and applications, our result may also lend itself to applications in other fields outside of radiotherapy modelling.

The remainder of this paper is set out as follows. In Sec. 6.3 we present the microscopic model of normal tissue cells adapted from the model of Stocks *et al.* [12] and a definition of NTCP. We use this model to explain the steps of our approximation

and derive our main results. This involves first writing the master equation, and subsequently approximating the dynamics by carrying out a Kramers–Moyal expansion and LNA. We then proceed to approximate the first-passage time across a boundary by considering the dynamics in a small region near the boundary marking the onset of NTC. This provides a Gaussian approximation of the first-passage times, and thus an approximation to NTCP. Following Hanin and Zaider [7] we then consider a more complicated model of normal tissue in Sec. 6.4. In this model there are two types of cells (normal and damaged), and we show how our method can be extended to systems with more than one degree of freedom. In the context of this model we also develop a second approximation method for NTCP. In Sec. 6.5 we combine models of cancerous cells and normal tissue to estimate the probability of complication-free tumour control, i.e., the probability that the tumour is controlled without complications in the normal tissue. In Sec. 6.6 we finally summarise our results. The Appendix contains further details of our analysis.

6.3 Logistic model of healthy tissue

6.3.1 Model definitions

We first focus on a model of normal tissue similar to that in Ref. [12], which is itself an individual-based extension to the deterministic dynamics considered in Ref. [7]. This existing work produced analytical descriptions of NTCP, but the analysis was restricted to the deterministic limit, in which intrinsic noise within the population is discarded. Our approach retains some of the effects of demographic noise on NTCP.

The model describes a well-mixed population of cells, we write N_t for the size of the population at time t. Cells can divide by mitosis at a rate b. We assume that overall growth is limited by spatial constraints and the presence of nutrients, or other regulatory mechanisms, so that b is a logistic function of N,

$$b_N = \begin{cases} b_0\left(1-\frac{N}{K}\right) & \text{if } N \leq K \\ 0 & \text{otherwise,} \end{cases} \tag{6.1}$$

where $b_0 > 0$ is a constant parameter. This indicates that the per capita birth rate decreases with increasing population size, and growth ceases completely when the carrying capacity K is reached; K is a model parameter and constant in time.

Cells can die due to natural causes and from external radiation. Natural death occurs with rate d. We note that explicitly separating death processes from birth events is necessary for a stochastic treatment of the model; basing the analysis on an effective net growth rate (i.e., $b_N - d$), as in Ref. [12], is insufficient to model the dynamics outside of the deterministic limit (models with different birth and death rates, but with the same net growth rate can lead to different results for NTCP in a stochastic setting).

External radiation damages cells mainly by inducing single or double strand breaks in their DNA [19]. The model captures these processes via a hazard function $h(t)$, denoting the per capita death rate due to radiation. This rate will generally depend on time, as determined by the details of the applied radiation protocol. For example, we consider the linear-quadratic (LQ) formalism of brachytherapy in Sec. 6.4.

The model can be summarised as a list of 'reactions', with notation similar to that used in chemical reaction systems. We write $\mathcal{N}$ to represent an individual normal cell. The dynamics are then given by

$$\begin{aligned} \mathcal{N} &\xrightarrow{b_0\left(1-\frac{N}{K}\right)} \mathcal{N}+\mathcal{N} && \text{(mitosis)},\\ \mathcal{N} &\xrightarrow{d} \emptyset && \text{(natural death)},\\ \mathcal{N} &\xrightarrow{h(t)} \emptyset && \text{(death due to radiation)}, \end{aligned} \tag{6.2}$$

where the rates above the arrows are per capita rates.

The deterministic rate equation for this system can be formulated heuristically as follows,

$$\frac{\mathrm{d}N}{\mathrm{d}t} = b_0 N\left(1-\tfrac{N}{K}\right) - [d+h(t)]N. \tag{6.3}$$

It can also be derived systematically from the lowest-order terms in an expansion in the inverse system size, as discussed below.

In the absence of radiation [i.e., when $h(t)=0$], the non-zero fixed point of Eq. (6.3) is given by $N^* = K\left(1-\frac{d}{b_0}\right)$. Since the population dynamics are stochastic, the size of the population fluctuates about this value. To simplify the notation we will use $K = \frac{\Omega}{1-d/b_0}$ in the following, such that—in the absence of radiation—the average population size is Ω.

6.3.2 Master equation

The process defined by Eqs. (6.2) can equivalently be described by a (chemical) master equation (CME). This is a set of ODEs describing the evolution in time of the probability for the population to be in each of the possible states, N. We write $P_N(t)$ for the probability that the population has size N at time t. The master equation is then given by

$$\begin{aligned}\frac{\mathrm{d}}{\mathrm{d}t}P_N(t) = &\left(\mathcal{E}^{-1}-1\right) Nb_0\left(1-\tfrac{N}{K}\right) P_N(t)\\ &+\left(\mathcal{E}-1\right) N\left[d+h\left(t\right)\right] P_N(t),\end{aligned} \tag{6.4}$$

where $\mathcal{E}$ is the step operator defined by its effect on a function f_N, i.e., we have $\mathcal{E}f_N = f_{N+1}$, and similarly, $\mathcal{E}^{-1}f_N = f_{N-1}$. The operators act on everything to their right.

6.3.3 Definition of normal-tissue complication probability and strategies to calculate it

Definition

An organ requires a minimum number of cells to function properly [20]. We introduce a threshold, L, and say that a normal tissue complication (NTC) is encountered when the number of cells in the population N_t falls below L. Given that N_t is a stochastic process, NTC will occur at different times in different realisations of the model dynamics (or potentially, it may never occur in a given realisation). This leads to the definition of normal tissue complication probability (NTCP). We assume that once NTC has been encountered in a given realisation of the dynamics, it cannot be repaired, even if the number of cells ultimately recovers to values above the threshold L. We therefore define NTCP(t) as the probability that, at some time before t, the population contained L cells or fewer. NTCP is then by definition an increasing function of time. We remark that this definition of NTCP(t) differs from one used previously in Ref. [12], which allowed NTCP(t) to decrease. In practice results using the two different definitions are often very similar.

Mathematically the calculation of NTCP constitutes a first-passage time problem [21]. More precisely, NTCP(t) is the cumulative distribution function of the

first-passage time through the threshold L. The methods we develop to approximate NTCP are therefore potentially applicable to a variety of other problems involving the estimation of first-passage time distributions, beyond the specific example of NTCP.

Strategies for the calculation or simulation of NTCP

Realisations of the process defined by Eqs. (6.2) can be generated using the stochastic simulation algorithm by Gillespie [22, 23]. In principle, a large ensemble of such simulations can be used to measure NTCP(t). However, in practice this approach is of limited use since a large number of runs need to be collected to obtain sufficient statistics. Simulations also offer relatively little in the way of mechanistic insight.

One can also find the NTCP(t) by direct numerical integration of Eq. (6.4). To do so, one must impose an absorbing boundary at L, i.e., the birth rate b_L would have to be set to zero so that once a trajectory has reached the threshold L it cannot recover to values above the threshold. In practice, this approach is computationally costly, especially in more realistic models where there are several different types of cells (see e.g., Sec. 6.4). The master equation is then a large set of coupled ODEs which would have to be integrated forward.

An alternative approach involves the use of generating functions (for general principles see for example Ref. [24]). However, this technique is usually only viable for relatively simple models. For example, generating functions can sometimes be calculated analytically when per capita birth and death rates do not depend on the current population size, i.e., when b_N is independent of N. This indicates that different cells reproduce and die independently of each other, and for such models explicit equations for both TCP and NTCP can, in principle, be obtained based on generating functions. This is not the case in the above logistic growth process however, which involves interaction between cells due to the overall carrying capacity. A notable example of an exact calculation using generating functions is the work of Zaider and Minerbo in Ref. [8] who obtain TCP in closed form for a linear-birth death process with time-dependent death rate (the time dependence is due to irradiation of the population). Their result for TCP can be expressed in terms of the solution of the rate equation describing the population in the deterministic limit (see also Ref. [25]). It is important to note though the result of Ref. [8] for TCP is valid for populations of any finite size,

whereas the approximation of NTCP in Ref. [12] discards intrinsic fluctuations.

Given the limitations of these numerical and analytical methods, we develop and use an approximation to estimate the NTCP. The approach is based on Kramers–Moyal expansion techniques [24,26] and retains features of the intrinsic noise resulting from the finiteness of the population of cells. At the same time, we assume that the population is sufficiently large so that the jump process defined by the master equation (6.4) can be approximated by a stochastic differential equation (SDE).

6.3.4 Kramers–Moyal expansion and linear-noise approximation

Kramers–Moyal expansion and Fokker–Planck equation

The expansion method is based on the assumption of a large, but finite population, as will be explained in further detail below. We will refer to Ω as the system size, in-line with previous literature [24,26]. As a first step we introduce the population density $n_t = N_t/\Omega$; that is, the population size at time t divided by the typical system size. We re-scale the threshold for the onset of NTC in the same way and write $\ell = L/\Omega$; NTC thus occurs when $n_t \leq \ell$. We also introduce a re-scaled carrying capacity and write $k = K/\Omega$. Given our above choice $K = \frac{\Omega}{1-d/b}$, we have $k = (1-d/b)^{-1}$.

Re-writing functions of N as functions of $n = N/\Omega$, we find $\mathcal{E}^{\pm 1} f(n) = f(n \pm 1/\Omega)$ for the action of the step operator. We proceed to consider the limit where the system size is large, $\Omega \gg 1$. In this limit one can expand

$$\mathcal{E}^{\pm 1} = 1 \pm \frac{1}{\Omega}\frac{\partial}{\partial n} + \frac{1}{2\Omega^2}\frac{\partial^2}{\partial n^2} + \dots \ . \tag{6.5}$$

Substituting this into the master equation (6.4) results in a Fokker–Planck equation for the probability density $\Pi(n,t)$,

$$\frac{\partial}{\partial t}\Pi(n,t) = -\frac{\partial}{\partial n}\mu(n,t)\Pi(n,t) + \frac{1}{2\Omega}\frac{\partial^2}{\partial n^2}\sigma^2(n,t)\Pi(n,t), \tag{6.6}$$

where we have neglected higher-order terms in Ω^{-1}. The probability of finding the random process n_t with a value in the interval $[n, n+\mathrm{d}n)$ at time t is $\Pi(n,t)\mathrm{d}n$.

For the current model, the drift and diffusion terms in Eq. (6.6) are given by

$$\mu(n,t) = nb_0\left(1-\frac{n}{k}\right) - n\left[d+h(t)\right], \tag{6.7a}$$

$$\sigma^2(n,t) = nb_0\left(1-\frac{n}{k}\right) + n\left[d+h(t)\right], \tag{6.7b}$$

respectively. Equation (6.6) describes the statistics generated by solutions of the Itō SDE

$$\mathrm{d}n_t = \mu(n_t,t)\mathrm{d}t + \Omega^{-1/2}\sigma(n_t,t)\mathrm{d}W_t, \tag{6.8}$$

where W_t is a standard Wiener process.

In principle, trajectories of this SDE can be generated in simulations, for example using the Euler–Maruyama method [27]. These simulations are more efficient than simulating the original model, in particular the population size only enters in the noise strength and does not affect computing time required to generate a set number of realisations. However, our aim is to make analytical progress. This requires further approximation, first because $\mu(n_t,t)$ is a non-linear function of n_t, and more importantly because the noise in Eq. (6.8) is multiplicative. We proceed by making a further simplification using the LNA [24,26], effectively turning multiplicative noise into additive noise.

Linear-noise approximation

To carry out the LNA we introduce the stochastic process ξ_t via the transformation [26]

$$n_t = \phi(t) + \Omega^{-1/2}\xi_t, \tag{6.9}$$

where $\phi(t)$ is a deterministic function of t, to be determined shortly.

We next substitute this ansatz into Eq. (6.8), and expand in powers of $\Omega^{-1/2}$. From the two lowest-order terms we find

$$\frac{\mathrm{d}\phi}{\mathrm{d}t} = \mu\left[\phi(t),t\right], \tag{6.10a}$$

$$\mathrm{d}\xi_t = \mu'\left[\phi(t),t\right]\xi_t\mathrm{d}t + \sigma\left[\phi(t),t\right]\mathrm{d}W_t, \tag{6.10b}$$

where $\mu'\left[\phi(t),t\right]$ is the derivative of the drift $\mu(n,t)$ with respect to n, evaluated at $\phi(t)$ and t.

The first of these equations indicates that $\phi(t)$ is the solution of a deterministic rate equation. Up to re-scaling of N and K this rate equation is identical to Eq. (6.3). The SDE (6.10b) describes fluctuations about this deterministic trajectory, due to demographic noise. We note that the LNA is only valid provided corrections to the deterministic dynamics remain small; if this is not the case higher-order terms in the system-size expansion become important. The approximation is generally appropriate if the deterministic trajectory is locally attracting, i.e., if $\mu'[\phi(t), t] < 0$ at all times. This condition is fulfilled in the present model.

The linear SDE (6.10b) can be solved straightforwardly [24,26,28], and, within the LNA, the distribution of n_t is found to be Gaussian, centred around the solution $\phi(t)$ of Eq. (6.10a),

$$\Pi(n,t) = \frac{1}{\sqrt{2\pi\Omega^{-1}\Sigma^2(t)}} \exp\left(-\frac{[n-\phi(t)]^2}{2\Omega^{-1}\Sigma^2(t)}\right). \tag{6.11}$$

The variance of this distribution, $\Omega^{-1}\Sigma^2(t)$, is a function of time, and can be obtained from the solution of

$$\frac{\mathrm{d}\Sigma^2}{\mathrm{d}t} = 2\mu'\left[\phi(t),t\right]\Sigma^2(t) + \sigma^2\left[\phi(t),t\right], \tag{6.12}$$

see e.g., Ref. [28].

For some cases Eqs. (6.10a) and (6.12) can be solved exactly, and one can obtain an analytical expression for $\Pi(n,t)$ in Eq. (6.11). We discuss this in the context of the current model below. For the general case, these equations can be integrated forward numerically, using standard Runge–Kutta methods. This only requires the integration of two ODEs.

Approximation of NTCP(t)

We now proceed to estimate NTCP using the outcome of the LNA. Taking Eqs. (6.10a) and (6.10b) as a starting point, the calculation of NTCP amounts to a first-passage time problem for a SDE with time-dependent drift and noise strength. Equation (6.10b) describes an Ornstein–Uhlenbeck process with time-dependent rates [24]. Due to the time-dependence of $\phi(t)$ in Eq. (6.10a), calculating NTCP amounts to calculating the first-passage time of this Ornstein-Uhlenbeck process through a moving boundary. While the first-passage time distribution of Ornstein–Uhlenbeck processes is available

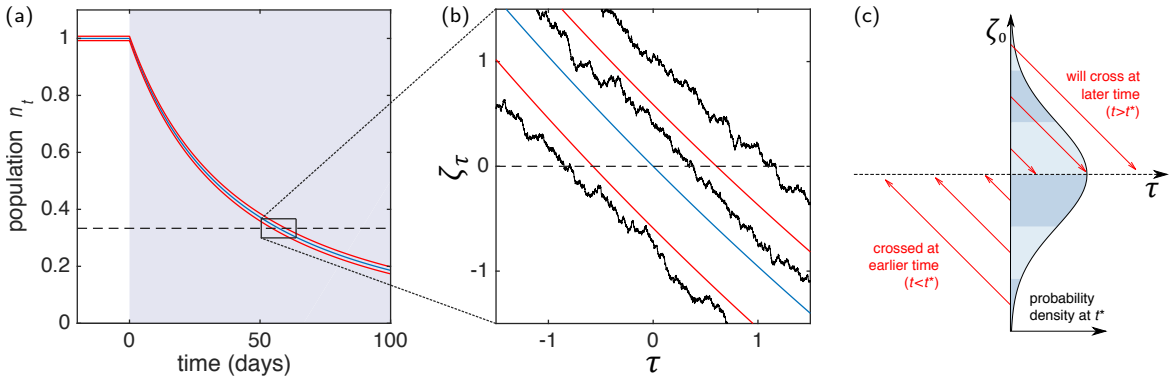

Figure 6.1: *Population size as a function of time for the model in Sec. 6.3.1.* In this set-up constant radiation acts from a given time, here chosen to be $t = 0$. The size of the population then decreases and falls below the threshold for the onset of NTCs. Panel (a): The central, blue line shows the deterministic trajectory [Eq. (6.10a)], the red lines show a band of one standard deviation as predicted by the LNA, see Eq. (6.12). The shading of the background indicates the rate of cell death due to radiation $h(t)$. The dashed line is the threshold for onset of NTC. Panel (b): Magnified look at the crossing region, shown in the re-scaled coordinates τ and ζ. Shown are three stochastic trajectories (black noisy lines) from simulation of SDE (6.8); they are approximately linear with gradient minus one, as predicted by Eq. (6.15). Panel (c): Schematic representation of our approximation. We start from the Gaussian distribution obtained within the LNA [Eq. (6.11)] and project trajectories onto the time axis, assuming that their behaviour is linear with slope minus one. Model parameters are given in Table 6.2 [parameter set (D)].

for constant rates and a static boundary [29], studies of instances with time-dependence are often based on approximation schemes for specific cases; examples can be found in Refs. [30, 31].

To make progress we therefore use a further approximation. We focus on cases in which the deterministic trajectory $\phi(t)$ crosses the threshold $\ell = L/\Omega$, as illustrated in Fig. 6.1(a); we write t^* for this time. The exact value of t^* will depend on the applied radiation protocol and the other model parameters. The calculation of NTCP(t) by Stocks *et al.* [12] is based on this deterministic contribution, and within their calculation NTCP(t) $= \Theta(t - t^*)$ is a Heaviside step function [$\Theta(u) = 1$ for $u \geq 0$, and $\Theta(u) = 0$ otherwise]. Our aim is to build on the results in Ref. [12] and to capture some of the influence of intrinsic fluctuations on NTCP.

As a next step we look at the dynamics of Eqs. (6.10a) and (6.10b) in a time window around t^*, as shown in Fig. 6.1(b). Some trajectories of the stochastic system will cross the threshold ℓ before t^*, and others after t^*. We expect these fluctuations in the crossing time to decrease as the system-size parameter Ω is increased. To evaluate this

	Coordinate	Interpretation	Relations
(A)	N_t	number of individuals in population at time t	—
(B)	n_t	population density	$n_t = N_t/\Omega$
(C)	$\phi(t)$	deterministic (mean-field) trajectory	$n_t = \phi(t) + \Omega^{-1/2}\xi_t$
	ξ_t	deviation from mean-field path due to linear noise	
(D)	ζ_τ	re-scaled population near boundary $\ell = L/\Omega$	$n_\tau = \ell + \Omega^{-1/2}\zeta_\tau$
	τ	re-scaled time near deterministic crossing time t^*	$t = t^* + \frac{\Omega^{-1/2}}{-\mu(\ell,t^*)}\tau$

Table 6.1: *Summary of the different coordinate systems used to describe the population in the model of Sec. 6.3.1.* Original coordinates (A) appear in the master equation (6.4), while coordinates (B) and (C) are used in the Kramers–Moyal expansion and linear-noise approximation, respectively [see Eqs. (6.8) and (6.10)]. Coordinates (D) are used for our analysis of the dynamics in the narrow, boundary-crossing region. The subscript t (or τ) is used to denote random processes.

further we consider the Gaussian distribution for the population density n_{t^*} obtained by evaluating Eq. (6.11) at time t^*. By construction, this distribution is centred on ℓ, as shown in Fig. 6.1(c). We now proceed on the basis that trajectories with values $n_{t^*} > \ell$ will first cross the threshold at a time greater than t^*, and estimate this time of crossing from the dynamics near t^*. Similarly, trajectories with $n_{t^*} < \ell$ have already crossed the threshold, and we estimate how long before t^* this has occurred. This procedure implies several assumptions, for example a trajectory with $n_{t^*} > \ell$ may have had its first crossing before t^* and then returned to values n_t above ℓ due to further fluctuations. This is not captured by our estimate of NTCP.

In order to focus on the dynamics in a time window near t^*, it is useful to introduce re-scaled coordinates

$$t = t^* - \frac{\Omega^{-1/2}}{\mu(\ell, t^*)}\tau, \tag{6.13a}$$

$$n_\tau = \ell + \Omega^{-1/2}\zeta_\tau. \tag{6.13b}$$

Considering values of τ and ζ of order Ω^0 allows us to magnify the region around t^* where boundary crossings are likely (ζ_τ refers to the random process, while ζ is a value in the process's state space). In these coordinates, the crossing of the deterministic trajectory occurs at $\tau = 0$, and the position of the threshold is at $\zeta = 0$. We note that $\mu(\ell, t^*) < 0$ so that positive values of the re-scaled time ($\tau > 0$) correspond to $t > t^*$. A summary of the coordinates used in our analysis is given in Table 6.1.

Substituting the new coordinates into Eq. (6.6), and writing $\widetilde{\Pi}(\zeta,\tau)$ for the probability density in these coordinates, we find

$$\frac{\partial}{\partial\tau}\widetilde{\Pi}(\zeta,\tau) = \frac{1}{\mu(\ell,t^*)}\frac{\partial}{\partial\zeta}\left[\mu(\ell+\Omega^{-1/2}\zeta,t)\widetilde{\Pi}(\zeta,\tau)\right] + \frac{1}{\mu(\ell,t^*)}\frac{1}{2\Omega^{1/2}}\frac{\partial^2}{\partial\zeta^2}\left[\sigma^2(\ell+\Omega^{-1/2}\zeta,t)\widetilde{\Pi}(\zeta,\tau)\right]. \tag{6.14}$$

Expanding in powers of $\Omega^{-1/2}$ we find to lowest order $\frac{\partial}{\partial\tau}\Pi(\zeta,\tau) = \frac{\partial}{\partial\zeta}\Pi(\zeta,\tau)$, i.e., near the threshold the dynamics of the system can be approximated by

$$\zeta_\tau = \zeta_0 - \tau, \tag{6.15}$$

where ζ_0 is the location of the path at time $\tau = 0$ (i.e., at $t = t^*$). Fig. 6.1 (b) shows a number of different stochastic trajectories in this region. Broadly, they travel along approximately parallel straight paths of gradient minus one (in the coordinate system of τ and ζ).

We now use this result to approximate the distribution of crossing times. To do this we estimate when a particular trajectory located at ξ_0 at time t^* crosses (or did cross) the threshold. We write $\tau_\times(\zeta_0)$ for this crossing time in the re-scaled coordinates. Using Eq. (6.15) we find

$$\tau_\times(\zeta_0) = \zeta_0\ . \tag{6.16}$$

We show this schematically in Fig. 6.1(c). We now combine this with the Gaussian distribution for ξ_0 obtained from the LNA, also shown in Fig. 6.1(c). Equation (6.11), evaluated at $t = t^*$, can be written as

$$\Pi(\zeta_0) = \frac{1}{\sqrt{2\pi\Sigma^2(t^*)}}\exp\left(-\frac{\zeta_0^2}{2\Sigma^2(t^*)}\right), \tag{6.17}$$

and we use this together with Eq. (6.16) to approximate the distribution of first-passage times $t_\times$ as

$$p(t_\times) = \sqrt{\frac{\Omega\mu^2(\ell,t^*)}{2\pi\Sigma^2(t^*)}}\exp\left(-\frac{\Omega\mu^2(\ell,t^*)}{2\Sigma^2(t^*)}\,(t_\times - t^*)^2\right). \tag{6.18}$$

Using the definition of NTCP as outlined above we find

$$\mathrm{NTCP}(t) = \frac{1}{2}\left[1 + \mathrm{erf}\left(\frac{(t-t^*)\sqrt{\Omega}\mu(\ell,t^*)}{\sqrt{2}\Sigma(t^*)}\right)\right], \tag{6.19}$$

where erf is the error function.

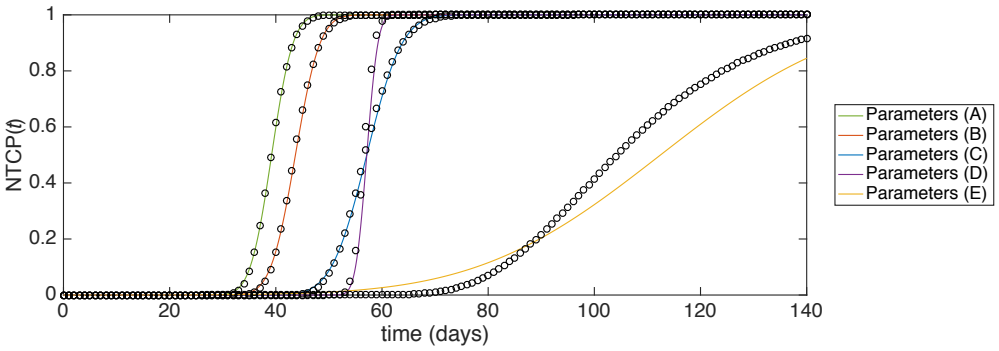

Figure 6.2: *NTCP as a function of time for the logistic model of healthy tissue in Sec. 6.3.1.* Black circles are obtained from numerical integration of the master equation of the original model [Eq. (6.4)]. Coloured solid lines show the approximation of Eqs. (6.23) and (6.24). Model parameters are given in Table 6.2.

Parameter	Definition	Value				
		(A)	(B)	(C)	(D)	(E)
b_0	mitosis rate (day^{-1})	0.019	0.019	0.019	0.019	0.038
d	natural death rate (day^{-1})	0.002	0.002	0.002	0.002	0.004
h_0	irradiated death rate (day^{-1})	0.035	0.032	0.026	0.026	0.026
Ω	typical population size (see text)	500	500	500	5000	500
ℓ	threshold for onset of NTC	1/3	1/3	1/3	1/3	1/3

Table 6.2: *Five sets of parameters used in Fig. 6.2 for the logistic model of healthy tissue.* These parameter sets are the same as those considered in Ref. [12], but we have defined separate mitosis and natural death rates to be able to analyse stochastic effects in finite populations (see text). The ratio of mitosis and natural death was chosen as $10:1$, consistent for example with Ref. [7].

Closed-form approximation of NTCP for model with logistic growth and constant radiation

We now test this approximation scheme on the logistic growth model defined in Eq. (6.2). We focus on a particularly simple case where there is no radiation prior to a certain time, and a constant rate of death due to radiation thereafter. We choose time $t = 0$ as the point at which radiation sets in, so that the hazard function $h(t)$ is the step function

$$h(t) = \begin{cases} 0 & \text{for } t < 0, \\ h_0 & \text{for } t \geq 0. \end{cases} \tag{6.20}$$

We primarily consider radiation of this type as a simple initial example, following the study of NTCP in Ref. [12]. More complicated radiation protocols will be discussed below.

We assume that the dynamics of the population start long before $t = 0$, so that the stationary state of the master equation (6.4) [with $h(t) = 0$] is reached by $t = 0$. The mean and variance of this distribution are given by the fixed points of Eqs. (6.10a) and (6.12), using μ and σ^2 for the logistic model and setting $h(t) = 0$. We have

$$\phi(t=0) = 1, \tag{6.21a}$$

$$\Sigma(t=0) = \frac{d}{b_0 - d}. \tag{6.21b}$$

At times $t \geq 0$, Eqs. (6.10a) and (6.12) are given by

$$\frac{\mathrm{d}\phi}{\mathrm{d}t} = \phi b_0 \left(1 - \frac{\phi}{k}\right) - \phi\left[d + h_0\right], \tag{6.22a}$$

$$\frac{\mathrm{d}\Sigma^2}{\mathrm{d}t} = 2\left\{b_0\left(1 - \frac{2\phi}{k}\right) - \left[d + h_0\right]\right\}\Sigma^2 + \phi b_0\left(1 - \frac{\phi}{k}\right) + \phi\left[d + h_0\right]. \tag{6.22b}$$

Eq. (6.22a) can be solved in closed form subject to the initial condition $\phi(0) = 1$. From the resulting deterministic trajectory $\phi(t)$ one then finds the passage time t^* of the deterministic trajectory as

$$t^* = \frac{1}{b_0 - d - h_0} \log\left(\frac{h_0 \ell}{b_0 \ell - d\ell - b_0 + d + h_0}\right), \tag{6.23}$$

assuming the fixed point of the deterministic trajectory is below the boundary ℓ. Next we turn to Eq. (6.22b) in order to find $\Sigma^2(t^*)$. For constant radiation the path $\phi(t)$ is monotonically decreasing in time. This allows us to trade the time derivative in Eq. (6.22b) for a derivative with respect to ϕ, resulting in a linear ODE for Σ^2 as a function of ϕ. For our specific example this ODE can be solved in closed form, and we find the variance of first-passage times as

$$\begin{aligned}\frac{\Sigma^2\left(t^*\right)}{\Omega\mu^2(\ell, t^*)} =& \frac{5b + \frac{2(b_0-d)d}{h_0} + \frac{(b_0-2d)h_0}{b_0-d} - \frac{b_0+d+h_0}{\ell} + \frac{(b_0-d)(b_0-d-h_0)(d+h_0)}{[d+h_0+b_0(\ell-1)-d\ell]^2} - \frac{(b_0-d)[b_0+3(d+h_0)]}{d+h_0+b_0(\ell-1)-d\ell}}{\Omega(b_0 - d - h_0)^3} \\ &+ \frac{2(b_0 - d)(b_0 + 2d + 2h_0)\log\left(\frac{h_0\ell}{b_0\ell - d\ell - b_0 + d + h_0}\right)}{\Omega(b_0 - d - h_0)^4}.\end{aligned} \tag{6.24}$$

This can then be used in Eq. (6.19) to obtain NTCP(t).

In Fig. 6.2 we show the resulting NTCP as a function of time for several sets of model parameters; these parameter sets are summarised in Table 6.2, and were previously motivated and used in Ref. [12] to consider normal tissue complications

arising from the treatment of prostate cancer. For the parameters shown, the standard deviation in the time for NTCP onset varies from 3% and 21% of the mean onset time. In order to test the accuracy of our approximation, we have also obtained NTCP(t) for the original model by numeral integration of the master equation Eq. (6.4); these values are shown as black circles in Fig. 6.2. These results are compared with the analytical approximations in Eqs. (6.19) and (6.24), and for most of the parameter sets tested we find good agreement. The approximation works noticeably less well for parameter set (E) than for the other four sets. In this case, the speed with which the deterministic path crosses the boundary is lower than for the other parameter sets. This leads to a longer time window around t^* within which crossings are likely, and thus a larger amount of error in our approximation.

6.4 Extended model of normal and doomed cells

6.4.1 Model definitions

Hanin and Zaider [7] proposed a model which adds complexity by including radiation-damaged cells. In this model, damaged cells continue to occupy the limited volume available to the population. Damaged cells also carry out their functions, but fail to proliferate. The presence of such cells has been offered an explanation for the observation that, after irradiation, an initial lag period occurs before re-population [7, 32]. Similar models have been proposed for tumour cells for a more realistic calculation of TCP, where the population is divided into radiation-damaged and unaffected tumour cells [33].

As before there are 'normal cells' $\mathcal{N}$ which carry out the functions of the organ; these cells have the ability to proliferate. However, once damaged by radiation, a cell does not vanish immediately; rather, it becomes a 'doomed cell' $\mathcal{X}$ [7]. Doomed cells continue to contribute to the normal functions of the organ, however they are unable to proliferate. Thus, although they may temporarily aid the function of the organ, they ultimately die without reproduction. Doomed cells also consume resources and so are in direct competition with the normal cells. As a result of this, the per capita mitosis (birth) rate of normal cells decreases as the total size of the population of both

types increases. The dynamics of the model can be summarised as follows:

$$\begin{aligned}
\mathcal{N} &\xrightarrow{b_0\left(1-\frac{N+X}{k\Omega}\right)} \mathcal{N}+\mathcal{N} && \text{(mitosis of normal cells)},\\
\mathcal{N} &\xrightarrow{h(t)} \mathcal{X} && \text{(radiation damage)},\\
\mathcal{N} &\xrightarrow{d_1} \emptyset && \text{(death of normal cell)},\\
\mathcal{X} &\xrightarrow{d_2} \emptyset && \text{(death of doomed cell)}.
\end{aligned} \tag{6.25}$$

We write N and X for the numbers of normal and doomed cells, respectively. As before, the constant $k \equiv (1 - d_1/b_0)^{-1}$ is chosen so that—in the absence of radiation—the stationary average size of the population of normal cells is Ω. An NTC is assumed to arise when the total number of functional cells, $N + X$, falls below a threshold L.

Writing $s = (N + X)/\Omega$ for the (re-scaled) total number of functional cells in the population, and $x = X/\Omega$ for the (re-scaled) number of doomed cells, one has the following rate equations in the deterministic limit,

$$\frac{\mathrm{d}s}{\mathrm{d}t} = b_0\left(1-\frac{s}{k}\right)(s-x) - d_1(s-x) - d_2 x, \tag{6.26a}$$

$$\frac{\mathrm{d}x}{\mathrm{d}t} = h(t)(s-x) - d_2 x. \tag{6.26b}$$

In this example, we consider brachytherapy where there is a time-varying dose of radiation acting on the population of normal cells, resulting from the decay of a radioactive implant. The effect of this type of radiation on the population of normal cells is obtained using the linear-quadratic (LQ) formalism, which is well established in the modelling of brachytherapy [34–36]. This formalism accounts for the degradation of the radioactive implant, both linear and quadratic tissue responses to radiation, and DNA repair. This leads to a time-dependent radiation hazard rate for the conversion of normal cells into doomed cells:

$$h(t) = \alpha R_0 e^{-\lambda t} + \frac{2\beta R_0^2 e^{-\lambda t}}{\gamma - \lambda}\left(e^{-\lambda t} - e^{-\gamma t}\right), \tag{6.27}$$

where $\alpha, \beta, \gamma, \lambda$ and R_0 are model parameters; R_0 in particular denotes the initial dose rate. Further details are given in 6.7. We consider a specific set of realistic parameters, proposed by Hanin and Zaider [7] and summarised in Table 6.3. These parameters were chosen to model the treatment of prostate cancer, where the normal-tissue complication refers to grade 2, or larger, toxicity ('GU2+') of the genitourinary tract.

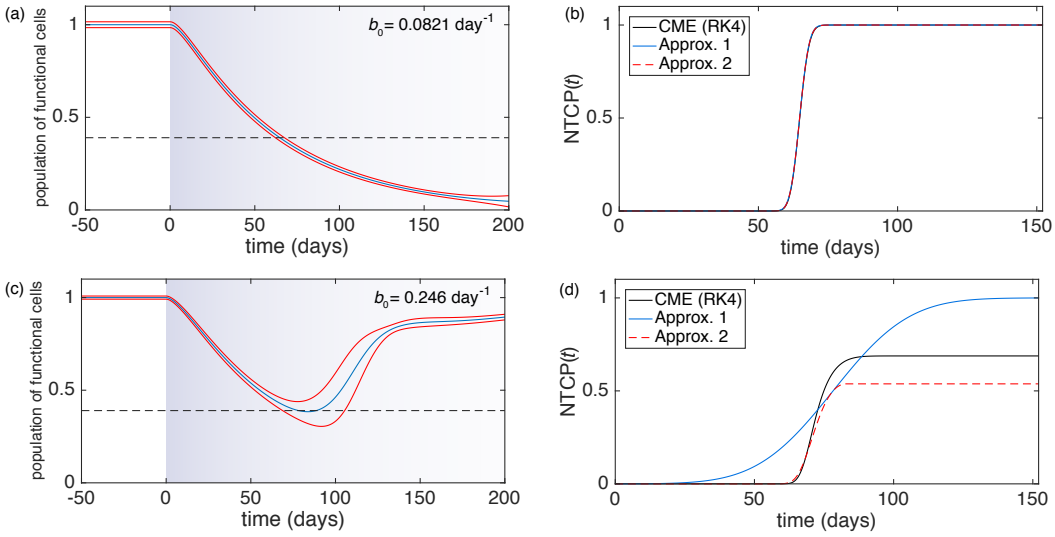

Figure 6.3: *Behaviour of the model with normal and damages cells defined in Sec. 6.4.1.* Panels (a) and (c): Population density for number of functional cells as a function of time for two different parameter sets (see Table 6.3). The central blue line shows the deterministic trajectory [Eq. (6.26b)], red lines indicate a band of one standard deviation as predicted by the linear-noise approximation. The shading of the background indicates the rate of radiation damage $h(t)$. Panels (b) and (d): NTCP as a function of time. We compare the results of our two approximations with the outcome of numerical integration of the (chemical) master equation (CME) using a Runge–Kutta scheme (RK4).

6.4.2 Alternative approximation for NTCP

Results for this model are presented in Fig. 6.3. We first focus on the deterministic dynamics, indicated by the blue lines in panels (a) and (c). In panel (a) the mitosis rate b_0 is sufficiently low for deterministic trajectory to fall below the threshold ℓ for the onset of NTCs. The approximation for NTCP developed in Sec. 6.3.4 can be applied, as discussed in more detail in Sec. 6.4.3.

The second parameter set in Table 6.3 describes a case with a higher mitosis rate b_0. As shown in Fig. 6.3 (c), the solution of the deterministic rate equations then only briefly falls below the threshold ℓ. The number of functional cells then increases again to values above ℓ. In the stochastic system we expect only a fraction of trajectories to cross the threshold; some realisations may never fall below ℓ, and hence NTCP(t) can be expected to take a long-time limit below one. This cannot be captured by the approximation method in Sec. 6.3.4.

With this in mind, we propose the following improved method of estimating NTCP. Within the LNA, at each moment in time t the distribution of the population of interest

Parameter	Definition	Fig. 6.3 (a, b)	Fig. 6.3 (c, d)
b_0	mitosis rate (day^{-1})	0.0821	0.246
d_1	normal cell death rate (day^{-1})	0.0164	0.0164
d_2	irradiated cell death rate (day^{-1})	0.0164	0.0164
Ω	population size	1000	1000
$\ell = \frac{L}{\Omega}$	critical fraction of population	0.39	0.39
α	LQ model parameter ($\mathrm{G\,y}^{-1}$)	0.109	0.109
β	LQ model parameter ($\mathrm{G\,y}^{-2}$)	0.0364	0.0364
γ	rate of DNA repair (day^{-1})	23.7	23.7
R_0	initial dose rate of implant ($\mathrm{G\,day}^{-1}$)	1.68	1.68
λ	decay rate (day^{-1})	0.0117	0.0117

Table 6.3: *Parameters used in Fig. 6.3.* Similar parameters were previously proposed in Ref. [7]. We have explicitly included normal-cell birth and death and made the assumption that $d_1 = d_2$.

(in this case s_t) is approximately normal with a mean $\phi(t)$ and variance $\Sigma^2(t)$ given by Eqs. (6.10a) and (6.12), respectively. The amount of probability below the threshold ℓ at a given time is then obtained as[1]

$$Q(t) = \frac{1}{2}\left[1 + \mathrm{erf}\left(\frac{\sqrt{\Omega}[\ell - \phi(t)]}{\sqrt{2}\Sigma(t)}\right)\right]. \tag{6.28}$$

We now estimate NTCP(t) as the maximum amount of probability below the threshold at any earlier time $t' \leq t$, i.e.,

$$\mathrm{NTCP}(t) = \max_{t' \leq t} Q(t'). \tag{6.29}$$

Further steps of the mathematical evaluation are presented in 6.8.

We briefly comment on the limitations of this approximation, before we discuss the results for the model of normal and doomed cells. Equation (6.29) provides a lower bound for NTCP of the process described by the LNA. This can be seen as follows. At a given time t, let the maximum in Eq. (6.29) have occurred at a time $t_m \leq t$; the estimate for NTCP(t) is then $Q(t_m)$. Consider now a trajectory with a total population density above the boundary at time t_m, $s_{t_m} > \ell$. Such a trajectory does not contribute to NTCP(t) within our approximation, even though it may have well have attained population sizes below threshold before t_m, or go below threshold between t_m and t. The above approximation therefore underestimates NTCP. We note that the SDE obtained in the LNA is itself an approximation, so the above calculation is not necessarily a lower bound to the NTCP of the discrete population dynamics from which we started.

[1] We note that the quantity $Q(t)$ in Eq. (6.28) corresponds to NTCP as defined in Ref. [12].

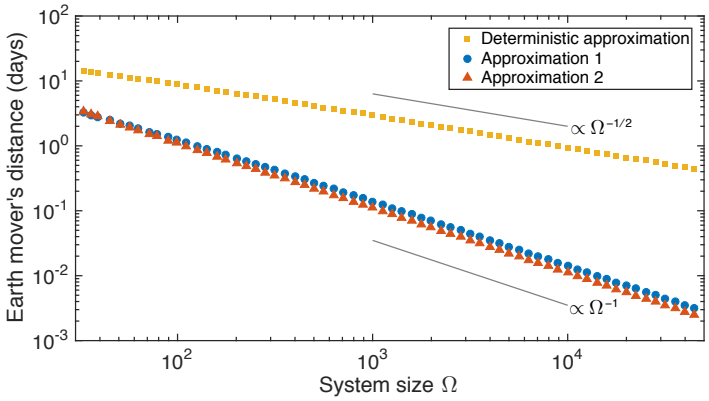

Figure 6.4: *Measure of error for the predictions of NTCP for the model in Sec. 6.3.1.* We use the Earth Mover's Distance (EMD) [37] as a measure of distance between two probability distributions. Each set of symbols shows the EMD of the distribution of first-passage times obtained from the different approximations relative to the distribution obtained for the original model obtained by numerical integration of the master equation (6.4). We compare three approximations: the deterministic approximation from Ref. [12] (i.e., the distribution of first-passage times is a delta-peak at the deterministic crossing time t^*), and Approximations 1 and 2 as described in the text. Results are shown as a function of the population-size parameter Ω. The data indicates that the EMD of Approximations 1 and 2 from the original model scales as Ω^{-1} with the typical size of the population; similar scaling is also observed using the Kullback–Leibler divergence (not shown). For the deterministic approximation the EMD decays much more slowly with the system-size parameter ($\propto \Omega^{-1/2}$).

Despite these limitations, the method provides useful estimates for NTCP. For example, NTCP(t) obtained from Eqs. (6.28) and (6.29) for the model in Sec. 6.3.1 does not significantly differ from the predictions of the method discussed in Sec. 6.3.4. To keep the language compact we will refer to the procedure in Sec. 6.3.4 as Approximation 1 from now on, and to that in Eqs. (6.28) and (6.29) as Approximation 2. A quantitative comparison of the distributions of first-passage time from the two approximations for the model in Sec. 6.3.1 is shown in Fig. 6.4. The data indicates that Approximation 2 provides an improvement relative to Approximation 1. Both methods do considerably better than the deterministic approximation in Ref. [12].

To compare the three approximations we have use the Earth-Movers distance (EMD), also known as the Wasserstein metric [37]. Intuitively, it is a measure of the amount of 'effort' needed to turn one distribution into the other; it is the amount of probability that needs to be moved weighted by the distance it has to be moved. We choose this rather than, say, the Kullback–Leibler divergence [38] or total variation distance since the distribution of first-passage times from the deterministic approach is a Dirac delta-distribution [12] which results in infinite Kullback–Leibler divergence. The EMD gives a more useful measure of error.

6.4.3 NTCP for model of normal and doomed cells

For the model with normal and doomed cells Approximation 2 can provide a significantly improved prediction of NTCP compared to Approximation 1, as we will discuss in this section. In this context it is useful to distinguish the cases in which normal tissue complication occurs with certainty at long times and those in which long-time NTCP stays below one.

Certain normal tissue complication at long times

For the first set of parameters in Table 6.3 normal-tissue complication occurs with probability one at long times. We show results in panel (a) of Fig. 6.3. The source of radiation is implanted at time zero, assuming that the population of normal cells is at its stationary state at this time. The population of functional cells then decreases monotonously, and the number of functional cells crosses the threshold for the onset of NTC. Panel (b) shows the estimates for NTCP as a function of time for Approximation

1 and Approximation 2. Their predictions are largely indistinguishable, and they both agree well with results for the original model found by numerical integration of the master equation.

We note that for this choice of parameter values, carrying out the numerical integration of the master equation takes approximately 10^5 times longer than to evaluate each of the two approximations. This is because the master equation consists of a set of Ω^2 coupled ODEs, whereas evaluation of each of the approximations only involves integrating forward five ODEs (for the means of the two degrees of freedom, their variances and the covariance). Thus, the approximation methods offer a significant increase in efficiency for large populations, at moderate reduction of accuracy.

Uncertain onset of normal tissue complication

In panels (c) and (d) of Fig. 6.3 we show the same quantities, but for a different choice of birth rate (see Table 6.3). The deterministic path barely crosses the boundary ℓ, and for this choice of parameters only a fraction of trajectories of the stochastic model will lead to an onset of NTC. In this case, the predictions of the two approximations are widely different. Approximation 1 assumes a Gaussian distribution of first-passage times and deviates significantly from the NTCP seen in the original model. Most notably, this approximation predicts that all trajectories eventually cross the boundary so that $\mathrm{NTCP}(t) \to 1$ at large times. Although this is not the case for typical population size used in this example ($\Omega = 1000$), we remark that for $\Omega \to \infty$ NTC becomes certain at long times in the original model for the present parameter set.

As seen in Fig. 6.3 (d) Approximation 2 outperforms Approximation 1. This is because, in the narrow region where boundary-crossings are likely, there is a significant change in the drift for the total population size; the sign of the drift changes from negative to positive. Approximation 2 takes this into account, whereas Approximation 1 is based on constant drift within the region near the boundary ℓ. Unlike Approximation 1, Approximation 2 does not (wrongly) predict that all trajectories eventually cross the boundary. Instead $\mathrm{NTCP}(t)$ remains below unity at $t \to \infty$ within Approximation 2.

6.5 Complication-free tumour control

6.5.1 Motivation

The objective of radiation therapy is to successfully eliminate cancerous cells while avoiding further complications from damaging normal tissue cells. In the preceding sections, we outlined analytical approximations for the efficient calculation of NTCPs. Tumour control probabilities—the probability of eliminating all cancer cells—from a stochastic birth-death model have been previously considered by Zaider and Minerbo [8]; the authors derive a general equation for the probability of the elimination of all tumour cells. In this section, we combine these two results for NTCP and TCP respectively to investigate how, in principle, mathematical models can be used to optimise the application of radiation therapy to achieve complication-free tumour control. We begin by motivating an extension to the model described in Sec. 6.3 to include the growth of cancerous cells. For completeness, we then proceed by briefly reviewing Zaider and Minerbo's result describing TCP.

6.5.2 Model definitions

We consider a model which contains both normal cells $\mathcal{N}$ and cancerous cells $\mathcal{C}$. The two populations are assumed to be spatially separated from each other. The normal cells are as described in Sec. 6.3: they undergo mitosis with a rate which depends on the number of normal cells, leading to logistic growth. They are also subject to a natural death with rate d_1, and to death from a source of radiation with hazard function $h_1(t)$. We label the rates pertaining to normal cells with the subscript 1, and similarly subscript 2 for cancerous cells. Cancerous cells, on the other hand, undergo mitosis with a constant rate b_2 [8]; numerical evidence suggests that the resulting exponential growth characterise tumours of small sizes well [39]. Cancer cells are also subject to a natural death with a rate d_2 and to death from a source of radiation with

hazard function $h_2(t)$. The model can be summarised by the following reactions:

$$\begin{array}{lll} \mathcal{N} \xrightarrow{b_1\left(1-\frac{N}{k\Omega}\right)} \mathcal{N}+\mathcal{N}, & \mathcal{C} \xrightarrow{b_2} \mathcal{C}+\mathcal{C}, & \text{(mitosis)}, \\ \mathcal{N} \xrightarrow{d_1} \emptyset, & \mathcal{C} \xrightarrow{d_2} \emptyset, & \text{(natural death)}, \\ \mathcal{N} \xrightarrow{h_1(t)} \emptyset, & \mathcal{C} \xrightarrow{h_2(t)} \emptyset, & \text{(irradiated death)}. \end{array} \tag{6.30}$$

Although both cells are subject to the same source of radiation, the hazard functions $h_1(t)$ and $h_2(t)$ for the two cell types can differ. This is because each cell type differs in its susceptibility to radiation and in their ability to repair damaged DNA. We again consider the case of brachytherapy, as in Sec. 6.4. The hazard function is as in Eq. (6.27), where the parameters $\alpha_{1,2}$, $\beta_{1,2}$, and $\gamma_{1,2}$ depend on the cell type. We also assume that, due to the presumed spatial separation of normal tissue and cancerous cells, the treatment can be targeted such that each cell type absorbs a different fraction of the total dose rate. This is incorporated into the hazard function by replacing the initial dose rate R_0 with an effective dose rate $\theta_{1,2}R_0$. The parameters describing the initial dose rate R_0 and the decay rate λ are characteristics of the radioactive implant and are thus common to the hazard function of both cell types. As before, we initialise the population of normal cells in its stationary state. We let there be initially C_0 cancer cells.

6.5.3 Tumour control probability, normal-tissue complication probability, and probability of complication-free control

We now consider the probability as a function of time of eliminating all cancer cells—TCP(t). Similarly to the calculation of NTCP(t), this is mathematically a first-passage time problem. Zaider and Minerbo [8] developed an analytical description for TCP for the linear dynamics of cancerous cells described above. This was achieved using a generating-function. This approach is feasible due to two features of the problem: (i) the model is linear (i.e., cells do not interact with each other), and (ii) the boundary of interest for TCP is at zero (i.e., extinction of tumour cells). The result for TCP(t) is [8]

$$\mathrm{TCP}(t) = \left[1 - \frac{C(t)/C_0}{1 + b_2 \int_0^t \mathrm{d}t' \frac{C(t)}{C(t')}}\right]^{C_0}, \tag{6.31}$$

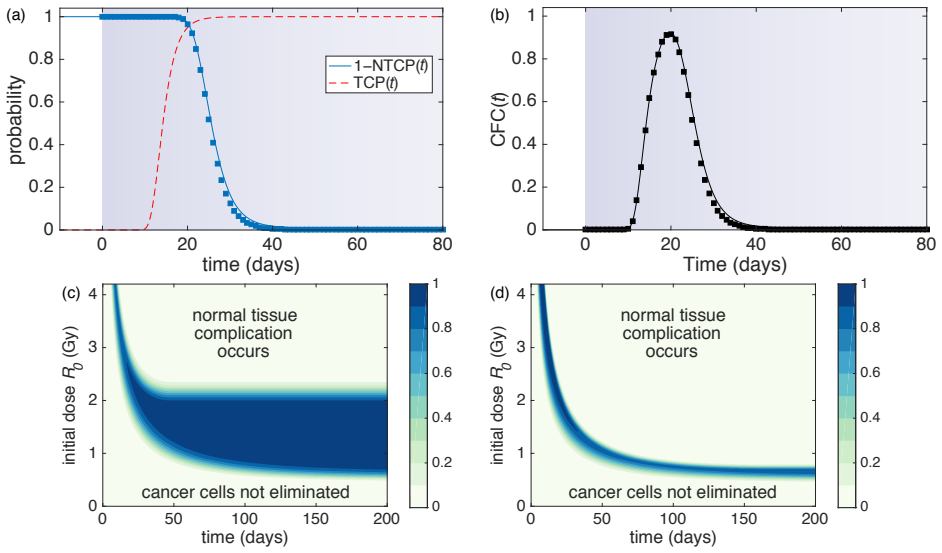

Figure 6.5: *TCP, NTCP and probability of CFC for the model in Sec. 6.5.2.* Panel (a): Probability that normal tissue complication has not yet occurred, $1 - \mathrm{NTCP}(t)$, as predicted by Approximation 2 (blue line) and from numerical integration of the master equation (blue squares). Probability that the tumour is successfully eliminated $\mathrm{TCP}(t)$ (dashed red line). TCP is calculated as in Ref. [8]. The shading of the background indicates the hazard function $h(t)$. Initial dose $R_0 = 2.5\mathrm{G\,y}$. Panel (b): Resulting probability of complication-free tumour control $\mathrm{CFC}(t)$. Black line is using Approximation 2 for NTCP and TCP as in Ref. [8]; results from direct numerical integration of the master equation are shown as black squares. Panels (c) and (d): $\mathrm{CFC}(t)$ for different values of the initial dose R_0, and for two different sets of model parameters (see Table 6.4).

where $C(t)$ is the deterministic path for number of cancerous cells, given by

$$\frac{\mathrm{d}C}{\mathrm{d}t} = [b_2 - d_2 - h_2(t)]\, C(t). \tag{6.32}$$

Even though the expression involves the deterministic trajectory $C(t)$ we stress again that this result is exact for arbitrary population sizes, and does not imply any approximations. While Eq. (6.32) cannot be solved analytically in most cases, the equation can be integrated numerically for an efficient calculation of TCP(t). The analysis reviewed here has also been extended to consider more complicated models, including the different stages of the cell cycle [9–11].

Complication-free tumour control (CFC) refers to the elimination of all cancer cells while maintaining enough normally functioning tissue for an organ to operate without complications [40]. The probability of CFC as a function of time is therefore given by [40]

$$\mathrm{CFC}(t) = \mathrm{TCP}(t)\,[1 - \mathrm{NTCP}(t)]\,. \tag{6.33}$$

We remark that Eq. (6.33) implies an equal weighting of the importance of tumour control and NTCs. In the most extreme cases, for example where NTCs relate to organ failure this is justified. In other cases, for example when NTC refers to increased urinal frequency, a complication may be preferable to a potentially life-threatening tumour. In such cases, Eq. (6.33) can be modified by appropriately weighting the two probabilities to maximise a 'quality of life' measure in accordance with clinical experience [41].

Fig. 6.5 (a) shows the probabilities $1-\mathrm{NTCP}(t)$ and TCP(t) for the model defined in Sec. 6.5.2, and for a specific choice of parameters (see Table 6.4). These quantities are obtained by Approximation 2 for NTCP, and Eq. (6.31) for TCP. Similarly, Fig. 6.5 (b) shows CFC(t) and compares the results from our approximation to those of numerical integration of the master equation. For this choice of parameters we find a non-trivial time (~ 20 days) which maximises the probability of CFC. In the case of a temporary brachytherapy implant, this would indicate the optimum moment for removal.

The analysis provided here allows us to investigate the optimum application of brachytherapy to maximise the likelihood of CFC. We consider a fixed set of parameters describing the cellular birth rates, death rates, susceptibilities and repair rates, shown in Table 6.4. We consider a temporary implant of a certain radioisotope, ^{125}I, which

Case	b day^{-1}	d day^{-1}	α G y^{-1}	β G y^{-2}	γ day^{-1}	threshold for NTC ℓ	frac. of dose absorbed θ	pop. size
Fig. 6.5 (a–c)								
TCP	0.0165	0.0015	0.2	0.05	8.35		1.0	$C_0 = 10^3$
NTCP	0.055	0.005	0.1	0.01	8.35	0.5	0.2	$\Omega = 10^3$
Fig. 6.5 (d)								
TCP	0.02	0.005	0.2	0.05	2.27		1.0	$C_0 = 10^3$
NTCP	0.0067	0.0017	0.1	0.01	2.27	0.2	0.4	$\Omega = 10^3$

Table 6.4: Parameters used in Fig. 6.5, along with $\lambda = 0.0117$ day^{-1}. The parameters in the upper two rows were previously used to model brachytherapy as a treatment for prostate cancer, where the normal tissue complication refers to rectal proctitis [12]. The parameters in the bottom row are hypothetical, used to show that a change in the optimum treatment strategy may result upon variation of parameters.

has a decay rate of $\lambda = 0.0117$ day^{-1}. In order to achieve CFC, we assume we are able to control the initial dose rate R_0 (i.e., the size of the radioactive seed) and the time at which the implant is removed.

Fig. 6.5 (c) shows the probability of CFC for different values of time and initial dose, again efficiently generated using Approximation 2 for NTCP and Eq. (6.31) for TCP. With the exception of the population sizes, the parameters we choose here were previously used to model the treatment of prostate carcinoma [12] consistent with experimentally collected parameters [42]. In this context NTC refers to acute radiation proctitis [43]. For these parameters, the optimal strategy involves an initial dose of size 1.7 G y and removal at a time over 50 days. Using this initial dose, the probability of CFC(t) does not decrease at large times, providing a large window for the removal of the implant or allowing the use of a permanent implant. This is not the case for all parameters; the optimum strategy may require the timely removal of the implant. An example of this is shown in Fig. 6.5 (d), which shows CFC(t) for parameters where the cancer cells have a three-fold higher growth rate than normal cells. The probability of CFC is peaked when implanting a high dose of radiation for a short time. For this case, we see the band where CFC is likely is narrow, indicating that such a treatment may be very sensitive to the time of removal of the implant.

6.6 Conclusions

To summarise, we have derived approximations for the distribution of first-passage times through a boundary of a stochastic birth-death model. These approximations

capture effects of fluctuations in the population discarded in previous approaches. The improvements rely on an expansion in the inverse typical size of the population. One can therefore expect the approach to be particularly useful for large, but finite populations. Intrinsic noise is then weak, but not always weak enough to be ignored altogether. It is worth noting that the methods we have developed do not require the birth-death model to be linear, for example we have considered logistic growth. Our analysis was presented in the context of normal tissue complication probabilities for radiotherapy treatment, however these mathematical results may also have wider applicability to other problems in which first-passage times of stochastic processes are of interest [44].

We note that NTCP takes the form of an error function in our approximation. This functional form has previously been reported in statistical models of NTCP, see for example Ref. [5]. This indicates that NTCP can be different from zero or one for intermediate doses of radiation; NTC then occurs (or does not occur) as a random process. This is the case as well in our model; the source of stochasticity is the intrinsic noise in the population of functional cells, i.e., random birth and death events. It is not clear however what exactly the origin of uncertainty is in statistical models of NTCP. Intrinsic stochasticity within functional subunits, or resulting from small numbers of stem cells may be potential sources of randomness, but other factors are likely to contribute as well.

We have obtained approximations of NTCP for models of normal tissue with a single type of cell and for an extended model with two different cell types. Our results demonstrate that these approximations can lead to a significant increase in efficiency over simulation methods, at a moderate loss of accuracy. This is the case particularly when the underlying model becomes complex and has many different internal states. In the final part of the paper we showed how approximations of NTCP and TCP can be used to estimate the probability of complication-free tumour control. We have demonstrated how the analytical approximations can be used for the efficient identification of optimised parameters for treatment planning in brachytherapy. Our analysis is limited to stylised models, and we do not claim direct clinical applicability. However, we hope that the methods we have developed can be adapted to more realistic populations of cancerous cells and normal tissue.

6.7 Appendix A: The LQ formalisation

We briefly review the LQ formalism for a radioactive implant [34–36]. We first consider the reaction describing death due to irradiation. The LQ formalism relates the mean surviving fraction of cells ψ to the total dose delivered in a time interval $[0, t]$, $D(t)$:

$$\psi(t) = e^{-\alpha D(t) - \beta q(t) D(t)^2}. \tag{6.34}$$

Here, there are two radiosensitivity parameters, α and β, which describe a tissue's linear and quadratic responses to a source of radiation, respectively. For a radioactive source exponentially decaying with rate λ and with an initial dose rate R_0, the total dose delivered by time t is given by $D(t) = R_0/\lambda\,[1 - \exp(-\lambda t)]$. The function $q(t)$ in Eq. (6.34) is the Lea–Catcheside protraction factor [45], which is specific to the method of treatment involved. In the case of brachytherapy it is given by

$$q(t) = \frac{2(\lambda t)^2}{(\gamma t)^2(1 - \lambda^2/\gamma^2)\,(1 - e^{-\lambda t})^2}\left[e^{-(\lambda+\gamma)t} + \gamma t\left(\frac{1 - e^{-2\lambda t}}{2\lambda t}\right) - \frac{1 + e^{-2\lambda t}}{2}\right]. \tag{6.35}$$

Here, γ is the rate at which radiation-damaged cells repair their DNA. The fractional change in the population over an infinitesimal time $\dot{\psi}(t)/\psi(t)$ gives the hazard function $h(t)$. This is found to be given by [12]

$$h(t) = \alpha R_0 e^{-\lambda t} + \frac{2\beta R_0^2 e^{-\lambda t}}{\gamma - \lambda}\left(e^{-\lambda t} - e^{-\gamma t}\right). \tag{6.36}$$

6.8 Appendix B: Evaluation of Approximation 1 for the model of normal and doomed cells in Sec. 6.4.1

We write N_t for the number of normal cells at time t and X_t for the number of doomed cells. We are interested in the population of total functional cells, $S_t \equiv N_t + X_t$. Specifically, we are interested in the time S_t first passes a boundary L. The master

equation can be formulated in terms of S and X:

$$\begin{aligned}\frac{\mathrm{d}}{\mathrm{d}t}P_{S,X}(t) = &\left(\mathcal{E}_S^{-1}-1\right) b_0(S-X)\left(1-\frac{S}{k\Omega}\right)P_{S,X}(t)\\ &+\left(\mathcal{E}_X^{-1}-1\right) h(t)(S-X)P_{S,X}(t)\\ &+\left(\mathcal{E}_S^{+1}-1\right) d_1(S-X)P_{S,X}(t)\\ &+\left(\mathcal{E}_S^{+1}\mathcal{E}_X^{+1}-1\right) d_2 X P_{S,X}(t),\end{aligned} \tag{6.37}$$

where $P_{S,X}(t)$ is the probability that random processes S_t, X_t have the values S, X at time t. The operator $\mathcal{E}_S$ is the step operator affecting the size of the total population, and $\mathcal{E}_X$ is the step operator affecting the number of doomed cells, i.e. $\mathcal{E}_S f_{S,X} = f_{S+1,X}$ and $\mathcal{E}_X f_{S,X} = f_{S,X+1}$.

We proceed by approximating the master equation via a Kramers–Moyal expansion. First, we introduce re-scaled processes $s_t = S_t/\Omega$ and $x_t = X_t/\Omega$, and then expand the step operators in the limit $\Omega \gg 1$. We arrive at the Fokker–Planck equation

$$\begin{aligned}\frac{\partial}{\partial t}\Pi(s,x,t) = &-\frac{\partial}{\partial s}\left[b_0\left(1-\tfrac{s}{k}\right)(s-x)-d_1(s-x)-d_2x\right]\Pi(s,x,t)\\ &-\frac{\partial}{\partial x}\left[h(t)(s-x)-d_2x\right]\Pi(s,x,t)\\ &+\frac{1}{2\Omega}\frac{\partial^2}{\partial s^2}\left[b_0\left(1-s\right)(s-x)+d_1(s-x)+d_2x\right]\Pi(s,x,t)\\ &+\frac{1}{2\Omega}\frac{\partial^2}{\partial x^2}\left[h(t)(s-x)+d_2x\right]\Pi(s,x,t)\\ &+\frac{1}{\Omega}\frac{\partial}{\partial s}\frac{\partial}{\partial x}\,d_2x\Pi(s,x,t),\end{aligned} \tag{6.38}$$

where we have neglected higher-order terms in Ω^{-1}. This Fokker–Planck equation can equivalently be written as an SDE:

$$\begin{pmatrix}\mathrm{d}s_t\\ \mathrm{d}x_t\end{pmatrix} = \boldsymbol{\mu}(s_t,x_t)\mathrm{d}t + \frac{1}{\Omega^{1/2}}\mathbf{B}(s,x,t)\begin{pmatrix}\mathrm{d}W_t^{(1)}\\ \mathrm{d}W_t^{(2)}\end{pmatrix}, \tag{6.39}$$

where the drift is given by

$$\boldsymbol{\mu}(s,x) = \begin{pmatrix}b\left(1-\frac{s}{k}\right)(s-x)-d_1(s-x)-d_2x\\ h(t)(s-x)-d_2x\end{pmatrix}. \tag{6.40}$$

The diffusion $\mathbf{B}(s,x,t)$ is the positive-semidefinite matrix satisfying

$$\mathbf{B}^2(s,x,t) = \begin{pmatrix}b\left(1-\frac{s}{k}\right)(s-x)+d_1(s-x)+d_2x & d_2x\\ d_2x & h(t)(s-x)+d_2x\end{pmatrix}. \tag{6.41}$$

We proceed by linearising the SDE (6.39). Let $s_t = \phi_1(t) + \Omega^{-1/2}\xi_{1t}$ and $x_t = \phi_2(t) + \Omega^{-1/2}\xi_{2t}$, where $\phi_1(t)$ and $\phi_2(t)$ are the deterministic functions of time. Substituting and collecting lowest order terms, we see these functions are given by the ODEs

$$\frac{\mathrm{d}\phi_1}{\mathrm{d}t} = \left(1 - \frac{\phi_1}{k}\right) b(\phi_1 - \phi_2) - d_1(\phi_1 - \phi_2) - d_2\phi_2, \tag{6.42a}$$

$$\frac{\mathrm{d}\phi_2}{\mathrm{d}t} = h(t)(\phi_1 - \phi_2) - d_2\phi_2, \tag{6.42b}$$

i.e., we recover Eqs. (6.26b).

The random processes ξ_{1t} and ξ_{2t} describe deviations from this deterministic trajectory, and are of the Ornstein–Uhlenbeck type

$$\mathrm{d}\boldsymbol{\xi}_t = \mathbf{A}(\phi_1, \phi_2, t)\,\boldsymbol{\xi}_t \mathrm{d}t + \mathbf{B}(\phi_1, \phi_2, t)\,\mathrm{d}\boldsymbol{W}_t, \tag{6.43}$$

where $\mathbf{A}(\phi_1, \phi_2, t)$ is given by

$$\mathbf{A}(\phi_1, \phi_2, t) = -\begin{pmatrix} b\left(1 - 2\frac{\phi_1}{k} + \frac{\phi_2}{k}\right) - d_1 & b\left(\frac{\phi_1}{k} - 1\right) + d_1 - d_2 \\ h(t) & -h(t) - d_2 \end{pmatrix}. \tag{6.44}$$

We note that the argument of $\mathbf{B}$ in Eq. (6.43) is now given by ϕ_1 and ϕ_2, so that the noise is additive rather than multiplicative.

We are interested in the variation of the total population size from the deterministic path $\langle \xi_{1t}^2 \rangle$; we remark that by construction $\langle \xi_{1_t} \rangle = \langle \xi_{2t} \rangle = 0$. The variances and covariance of ξ_{1t} and ξ_{2t} can be seen to evolve in time as follows [28]

$$\frac{\mathrm{d}\langle \xi_{1t}^2 \rangle}{\mathrm{d}t} = 2A_{11}\langle \xi_{1t}^2 \rangle + 2A_{12}\langle \xi_{1t}\xi_{2t} \rangle + (B_{11})^2 + (B_{12})^2, \tag{6.45a}$$

$$\frac{\mathrm{d}\langle \xi_{2t}^2 \rangle}{\mathrm{d}t} = 2A_{22}\langle \xi_{2t}^2 \rangle + 2A_{21}\langle \xi_{1t}\xi_{2t} \rangle + (B_{22})^2 + (B_{21})^2, \tag{6.45b}$$

$$\frac{\mathrm{d}\langle \xi_{1t}\xi_{2t} \rangle}{\mathrm{d}t} = A_{21}\langle \xi_{1t}^2 \rangle + A_{12}\langle \xi_{2t}^2 \rangle + (A_{11} + A_{22})\langle \xi_{1t}\xi_{2t} \rangle + B_{11}B_{21} + B_{12}B_{22}. \tag{6.45c}$$

For a given set of parameters, we numerically integrate the five coupled Eqs. (6.42) and Eqs. (6.45). This provides the mean and covariance matrix for the bivariate Gaussian distribution of the number of normal and doomed cells as a function of time. For Approximation 1, the time t^* is defined by $\phi_1(t^*) = \ell$; this is the point in time when the total number of functional cells crosses the threshold for onset of NTC. The variance of the number of functional cells at this time is given by $\Sigma^2(t^*) = \langle \xi_{1t^*}^2 \rangle$ within the LNA. We then use Eq. (6.19), where $\mu(\ell, t^*)$ is to be replaced by the right-hand side of Eq. (6.42a), evaluated at t^*.

Approximation 2 is computed using Eq. (6.28), replacing $\phi(t)$ by $\phi_1(t)$, and $\Sigma^2(t)$ by $\left\langle {\xi_1}_t^2 \right\rangle$, respectively.

6.9 Bibliography

[1] P. G. Hufton, E. Buckingham-Jeffery, and T. Galla. Calculating normal tissue complication probabilities and probabilities of complication-free tumour control from stochastic models of population dynamics. *arXiv preprint arXiv:1803.08595* (2018).

[2] E. Martinez, A. Daidone, C. Gutierrez, J. Pera, A. Boladeras, F. Ferrer, F. Pino, J. F. Suarez, A. Polo, and F. Guedea. Permanent seed brachytherapy for clinically localized prostate cancer: Long-term outcomes in a 700 patient cohort. *Brachytherapy* **14**, 166 (2015).

[3] N. Tanaka, I. Asakawa, M. Hasegawa, and K. Fujimoto. Urethral toxicity after LDR brachytherapy: experience in Japan. *Brachytherapy* **14**, 131 (2015).

[4] J.-C. Horiot, P. Bontemps, W. Van den Bogaert, R. Le Fur, D. van den Weijngaert, M. Bolla, J. Bernier, A. Lusinchi, M. Stuschke, J. Lopez-Torrecilla, *et al.* Accelerated fractionation (AF) compared to conventional fractionation (CF) improves loco-regional control in the radiotherapy of advanced head and neck cancers: results of the EORTC 22851 randomized trial. *Radiother. Oncol.* **44**, 111 (1997).

[5] J. T. Lyman. Complication Probability as Assessed from Dose-Volume Histograms. *Radiat. Res.* **104**, S13 (1985).

[6] A. Niemierko and M. Goitein. Modeling of normal tissue response to radiation: The critical volume model. *Int. J. Radiat. Oncol. Biol. Phys.* **25**, 135 (1993).

[7] L. Hanin and M. Zaider. A mechanistic description of radiation-induced damage to normal tissue and its healing kinetics. *Phys. Med. Biol.* **58**, 825 (2013).

[8] M. Zaider and G. Minerbo. Tumour control probability: a formulation applicable to any temporal protocol of dose delivery. *Phys. Med. Biol.* **45**, 279 (2000).

[9] A. Dawson and T. Hillen. Derivation of the tumour control probability (TCP) from a cell cycle model. *Comput. Math. Methods Med.* **7**, 121 (2006).

[10] A. Maler and F. Lutscher. Cell-cycle times and the tumour control probability. *Math. Med. Biol.* **27**, 313 (2009).

[11] T. Hillen, G. De Vries, J. Gong, and C. Finlay. From cell population models to tumor control probability: including cell cycle effects. *Acta Oncol.* **49**, 1315 (2010).

[12] T. Stocks, T. Hillen, J. Gong, and M. Burger. A stochastic model for the normal tissue complication probability (NTCP) and applications. *Math. Med. Biol.* **34**, 469 (2017).

[13] P. Stavrev, N. Stavreva, A. Niemierko, and M. Goitein. Generalization of a model of tissue response to radiation based on the idea of functional subunits and binomial statistics. *Phys. Med. Biol.* **46**, 1501 (2001).

[14] S. L. Tucker, M. Zhang, L. Dong, R. Mohan, D. Kuban, and H. D. Thames. Cluster model analysis of late rectal bleeding after IMRT of prostate cancer: A case–control study. *Int. J. Radiat. Oncol. Biol. Phys.* **64**, 1255 (2006).

[15] E. Rutkowska, C. Baker, and A. Nahum. Mechanistic simulation of normal-tissue damage in radiotherapyimplications for dosevolume analyses. *Phys. Med. Biol.* **55**, 2121 (2010).

[16] M. D'Andrea, M. B. Benassi, and L. Strigari. Modeling Radiotherapy Induced Normal Tissue Complications: An Overview beyond Phenomenological Models. *Comput. Math. Methods Med* **2016**, 2796186 (2016).

[17] J. Hendry and H. Thames. The tissue-rescuing unit. *Br. J. Radiol.* **59**, 628 (1986).

[18] A. W. Konings, R. P. Coppes, and A. Vissink. On the mechanism of salivary gland radiosensitivity. *Int. J. Radiat. Oncol. Biol. Phys.* **62**, 1187 (2005).

[19] R. G. Dale and B. E. Jones. *Radiobiological modelling in radiation oncology.* British Institute of Radiology, London (2007).

[20] V. P. Bond, T. M. Fliedner, and J. O. Archambeau. *Mammalian radiation lethality: a disturbance in cellular kinetics.* Academic Press, Cambridge MA (1965).

[21] S. Redner. *A guide to first-passage processes.* Cambridge University Press, Cambridge (2001).

[22] D. T. Gillespie. A general method for numerically simulating the stochastic time evolution of coupled chemical reactions. *J. Comput. Phys.* **22**, 403 (1976).

[23] D. T. Gillespie. Exact stochastic simulation of coupled chemical reactions. *J. Phys. Chem.* **81**, 2340 (1977).

[24] C. W. Gardiner. *Handbook of Stochastic Methods.* Springer-Verlag, Berlin (2004).

[25] J. Gong, M. M. Dos Santos, C. Finlay, and T. Hillen. Are more complicated tumour control probability models better? *Math. Med. Biol.* **30**, 1 (2013).

[26] N. G. van Kampen. *Stochastic Processes in Physics and Chemistry.* North-Holland, Amsterdam (2007).

[27] P. E. Kloeden and E. Platen. *Numerical Solution of Stochastic Differential Equations.* Springer-Verlag, Berlin (1992).

[28] H. Risken. *The Fokker–Planck Equation: Methods of Solution and Applications.* Springer-Verlag, Berlin (1989).

[29] L. M. Ricciardi and S. Sato. First-passage-time density and moments of the Ornstein-Uhlenbeck process. *J. Appl. Probab.* **25**, 43 (1988).

[30] Y. Madec and C. Japhet. First passage time problem for a drifted Ornstein–Uhlenbeck process. *Math. Biosci.* **189**, 131 (2004).

[31] C.-F. Lo and C.-H. Hui. Computing the first passage time density of a time-dependent Ornstein–Uhlenbeck process to a moving boundary. *Appl. Math. Lett.* **19**, 1399 (2006).

[32] E. J. Hall and A. J. Giaccia. *Radiobiology for the Radiologist.* Lippincott Williams & Wilkins, Philadelphia PA (2006).

[33] A. V. Ponce Bobadilla, P. K. Maini, and H. Byrne. A stochastic model for tumour control probability that accounts for repair from sublethal damage. *Math. Med. Biol.* page dqw024 (2017).

[34] D. J. Brenner and D. E. Herbert. The use of the linear-quadratic model in clinical radiation oncology can be defended on the basis of empirical evidence and theoretical argument. *Med. Phys.* **24**, 1245 (1997).

[35] D. J. Brenner. The linear-quadratic model is an appropriate methodology for determining isoeffective doses at large doses per fraction. In *Seminars in radiation oncology*, volume 18, pages 234–239. Elsevier (2008).

[36] J. F. Fowler. 21 years of biologically effective dose. *Br. J. Radiol.* **83**, 554 (2010).

[37] A. L. Gibbs and F. E. Su. On choosing and bounding probability metrics. *Int. Stat. Rev.* **70**, 419 (2002).

[38] S. Kullback and R. A. Leibler. On information and sufficiency. *Ann. Math. Stat* **22**, 79 (1951).

[39] H. McAneney and S. O'Rourke. Investigation of various growth mechanisms of solid tumour growth within the linear-quadratic model for radiotherapy. *Phys. Med. Biol.* **52**, 1039 (2007).

[40] A. J. Mundt and J. C. Roeske. *Intensity modulated radiation therapy: a clinical perspective*, volume 1. PMPH-USA, Shelton CT (2005).

[41] P. Kallman, B. K. Lind, and A. Brahme. An algorithm for maximizing the probability of complication-free tumour control in radiation therapy. *Phys. Med. Biol.* **37**, 871 (1992).

[42] D. J. Carlson, R. D. Stewart, X. A. Li, K. Jennings, J. Z. Wang, and M. Guerrero. Comparison of in vitro and in vivo α/β ratios for prostate cancer. *Phys. Med. Biol.* **49**, 4477 (2004).

[43] A. U. Kishan and P. A. Kupelian. Late rectal toxicity after low-dose-rate brachytherapy: incidence, predictors, and management of side effects. *Brachytherapy* **14**, 148 (2015).

[44] R. Metzler, G. Oshanin, and S. E. Redner. *First-Passage Phenomena and Their Applications*. World Scientific, Singapore (2014).

[45] D. Lea and D. Catcheside. The mechanism of the induction by radiation of chromosome aberrations in Tradescantia. *J. Genet.* **44**, 216 (1942).

Chapter 7

Conclusions

Throughout this thesis we have considered the stochastic dynamics of systems in time-varying environments. The thesis is broadly composed of chapters of two types of content: Chapters 2 and 5 are focussed on developing new mathematical methods, while Chapters 3 and 4 are more focussed on specific applications in biology; Chapter 6 contains both new methods and applications.

The major result of the first two of these methods chapters is a palette of approximations schemes, which provides reduced descriptions of systems in switching environments when either the system is large, the environmental switching is fast, or both (Fig. 5.8). In Chapter 2, we developed a systematic expansion method in the limit of a large system for describing the dynamics of systems coupled to a Markovian switching environment. The lowest order of this expansion is the piecewise-deterministic Markov process which ignores demographic noise; for this process we provided the general stationary distribution for the simplest case of a single systemic species and a two-state environment. Considering the next order in this expansion allowed us incorporate the effects of demographic noise into the approximation, resulting in the description as a piecewise-diffusive process. Using the linear-noise approximation, we were able to find an analytical approximation for the stationary distribution of this process, which produced marked improvements over the PDMP description when compared to simulations of the full, individual-based model. We demonstrated the validity of our approach by considering models with complications including nonlinear reaction rates, situations in which the environmental switching depends on the state of the population, and systems where there are multiple attractors. A limitation of this work is that

analytical approximations to stationary distributions were only possible for the case of a single systemic species in a two-state environment; outside of these conditions, the equations describing the stationary state of the PDMP could not be solved. For such cases it is possible that other approaches, such as those based on the WKB method as considered in Refs. [1–6], may produce analytical results.

The second methods chapter (Chapter 5) concerned the dynamics of a system in a switching environment, where the environmental switching happened on a faster time scale than the systemic reactions. We described a new expansion in the limit of fast, but finite, environmental switching. Considering only the lowest-order terms in this expansion resulted in the adiabatic description where environmental noise is disregarded entirely, which is closely related to the quasi-stationary state approximation. Incorporating sub-leading order terms into the expansion resulted in a reduced master equation in which bursting events (occasions where two events happen simultaneously) occurred. We showed how this reduced master equation offered a more accurate description than the adiabatic description, by comparing stationary distributions and power spectra with the full model.

The second half of Chapter 5 combined expansions in powers of the inverse switching time scale with expansions in the inverse system size, resulting in the table of approximations Fig. 5.8. This involved introducing new approximations, and putting existing approximations into a wider context. We expect many of these approximations to be useful in their relevant limit. In particular, we identified the "SDE with switching and demographic noise" (the centre box in Fig. 5.8) as an ideal candidate for the facilitation of future research, since it incorporates both demographic and environmental sources of noise and takes a form which allows for analytical progress or at least efficient simulation. We demonstrated these approaches for a number of different applications, biological and otherwise. While this chapter provided useful results when their is a large time-scale separation between system and environment, I remark that the dynamics for general time scales remains an open challenge.

Another major component of Chapter 5 considered master equations with negative 'rates'. We showed how, in some circumstances, such rates occur from the expansion of the master equation in the fast-switching limit; these rates show similarities to cases in open quantum systems. We showed how such dynamics can lead to negative

'probabilities', which occur on time scales shorter than that of the environment. In our classical setting, we reviewed an existing simulation algorithm for producing sample paths from master equations with negative rates and showed this failed to capture statistical features of the full model. We proposed a new tau-leaping scheme for generating trajectories for the case of negative rates in Chapter 5.

New methods were also developed in Chapter 6; we devised techniques for approximating first passage times for systems with a continuous, deterministic environment. These approaches relied on the assumption of a large system size, and mathematically utilised an expansion in powers of the inverse systems-size parameter. Here, I remark that this approach is equally valid in other weak-noise cases, such as the "SDE with switching and demographic noise" presented in Chapter 5. Since weak-noise limits are commonplace in statistical physics, we believe our results may be applicable to a range of problems. This could potentially include other areas where first-passage times are of interest, such as financial risk [7].

Chapter 6 considered a specific biological application; we studied normal tissue complication probabilities arising in the treatment of cancer. We showed how the probability for the onset of a normal tissue complication could be approximated for a one-dimensional logistic growth model under a particular radiotherapy protocol. We later extended this by considering a more complicated model containing both normal and radiation-damaged cells. In all cases we found our approximations constituted a more efficient approach to finding the first passage times than integration of the master equation, at a moderate loss of accuracy, for sufficiently large systems. Lastly, we combined our approximation for NTCP with an existing result describing tumour control probabilities, in order to estimate the probability of a complication-free cure. Using these two approaches we were able to efficiently sweep the parameter space describing different brachytherapy protocols, we and demonstrate how the probability of a complication-free cure can be theoretically maximised.

Chapter 3 was the first of the application-focused Chapters. Here we used the results of Chapter 2 to study a stylised model characterising bet-hedging, in which cells switch between phenotypes to endure varying environmental conditions. We began by defining an individual-based model, and proceeded to approximate the dynamics in the limit of a large system as a piecewise-deterministic Markov process. This allowed

us to obtain a closed-form solution for the average growth rate for a population. We compared the cases of Markovian environmental switching and a periodic environment. Our main conclusions were: (i) when the environmental switching rates are slow, the growth-maximising phenotypic strategy is achieved when the phenotypic switching rates match the environmental switching rates. This is the case for both stochastic and periodic environmental dynamics; however, the stochastic regime had different behaviour for environments of intermediate speeds; (ii) for both stochastic and periodic environments, heterogeneity is favoured at low environmental switching rates, while homogeneity is favoured when the environment switches quickly. Stochastic environments, however, favour heterogeneity over a larger range of environmental dynamics than strictly periodic environments; (iii) instantaneous growth rates are universally higher in the case of stochastic environments than in the periodic case; (iv) the model can be interpreted as a host-pathogen interaction, in which the host tries to choose environmental switching so as to minimise the growth of the pathogen, and in which the pathogen chooses its phenotypic-switching strategy to optimise its growth rate. We showed how this could leak to a mutual best-response scenario. The mathematical approach developed in this Chapter may allow for studies into other ecological models of competition in dynamic random external conditions.

In Chapter 4 we considered a model of mouse embryonic stem cells. We considered an experimentally-inferred network topology and, using a number of simplifying assumptions to the molecular logic and dynamics, we extended this to a microscopic model with a large number of species (i.e., three external inputs, 12 genes, and 12 transcription factors) and a large number of interactions. We approximated the dynamics of the individual-based model in the limit of a large system as a piecewise-deterministic Markov process; this provided an efficient scheme for simulating the dynamics, and we found an decrease in simulation time of order 10^3 when compared to Gillespie simulation. Thanks to this increase in speed, we were able to perform a large number of simulations using different parameters, and find which of those best characterised a number experimental results. We found parameters which matched the Boolean-expression data of Dunn *et al.* [8] spanning very different gene-switching regimes (slow, intermediate, and fast), suggesting that mean expression data is insufficient for uniquely determining the parameters of high-dimensional networks. However,

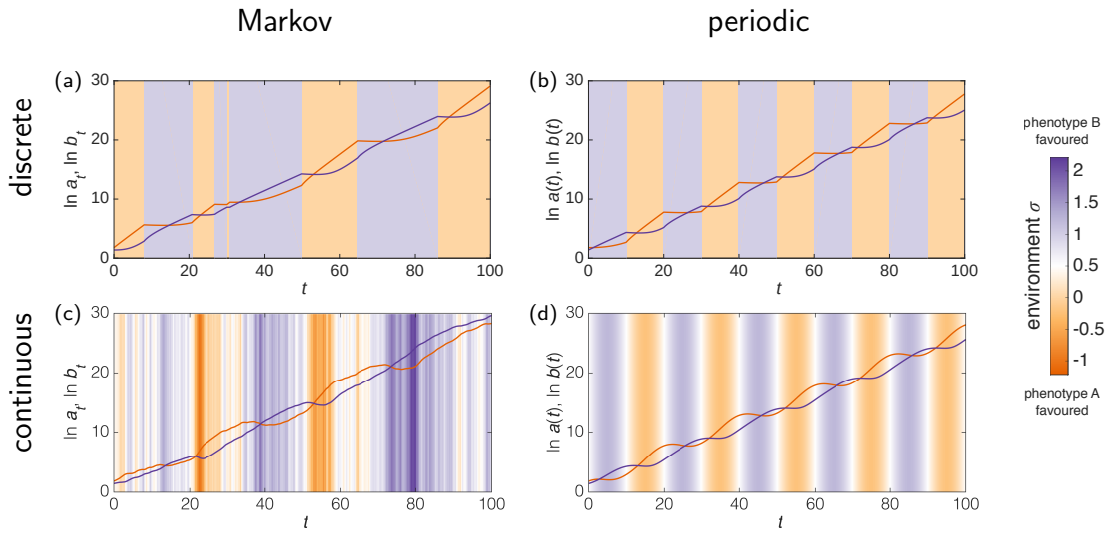

Figure 7.1: Growth for the model of phenotypic switching model (Chapter 3) with different environmental dynamics. Typical trajectories for the case of (a) a discrete Markovian environment, (b) a discrete periodic environment, (c) a continuous Markovian environment, and (d) a continuous periodic environment. The populations of phenotypes A and B are orange and purple lines, respectively. The background shading indicates the state of the environment. Simulations use parameter set Table 3.1 (b), environmental switching rates are $\lambda_0 = 0.10$, $\lambda_1 = 0.10$, and phenotypic switching rates $p = 0.028$, $q = 0.043$. See Appendix 7.1 for details.

we identified the intermediate regime of gene switching, in which genetic-switching rates are comparable to system reaction rates, as most consistent with other single-cell measurements [9, 10]. We also found that this intermediate regime had a much faster response to changing external signals than the fast-switching regime.

The work in my thesis leaves open several areas for future research which, if I had more time, I would have liked to explore. One direction I would have liked to take this research is towards considering continuous, stochastic environments. Models with reaction rates which vary according to an SDE were recently considered in Refs. [5, 11, 12]. Dynamics of such a type pose both a technical challenge and could have important applications. Examples of these different environmental dynamics are shown in Fig. 7.1. Here, I show trajectories for the model of population growth considered in Chapter 3, which was used to describe phenotypic bet-hedging in a fluctuating environment. Panels (a–d) indicate four different environmental dynamics: Markovian switching, periodic switching, continuous stochastic, and continuous periodic, respectively (details are given in Appendix 7.1). In Chapter 3 we focused on the former two environmental dynamics. In the context of the model therein, however, continuous

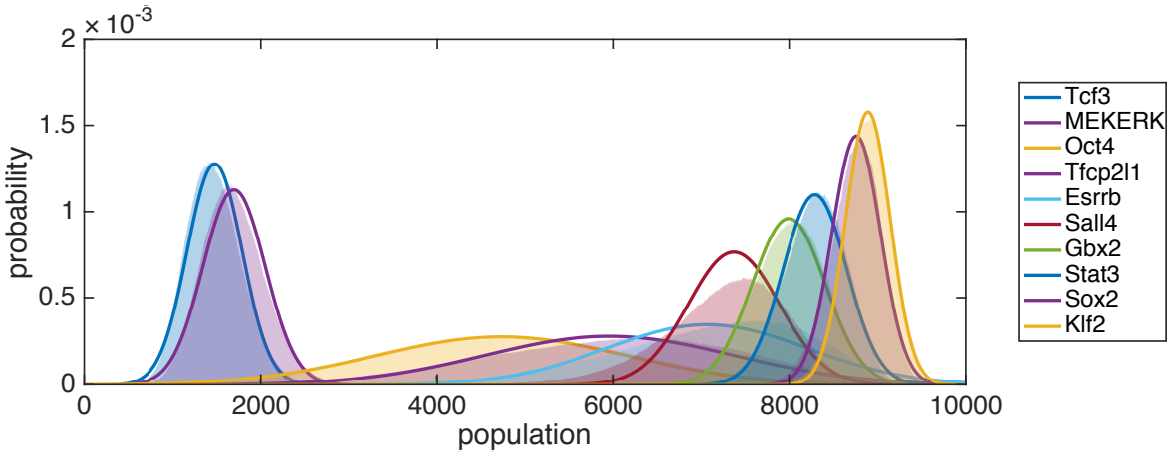

Figure 7.2: Stationary distributions for the populations of transcription factors for the model of mouse embryonic stem cells considered in Chapter 4. The fast switching parameters shown in Fig. 4.2 are used, along with external inputs LIF+2i. Histograms show the results from 48 hours of Gillepsie simulations of the full individual-based model. Solid lines show analytical approximations found by considering the SDE with switching and demographic noise from Chapter 5 and linearising around the fixed point; they were obtained in less than a second.

environments may be appropriate to describe continuous fluctuations in temperature, the availability of nutrients, or the intensity of light. For the model with a continuous stochastic environment, there is no obvious analytical solution for the average growth rates. Further analysis of the average growth rates (and thus the optimal strategies) could therefore come from either Monte Carlo simulations, or numerical integration of the Fokker–Planck equation describing the joint distribution of the phenotypes and environment $\Pi(\phi, \sigma)$. Such methods will be considerably more computationally expensive than the integral solution we produced for the discrete case in this thesis.

We also note that different processes for a continuous environment are likely to produce very different results. Panel (c) shows an Ornstein–Uhlenbeck process which 'lingers' (i.e., is most likely to be found) around the mean environmental state. Such a 'mean' environment is not part of the model with discrete states. Panel (d) shows a periodic continuous environment with sinusoidal time dependence which, on the other hand, spends more time at the two extremes. Alternative stochastic environmental processes could be conceived which behave more similarly to the discrete switching or sinusoidal cases, for example by involving motion in a double-well potential.

Considered as a whole, this thesis forms a consistent body of work describing the dynamics of systems in switching environments. In this way, each chapter is

relevant to some or all of the others. An example of this is demonstrated in Fig. 7.2, where I show how the theory developed in Chapter 5 applies to the model considered earlier in Chapter 4; The figure shows stationary distributions of the populations of transcription factors for the model of mouse embryonic stem cells considered in Chapter 4. The parameters charactering the limit of fast genetic switching are used (see Fig. 4.2). The coloured histograms show the the results found from 48 hours of Gillespie simulation of the the full, individual-based model. Later in the course of my PhD studies (Chapter 5), we developed new approximations for the dynamics of systems in fast-switching environments, and also approximations for large systems. For the model of Chapter 4, we consider the "SDE with switching and demographic noise", since it includes both sources of noise. Following a linearisation of the noise terms, the stationary distributions of these SDEs can be calculated. The results from this approximation are shown as solid lines in Fig. 7.2; this took less than a second to calculate. The agreement of these two approaches, and the computational benefit from using our approximation, suggest that our results may be useful in future research. It is my hope the inter-applicability and interconnectivity of the material in this thesis can be considered one of its strengths.

The techniques described in the thesis help in completing our understanding of processes involving both intrinsic and extrinsic noise. While existing dynamical approximations to switching environments, the PDMP or the adiabatic description (QSSA), each ignore one source of noise, we have here developed methods for retaining (to some approximation) both sources of noise. As discussed in the opening chapter, relevant applications are widespread including genetic networks and predator-prey models. Since publication of our first paper [13] in 2016, it has been cited a number of times by other authors (16 at the time of writing), in papers ranging from studies of voter behaviour [14] to predator-prey models [15]. It is my hope that the methods developed here will be used in future applications considering systems in switching environments.

7.1 Appendix A: Additional environmental dynamics

In Fig. 7.1 (c) I show the model described in Chapter 3 but where the environment is described by an Ornstein–Uhlenbeck process

$$\mathrm{d}\sigma_t = \theta\,(m - \sigma_t)\,\mathrm{d}t + s\,\mathrm{d}W_t, \tag{7.1}$$

where parameters θ, m, and s are chosen so that the Ornstein–Uhlenbeck process has the same mean, variance, and auto-correlation time as the telegraph process in Chapter 3. I remark that this Ornstein–Uhlenbeck process allows the environmental state σ to be greater than 1 and to be smaller than 0. The corresponding growth rates are assumed to be of the form $\mu^{A,B}(\sigma) = (1-\sigma)\mu_0^{A,B} + \sigma\mu_1^{A,B}$.

Similarly, in Fig. 7.1 (d) I consider a continuous periodic environment described by

$$\sigma(t) = A\sin(2\pi t/T) + m, \tag{7.2}$$

where parameters A, T and m are chosen so the the mean, variance, and period are the same as the discrete case in Chapter 3. In the periodic case the population dynamics converge to a limit cycle, and one can, in principle, numerically find the average growth rate by considering the growth over a single period after a transient time.

7.2 Bibliography

[1] A. Kamenev, B. Meerson, and B. Shklovskii. How Colored Environmental Noise Affects Population Extinction. *Phys. Rev. Lett.* **101**, 268103 (2008).

[2] M. Assaf, A. Kamenev, and B. Meerson. Population extinction in a time-modulated environment. *Phys. Rev. E* **78**, 041123 (2008).

[3] M. Assaf, E. Roberts, and Z. Luthey-Schulten. Determining the Stability of Genetic Switches: Explicitly Accounting for mRNA Noise. *Phys. Rev. Lett.* **106**, 248102 (2011).

[4] M. Assaf, M. Mobilia, and E. Roberts. Cooperation Dilemma in Finite Populations under Fluctuating Environments. *Phys. Rev. Lett.* **111**, 238101 (2013).

[5] M. Assaf, E. Roberts, Z. Luthey-Schulten, and N. Goldenfeld. Extrinsic noise driven phenotype switching in a self-regulating gene. *Phys. Rev. Lett.* **111**, 058102 (2013).

[6] E. Roberts, S. Be'er, C. Bohrer, R. Sharma, and M. Assaf. Dynamics of simple gene-network motifs subject to extrinsic fluctuations. *Phys. Rev. E* **92**, 062717 (2015).

[7] R. Metzler, G. Oshanin, and S. E. Redner. *First-Passage Phenomena and Their Applications*. World Scientific, Singapore (2014).

[8] S.-J. Dunn, G. Martello, B. Yordanov, S. Emmott, and A. Smith. Defining an essential transcription factor program for naive pluripotency. *Science* **344**, 1156 (2014).

[9] Z. S. Singer, J. Yong, J. Tischler, J. A. Hackett, A. Altinok, M. A. Surani, L. Cai, and M. B. Elowitz. Dynamic heterogeneity and DNA methylation in embryonic stem cells. *Mol. Cell.* **55**, 319 (2014).

[10] R. M. Kumar, P. Cahan, A. K. Shalek, R. Satija, A. J. DaleyKeyser, H. Li, J. Zhang, K. Pardee, D. Gennert, J. J. Trombetta, *et al.* Deconstructing transcriptional heterogeneity in pluripotent stem cells. *Nature* **516**, 56 (2014).

[11] M. Assaf, M. Mobilia, and E. Roberts. Cooperation dilemma in finite populations under fluctuating environments. *Phys. Rev. Lett.* **111**, 238101 (2013).

[12] E. Roberts, S. Be'er, C. Bohrer, R. Sharma, and M. Assaf. Dynamics of simple gene-network motifs subject to extrinsic fluctuations. *Phys. Rev. E* **92**, 062717 (2015).

[13] P. G. Hufton, Y. T. Lin, T. Galla, and A. J. McKane. Intrinsic noise in systems with switching environments. *Phys. Rev. E* **93**, 052119 (2016).

[14] J. Hidalgo, S. Suweis, and A. Maritan. Species coexistence in a neutral dynamics with environmental noise. *J. Theor. Biol.* **413**, 1 (2017).

[15] R. West, M. Mobilia, and A. M. Rucklidge. Survival behavior in the cyclic Lotka-Volterra model with a randomly switching reaction rate. *Phys. Rev. E* **97**, 022406 (2018).